Author/s:
Wilson, Kayla Roberta

Title:
Exploiting immunoreceptor regulation for immunity

Date:
2021

Persistent Link:
https://hdl.handle.net/11343/297352

# Exploiting immunoreceptor regulation for immunity

Kayla Roberta Wilson

ORCID: 0000-0003-2023-7964

Submitted in total fulfilment of the requirements of the degree of Doctor of Philosophy

October 2021

Department of Biochemistry and Pharmacology

The University of Melbourne

# Abstract

Dendritic cells (DCs) are critical for the activation of immune responses. As such, there is a lot of interest in understanding their biology so they can be more easily exploited for improved immune responses to vaccines. This thesis has interrogated two key molecules necessary for the generation and function of DCs – FMS-like tyrosine kinase 3 (Flt3) and major histocompatibility complex class II (MHC II).

It is well established that the number of DCs in normal (1–4) and malignant tissues (5) is reliant on the Flt3/Flt3 ligand (Flt3L) signaling cascade. Therefore, manipulation of this pathway is an attractive solution to improve immune outcomes. Currently, clinical strategies rely upon administration of Flt3L, however, improved understanding of the expression and regulation of Flt3 could lead to more sophisticated and long-lasting approaches.

In Chapter Three of this thesis, I show that terminally differentiated splenic DCs express and regulate Flt3. Differential expression of Flt3 is observed between different DC subsets and activation states. Furthermore, I demonstrate changes to the biology of DCs when they express Flt3-internal tandem duplication (ITD) – the most common mutation observed in acute myeloid leukemia (6). Mice expressing Flt3-ITD have expanded numbers of splenic DCs with altered cell surface phenotype including increased MHC expression. Overall, we found the mutation does not impact cross-presentation, however, it does significantly improve MHC II antigen presentation, with consequences for DC function and T cell immunity.

In Chapter Four, I further interrogated the Flt3 pathway by investigating the genetic machinery that regulates Flt3 in DCs. Using CRISPR/Cas9 genome-wide screens, I identified several novel regulators of Flt3. These included *Mediator 25 (Med25)*, which encodes a subunit of the Mediator complex, and *Ubiquitin-specific peptidase 22 (USP22)*, which encodes a subunit of the Spt-Ada-Gcn5 Acetyltransferase (SAGA) complex. Both genes have undescribed roles in DCs however my findings suggest they promote and repress the transcription of *Flt3*, respectively.

In Chapter Five, I tackled DC manipulation from another angle by investigating the impact of MHC II ubiquitination on DC function and immunity. I found MHC II ubiquitination controls DC numbers and function, with mice lacking MHC II ubiquitination (*MHC IIKR*$^{KI/KI}$) having a reduced number of DCs with altered cell surface phenotype, antigen proteolysis and cytokine secretion. These changes ultimately lead to impaired immunity, with reduced *in vivo* T cell priming, cytotoxic T cell and humoral responses observed.

In summary, I have broadened the understanding of DC biology by comprehensively studying pathways which promote the generation and function of these unique immune cells. As a result, this thesis will assist in the design of vaccines which exploit DCs for improved immunity.

# Declaration

This is to certify that

I. This thesis comprises only my original work towards the PhD except where indicated in the Preface.

II. Due acknowledgements have been made in the text to all other materials used.

III. This thesis is less than 100,000 words in length, exclusive of tables, bibliographies, and appendices.

Kayla Roberta Wilson

October 2021

# Preface

This work was conducted in the laboratories of Associate Professor Justine D. Mintern and Professor Jose A. Villadangos at the University of Melbourne. The work was funded by the grants from the National Health and Medical Research Council and Australian Research Council. My studies were supported by The Australia Government Research Training Program (RTP) Scholarship.

The contribution of others is acknowledged below, with the proportion of original work by the Author indicated:

**Introduction:** A proportion of the introduction is from a review published in *Immunology and Cell Biology*. The specific contributions from the named authors are listed in the section below "Publications arising from this thesis".
Proportion of original work by the Author: 90%.

**Chapter 3:** This study is a manuscript in progress. The specific contributions from the named authors are listed in the section below "Publications arising from this thesis". In addition, cell sorting was carried out by Dr. Matt Burton, Dr. Eleanor Jones, and Dr. Paul Lau (Murdoch Children's Research Institute, MCRI). Proportion of original work by the Author: 98%.

**Chapter 4:** The introduction to Chapter 3 is from a review published in *Immunology and Cell Biology.* The specific contributions from the named authors are listed in the section

below “Publications arising from this thesis”. In addition, Dr. Stephen Wilcox from the Genomics Hub performed the Illumina Sequencing and Dr. Shani Amarasignhe performed the EdgeR analysis of the CRISPR/Cas9 genome-wide screens utilized in this chapter. Cell sorting was carried out by Dr. Matt Burton, Dr. Eleanor Jones, and Dr. Paul Lau (MCRI). Proportion of original work by the Author: 90%.

**Chapter 5:** This study was a collaborative work published in the *Journal of Immunology* (see below). The specific contributions from all the named authors are listed below. Proportion of original work by the Author: 70%.

# Publications arising from this thesis

Wilson KR, Villadangos JA, Mintern JD (2021) Dendritic cell Flt3 – regulation, roles and repercussions for immunotherapy. *Immunology and Cell Biology*. 99(9):962-921. (**Chapter 1, Chapter 4**)

Contributions: KR Wilson: Conceived the study, prepared the figures, drafted the manuscript and edited the manuscript. JA Villadangos: Conceived the study, edited the manuscript, supervision and funding acquisition. JD Mintern: Conceived the study, edited the manuscript, supervision and funding acquisition.

Wilson KR, Villadangos JA, Mintern JD (2021) The impact of Flt3-ITD mutation on dendritic cell function. *Manuscript prepared for publication* (**Chapter 3**)

Contributions: KR Wilson: Conceived the study, designed, performed and analyzed all experiments, prepared the figures, drafted the manuscript and edited the manuscript. JA Villadangos: Conceived the study, edited the manuscript, supervision and funding acquisition. JD Mintern: Conceived the study, edited the manuscript, supervision and funding acquisition

Wilson KR, Jenika D, Blum AB, Macri C, Xu B, Liu H, Schriek P, Schienstock D, Francis L, Makota FV, Ishido S, Mueller S, Lahoud MH, Caminschi I, Edgington-Mitchell L.E, Villadangos JA, Mintern JD (2021) MHC II ubiquitination regulates dendritic cell function and immunity. *The Journal of Immunology*. 207:1-10. (**Chapter 5**)

Contributions: KR Wilson: Conceived the study, designed and analyzed the majority of FACS experiments, prepared the figures, drafted the manuscript and edited the manuscript. In addition, the following experiments were carried out by KR Wilson: Quantification of splenic immune cell subsets, cell surface phenotyping, OVA-Cy5 internalization, DQ-BSA antigen proteolysis, pHrodo fluorescence, cytokine secretion, *ex vivo* antigen presentation assays, *in vitro* antigen presentation assays, Tfh induction and antibody production assays. D Jenika: Performed the cytotoxic T lymphocyte assays and the T cell characterization assays. AB Blum: Performed the *in vivo* antigen presentation assays and preliminary uptake experiments. C Macri: Performed the *in vivo* antigen presentation assays and proteolysis assays. B Xu: Performed the protease activity assay and cystatin C immunoblots. H Liu: Conceived the study, performed DC numbers and antibody response experiments. P Schriek: Performed DC numbers and cell surface phenotype experiments. D Schienstock: performed preliminary microscopy experiments. L Francis: Performed DC numbers experiments. FV Makota: Performed the *in vivo* antigen presentation assays. S Ishido: generated the *MHC IIKR*$^{KI/KI}$ mice. S Mueller: provided resources and critical review. MH Lahoud: provided resources and critical review. I Caminschi: provided resources and critical review. L.E Edgington-Mitchell: provided resources and critical review. JA Villadangos: Conceived the study, edited the manuscript, supervision and funding acquisition. JD Mintern: Conceived the study, edited the manuscript, supervision and funding acquisition.

# Evidence of Research Output

## Publications

Wilson KR, Liu H, Healey G, Vuong,V, Ishido S, Herold, MJ, Villadangos JA,Mintern, JD (2018) MARCH1-mediated ubiquitination of MHC II impacts the MHC I antigen presentation pathway. *PLoS One*. 13, 1–16

Liu H, Wilson KR, Schriek P, Macri C, Blum AB, Francis L, Heinlein M, Nataraja C, Harris J, Jones SA, Gray DHD, Villadangos JA, Mintern JD, (2020) Ubiquitination of MHC II is required for the development of regulatory but not conventional $CD4^+$ T cells. *The Journal of Immunology.* 5, 1207–1216

Wilson KR, Villadangos JA, Mintern JD (2021) Dendritic cell Flt3 – regulation, roles and repercussions for immunotherapy. *Immunology and Cell Biology.* 99(9):962-921

Wilson KR, Jenika D, Blum AB, Macri C, Xu B, Liu H, Schriek P, Schienstock D, Francis L, Makota FV, Ishido S, Mueller S, Lahoud MH, Caminschi I, Edgington-Mitchell L.E, Villadangos JA, Mintern JD (2021) MHC II ubiquitination regulates dendritic cell function and immunity. *The Journal of Immunology*. 207:1-10.

Schriek P, Liu H, Ching AC, Huang P, Gupta N, Wilson KR, Tsai MH, Yan Y, Macri C, Dagley LF, Infusini G, Webb AI, McWilliam HEG, Ishido S, Mintern JD, Villadangos JA. (2021) Physiological Substrates and Ontogeny-Specific Expression of

the Ubiquitin Ligases MARCH1 and MARCH8. *Current Research in Immunology*. (Accepted for publication).

Liu H, Wilson KR, Firth A, Macri C, Schriek P, Blum AB, Villar J, Wormald S, Shambrook M, Xu B, Lim HJ, McWilliam HEG, Hill AF, Edgington-Mitchell LE, Caminischi I, Lahoud M, Segura E, Herold M, Villadangos JA, Mintern JD. (2021) Ubiquitin-like protein 3 (UBL3) is required for MARCH ubiquitination of major histocompatibility complex class II and CD86 in mouse and human antigen presenting cells. (Submitted for publication)

## Conferences

2018

- The AVID Meeting 2018 – Poster presentation
- ASMR VIC Student Symposium – ten-minute oral presentation
- University of Melbourne Biochemistry and Molecular Biology Graduate Retreat – five-minute oral presentation
- ASI IgV Annual Scientific Meeting – Poster presentation
- VIIN Young Investigators Symposium – Poster presentation
- Peter Doherty Institute work in progress seminar – fifteen-minute oral presentation

2019

- Lorne Infection and Immunology – Poster presentation
- ASMR VIC Student Symposium – three-minute oral presentation

- University of Melbourne Biochemistry and Molecular Biology Graduate Retreat – ten-minute oral presentation
- VIIN Young Investigators Symposium – Poster presentation
- University of Melbourne Biochemistry and Molecular Biology Data Club – ten-minute presentation

2020

- Lorne Infection and Immunology – Poster presentation
- University of Melbourne Biochemistry and Molecular Biology Graduate Retreat – ten-minute oral presentation
- ASI IgV Annual Scientific Meeting – three-minute oral presentation
- University of Melbourne MDHS Graduate Research Conference – fifteen-minute oral presentation

# Acknowledgements

Over the last four years, I have had the opportunity to wholeheartedly throw myself into this Doctor of Philosophy – a feat that has been as exciting as it has been challenging. Attaining this level of education is a massive privilege that would not be possible without the mentorship and support of numerous individuals.

First and foremost, acknowledgement must be made to my PhD supervisors, Justine Mintern and Jose Villadangos. Justine, thanks for being a great supervisor! You have continuously pushed me to do better and have given me ample opportunity to do so. Thank you for always laughing with me when things didn't go as planned and for giving me just-the-right amount of support and freedom to confidently explore and learn. Jose, thank you for your support and patience over the years. I appreciate all the feedback, knowledge, and enthusiasm you provided me during our "FtF" meetings.

To my PhD committee, Ian van Driel, Katrina Binger, Meredith O'Keeffe and Sammy Bedoui, thank you for giving me a safe space to present and discuss my data. You provided a wealth of knowledge that helped shape this thesis.

Thank you to the WEHI genomics hub, particularly Stephen Wilcox and Shani Amarasinghe, for assistance with the library data and analysis. Thank you to Bangyan Xu for assistance with the protease analysis (and the many laughs during our long, cold DC preps).

Thank you to the Bio21 animal facility, especially Sam, Shasta, Charlotte, Lee, Carlos, and Max who were always happy to help with animal experiments.

Thanks must also go the past and present members of the Mintern and Villadangos labs who provided a fun place to work and learn. Specifically, thank you to Jo for keeping our lab running smoothly and always being up for some fun. Christophe, thank you for all the knowledge you passed onto me, but more importantly, thank you for always laughing at/with me when everything went wrong/on fire. Haiyin and Nishma, words cannot describe how much your mentorship and friendship means to me. I appreciate all the advice, laughs, and snacks we have shared over the years.

One of the best things I have gained from this doctorate is a crazy group of friends – Erin, Annabelle (and Michael), Beth, Yoon Hee and Emily. We have laughed, and occasionally cried, our way through these PhD years. I am so happy I experienced this with you and am so proud of what we have achieved.

To my mom, Gav, Ty and Trav – we did it! Dankie for all the sacrifices you have made and continue to make for me. Please know this thesis is largely due to all the red wine you have supplied and your unwavering belief in me. To my fiancé, James, and our cat, Cheddar, you are the best (around). I appreciate all the love, support, and patience you have given me, especially when my priorities were out of whack. I love you.

# Table of Contents

# List of Abbreviations

| | |
|---|---|
| ACT | adoptive T cell transfer |
| ADAM10 | a disintegrin and metalloproteinase 10 |
| ADAM17 | a disintegrin and metalloproteinase 17 |
| AITD | autoimmune thyroid disease |
| APC | antigen presenting cells |
| BMDC | bone marrow-derived DC |
| BSS | balanced salt solution |
| Btk | Bruton's tyrosine kinase |
| CAR | chimeric antigen receptor |
| cDC | conventional dendritic cell |
| CIITA | class II major histocompatibility transactivator |
| CLIP | class II associated invariant chain peptide |
| DAPI | diamidino phenylindole |
| DC | dendritic cell |
| Dox | Doxycycline |
| DUB | deubiquitinating enzyme |
| ERK | extracellular signal-related kinase |
| Flt3 | FMS-like tyrosine kinase 3 |
| Flt3L | FMS-like tyrosine kinase 3 ligand |
| G-CSF | granulocyte colony-stimulating factor |
| GeCKO | Genome-scale CRISPR Knock-Out |
| GM-CSF | granulocyte macrophage colony stimulating factor |
| gMFI | geometric mean fluorescence intensity |
| GVHD | graft-versus-host-disease |
| HLA | Human leukocyte antigen |
| ICE | Inference of CRISPR Edits |
| Ii | In |
| IL | interleukin |
| ILV | Intraluminal vesicle |

| | |
|---|---|
| InDels | insertions and deletions |
| ITD | internal tandem duplication |
| LN | lymph node |
| LPS | lipopolysaccharide |
| M-CSFR | macrophage colony-stimulating factor receptor |
| MARCH | membrane-associated RING-CH |
| MCS-F | macrophage colony-stimulating factor |
| MEP | megakaryocyte erythrocyte progenitor |
| MHC | major histocompatibility complex |
| MHC I | major histocompatibility complex class I |
| MHC II | major histocompatibility complex class II |
| MIIC | major histocompatibility complex class II compartment |
| MVB | multivesicular body |
| NEM | N-ethylmaleimide |
| NK | natural killer |
| OVA | ovalbumin |
| PAMP | pathogen associated molecular pattern |
| PD-1 | programmed cell death-1 |
| pDC | plasmacytoid dendritic cell |
| PDGFR | platelet-derived growth factor receptor |
| PI3K | phosphatidylinositol 3 kinase |
| pMHC II | peptide loaded major histocompatibility complex II |
| poly I:C | Polyinosinic:polycytidylic acid |
| PRR | pattern recognition receptor |
| PTEN | phosphatase and tensin homolog |
| RA | rheumatoid arthritis |
| RBR | RING between RING |
| RCRB | red cell removal buffer |
| RING | really interesting new gene |
| S6K | S6 kinase beta-1 |
| SCFR | mast/stem cell growth factor receptor |
| SHC | SHC adaptor protein 1 |

| | |
|---|---|
| STAT3 | signal transducers and activators of transcription 3 |
| TCR | T cell receptor |
| TID | tumor-infiltrating dendritic cells |
| TLR | toll-like receptor |
| TM | transmembrane |
| TNFα | tumor necrosis factor α |
| Treg | regulatory T cell |

# List of Figures

# List of Tables

# Chapter 1 - Introduction

Sections of this chapter were published in Immunology & Cell Biology (2021). The specific contributions of authors are disclosed in the "Preface" and "Publications arising from this thesis" sections of this thesis. The published manuscript can be found in Appendix 1.

# Introduction

An exciting advance to immunotherapy against infection, cancer and autoimmunity is to exploit the biology of dendritic cells (DCs) (7). DCs are unrivalled in their ability to acquire, process and present antigenic peptide to T cells. Discovered in 1973 (8), they are a functionally and phenotypically heterogenous population of cells that are widely distributed throughout the body. Under steady state conditions, DCs are well-equipped at acquiring and processing antigen but poor at inducing immunity. Interactions between immature DCs and naïve T cells can lead to tolerance, are important in shaping T cell development in the thymus and maintaining T cell populations in the peripheral lymphoid organs. Upon encounter with inflammatory stimuli DCs undergo maturation. Inflammatory stimuli include pathogen associated molecular patterns (PAMPs) which are recognized by pattern recognition receptors (PRRs) on DCs in addition to inflammatory cytokines (9). Mature DCs have elevated major histocompatibility complex (MHC), costimulatory molecules and inflammatory cytokines and migrate to T cell zones of secondary lymphoid organs where they can initiate immune responses. DC interaction with T cells can be a double-edged sword, with DCs capable of not only initiating immune responses against non-self but also initiating autoimmunity.

To manipulate DCs in clinical settings, it is important to understand the major signaling cascade that generates these cells, FMS-like tyrosine kinase 3 (Flt3)/Flt3 ligand (Flt3L), and the proteins responsible for antigen presentation, MHC molecules.

## 1.1 FMS-like tyrosine kinase 3

### FMS-like tyrosine kinase 3 (Flt3) receptor

The *Flt3* gene encodes a type III receptor tyrosine kinase in the same family as macrophage colony-stimulating factor (M-CSF) receptor (M-CSFR), mast/stem cell growth factor receptor (SCFR/c-KIT/CD117) and platelet-derived growth factor receptors A and B (PDGFR-A and -B). These receptors share a similar structure with five extracellular immunoglobulin-like domains, one transmembrane domain, one juxtamembrane domain and two tyrosine kinase domains (**Figure 1.1**). Flt3 expression is restricted to hematopoietic stem cells and DCs (10).

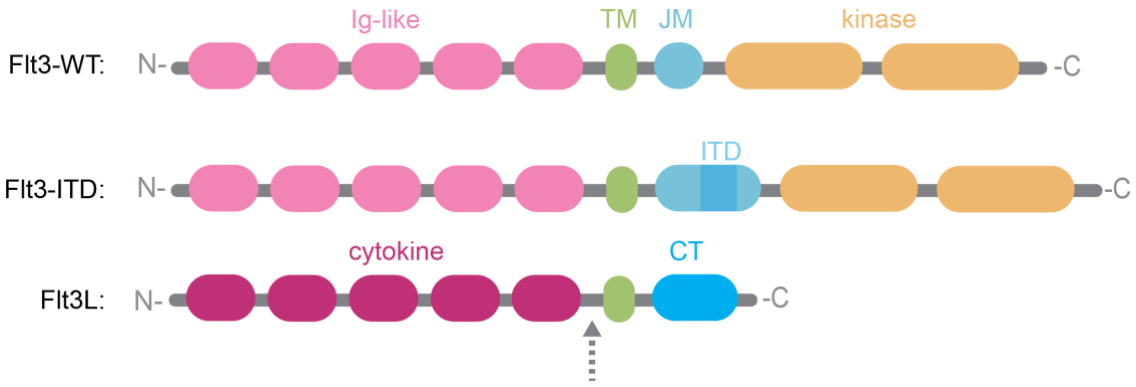


**Figure 1. The structure of Flt3 and Flt3L**. Flt3 comprises five extracellular immunoglobulin (Ig)-like domains at the N-terminus. These are followed by one transmembrane (TM) domain and a juxtamembrane (JM) domain. The C-terminus comprises 2 tyrosine kinase domains. The most common mutation in the *Flt3* gene is the internal tandem duplication (ITD), where an in-frame duplication of exons 14 and 15

is present in the JM domain. Membrane-bound Flt3L comprises 5 extracellular domains, one TM domain and one cytosolic tail (CT). Arrow indicates cleavage site to form soluble Flt3L.Figure from (11).

## Flt3 ligand (Flt3L)

The ligand for Flt3 is Flt3 ligand (Flt3L), a type I transmembrane protein in the same family as the ligands for SCFR and M-CSFR. It comprises five extracellular domains, a transmembrane domain and a cytosolic tail (**Figure 1**). There are three main isoforms of Flt3L. The first isoform, found in both humans (12, 13) and mice (14), is cleavable membrane-bound Flt3L which can form soluble Flt3L. Flt3L can also be generated as a soluble protein which lacks a membrane anchor (12–14). This occurs due to an early stop-codon which is introduced into Flt3L due to exon skipping. The last isoform is membrane-tethered and cannot be cleaved (15). Like soluble Flt3L, membrane-tethered Flt3L occurs due to alternative splicing and results in a protein that lacks the cleavage site. While all forms are biologically active, the abundance of each differs between species. In humans, the most common form is the cleavable membrane-bound Flt3L (15), whereas in mice the most common form is the membrane-tethered Flt3L (13, 15). It is currently unclear whether the different isoforms perform different functions.

In contrast to the Flt3 receptor, Flt3L mRNA is expressed by most hematopoietic and non-hematopoietic tissues (13, 14). Even so, in healthy individuals serum Flt3L levels are low (16). The non-hematopoietic sources have not been studied extensively; however, for the hematopoietic source it has been shown that T cells secrete Flt3L (17).When lethally irradiated *Flt3L*$^{-/-}$ mice are reconstituted with bone marrow from mice lacking T cells (*CD3ε*$^{-/-}$) there is a significant reduction in serum Flt3L in comparison to *Flt3L*$^{-/-}$ mice

reconstituted with wild type bone marrow (17). In particular, $CD4^+$ T cells were found to secrete higher amounts of Flt3L than $CD8^+$ T cells when stimulated *ex vivo* with anti-CD3ε and anti-CD28 antibodies (17). In T cells, Flt3L is stored intracellularly and colocalizes with Golgi-resident proteins (16, 18). Trafficking to the cell surface can be induced by cytokines which signal through the common γ receptor chain though the mechanism involved is unclear (18). The metalloprotease TNFα converting enzyme (TACE/ADAM17) cleaves membrane-bound Flt3L to soluble Flt3L (19).

Recently, there has been evidence of additional hematopoietic sources of Flt3L during steady-state conditions. Whilst not as highly expressed as in T cells, *Flt3L* is detected in conventional DC (cDC) subset 2 (cDC2) with low levels of soluble Flt3L detected in primary murine cDC2 cultures. The metalloprotease responsible for cleaving cDC2 Flt3L is a disintegrin and metalloproteinase 10 (ADAM10) (20). Mice lacking ADAM10 specifically in DCs have increased surface cDC2 Flt3L, reduced serum Flt3L and significantly reduced splenic cDC2 (defined as $CD11b^+$ $CD4^+$ $ESAM^+$) (20). This is the first paper to provide evidence for differential roles of Flt3L isoforms, with cleaved soluble Flt3L, not membrane-bound or tethered, required for the development and maintenance of $ESAM^+$ cDC2. It is currently unclear why splenic cDC2 preferentially require soluble Flt3L, though it has been suggested this improves accessibility of the ligand (20).

**Flt3/Flt3L signaling**

Once activated, Flt3 signals via mitogen-activated protein kinase (MAPK), phosphatidylinositol 3 kinase (PI3K) and signal transducers and activators of

transcription 3 (STAT3) pathways (**Figure 2**). Flt3 signaling is also implicated in the indirect regulation of other signaling pathways given that in the absence of Flt3, DCs and their progenitors are more responsive to other growth factors (such as M-CSF and stem cell factor) and can activate additional pathways (21).

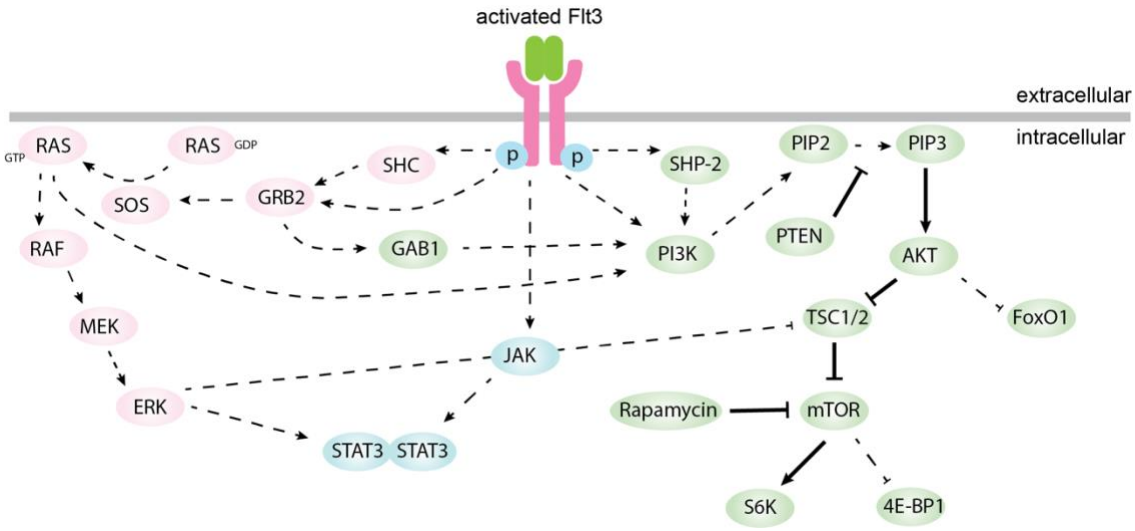


**Figure 2. Signaling pathways induced by activated Flt3.** Flt3 signals through 3 pathways –MAPK (pink), STAT3 (blue) and PI3K (green). Dashed arrows indicate pathways that have only been demonstrated using transformed cell lines (not DCs) whereas solid lines indicate pathways confirmed in DCs or DC progenitors. Figure from (11).

The MAPK pathway is implicated in Flt3 signaling in different cell lines overexpressing wild type Flt3. Once stimulated with Flt3L, increased activation of SHC adaptor protein 1 (SHC) and extracellular signal-related kinase (ERK)1/2 is observed (22). While this likely occurs in DCs, it has yet to be shown. The PI3K pathway is also implicated in Flt3 signaling. Flt3-mediated PI3K activation has been demonstrated in DCs (23). Indeed, *in vivo* administration of Flt3L leads to increased phosphorylation of ribosomal protein S6 kinase beta-1 (S6K) in splenic cDCs. Congruent to this, global or DC-specific deletion of phosphatase and tensin homolog (PTEN), an inhibitor of AKT and downstream of PI3K

signaling, leads to an increase in the number of DCs suggesting an important role of Flt3L-induced PI3K signaling in DC regulation (23). Finally, activation of STAT3 is critical for DC development and occurs following Flt3L stimulation (24). Consequently, mice lacking STAT3 in hematopoietic cells have fewer DCs which cannot be rescued by Flt3L treatment (24). Similarly, forced expression of STAT3 leads to increased DC developmental potential (1).

**Flt3 and DC development**

Single cell analysis has revealed the development of terminally differentiated DCs is a continuous process whereby progenitor cells progressively differentiate (25). DC development is dependent on Flt3/Flt3L signaling. As such, all cells that differentiate into cDCs and pDCs express Flt3 (4, 26). Surface expression of Flt3 differs, with the highest expression observed for splenic cDC1 and the lowest for pre-cDC1 and pre-cDC2 (27). It should be noted that not all DCs rely on Flt3. Indeed, Langerhans cells, an epidermal-resident DC, are unaffected by loss of Flt3 signaling (28), indicating their establishment and maintenance is Flt3-independent. The critical role of Flt3 in cDC and pDC development has been reinforced by studies overexpressing Flt3 (1). Onai and colleagues showed $Flt3^-$ hematopoietic progenitors, such as the megakaryocyte erythrocyte progenitor, MEP, cannot produce cDC or pDC irrespective of Flt3L stimulation. However, upon *Flt3* introduction, these progenitors can give rise to cDC and pDC (1). Further to this, lethally irradiated mice have reduced cDCs and pDCs following reconstitution with $Flt3L^{-/-}$ bone marrow. Similarly, lethally irradiated $Flt3L^{-/-}$ mice reconstituted with wild type bone marrow have reduced cDCs and pDCs (17). This not only demonstrates the importance of Flt3 signaling in DC development but also highlights

the importance of hematopoietic sources of Flt3L, particularly $CD4^+$ T cells. Further evidence of the critical role of Flt3 in haematopoietic development comes from studies showing an increase in DC and progenitor number when Flt3L is administered to mice (2–4) or humans (29). Other growth factors, such as granulocyte colony-stimulating factor (G-CSF) increase DC numbers however they are incapable of expanding DCs to the same extent as Flt3L (2). Although increased cellularity is not observed in the bone marrow of Flt3L treated mice, there is an increase in the number of B cell and DC precursors and their mobilization (3). In support of this, when Flt3L-treated and untreated splenocytes are depleted of cDCs and transferred into irradiated recipients there is an increase in DCs originating from Flt3L-treated splenocytes (3). This is indicative of increased DC progenitors in Flt3L-treated spleens.

A greater understanding of Flt3 signaling on hematopoiesis has been gained from mice lacking *Flt3* (*Flt3*$^{-/-}$) (30) or *Flt3L* (*Flt3L*$^{-/-}$) (31). Initially *Flt3*$^{-/-}$ mice were described to have no changes in cellularity except for reduced bone marrow B cell progenitors (30). However, more recent analysis using complex multicolor immunophenotyping has revealed additional decreases in lymphoid (3) and nonlymphoid (28) DCs. A similar, albeit more severe, phenotype is observed in *Flt3L*$^{-/-}$ mice. Mice lacking *Flt3L*$^{-/-}$ have reduced DC progenitors (31). In addition, significant reductions in lymphoid (3, 21, 31) and non-lymphoid DCs (28) are observed. *Flt3L*$^{-/-}$ mice also have reduced natural killer (NK) cells (31). This indicates Flt3 signaling regulates early progenitor cells involved in the differentiation of several lineages. In competitive bone marrow transplantation experiments *Flt3*$^{-/-}$ bone marrow cells are unable to reconstitute DCs (3) and other lineages (3, 30) to the same extent as wild type bone marrow. In addition, by assessing

bromodeoxyuridine (BrdU) incorporation into *Flt3*$^{-/-}$ and wild type splenic DCs, Waskow *et al*. demonstrated that *Flt3*$^{-/-}$ DCs in the periphery are unable to proliferate to the same extent as their wild type counterparts (3). Therefore, Flt3 signaling regulates not only the differentiation and mobilization of progenitor DCs, but also plays a role in the homeostatic division of cDCs in peripheral lymphoid organs. More recent analysis suggests that while the earlier stages of cDC1 development require Flt3 signaling, the final stage is independent of this pathway (27). Similar proportions of cDC1 are generated when purified splenic pre-cDCs (CD11c$^{+}$ MHC II$^{int}$ Flt3+ SiRP$\alpha^{int}$) were cultured *in vitro* with feeder cells with and without Flt3L. This contrasts with cDC2, that are significantly reduced in the absence of Flt3L (27). This is surprising given cDC1 express higher Flt3 than cDC2 (27), and suggests Flt3 may play other important roles in cDC1.

**Flt3 and immune responses**

Flt3-mediated DC homeostasis is important for regulating normal immune responses, mainly due to its indirect effect on T cell homeostasis. DC numbers highly correlate with regulatory T cell (Treg) numbers. Flt3L administration increases Tregs and Flt3 depletion reduces Tregs (32, 33). This relationship is observed in humans, with Flt3L treatment causing significant expansion of Tregs (34). Alterations to T cell compartments are independent of thymic Treg production as Flt3L administration increases splenic Tregs in thymectomized mice (32). DCs regulate Treg proliferation in the periphery (32–34) . Given the relationship between DCs and Tregs, aberrant DC Flt3 signaling may alter immunosurveillance in cancer (35).

Serum Flt3L levels, and as a result DC and T cell numbers, vary during different disease states. Dramatic increases in serum Flt3L are often observed in conditions of decreased progenitors, for example patients undergoing high-dose chemotherapy (16). Increased Flt3L is also evident at inflammation sites, such as following *Plasmodium* infection (36). While $CD4^+$ T cells and cDC2 may be responsible for steady-state levels of Flt3L, this may not be the case in the presence of reduced hematopoietic progenitors, inflammation, or infection. Indeed, mast cells, not $CD4^+$ T cells, are a major source of Flt3L during *Plasmodium* infection (36). Similarly, in cancer, natural killer (NK) cells produce Flt3L at the tumor site (5). Increases in Flt3L during infection and cancer play important protective roles by expanding DCs capable of presenting exogenous antigen by MHC I (cross-presenting cDC1) and improving $CD8^+$ T cell responses.

**Exploiting Flt3/Flt3L signaling in immunotherapy and vaccination**

There is significant interest in exploiting DCs in tumor immunotherapy. This is because of their excellent ability to capture and present antigen, in addition to trafficking to T cell zones. Unfortunately, harnessing the power of DCs has proved difficult due to their rare number in healthy and malignant tissues. Indeed, assessment of tumor infiltrating immune cells shows DCs to be the rarest cell type (37, 38). Whilst the number of tumor infiltrating DCs (TIDs) may be small, the role they play in tumor clearance is anything but. Cross-presenting cDC1 ($CD141^+$/$BDCA3^+$ in humans and $CD103^+$ in mice) are essential in solid tumor clearance. Mice lacking cross-presenting DCs (*Batf3*$^{-/-}$) have decreased $CD8^+$ T cell recruitment and increased tumor burden following tumor inoculation (38, 39). Similarly, high expression of $BDCA3^+$-related gene expression in melanoma correlates with increased overall patient survival (5). This dramatic phenotype is due to an increase

in $CD8^+$ T cell activation and infiltration (39). Indeed, while a number of tumor-infiltrating immune cells, such as macrophages, can capture tumor-associated antigen, only cross-presenting TIDs are able to traffic to, and activate, $CD8^+$ T cells in the tumor and at tumor draining lymph nodes (37, 38). The normal number of TIDs is reliant on Flt3L production by NK cells, with a decrease in cross-presenting TIDs in mice lacking NK cells (36). In agreement with this, the number of NK cells correlates with *Flt3L* gene expression and $BDCA3^+$ DC numbers in human melanoma (36).

The Flt3/Flt3L signaling cascade is being targeted to manipulate the number of cross-presenting TIDs to improve anti-tumor immune responses. Administration of Flt3L to mice and humans significantly expands cross-presenting TIDs and their progenitors (37, 38, 40, 41). This promotes anti-tumor immunity in mice with solid tumors (41, 42). Improved outcomes occur when Flt3L is used together with a stimulatory agent and checkpoint inhibitors. Mice treated with Flt3L in combination with poly I:C (TLR3 agonist), mAb specific for programmed cell death-1 (PD-1) with and without irradiation have significantly reduced primary and secondary tumor growth and increased survival (37, 40, 43). This phenotype is reliant on cross-presenting $CD103^+$ DC and $CD8^+$ T cells (37, 40). The former is essential for anti-PD-1 therapy (43). Including Flt3L in combination therapy appears promising in clinical trials, with increased tumor regression in B cell lymphoma patients treated with Flt3L, irradiation and poly I:C (40).

Adoptive T cell transfer (ACT) is an immunotherapy where patients are infused with T cells that are expanded *in vitro*. Importantly, these T cells can be genetically modified to improve their anti-cancer efficacy. For example, chimeric antigen receptor (CAR) T cells

are engineered to express receptors specific for tumor antigens. In mice reconstituted with *Batf3*$^{-/-}$ bone marrow, adoptively transferred T cells were unable to migrate to the tumor site (39). However, once reconstituted with activated DCs, this phenotype was rescued (39). It is therefore possible that Flt3L, in combination with a TLR agonist, could potentiate ACT. Indeed, increased proliferation of adoptively transferred OT-I cells occurs in B16-OVA bearing mice treated with Flt3L and poly I:C (37). CAR T cells have been engineered to express and secrete Flt3L (41). Lai and colleagues demonstrate Flt3L-CAR T cells improve tumor clearance, especially in combination with poly I:C and anti-4-1BB (CD137) . This is dependent on cDC1, with no significant reduction in tumor size observed in *Batf3*$^{-/-}$ mice. Importantly, Flt3L-CAR T cell therapy increases the host anti-tumor response with an increase in endogenous DC and T cells (41). In addition, improved host TCR diversity is observed. As a result, when mice are rechallenged with tumors lacking antigen, anti-tumor responses are improved.

Flt3/Flt3L signaling has been exploited for vaccines against infection. Incorporation of Flt3L into vaccines against infectious agents can enhance immunity by increasing DC numbers and infiltration. Following subcutaneous immunization with DC-targeted antigen there is an increase in serum Flt3L alongside alterations in DC composition in skin-draining LNs (44). Mice treated with Flt3L during immunization display increased antigen uptake, and upon antigen recall, improved $CD4^+$ T cell interferon gamma (IFNγ) production, $CD4^+$ T cell expansion and increased serum IgG. In addition, Flt3L treatment expands $CD8^-$ $CD24^+$ precursors of cDC1 (45). Mice vaccinated with these DC precursors prior to viral infection have increased specific memory T cell expansion and decreased viral load in comparison to mice vaccinated with cDC1 (45). During early stages of

influenza A virus infection, there is a decrease in Flt3L and cDCs, impacting immune outcomes (46). By treating mice with a Flt3L-encoding plasmid prior to infecting with influenza, Beshara and colleagues exploited the Flt3/Flt3L signaling pathway and effectively increased the number of DC progenitors and lung DCs, in addition to reducing the number of tissue-damaging inflammatory monocytes. This strategy protected mice against secondary bacterial infections (46).

**Flt3 and autoimmunity**

While increased Flt3/Flt3L signaling may be desirable during infection and cancer, a genome-wide association study of more than 30,000 autoimmune thyroid disease (AITD) cases highlights this pathway can also elicit autoimmune disease (47). Saevarsdottir and colleagues identified an intron variant of Flt3 impacting AITD, systemic lupus, rheumatoid arthritis (RA) and coeliac disease risk (47). The intron variant has a premature stop codon predicted to generate a truncated non-functional protein. The reduction in Flt3 correlates with increased serum Flt3L and expansion of myeloid cells, indicative of a positive feedback loop between Flt3 receptor and ligand (47). This is the first study to detail a germline mutation in *Flt3* leading to increased risk of autoimmunity. Increased Flt3L is a well-established hallmark of autoimmunity. Indeed, RA patients not only exhibit increased serum Flt3L but also significantly increased Flt3L in the synovial fluid of their joints, where most inflammation and tissue damage is observed (48). It is hypothesized that increased Flt3L exacerbates autoimmunity in RA. In support of this, increased arthritis pathogenesis is observed in mice administered with Flt3L (48).

In contrast, Flt3/Flt3L signaling can dampen autoimmunity via expansion of Tregs. Flt3L pre-treatment prevents death due to graft-versus-host-disease (GVHD) and protects mice against type 1 diabetes and inflammatory bowel disease (32, 33). In part this is due to increased cDC1s with protection lost when Tregs are depleted (33). Unsurprisingly, the relationship between Tregs and DCs is also observed in mice harboring Flt3-ITD mutations, with progressively increased Tregs in $Flt3^{ITD/+}$ and $Flt3^{ITD/ITD}$ mice (35). Indeed, when Tregs are selectively depleted with diphtheria toxin in $Flt3^{ITD/+}FoxP3^{DTR\text{-}GFP}$ or $Flt3^{+/+}FoxP3^{DTR\text{-}GFP}$ mice, there was faster reconstitution of Tregs in $Flt3^{ITD/+}$ mice (35).

## 1.2 Major histocompatibility complex class II (MHC II)

Besides manipulating the number of DC, immune outcomes can be controlled by manipulating antigen presentation. Classically, presentation of cytosolic-derived antigen occurs on MHC class I (MHC I) to $CD8^+$ T cells whereas presentation of exogenous antigen occurs on MHC class II (MHC II) to $CD4^+$ T cells.

Presentation of antigen to T cells is critical for the activation of immune responses. In addition, it plays important roles in T cell selection in the thymus – a process termed "central tolerance" (reviewed in (49)). According to the affinity model of thymocyte selection, the development of T cells from thymocytes is dependent on the interaction between TCR and peptide-loaded MHC. To survive, thymocytes require weak interactions between TCR and peptide-loaded MHC (positive selection). Interactions that are too strong lead to apoptosis-induced death (negative selection) or Treg differentiation.

Notably, MHC expression on DCs, in addition to thymic epithelial cells, is critical to this process (reviewed in (50)). MHC II expression in peripheral lymphoid organs is also important for the maintenance of peripheral tolerance (50). Indeed, antigen presentation by immature DCs to T cells in the absence of inflammation can promote T cell anergy or deletion.

MHC II can also act as a signaling receptor (reviewed in (51)). Once engaged, MHC II activates a diverse range of signaling pathways which can promote proliferation, apoptosis, and cytokine production. In fact, it has been shown that intracellular MHC II in macrophages and BMDCs interacts with Bruton's tyrosine kinase (Btk) to form a signaling platform which includes MyD88 and TRIF (52). This interaction is mediated through CD40 and allows for TLR signaling. As such, cells lacking MHC II produce less proinflammatory cytokines following TLR stimulation (52).

**MHC II trafficking**

MHC II is comprised of two glycoproteins, α and β chain, which are non-covalently bound (53, 54). In humans, there are three isoforms of MHC II: HLA-DM, -DQ and -DR. In mice there are two isoforms of MHC II known as H2-A and H2-E. In addition to the classical MHC II molecules, there are non-classical molecules which assist in trafficking MHC II. These include HLA-DM and HLA-DO (known as H2-M and H2-O in mice). Expression of classical and non-classical MHC II, in addition to invariant chain (Ii) is under the control of Class II major Histocompatibility Complex Transactivator (CIITA, encoded by *MHC2TA*). Since CIITA does not bind to DNA directly, it requires other genes to promote MHC II transcription. These include regulatory factor (RF) X5 (RFX5),

RF X associated protein (RFXAP) and RF X associated ankyrin containing protein (RFXANK) which form a complex upstream of MHC II. Once bound, these proteins recruit cAMP-response element binding protein (CREB) and nuclear transcription factor Y subunit alpha (NFY). Together, this forms the MHC II "enhanceosome" which CIITA binds to and promotes MHC II transcription (reviewed in (55, 56)).

As shown in **Figure 3**, MHC II is transcribed and translated before it forms αβ dimers in the ER. Here, Ii binds to the MHC II peptide binding groove to form Ii-MHC II. This association improves the stability of MHC II (57) and prevents the premature binding of antigenic peptides (58). Ii contains sorting motifs which target MHC II to a late endosomal compartment called MHC II compartment (MIIC) (59, 60), via the trans-Golgi network (61) or cell membrane (62, 63). Here, Ii is degraded by proteases, such as cathepsin S, to a smaller peptide called class II-associated invariant chain peptide (CLIP) (64–66). CLIP is finally removed by HLA-DM to expose the peptide binding groove (67–69). This step is essential for antigen presentation and mice that lack HLA-DM are defective in antigen presentation (70). HLA-DM is regulated by HLA-DO, which competitively inhibits binding to MHC II (71). In addition, it has recently been demonstrated that the cation channels transmembrane protein 176A and B (TMEM176A/B) regulate the expression of HLA-DM in murine cDC2, with elevated HLA-DM (H2-M) protein expression observed in cDC2 lacking TMEM176A/B (72). This leads to reduced MHC II-CLIP and impairs $CD4^+$ T cell priming (72). Once MHC II is fully exposed, it can bind 13-25 residue long self- and non-self peptides or even entire proteins (reviewed in (73)). Once loaded, MHC II traffics to the cell surface via tubulovesicular endosomes (74). It has been shown that peptide-loaded MHC II (pMHC

II) localize at the cell surface in lipid rafts. This clustering is thought to increase the chance of antigen-specific CD4$^+$ T cells finding their cognate antigen (reviewed in (75)).

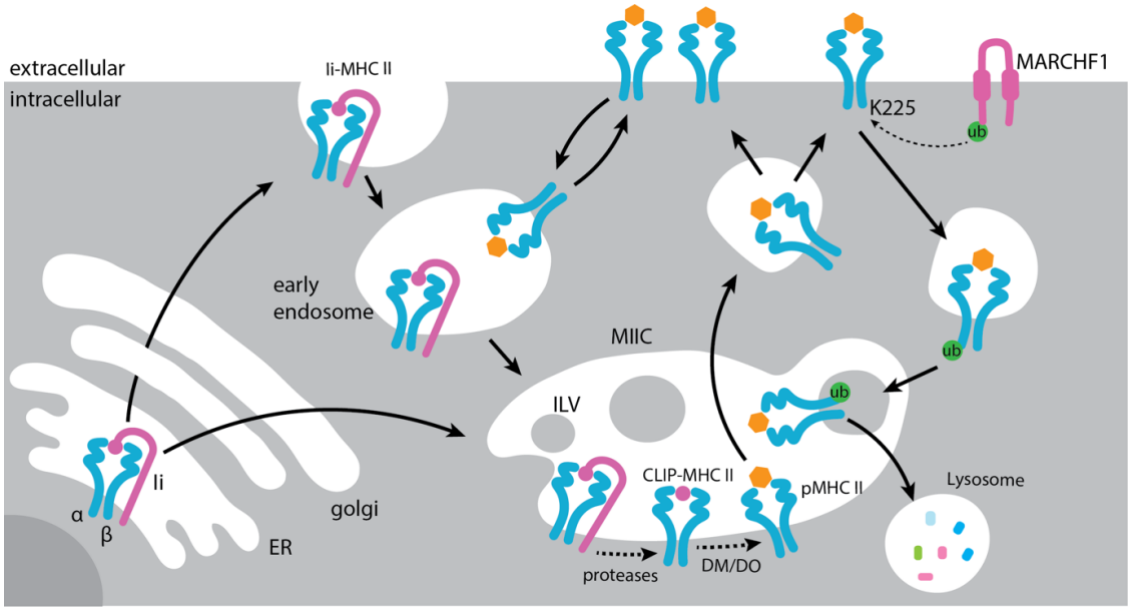


**Figure 3. The trafficking of MHC II.** The α and β chains of MHC II dimerize in the endoplasmic reticulum (ER). Once bound to the invariant chain (Ii), Ii-MHC II traffics to the MHC II endosomal compartment (MIIC). Trafficking to MIIC can occur directly or via the cell surface. Proteases in MIIC partially degrade Ii to a smaller peptide called "class II-associated invariant chain peptide" (CLIP). CLIP is then degraded by HLA-DM, which is regulated by HLA-DO. Once the peptide-binding groove of MHC II is exposed it can bind peptide antigen and forms pMHC II. This traffics to the cell surface to present to CD4$^+$ T cells. Surface pMHC II can recycle between the cell surface and early endosome. Alternatively, the β chain of pMHC II can be ubiquitinated at lysine 225 (K225) by MARCH1. Ubiquitination promotes MHC II degradation via the lysosomal pathway.

## Peptide-MHC II trafficking

Once at the cell-surface pMHC II is rapidly internalized (76) but can recycle back to the cell surface with the same or newly acquired peptide (77–80). The latter is thought to improve the repertoire of peptides available for T cell recognition and has been shown to be critical for the presentation of some antigens. For example, the S3 epitope of influenza is only presented on MHC II via the recycling pathway (81). Alternate to recycling,

pMHC II can be sorted into intraluminal vesicles (ILVs) destined to be degraded by the lysosomal pathway.

MHC II expression changes dramatically depending on the activation status of DCs. In resting DCs, the majority of MHC II is stored intracellularly in multivesicular bodies (MVBs) with little MHC II found on the cell surface (74, 76, 82, 83). While MHC II is continuously synthesized, it is degraded quickly with a half-life of ~10 hours (76). It is thought that this prevents irrelevant peptide accumulating at the cell surface during steady-state conditions, which in turn safeguards against excessive immune responses (76). Once activated, however, the MVBs once storing MHC II become tubular and lose their ILVs. This allows for the redistribution of MHC II to the cell surface (82). As such, the cell surface expression of MHC II significantly increases and the intracellular pool is lost (76, 82–84). In addition, the rate of MHC II synthesis is transiently increased before being shut down (76, 83). This is due to a shut down in the gene expression of CIITA (85). Interestingly though, the half-life of MHC II increases to ~100 hours (76). These changes, alongside a reduction in endocytosis (86, 87), ensure that only peptides acquired at the site of inflammation accumulate at the cell surface and are presented to T cells, a process termed “antigenic memory” (88).

The stability of MHC II in DCs is dependent on their ubiquitination status. Ubiquitination of MHC II was first described in 2006 in studies that showed when the single lysine (K225) on the β chain of MHC II is mutated to arginine (MHC IIKR) or alanine (MHC IIKA) the cell surface expression of MHC II increases. In addition, they found that while MHC II is ubiquitinated in wild type cells, K225R/A leads to a loss of this ubiquitination

(89–91). Later, it was confirmed that the E3 ligase responsible for MHC II ubiquitination in B cells (92) and DCs (93) is the Membrane Associated RING-CH-type finger 1 (MARCH1). Mice lacking MARCH1 (*Marchf1*$^{-/-}$) (92) or expressing MHC IIKR (*MHC IIKR*$^{KI/KI}$) (94) lack MHC II ubiquitination and have elevated MHC II cell surface expression. We have recently shown MARCH1-mediated MHC II ubiquitination occurs in all professional and "atypical" hematopoietic antigen presenting cells (95).

**Regulation of cell surface MHC II expression**

While MARCH1 has a striking effect on MHC II expression, its endogenous expression is difficult to detect (93, 96). This is due to a low abundance in *Marchf1* mRNA (97) in addition to MARCH1 autoubiquitination leading to a short half-life (98). Interestingly, when investigating the expression of *Marchf1* mRNA it was found to decrease following activation of human monocyte-derived DCs (93, 96), murine cDC (99, 100), B cells (100) and to a lesser extent pDC (99). Whilst the pathways involved in this downregulation are currently unknown, it has been shown to cause a decrease in MHC II ubiquitination and an increase in MHC II stabilization (90, 91). A similar effect is observed when *Marchf1* is forcibly downregulated in immature DCs (93). Downregulation of *Marchf1* during DC activation is thought to assist with antigenic memory.

In addition to DC activation, *Marchf1* is regulated by IL-10. In macrophages and monocytes, exposure to IL-10 leads to increased *Marchf1* expression (101, 102). This promotes MHC II ubiquitination and decreases MHC II cell surface expression, which is rescued in *Marchf1*$^{-/-}$ mice (101, 102). Initially IL-10 was thought to have the same effect on DCs. Indeed, it was shown that DCs treated with IL-10 or incubated with Tregs (which

produce IL-10) have reduced MHC II expression and increased *Marchf1* expression (103, 104). However, it was later demonstrated that this was due to IL-10 inhibiting DC activation, with reduced MHC II and CD86 expression also observed in *Marchf1*$^{-/-}$ DCs treated with IL-10 (101). In contrast to the aforementioned cells, IL-10 has been shown to reduce *Marchf1* expression in B cells (105). Together, these studies stress the importance for future experiments investigating the intricacies of MARCH1 regulation.

The expression of MHC II is also regulated by CD83. Mice harboring a mutated form of CD83 (*CD83*$^{anu/anu}$) have reduced MHC II and CD86 cell surface expression on DCs and B cells (103), in addition to thymic epithelial cells (106, 107). This phenotype is rescued when MHC II is mutated to MHC IIKR (103), indicating a role for ubiquitination. Indeed, it was demonstrated that CD83 regulates MHC II expression by binding to MARCH1 in DCs and B cells, or MARCH8 in thymic epithelial cells (103). This association prevents MARCH1 from ubiquitinating MHC II or CD86 and leads to an increase in their cell surface expression. Interestingly, CD83 expression is upregulated during DC activation (103). This, along with decreased *Marchf1* expression, promotes increased MHC II cell surface expression in activated DCs.

Besides MARCH1, CD83 and IL-10, MHC II expression is also impacted by the length of its polyubiquitin chain. In immature DCs, the majority of MHC II resides in late endocytic compartments whereas in B cells the majority of MHC II resides at the cell surface. Interestingly, DC MHC II has a polyubiquitin chain of 4-6 molecules long while B cell MHC II has 2-3 ubiquitin molecules (90). It has been suggested that the ubiquitin

chain length alters the architecture of MHC II which in turn impacts the recognition of MHC II by the endosomal sorting machinery (90).

**Regulation of MHC II trafficking by ubiquitination**

There are two hypotheses as to how MARCH1-mediated MHC II ubiquitination leads to reduced cell surface expression. Firstly, ubiquitination could increase MHC II internalization from the cell surface. To measure endocytosis, studies have monitored the internalization of anti-MHC II antibody from the cell surface in BMDCs, human monocyte-derived DCs or D1 cells (90, 91, 93). Here, they have found that cells lacking MHC II ubiquitination have less intracellular accumulation. Using a quenchable fluorescently tagged internalization probe (108), our lab has shown reduced MHC II internalization in *Marchf1*$^{-/-}$ (109) and *MHC IIKR*$^{KI/KI}$ splenic cDC (110).

This is, however, in contrast to studies using BMDCs or B cells from *Marchf1*$^{-/-}$ and *MHC IIKR*$^{KI/KI}$ mice where no significant difference in anti-MHC II antibody accumulation was observed (92, 94). An alternative hypothesis is that MHC II ubiquitination prevents MHC II recycling. To investigate this question, studies have used reversible biotinylation assays whereby cell surface proteins are labelled with cleavable biotin. After allowing internalization to occur, cell surface biotin is cleaved before reculturing cells and allowing recycling to occur. In these studies, it was found that the lack of MHC II ubiquitination increases MHC II recycling (100). It should be noted that these studies were carried out using different cells (for example BMDCs with forced expression of MHC II vs endogenous MHC II expression in primary splenic DCs) which could account for the contradictory conclusions drawn by different groups. In addition,

the measure for endocytosis and recycling between assays varied with fluorescently tagged antibodies, internalization probes and cleavable biotin used (111).

**Role of MHC II ubiquitination in immunity**

The functional role of MHC II ubiquitination in immunity is unclear. An appealing hypothesis is that MHC II ubiquitination suppresses antigen presentation and prevents detrimental immune responses.

Given the important role of MHC II in T cell development it is expected that mice lacking MHC II ubiquitination would have altered T cell compartments. However, when investigating immune cell populations in *MHC IIKR*$^{KI/KI}$ mice one study found no significant changes (112). Our lab, and others, have confirmed that conventional T cells are unaltered in the absence of MHC II ubiquitination, however, reduced numbers of Tregs are observed (110, 113, 114). We have recently demonstrated that this reduction is due to reduced number of thymic Treg precursors (110). Since this phenotype is not observed in *March8*$^{-/-}$ mice, the expression of MHC II on thymic DCs is important for the development of Tregs.

Altered DC function is observed when investigating the ability of DCs to produce pro-inflammatory cytokines in response to LPS, with *Marchf1*$^{-/-}$ and *MHC IIKR*$^{KI/KI}$ DCs secreting reduced IL-12 and TNFα (115–117). How this altered DC function impacts immune outcomes is unclear though, with different *in vitro* studies concluding antigen presentation by *MHC IIKR*$^{KI/KI}$ DCs is increased, unchanged and reduced. This discrepancy is largely due to different assays, antigen and cells being employed (116).

Importantly, these studies have made conclusions about overall antigen presentation when they are in fact assessing different aspects of antigen presentation. For example, one study concluded that *MHC IIKR*$^{KI/KI}$ BMDCs have improved antigen presentation as they were able to stimulate $CD4^+$ T cells for a longer period of time following incubation on ice with the ovalbumin peptide $OVA_{323-339}$ (100). This is likely due to increased MHC II expression and does not take into consideration antigen uptake or proteolysis. In contrast, studies have concluded *MHC IIKR*$^{KI/KI}$ DCs have reduced antigen presentation to $CD4^+$ T cells following exposure to ovalbumin *in vitro* (116). We have previously reported that altered MHC II ubiquitination impacts the expression of MHC I and that this is associated with reduced cross-presentation of cell-associated antigen (109). Importantly, these *in vitro* studies do not reveal which aspect of antigen presentation is affected or the consequences on immune responses *in vivo*. Recently, it was demonstrated that *MHC IIKR*$^{KI/KI}$ mice have reduced $CD4^+$ T cell priming *in vivo* following OVA-CFA immunization (117). While this paper was the first to hint at a role of MHC II ubiquitination in the regulation of immunity *in vivo*, several questions remain, including the impact of MHC II ubiquitination on DC function in addition to $CD8^+$ T cell responses.

How MHC II ubiquitination affects the development of Tregs, DC cytokine secretion and antigen presentation of MHC II and MHC I is currently unclear. MHC II has been shown to cluster in cell surface lipid raft domains. Elevated MHC II expression has been shown to disrupt these domains and impair DC engagement with thymocytes and Treg development *in vitro* (113). It is possible that altered lipid rafts may account for some of the other changes observed in *MHC IIKR*$^{KI/KI}$ cDC, particularly given that MHC I and MHC II have been shown to cluster together (109, 118, 119). It has also been suggested

that MHC II stabilization at the cell surface may cause DCs to interact with "certain factors" *in vivo*, which alter DC function (115). What these factors are or how they may interact with DCs is unknown.

## 1.3 Aims of this thesis

The major aim of this thesis is to improve the understanding of DCs such that they are easier to manipulate for improved immune responses to vaccines against infection and cancer.

The specific aims are:

I. To explore the expression of wild type and mutated Flt3 (Flt3-ITD) in DCs and assess the impact of Flt3-ITD on DC function.
II. To uncover the molecular machinery involved in DC Flt3 regulation, using CRISPR/Cas9 genome-wide screens.
III. To investigate the impact of MHC II ubiquitination on DC function and immune outcomes.

# Chapter 2 - Materials and Methods

## 2.1 Media and buffers

### Culture media

Complete DMEM

Dulbecco's modified Eagle medium (DMEM) (Peter Doherty Institute for Infection and Immunity Media Preparation Unit, PDI MPU) supplemented with 10% (v/v) fetal bovine serum (FBS; Gibco) and 100 U/mL penicillin and 100 µg/mL streptomycin (PDI MPU).

Complete IMDM

Iscove's Modified Dulbecco's Medium (IMDM) GlutaMAX™ (Gibco) supplemented with 10% (v/v) FBS (Gibco), 100 U/mL penicillin and 100 µg/mL streptomycin (PDI MPU), 50 µM β-mercaptoethanol (Gibco).

Complete RPMI

RPMI 1640 with 33.6 mM hydroxyethyl piperazineethanesulfonic acid (HEPES) (PDI MPU), 1 µM sodium pyruvate, 24 mM sodium bicarbonate, 10% (v/v) FBS (Gibco), 100 µM β-mercaptoethanol (Gibco), 100 U/mL penicillin and 100 µg/mL streptomycin (PDI MPU) and 2mM GlutaMAX™.

**Buffers**

EDTA-BSS

Mouse tonicity balanced salt solution supplemented with EDTA. Double distilled water containing 150 mM sodium chloride, 4 mM potassium chloride, 12 μM sodium dihydrogen orthophosphate, 24 μM disodium hydrogen orthophosphate, 15 mM HEPES and 5 mM ethylenediaminetetraacetic acid (EDTA) (PDI MPU).

EDTA-BSS 2% FBS

EDTA-BSS with 2% (v/v) FBS (Gibco).

FBS-EDTA

FBS (Gibco) supplemented with 10% (v/v) 0.1 M EDTA (Univar).

NP40 lysis buffer

0.5% (v/v) IGEPAL CA-630 (Sigma-Aldrich), 50 mM Tris-Cl (pH 7.5, Astral Scientific), 5 mM $MgCl_2$ (Sigma-Aldrich), cOmplete Protease Inhibitor Cocktail (Roche) and PhosSTOP (Sigma-Aldrich).

NET wash buffer

MilliQ water containing 0.5% (v/v) IGEPAL CA-630, 50 mM Tris-Cl (pH 7.5, Astral Scientific), 150 mM NaCl (Sigma-Aldrich), 5 mM EDTA (Univar).

Phosphate buffered saline (PBS)

MilliQ water with 145 mM NaCl, 7.5 mM disodium hydrogen orthophosphate and 2.8 mM sodium dihydrogen orthophosphate (PDI MPU).

PBS-Tween 20 (PBST)

PBS with 0.1 % (v/v) Tween-20 (Sigma-Aldrich).

RPMI-2% FBS.

RPMI 1640 (PDI MPU) with 2% (v/v) FBS (Gibco)

Sodium dodecyl sulphate (SDS) sample buffer (3x)

MilliQ water with 0.2 M Tris-Cl (pH 6.8, Astral Scientific), 12% w/v SDS (Amresco), 30% (v/v) glycerol (Univar), 15% (v/v) β-mercaptoethanol (Gibco) and 0.02% (w/v) bromophenol blue (Sigma-Aldrich).

## 2.2 Mice

C57BL/6JArc (wild type) mice were used at 6 – 12 weeks of age. All mice were bred and maintained in specific pathogen-free conditions at the Melbourne Bioresources Platform at Bio21 Molecular Science and Biotechnology Institute. Experimental procedures were approved by the Animal Ethics Committee of the University of Melbourne (1714375).

## 2.3 Primary cells

**Dendritic cells**

Primary splenic DCs were isolated as previously described (120). In brief, spleens were finely chopped with scissors and digested in 7 mL RPMI-2% FBS containing 140 μg/mL DNaseI (Roche) and 1 mg/mL collagenase type 3 (Worthington Biochemicals) for 20 min at room temperature with constant agitation. Intercellular clusters were disrupted by addition of further 10 mM EDTA and agitation for 5 min at room temperature. Light density cells were isolated by density gradient separation in 1.077 g/cm$^3$ Nycodenz, 5 mL per 4 spleens (Nycomed Pharma). The upper ~9 ml were collected, washed in EDTA-BSS-2% FBS, then resuspended in a depletion cocktail containing the following rat anti-mouse mAbs: anti-CD3 (Clone: KT3-1.1), anti-Thy1 (Clone: T24/31.7), anti-RBC (Clone: Ter119), anti-B220 (Clone: RA3-6B2), anti-Ly6c/g (Clone: RB6-8C5). Cells were incubated with cocktail (10 μL per $10^6$ cells) for 30 min at 4°C, washed, and incubated with BioMag anti-rat IgG-coupled magnetic beads (Qiagen) for 20 min at 4°C with continuous agitation. The DC-enriched supernatant was then recovered after magnetic depletion. This protocol yielded cell preparations with 70-85% CD11c$^+$ purity. cDC1 were defined as CD11c$^+$CD11b$^-$CD8$^+$ and cDC2 were defined as CD11c$^+$CD11b$^+$CD8$^-$.

## 2.4 Flow cytometry

For flow cytometry analysis, single cell suspensions were stained with antibodies in EDTA-BSS 2% FBS for 30 mins on ice. Cells were washed twice and resuspended in

EDTA-BSS 2% FBS with viability dye (DAPI or Propidium Iodide, Invitrogen). Samples were collected on the LSRFortessa (BD) and data analysis was performed using FlowJo software (FlowJo LLC) and Prism (Graphpad).

## 2.5 Antibodies

**Table 2.1 Flow cytometry antibodies.**

| Antigen | Clone | Supplier |
|---|---|---|
| CD8α | 53-6.7 | BioLegend |
| CD11c | N418 | BioLegend |
| CD40 | FGK45.5 | WEHI antibody facility |
| CD80 | 16-10A1 | WEHI antibody facility |
| CD86 | GL1 | BioLegend |
| CD135 (Flt3) | A2F10 | BioLegend |
| CD205 (DEC205) | NLDC-145 | WEHI antibody facility |
| MHC I | M1/42 | WEHI antibody facility/BioLegend |
| MHC II | M5/114 | WEHI antibody facility/BioLegend |
| XCR1 | ZET | BioLegend |

**Table 2.2 Immunoprecipitation and immunoblotting antibodies.**

| Antigen | Clone | Host | Supplier |
|---|---|---|---|
| CD135 (Flt3) | AF768 | Goat | R&D Systems |
| CD135 (Flt3) | 8F2 | Rabbit | Cell Signaling |
| Phosphotyrosine | 4G10 | Mouse | Sigma-Aldrich |
| Actin | A5060 | Rabbit | Sigma-Aldrich |
| Rabbit IgG H&L (HRP) | AB6741 | Rabbit | Abcam |
| Goat IgG H&L (HRP) | AB6721 | Goat | Abcam |

## 2.6 Cell culture

### Cell lines

HEK293T cells were originally obtained from the American Type Culture Collection (ATCC) and were maintained in Complete DMEM. Cells were kept in a humidified incubator with 10% atmospheric CO2 at 37°C and passaged at 80% confluency using Trypsin-Versene (PDI MPU).

MuTu DC1940 cells were a gift from Hans Acha-Orbea (121), and were maintained in Complete IMDM. Cells were kept in a humidified incubator with 10% atmospheric CO2 at 37°C and passaged at 70% confluency using EDTA-BSS 2% FBS, and by pooling adherent and non-adherent populations.

### Lentiviral transduction

To generate lentiviral particles, target, and packaging vectors (*Flt3* and *hBim* knockout cells: pMDL, RSV-REV and pMD2.G; GeCKO and Brie libraries: pCMV-VSV-G and psPAX2) were co-transfected into HEK293T cells using 10 μg/mL PEI 25K (Polysciences). Media was replaced after 24 h with target cell media. Supernatants were harvested after 24 h, filtered through a 45 μm PVDF membrane (Millipore) and frozen at -80°C or used for spinoculation. MuTu DC1940 cells were seeded into a 12- or 6 well culture plate with viral supernatants and 8 μg/mL polybrene (Sigma-Aldrich), and centrifuged for 2 hours at 2000 rpm and 32°C. After centrifugation, transduction media was replaced with fresh media and cells were analyzed after 72 h.

## 2.7 CRISPR knockout cell lines

### Plasmids

**Table 2.3 Plasmids for generating knockout cells.**

| Name | Description | Marker | Addgene # | Depositing lab |
|---|---|---|---|---|
| FUCas9Cherry | Stable SpCas9 expression plasmid | mCherry | 70182 | Marco Herold |
| FgH1tUTCyan | Dox-inducible gRNA expression plasmid | CFP | 85551 | Marco Herold |
| pMDLg/pRRE | Lentiviral packaging plasmid | - | 12251 | Didier Trono |
| pRSV-Rev | Lentiviral packaging plasmid | - | 12251 | Didier Trono |
| pMD2.G | Lentiviral packaging plasmid | - | 12259 | Didier Trono |
| pCMV-VSV-G | Lentiviral packaging plasmid (GeCKOv2, Brie) | Puromycin | 8454 | Bob Weinberg |
| psPAX2 | Lentiviral packaging plasmid (GeCKOv2, Brie) | Puromycin | 12260 | Didier Trono |

### Cloning gRNA expression plasmids

Target sequences for gRNAs were designed using the Broad Institutes gRNA design web portal (https://portals.broadinstitute.org/gpp/public/analysis-tools/gRNA-design) (122) by submitting the specific RefSeq ID of desired knockout targets. Suitable gRNAs were selected prioritizing lowest pick order number, N-terminal exons or catalytically active sites (where known). Oligonucleotides containing the desired gRNA target (see **Table 2.4**) and additional 5' overhang sequences (sense: 5' TCCC-; antisense: 5' AAAC-) were annealed, phosphorylated, and cloned into the FgH1tUTCyan vector (**Table 2.3**) using BsmBI restriction sites. Stbl3 chemically competent E. coli (Invitrogen) were heat shock transformed with ligated plasmids. Successful insertion of the gRNA target sequence into the vector was verified by Sanger sequencing (Australian Genome Research Facility).

**Table 2.4 CRISPR gRNA or crRNA target sequences and corresponding primers for PCR genotyping.**

| Gene | target sequence | PCR primer FOR | PCR primer REV |
|---|---|---|---|
| *hBim* | GCCCAAGAGTTGCGGCGTAT | N/A | N/A |
| *Neg control* | Integrated DNA Technologies (IDT) Alt-R CRISPR-Cas9 negative control crRNA #1 | | |
| *Flt3 #1* | GGTATATGAAGCGGCCACCG | ATGCAAACAGGTTCAATGCT | CGTGCGTTCATTATTTCAGC |
| *Flt3 #2* | GGTCTCTGTCACGTTCAAGA | TCTGAGGGTGGGTGTTAGGT | AAGCACACTAGGTCCCGAAG |
| *Med25* | TCTTTGCAGGTACTTCAACG | TTTCCTCCCTCAGACACAGG | TTTCCTCCCTCAGACACAGG |
| *Tcf7l2* | CGGAAACTTTCGGAGCGAGG | GCTGGCTGCGAAAACTTGTA | CAGGTCGGGGATCATGATGA |
| *RhoG* | CCAGGAGGATAGGCACGTCA | GGTCCTGCATCCTCTTGTGA | CAGGCAGCAACAACTTTGGA |
| *Hes1* | GTGTTGGGGAAATACCGCGC | GGCTGGATAGAAGGTAGGGG | CGTTGATCTGGGTCATGCAG |
| *KMT2C* | AGAACCATTATTAGTAAACG | TGAACCACTCCCACCAAGTT | CTGAAAAGGTACAGGCACAGG |
| *EP300* | CCTGACCCGTCTATGATCCG | AGACGTTGGAGGGCAATTTG | AGTCATCCGAGGCATCATGT |
| *ARIH1* | ATGTATCCGGGAGGTCAACG | GATAACCTGGATCTGGGCGA | GTATCCCATCCTCCGGCC |
| *Usp22* | TGCGTGGACTGATCAACCTG | CCACCTCCACGAACTCTGTA | GGACATCTCACAGACCAAGC |

## Generation of knockout cell lines

Stable SpCas9 expressing cells were generated by lentivirally transducing DC1940 cells with FUCas9Cherry and sorted for mCherry expression (Dr. Haiyin Liu, Mintern Lab). Knockout cells were then generated using a doxycycline-inducible dual-plasmid system (123) or the Alt-R CRISPR-Cas9 system (IDT).

For knockout cells generated with the doxycycline-inducible dual-plasmid system, gRNA-containing plasmids were lentivirally transduced into Cas9-expressing cells. gRNA expression was induced by incubation with 1 μg/mL doxycycline for 6 days. As a negative control, cells were transduced with a plasmid containing a mouse-unspecific gRNA sequence generated using human Bim (*hBim*). To enrich for knockout cells, cells were bulk sorted for $GFP^+mCherry^+CFP^+$.

For knockout cells generated with Alt-R CRISPR-Cas9 system, equimolar concentrations of Alt-R CRISPR-Cas9 crRNA and tracrRNA oligos were mixed in nuclease-free duplex buffer as per manufacturers protocol. To form a duplex, the oligo mix was incubated for 2 minutes at 95°C before cooling to room temperature. MuTu DC1940Cas9 cells were transfected in Opti-MEM (Gibco) with the duplexed oligos (30 μM final concentration of crRNA:tracrRNA) using Lipofectamine RNAiMax (Invitrogen) according to manufacturer's instructions. Cells were incubated in humidified incubator with 10% atmospheric CO2 at 37°C for 48 hours. To enrich for knockout cells, cells were stained for Flt3 and sorted on $GFP^+mCherry^+Flt3^+$ or $Flt3^-$.

To generate clonal cell lines, single cell sorting was carried out into three 96 well round bottom tissue culture plates with a BD Influx cell sorter. Surviving cell clusters were expanded and screened by Sanger sequencing.

*Generation of MuTu DC1940 cells stably expressing spCas9 was performed by Dr. Haiyin Liu, Mintern Lab, The Bio21 Institute). All cell sorting was performed at the Murdoch Children's Research Institute (Victoria, Australia).*

### Validation of knockout cell lines

To determine and quantify the exact induced insertions or deletions (InDels) in knockout cell lines, cells were lysed using QuickExtract (Epicentre) and subjected to PCR using the primers outlined in **Table 2.4**. The amplicons were separated on a 2% agarose gel and PCR bands were cut out and gel purified before analysis with Sanger sequencing (Australian Genome Research Facility). The relative contribution of different insertions and deletions (InDels) was quantified using Inference of CRISPR Edits (ICE) (124) analysis.

## 2.8 Biochemical Assays

### Flt3L stimulations

To investigate the impact of Flt3L on cell surface or total Flt3, equal number of MuTu DC1940 cells were treated with the indicated concentration of recombinant murine Flt3L (PeproTech) in Complete IMDM for the indicated times at 37°C. As a control, cells were treated with equivalent amount of PBS (carrier).

### Internalization assay

Recombinant murine Flt3L (PeproTech) conjugated to click sensor (sCy5-TCO) (Flt3L-sCy5-TCO) and quencher (sQSY-Tet) were generated as previously described (125) and gifted from Johnston Lab, Monash Institute of Pharmaceutical Sciences. For the internalization assay, cells were stained on ice for 30 min with Flt3L-sCy5-TCO after which they were washed twice to remove excess, unbound probe. Internalization was allowed by incubating cells in complete RPMI (primary DCs) or complete IMDM (MuTu

DC1940 cells) at 37°C. Cells were removed at specific time points and placed on ice, washed, phenotyped for surface markers and resuspended in media containing propidium iodide with or without 0.5 μM quencher. Cells were analyzed by flow cytometry. The quenching efficiency and percentage internalized Flt3L-sCy5-TCO was calculated as previously described (125).

**Flt3 Immunoprecipitation**

Cells were lysed on ice in NP40 lysis buffer at concentrations of $10^7$ cells/mL and nuclei were removed by 10 min centrifugation at 14,000 x g and 4°C. Lysates were pre-cleared once for 30 mins with uncoupled protein-G Sepharose beads, normal mouse serum and normal rat serum (all obtained from the Walter and Eliza Hall Institute) followed by a second 30 min pre-clear with uncoupled protein-G Sepharose beads only. To immunoprecipitate Flt3, 1 μg anti-Flt3 antibody and 50 μL of protein-G Sepharose beads were added to the lysate and incubated for 1 hour at 4°C with agitation. To immunoprecipitate biotinylated proteins, 50 μL streptavidin-agarose (Thermo Scientific) was added to the lysate. The beads were washed 3 times with NET wash buffer to remove unbound proteins. Flt3 was eluted by incubating the beads with 1x sample buffer for 5 mins at 95°C.

**Immunoblotting**

Immunoprecipitates or whole cell lysates from equal cell numbers were separated on a pre-cast Bolt 10% Bis-Tris Mini Protein gel run with 1x Bolt MOPS SDS running buffer (Invitrogen). Proteins were transferred onto PVDF membrane with iBlot 2 at 20V for 10 mins (Invitrogen). Blots were blocked in PBST containing 5% bovine serum albumin

(BSA, Sigma) for two hours at room temperature with agitation. Blots were then incubated with primary antibodies (anti-Flt3 or anti-actin) in PBST with 1% BSA overnight at 4°C with agitation. Blots underwent three washes with PBST prior to one hour incubation with HRP-conjugated secondary antibody in PBST with 1% BSA for one hour at room temperature with agitation. Chemiluminescence was determined using the ECL select substrate (GE Healthcare) acquired on a ChemiDoc MP imaging system (Bio-Rad) and analyzed with ImageJ.

**RT-PCR**

Equal numbers of MuTu DC1940 cells were pelleted and stored at -80C. RNA was extracted using RNeasy Mini Kit (Qiagen) as per manufacturers protocol. To remove genomic DNA, DNASE I amplification kit (Rowe Scientific) was used as per manufacturers protocol. cDNA was then synthesized using SensiFAST cDNA Synthesis kit (Bioline). RT-qPCR was performed using TaqMan Fast Advanced Master Mix (Applied Biosystems) with Flt3 (Mm00439016) FAM-MGB and HPRT (Mm03024075) FAM-MGB TaqMan probes (Applied Biosystems). Samples were run in technical triplicate on QuantStudio 6 Flex Real-Time PCR System (Applied Biosystems) in 384 well fast plates as per the PCR cycle below. For negative controls, a no reverse transcriptase sample was included for both probes.

| reagent | volume |
|---|---|
| Taqman Fast Advanced Master Mix (2x) | 5 µL |
| TaqMan Assay (20x) | 0.5 µL |
| Nuclease free water | 3.5 µL |
| Total | 10 µL |

| temperature | time | cycles |
|---|---|---|
| 50°C | 2 min | 1 |
| 95°C | 2 min | 1 |
| 95°C | 1 sec | 40 |
| 60°C | 20 sec | |

## 2.9 CRISPR/Cas9 genome-wide screens

### Library generation

To generate MuTu DC1940 cells expressing a genome wide library the mouse knockout pooled libraries genome-scale CRISPR-Cas9 knockout (GeCKO) v2 (126, 127) and Brie (122) were utilized. These were used in the lentiCRISPRv2 format (Addgene #1000000052 and Addgene #73632). The GeCKO library contains two half-libraries (Library A: 67,405 gRNA; Library B: 62,804 gRNA) targeting 20,611 genes. This study utilized Library A. The Brie library contains 78,637 gRNA targeting 19,674 genes. To amplify the library plasmid DNA, Endura ElectroCompetent cells (Lucigen) were transformed with library plasmids by electroporation, cultured and DNA was extracted from bacterial pellets using Plasmid Maxiprep Kit (Qiagen). Library plasmid DNA was co-transfected into HEK293T cells with pCMV-VSV-G and psPAX2 using PEI transfection.

To generate the library, GeCKOv2 lentivirus was used to transduce 72 $x10^6$ MuTu DC1940 cells at a multiplicity of infection (MOI) of 0.3 - 0.4 to achieve 300 – 400x coverage. For Brie, 185 $x10^6$ MuTu DC1940 cells were transduced at an MOI of 0.15 – 0.3 to achieve 300 – 600 x coverage. Cells were maintained for 3 days post-transduction prior to selection with 1 μg/mL puromycin.

*GeCKOv2 library amplification was performed by Dr. Hamish McWilliam (The Peter Doherty Institute).*

**Isolation of Flt3$^{hi}$ and Flt3$^{lo}$ populations**

For the GeCKOv2 library, cells were first stimulated with 100 ng/mL Flt3L for 1 hour. To isolate Flt3$^{hi}$ and Flt3$^{lo}$ cells, 3-5 x $10^8$ library expressing cells were stained with biotin-conjugated anti-Flt3 in EDTA-BSS 2%FBS for 30 mins on ice. Cells were washed twice and stained with streptavidin-APC for 30 mins on ice after which they were washed twice again and resuspend in propidium iodide (PI). Live cells were identified as GFP$^+$ PI$^-$ and 5% of the highest or lowest Flt3 expressing cells were sorted using BD Influx (Murdoch Children's Research Institute). 3-5 x $10^6$ sorted cells were recultured. One week later, ~1 x $10^8$ cells underwent a second sort to further enrich for the 5% of the highest or lowest Flt3 expressing cells.

**DNA isolation**

Genomic DNA was isolated from at least 3-5 x $10^7$ cells using Quick-DNA Midiprep Plus Kit (Zymo Research) as per manufacturer's instructions and the concentration was measured using BioPhotometer (Eppendorf).

**Targeted PCR**

For GeCKOv2, a two-step nested PCR was performed to generate ~280 bp amplicons which can be sequenced using Illumina MiSeq technology. The first set of primers (GeCKO F1 and F2) were designed to amplify the GeCKO backbone vector which surrounds the gRNA sequence. The second set of primers (GeCKO F37-48 and GeCKO R65-R70) were designed to anneal within the amplicon of the first PCR and attach Illumina adaptor sequences, offset staggers to introduce complexity, unique indexes for sample identification, bridge amplification sequences as well as vector specific sequences.

**Table 2.5 GeCKOv2 sequencing primers.**

| Primer | Sequence |
|---|---|
| F1 | AATGGACTATCATATGCTTACCGTAACTTGAAAGTATTTCG |
| R1 | TCTACTATTCTTTCCCCTGCACTGTTGTGGGCGATGTGCGCTCTG |
| F37 | AATGATACGGCGACCACCGAGATCTACACTCTTTCCCTACACGACGCTCTTCCGATCTGTA AACTCACCGGACTATCATATGCTTACCGTAAC |
| F38 | AATGATACGGCGACCACCGAGATCTACACTCTTTCCCTACACGACGCTCTTCCGATCTTCA AGAGATCGGACTATCATATGCTTACCGTAAC |
| F39 | AATGATACGGCGACCACCGAGATCTACACTCTTTCCCTACACGACGCTCTTCCGATCTGAA GGACACGGACTATCATATGCTTACCGTAAC |
| F40 | AATGATACGGCGACCACCGAGATCTACACTCTTTCCCTACACGACGCTCTTCCGATCTTAC AATCCGTCGGACTATCATATGCTTACCGTAAC |
| F41 | AATGATACGGCGACCACCGAGATCTACACTCTTTCCCTACACGACGCTCTTCCGATCTAGA ATGTTGCGGACTATCATATGCTTACCGTAAC |
| F42 | AATGATACGGCGACCACCGAGATCTACACTCTTTCCCTACACGACGCTCTTCCGATCTAAC ACGACCGGACTATCATATGCTTACCGTAAC |
| F43 | AATGATACGGCGACCACCGAGATCTACACTCTTTCCCTACACGACGCTCTTCCGATCTCGT ACAGATTCGGACTATCATATGCTTACCGTAAC |
| F44 | AATGATACGGCGACCACCGAGATCTACACTCTTTCCCTACACGACGCTCTTCCGATCTTCA GATGTACGGACTATCATATGCTTACCGTAAC |
| F45 | AATGATACGGCGACCACCGAGATCTACACTCTTTCCCTACACGACGCTCTTCCGATCTCAG CCATGCGGACTATCATATGCTTACCGTAAC |
| F46 | AATGATACGGCGACCACCGAGATCTACACTCTTTCCCTACACGACGCTCTTCCGATCTACG AGGCTAACGGACTATCATATGCTTACCGTAAC |
| F47 | AATGATACGGCGACCACCGAGATCTACACTCTTTCCCTACACGACGCTCTTCCGATCTGAA TAGCGACGGACTATCATATGCTTACCGTAAC |
| F48 | AATGATACGGCGACCACCGAGATCTACACTCTTTCCCTACACGACGCTCTTCCGATCTTAT CATTCCGGACTATCATATGCTTACCGTAAC |
| R65 | CAAGCAGAAGACGGCATACGAGATCGGTCTCGGCATTCCTGCTGAACCGCTCTTCCGATC TGAATTGAGGACAAGTTGATAACGGACTAGCCTTA |
| R66 | CAAGCAGAAGACGGCATACGAGATCGGTCTCGGCATTCCTGCTGAACCGCTCTTCCGATC TTCAACCACACAAGTTGATAACGGACTAGCCTTA |
| R67 | CAAGCAGAAGACGGCATACGAGATCGGTCTCGGCATTCCTGCTGAACCGCTCTTCCGATC TGTACAAGACTACAAGTTGATAACGGACTAGCCTTA |
| R68 | CAAGCAGAAGACGGCATACGAGATCGGTCTCGGCATTCCTGCTGAACCGCTCTTCCGATC TACAATGGAACAAGTTGATAACGGACTAGCCTTA |
| R69 | CAAGCAGAAGACGGCATACGAGATCGGTCTCGGCATTCCTGCTGAACCGCTCTTCCGATC TCGTCACTTCGACAAGTTGATAACGGACTAGCCTTA |
| R70 | CAAGCAGAAGACGGCATACGAGATCGGTCTCGGCATTCCTGCTGAACCGCTCTTCCGATC TTCCAGCGTTACAAGTTGATAACGGACTAGCCTTA |

To maintain the library coverage, 200 µg (for unsorted samples) or 60 µg (for sorted samples) were used in the first PCR. This was split into 100 µL PCR reactions, each containing 10 µg DNA each. The required amount of template DNA was calculated as follows, assuming a molecular weight of 1.8 x $10^{12}$ $\frac{g}{mol}$ per one mouse haploid genome (128):

$$\frac{200\ x\ 10^{-6} g}{1.8x10^{12}\ \frac{g}{mol}} = 111.1x10^{-18} mol$$

$$111.1\ x\ 10^{-18}\ x\ 6.022\ x\ 10^{23} = 66.9\ x\ 10^{6}\ haploid\ genomes = \ 33.5\ x\ 10^{6}\ diploid\ genomes$$

$$\approx 500x\ library\ size$$

The first and second PCR was performed using Herculase II Fusion DNA Polymerase (Agilent) and following conditions:

| **reagent** | **volume** |
|---|---|
| 5x Herculase reaction buffer | 20 µL |
| dNTP 10 mM each | 2.5 µL |
| F-primer 10 µM | 2.5 µL |
| R-primer 10 µM | 2.5 µL |
| Template DNA 10 µg | 62.5 µL |
| Herculase II Fusion Polymerase | 1 µL |
| $H_2O$ | 9 µL |
| Total | 100 µL |

| **temperature** | **time** | **cycles** |
|---|---|---|
| 95°C | 3 min | 1 |
| 95°C | 15 sec | 12** |
| 60°C | 30 sec | |
| 72°C | 30 sec | |
| 72°C | 7 min | 1 |

**The number of cycles for the second PCR increased to 28 cycles.

For Brie, a one-step PCR was performed to generate ~280 bp amplicons which can be sequenced using Illumina MiSeq technology. All samples received the same forward primer mix which comprised of 8 primers (LcV2-P5-0nt - LcV2-P5-8nt) with 0-8 nucleotide staggers which introduces complexity. Each sample received a unique reverse primer (LCv2-R1 – R18, R24, R25) which allowed for sample identification.

**Table 2.6 Brie sequencing primers.**

| Primer | Sequence |
|---|---|
| LcV2-P5-0nt | AATGATACGGCGACCACCGAGATCTACACTCTTTCCCTACACGACGCTCTTCC GATCTTTGTGGAAAGGACGAAACACCG |
| LcV2-P5-1nt | AATGATACGGCGACCACCGAGATCTACACTCTTTCCCTACACGACGCTCTTCC GATCTCTTGTGGAAAGGACGAAACACCG |
| LcV2-P5-2nt | AATGATACGGCGACCACCGAGATCTACACTCTTTCCCTACACGACGCTCTTCC GATCTGCTTGTGGAAAGGACGAAACACCG |
| LcV2-P5-3nt | AATGATACGGCGACCACCGAGATCTACACTCTTTCCCTACACGACGCTCTTCC GATCTAGCTTGTGGAAAGGACGAAACACCG |
| LcV2-P5-4nt | AATGATACGGCGACCACCGAGATCTACACTCTTTCCCTACACGACGCTCTTCC GATCTCAACTTGTGGAAAGGACGAAACACCG |
| LcV2-P5-6nt | AATGATACGGCGACCACCGAGATCTACACTCTTTCCCTACACGACGCTCTTCC GATCTTGCACCTTGTGGAAAGGACGAAACACCG |
| LcV2-P5-7nt | AATGATACGGCGACCACCGAGATCTACACTCTTTCCCTACACGACGCTCTTCC GATCTACGCAACTTGTGGAAAGGACGAAACACCG |
| LcV2-P5-8nt | AATGATACGGCGACCACCGAGATCTACACTCTTTCCCTACACGACGCTCTTCC GATCTGAAGACCCTTGTGGAAAGGACGAAACACCG |
| LcV2-R1 | CAAGCAGAAGACGGCATACGAGATCGGTTCAAGTGACTGGAGTTCAGACGT GTGCTCTTCCGATCTCCAATTCCCACTCCTTTCAAGACCT |
| LcV2-R2 | CAAGCAGAAGACGGCATACGAGATGCTGGATTGTGACTGGAGTTCAGACGTG TGCTCTTCCGATCTCCAATTCCCACTCCTTTCAAGACCT |
| LcV2-R3 | CAAGCAGAAGACGGCATACGAGATTAACTCGGGTGACTGGAGTTCAGACGT GTGCTCTTCCGATCTCCAATTCCCACTCCTTTCAAGACCT |
| LcV2-R4 | CAAGCAGAAGACGGCATACGAGATTAACAGTTGTGACTGGAGTTCAGACGTG TGCTCTTCCGATCTCCAATTCCCACTCCTTTCAAGACCT |
| LcV2-R5 | CAAGCAGAAGACGGCATACGAGATATACTCAAGTGACTGGAGTTCAGACGT GTGCTCTTCCGATCTCCAATTCCCACTCCTTTCAAGACCT |
| LcV2-R6 | CAAGCAGAAGACGGCATACGAGATGCTGAGAAGTGACTGGAGTTCAGACGT GTGCTCTTCCGATCTCCAATTCCCACTCCTTTCAAGACCT |
| LcV2-R7 | CAAGCAGAAGACGGCATACGAGATATTGGAGGGTGACTGGAGTTCAGACGT GTGCTCTTCCGATCTCCAATTCCCACTCCTTTCAAGACCT |
| LcV2-R8 | CAAGCAGAAGACGGCATACGAGATTAGTCTAAGTGACTGGAGTTCAGACGTG TGCTCTTCCGATCTCCAATTCCCACTCCTTTCAAGACCT |
| LcV2-R9 | CAAGCAGAAGACGGCATACGAGATCGGTGACCGTGACTGGAGTTCAGACGT GTGCTCTTCCGATCTCCAATTCCCACTCCTTTCAAGACCT |
| LcV2-R10 | CAAGCAGAAGACGGCATACGAGATTACAGAGGGTGACTGGAGTTCAGACGT GTGCTCTTCCGATCTCCAATTCCCACTCCTTTCAAGACCT |

| | |
|---|---|
| LcV2-R11 | CAAGCAGAAGACGGCATACGAGATATTGTCAAGTGACTGGAGTTCAGACGTG TGCTCTTCCGATCTCCAATTCCCACTCCTTTCAAGACCT |
| LcV2-R12 | CAAGCAGAAGACGGCATACGAGATTATGTCTTGTGACTGGAGTTCAGACGTG TGCTCTTCCGATCTCCAATTCCCACTCCTTTCAAGACCT |
| LcV2-R13 | CAAGCAGAAGACGGCATACGAGATATTGGATTGTGACTGGAGTTCAGACGTG TGCTCTTCCGATCTCCAATTCCCACTCCTTTCAAGACCT |
| LcV2-R14 | CAAGCAGAAGACGGCATACGAGATATACTCGGGTGACTGGAGTTCAGACGT GTGCTCTTCCGATCTCCAATTCCCACTCCTTTCAAGACCT |
| LcV2-R15 | CAAGCAGAAGACGGCATACGAGATTATGAGAAGTGACTGGAGTTCAGACGT GTGCTCTTCCGATCTCCAATTCCCACTCCTTTCAAGACCT |
| LcV2-R16 | CAAGCAGAAGACGGCATACGAGATGCACAGTTGTGACTGGAGTTCAGACGT GTGCTCTTCCGATCTCCAATTCCCACTCCTTTCAAGACCT |
| LcV2-R17 | CAAGCAGAAGACGGCATACGAGATCGTGGATTGTGACTGGAGTTCAGACGTG TGCTCTTCCGATCTCCAATTCCCACTCCTTTCAAGACCT |
| LcV2-R18 | CAAGCAGAAGACGGCATACGAGATTAGTAGAAGTGACTGGAGTTCAGACGT GTGCTCTTCCGATCTCCAATTCCCACTCCTTTCAAGACCT |
| LcV2-R24 | CAAGCAGAAGACGGCATACGAGATCGCATCAAGTGACTGGAGTTCAGACGT GTGCTCTTCCGATCTCCAATTCCCACTCCTTTCAAGACCT |
| LcV2-R25 | CAAGCAGAAGACGGCATACGAGATTAACTCAAGTGACTGGAGTTCAGACGT GTGCTCTTCCGATCTCCAATTCCCACTCCTTTCAAGACCT |

Like the GeCKOv2 library, 200 μg (for unsorted samples) or 60 μg (for sorted samples) were used in the PCR to maintain coverage. The PCR was performed using Herculase II Fusion DNA Polymerase (Agilent) and following conditions:

| **reagent** | **volume** |
|---|---|
| 5x Herculase reaction buffer | 20 μL |
| dNTP 10 mM each | 2.5 μL |
| F-primer 10 μM | 2.5 μL |
| R-primer 10 μM | 2.5 μL |
| Template DNA 10 μg | 60 μL |
| Herculase II Fusion Polymerase | 1 μL |
| $H_2O$ | 11.5 μL |
| Total | 100 μL |

| **temperature** | **time** | **cycles** |
|---|---|---|
| 95°C | 3 min | 1 |
| 95°C | 15 sec | 28 |
| 60°C | 30 sec | |
| 72°C | 30 sec | |
| 72°C | 7 min | 1 |

**Integrity and Quality Ascertainment of Amplicons**

Amplicon size distribution was ascertained using the Agilent Tapestation D1000 protocol. For Tapestation analysis, 3 µL of D1000 reagent buffer was mixed with 1 µL of sample PCR and placed in a well on a 96 well plate. The Tapestation was set up and sample assessment performed according to manufacturer's instructions, and appropriate amplicon quality was confirmed when a single band at ~250 bp was observed. From each sample of the plate, 5 µL was taken and pooled for purification.

**Bead purification of pooled amplicons**

To remove salts and primer-dimers, purification of PCR amplicons was carried out using AMPure magnetic size selection beads (Beckman Coulter). A 100 µL aliquot from the pooled samples was taken, added to an equal volume of beads and incubated for 5 min at room temperature. The tube with beads was attached to a magnetic stand, and beads were washed twice with 200 µL 80% ethanol, before being left to air dry for 5 minutes. DNA was eluted with 35 µL water for 5 min at room temperature. The quality and integrity of the samples was ascertained as described above.

**Next Generation Sequencing**

Each dual indexed library plate pool was quantified using the Agilent Tapestation and the Qubit™ DNA assay kit for Qubit 3.0. Fluorometer (Life Technologies). The indexed pool was diluted to 1.2 pM for sequencing on a NextSeq instrument as per manufacturer's instructions. For GeCKOv2, the 400-cycle kit was used to generate paired end reads. For Brie, the 75-cycle high output kit was used to generate paired end reads. The fastq sequence output file from the run was used for analysis, where Read 2 is used to identify the second index of the dual indexed library. *Sequencing and sequence read generation*

*was performed by Dr. Stephen Wilcox (The Walter and Eliza Hall Institute Genomics Hub).*

**Analysis of CRISPR/Cas9 libraries**

The GeCKOv2 and Brie library data was processed using EdgeR (129) and MAGeCK (130). EdgeR uses a negative binomial generalized linear model to compensate for over dispersed count data which may have been introduced by independent library infections. First, Cutadapt (131) was used to trim the reads such that the Illumina adaptor was removed. MAGeCK "count" command was then used to gRNA count tables. This step includes median normalization and mean-variance modelling to account for any variations between replicates. To determine gRNA and gene enrichment, the MAGeCK "test" command was used with the default parameters. Significant enrichment of gRNAs in experimental samples relative to controls was determined by false discovery rate adjustment of P-values. Enriched gRNAs with a fold change ratio of $> 2$ and false discovery rate $< 0.01$ were considered hits. *EdgeR analysis was performed by Dr. Shani Amarasinghe (The Walter and Eliza Hall Institute.*

# Chapter 3 - Publication: The impact of Flt3-ITD mutation on dendritic cell function

This chapter is a manuscript that has been prepared for publication. The specific contributions of each author are disclosed in the "Preface" and "Publications arising from this thesis" sections.

## ABSTRACT

Dendritic cells play an important role in the initiation of immune responses. Their development is dependent on the FMS-like tyrosine kinase 3 (Flt3) receptor. Flt3-internal tandem duplication (ITD) is one of the most common mutations in acute myeloid leukemia. Here we have used wild type and Flt3-ITD expressing mice to characterize Flt3 in dendritic cells (DCs) and determine the impact of Flt3-ITD on DC function. Terminally differentiated wild type splenic DCs expressed high level of Flt3 at the cell surface and intracellularly, were responsive to Flt3 ligand (Flt3L) and altered Flt3 expression following activation. Mice harboring Flt3-ITD mutation possessed expanded splenic plasmacytoid DC (BST-2$^{+}$ CD11c$^{int}$), conventional DC1 (cDC1, CD11c$^{+}$ CD8$^{+}$ CD11b$^{-}$), cDC2 (CD11c$^{+}$ CD8$^{-}$ CD11b$^{+}$), double positive cDC1 (CD11c$^{+}$ CD8$^{+}$ CD11b$^{-}$ CD103$^{+}$ CD86$^{+}$), noncanonical cDC1 (CD11c$^{+}$ CD8$^{+}$ CD11b$^{-}$ CD103$^{-}$ CD86$^{-}$) and single positive cDC1 (CD11c$^{+}$ CD8$^{+}$ CD11b$^{-}$ CD103$^{-}$ CD86$^{+}$). Flt3-ITD splenic DCs had reduced cell surface Flt3 and constitutively activated intracellular Flt3. The impact of the Flt3-ITD mutation differed depending on the DC subset examined, with significant changes in DC markers including major histocompatibility complex class I (MHC I) and II (MHC II).

Critical DC functions including cytokine secretion, antigen uptake, proteolysis and endosomal pH were altered with significant outcomes for antigen presentation. Therefore, the Flt3-ITD mutation and constitutive Flt3 activation has important consequences for terminally differentiated DC function.

# INTRODUCTION

FMS-like tyrosine kinase 3 (Flt3) is a receptor expressed on hematopoietic progenitors and terminally differentiated dendritic cells (DCs). The receptor binds to Flt3 ligand (Flt3L) which is produced by hematopoietic and non-hematopoietic tissues, with $CD4^+$ T cells known to secrete high amounts of Flt3L (17). Upon Flt3L stimulation, Flt3 is activated (phosphorylated) and signals via the mitogen-activated protein kinase (MAPK) (22), phosphatidylinositol 3 kinase (PI3K) (23) and signal transducers and activators of transcription 3 (STAT3) pathways (24). Flt3-dependent activation of these pathways is critical for the development of DCs (1, 23, 24). When administered to mice (2, 3) or humans (29, 132), Flt3L expands DCs and their progenitors. Similarly, mice lacking Flt3 (*Flt3*$^{-/-}$) (30) or Flt3L (*Flt3L*$^{-/-}$) (31) show significant defects in hematopoiesis with reduced lymphoid (3, 31) and nonlymphoid (28) DCs.

A few years after the discovery of *Flt3*, mutations were identified in patients with acute myeloid leukemia (AML) and acute lymphoblastic leukemia (ALL) (133). The most common mutation is the Flt3 internal tandem duplication (Flt3-ITD) which occurs due to in-frame duplications of 3 to ≥ 400 bp in the Flt3 juxtamembrane domain (134). Unlike wild type Flt3, Flt3-ITD is constitutively active regardless of ligand stimulation (135–

138). Flt3-ITD constitutively signals through MAPK (135–138), PI3K (136, 138), STAT3 (139, 140) and STAT5 (135–138). Overall, the Flt3-ITD mutation is prognostically unfavorable, with reduced overall survival and increased risk of relapse observed in Flt3-ITD$^{+}$ patients in comparison to patients without the mutation (6).

To investigate the impact of the Flt3-ITD mutation, mice harboring a human ITD in the mouse *Flt3* gene have been generated (Flt3$^{ITD/ITD}$) (141). Bone marrow cells and splenocytes from these mice show increased Flt3 and STAT5 phosphorylation, indicative of increased Flt3 signaling. The mutation leads to splenomegaly, leukocytosis and monocytosis which has been attributed to increased survival and cell cycling of bone marrow progenitor cells (141). The mice rarely develop leukemia, indicating the need for additional genetic mutations for development of this disease (141). Flt3$^{ITD/ITD}$ mice have a cell-intrinsic gene-dosage dependent increase in conventional DCs (cDC) and plasmacytoid DC (pDC) in the bone marrow, spleen, lymph nodes and thymus (35). In addition, increased late DC progenitors are present in the bone marrow and spleen. The largest DC expansion is noncanonical cDC, also known as "Cx$_3$CR1$^{+}$ CD8$^{+}$" or "CD8 look-alike" DCs (35, 142, 143). These have characteristics of cDC and pDC populations and have been identified in humans as "Axl$^{+}$ Siglec6$^{+}$ (AS DC/DC5)" (144) and "pre-DC" (145). In humans, noncanonical DCs stimulate allogenic T cells (144, 145), however little is known about their antigen presentation capacity.

Analysis of Flt3$^{ITD/+}$ DC subsets identified induction of genes related to immune tolerance (35). It has been suggested that the ITD mutation promotes tolerance which may allow for leukemogenesis (35). In agreement, Flt3$^{ITD/+}$ mice have a cell-extrinsic expansion of

regulatory T cells (Tregs) and murine $Flt3^{ITD/+}$ splenocytes are able to expand allogeneic T cells to a greater extent than wild type splenocytes in mixed leukocyte reactions (35).

In this study, expression of Flt3 and Flt3-ITD was characterized in DCs and the impact of Flt3-ITD on specific parameters of DC function determined. We identify Flt3-ITD results in functional changes in DCs. Besides being significantly expanded *in vivo*, $Flt3^{ITD/ITD}$ DCs have altered cell surface phenotype, cytokine secretion, antigen uptake, proteolysis and endosomal pH culminating in alterations in antigen presentation.

# MATERIALS AND METHODS

## Mice

C57BL/6JArc, B6.CH-2$^{bm-1}$ (BM-1), OT-II (146) x Ly5.1 and OT-I (147) x Ly5.1, Flt3$^{ITD/ITD}$ (141), and *IA*$\alpha^{-/-}$ (148) were used at 6-12 weeks of age. All mice were bred and maintained in specific pathogen–free conditions at the Department of Biochemistry and Molecular Biology of The University of Melbourne. Experiments were done in accordance with the Institutional Animal Care and Use Committee guidelines of the University of Melbourne.

## Isolation of immune cells

Primary spleen DCs were isolated as previously described (120). In brief, organs were finely chopped and digested in the presence of Dnase I (Roche) and collagenase type 3 (Worthington Biochemicals). Intercellular clusters were disrupted by addition of 10 mM EDTA. Light density cells were isolated by density gradient separation in 1.077 g/cm$^3$ Nycodenz (Nycomed Pharma). Upper fractions were collected, washed and subject to further enrichment by resuspending in a depletion cocktail containing the following rat anti-mouse mAbs specific for: CD3 (KT3-1.1), CD90 (T24/31.7), red blood cells (Ter119), B220 (RA3-6B2), Ly6G (IA8). For purification of plasmacytoid DC, the upper fractions were incubated with rat anti-mouse mAbs specific for CD3 (KT3-1.1), Thy1 (T24/31.7), red blood cells (Ter119), Ly6G (IA8) and CD19 (ID3). Cells were incubated with antibodies, washed, and incubated with BioMag anti-rat IgG-coupled magnetic beads (Qiagen). The DC-enriched supernatant was recovered by magnetic separation. Where required, DC were sorted to purity by flow cytometry on a Becton Dickinson Influx (Murdoch Children's Research Institute Flow Cytometry and Imaging facility).

cDC1 were defined as $CD11c^+$ $CD8^+$ $CD11b^-$, cDC2: $CD11c^+$ $CD8^-$ $CD11b^+$, cDC1 double positive cDC1 (DP cDC1): $CD11c^+$ $CD8^+$ $CD11b^-$ $CD103^+$ $CD86^+$, double negative cDC1 (DN cDC1): $CD11c^+$ $CD8^+$ $CD11b^-$ $CD103^-$ $CD86^-$, or single positive cDC1 (SP cDC1) $CD11c^+$ $CD8^+$ $CD11b^-$ $CD103^+$ $CD86^+$.

For T cell isolation, single cell suspensions were generated from lymph nodes. Cells were stained with rat anti-mouse mAbs specific for: Cells were stained with rat anti-mouse mAbs specific for: CD11b (M1/70), F4/80 (F4/80), red blood cells (TER119), Ly6G/-Ly6C (RB68C5), MHCII (M5/114), CD45R (RA36B2) and CD4 (GK1.5) for $CD8^+$ T cells or CD8 (53-6.7) for $CD4^+$ cells. Cells were washed and incubated with BioMag anti-rat IgG-coupled magnetic beads (Qiagen). After magnetic depletion, the $CD4^+$ or $CD8^+$ T cell-enriched supernatant was recovered. Purity was determined by flow cytometry.

For B cell isolation, single cell suspensions were generated from spleens. Cells were resuspended in EDTA-BSS medium 2% (v/v) FCS and gradient centrifugation was carried out with Ficoll-Paque™ PLUS (GE Healthcare). Mononuclear cells were isolated and negative selection was carried out by incubating the cells with FITC-conjugated antibodies against CD4 (GK1.5), Ly76 (TER119) and CD43 (S7). Cells were washed and incubated with anti-FITC microbeads (Miltenyi Biotec). The B cell enriched supernatant was collected after separation with LS magnetic columns (Miltenyi Biotec). Purity was determined by flow cytometry.

Cells were stained with mAbs specific for CD8α (53-6.7), CD11b (M1/70), CD11c (N418), CD19 (6D5), CD24 (M1/69), CD40 (FGK45.5), CD45R/B220 (RA3-6B2),

CD80 (16-10A1), CD86 (GL1), CD135/Flt3 (A2F10), CD172 (Sirpα), CD205/DEC205 (NLDC-145), CD274/PD-L1 (10F.9G2), CD317/BST2 (927), CD370/Clec9A (7H11), H-2Kb (AF6-8815), IgD (11-26c.2a), IgM (RMM-1), SiglecH (551), XCR1 (ZET) (all BioLegend). To obtain absolute cell numbers, an internal microsphere counting standard (BD Biosciences) was used. Analysis was performed with a Becton Dickinson LSRFortessa, FlowJo and Graphpad Prism software.

**Immunoprecipitation**

cDCs from wild type (+/+), heterozygote (+/ITD) or homozygote (ITD/ITD) littermates were isolated and stimulated in 100 ng/mL Flt3L in complete RPMI at 37ºC and 10% $CO_2$ for 0, 10 or 30 minutes. Cells were washed and lysed in 0.5% NP-40, 50 mM Tris-HCl pH 7.4, 5 mM $MgCl_2$ and cOmplete™ protease inhibitor cocktail (Roche). The lysate was pre-cleared with protein G-sepharose beads (WEHI Antibody Facility) and normal rat and mouse serum (WEHI Antibody Facility). Flt3 was precipitated with anti-Flt3 (AF768, R&D systems) antibody and protein-G sepharose beads. Proteins were eluted with reducing SDS sample buffer and analyzed by SDS-PAGE and immunoblotting.

**Immunoblotting**

Immune populations were isolated as previously described and cells were lysed in 0.5% NP-40, 50 mM Tris-HCl pH 7.4, 5 mM $MgCl_2$ and cOmplete™ protease inhibitor cocktail (Roche). Post-nuclear lysates were resolved by SDS-PAGE using 8% Bolt Bis-Tris Mini Protein Gels (Invitrogen) and proteins were transferred to Immunoblot PVDF membranes (Bio-Rad). Membranes were stained with primary antibodies against Flt3 (AF768, R&D systems), phosphorylated tyrosine (4G10, Sigma-Aldrich), actin (A5060, Sigma-Aldrich) or tubulin (DM1A, Abacm) followed by HRP-conjugated secondary antibodies.

**DC activation**

For *in vitro* activation assays, DCs were isolated and incubated overnight in complete RPMI with or without 0.5 μM CpG 1668 ODN (Bioneer) at 37ºC or 4ºC. For *in vivo* activation assays, mice were injected intravenously with 0.2 μM CpG or PBS.

**Cytokine secretion**

Splenic DC populations were isolated and cell sorted to purity. 1 x $10^5$ cells were incubated in the presence of 0.5 μM CpG, 50 ng/mL interferon gamma (Peptrotech) and 20 ng/mL granulocyte-macrophage colony-stimulating factor (GM-CSF, Peprotech). Supernatants were collected 18 hours later and stored at -20°C. Cytokine secretion was determined using the BD Cytometric Bead Array Mouse Inflammation kit according to the manufacturer's instructions (BD Biosciences).

***In vitro* antigen presentation assay**

Single cell suspensions were generated from lymph nodes of OT-I or OT-II mice and T cells were purified as previously described. Cells were washed with PBS 0.1% bovine serum albumin (BSA) and labelled with CellTrace Violet (CTV). Splenic wild type or ITD/ITD DC populations were isolated and cell sorted to purity as previously described. For antigen presentation with soluble OVA, 2.5 x $10^4$ DC were incubated with 100 μg/mL OVA (Worthington Biochemical) and 0.5 μM CpG at 37ºC and 10% $CO_2$. Cells were washed before plating with 5 x $10^4$ OT-I or OT-II cells in complete RPMI and 20 ng/mL GM-CSF (Peprotech). For OVA-coated splenocytes, single cell suspensions were generated from BM-1 (for OT-I) or IA$\alpha^{-/-}$ (for OT-II) mice. Red blood cells were lysed and splenocytes were incubated with 10 mg/mL ovalbumin (Sigma) in KDS-RPMI at 37ºC and washed. 2 x $10^5$ OVA-coated splenocytes were incubated with 2.5 x $10^4$ DC

and 5 x $10^4$ OT-I or OT-II cells in complete RPMI and 20 ng/mL GM-CSF (Peprotech). For both soluble OVA and OVA-coated splenocyte, cells were incubated for three days and stained with mAbs specific for CD8 (53-6.7, BioLegend) or CD4 (GK1.5; Walter and Eliza Hall Antibody Facility). The number of divided OT-II and OT-I was determined as the number of $CD4^+$ or $CD8^+$ $Ly5.1^+$ cells that had undergone CTV dilution. To obtain absolute cell numbers, an internal microsphere counting standard (BD Biosciences) was used.

**Antigen uptake, proteolysis and endosomal pH analyses**

To assess antigen uptake, 5 x $10^4$ purified DC were incubated with 50 μg/mL ovalbumin-Cy5 in complete medium for 0 – 90 minutes at 37°C. DCs were washed and the fluorescence measured by flow cytometry. As a control, DCs were pulsed with ovalbumin-Cy5 for 90 min at 4°C. To assess antigen proteolysis and endosomal pH, 2.5 x $10^5$ purified DCs were incubated with 20 μg/mL DQ-OVA (Life Technologies) or dextran-pHrodo for 15 min at 37°C. Cells were washed, resuspended in complete RMPI and chased for the indicated time. At each time point, cells were kept on ice and the fluorescence was measured by flow cytometry. As a control, DCs were pulsed with DQ-OVA or dextran-pHrodo for 15 min at 4°C. The signal was calculated for the 37°C chase time point by subtracting the gMFI at 4°C.

# RESULTS

**Flt3 expression by wild type splenic DCs.**

First, we investigated Flt3 expression in splenic immune cells. In agreement with previous studies (10, 27), cell-surface Flt3 was detected on splenic cDC1, cDC2 and pDC, but not T or B lymphocytes, with highest expression by cDC1, known to preferentially expand in response to Flt3L (149, 150) (**Figure 1A**). Total Flt3 protein expression was determined for purified cell populations with two forms of Flt3 detected by immunoblotting, similar to non-DC cell lines (151, 152) (**Figure 1B**). The higher molecular weight (MW, approximately 160 kDa) species is likely cell surface Flt3, given its slower migration due to being highly glycosylated, while the lower MW (approximately 130 kDa) band is likely intracellular Flt3. Flt3 was only detected by immunoblot in cells displaying it at the cell surface; cDC1, cDC2 and pDC. The detected pattern of Flt3 varied between DC populations, with pDC expressing a higher MW species of cell surface Flt3 than cDC1 or cDC2. To examine how Flt3L impacts DC Flt3, primary murine splenic DCs were isolated and stimulated with Flt3L (100 ng/mL) for 1 hour and cell surface Flt3 expression was determined by flow cytometry. Flt3 was significantly reduced on both cDC subsets following *in vitro* Flt3L stimulation (**Figure 1C**).

Flt3 expression during DC activation was characterized. Splenic DCs were purified and activated *in vitro* with toll-like receptor 9 (TLR9) agonist CpG 1668 ODN (Class B, 0.5 uM). Flt3 protein detected by immunoblotting showed an increase in intensity for the higher MW Flt3, and a loss of the lower MW Flt3, following CpG treatment (**Figure 1D**).

In agreement, elevated surface Flt3 was detected by flow cytometry (**Figure 1E**). To investigate if this was also the case following DC activation *in vivo*, mice were injected intravenously (IV) with CpG (0.2 μM) or PBS. DCs were purified one day later and Flt3 expression determined by flow cytometry (**Figure 1F**). In contrast to *in vitro* DC activation, a significant reduction in cell surface Flt3 was observed following administration of CpG. A short time course, with spleens harvested from mice 0 – 4 hours after CpG IV injection showed surface Flt3 loss by cDC1 as rapidly as one hour after CpG administration, while cDC2 displayed the first signs of surface Flt3 reduction four hours following CpG administration (**Figure 1G**). In all experiments, increased CD86 was used as a positive control for DC activation (**Figure 2**). Together, this data demonstrates that splenic DCs express and regulate Flt3 at steady state. Furthermore, splenic DCs regulate Flt3 during activation, with increased Flt3 observed on splenic DCs treated with CpG *in vitro* and reduced Flt3 observed on splenic DCs isolated from mice CpG-treated mice.

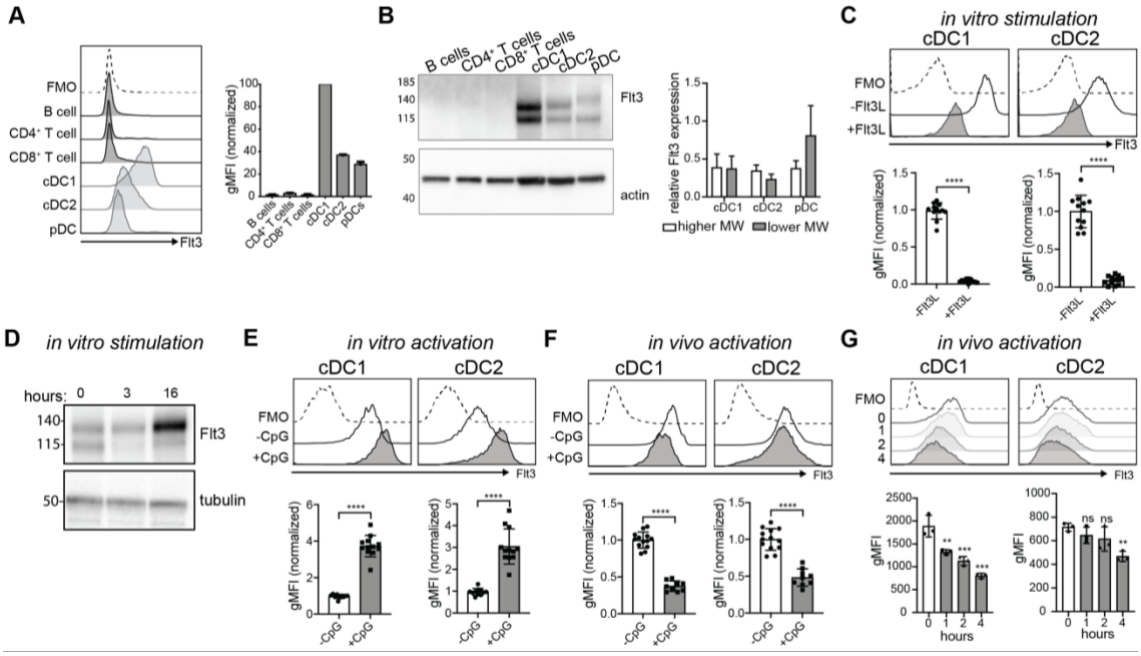


**Figure 1. Flt3 expression by splenic DCs.** (A) Representative histograms and quantification of surface Flt3 on splenocytes as determined by flow cytometry. Data is pooled from 2 independent experiments, with 2 spleens pooled in each experiment. The gMFI has been normalized to the maximum signal for each cell type. Bars are mean + SEM. (B) Purified cells were analyzed by immunoblotting and probed with anti-Flt3 (A2F10) or anti-actin (A5060) antibodies. Blot is representative of 3 independent experiments. Band intensities of the higher molecular weight (MW) species and lower MW Flt3 were quantified relative to actin. Bars are mean + SEM. (C) Splenic DCs were isolated and stimulated with (+) or without (–) Flt3L (100 ng/mL) for 1 hour at 37°C. Flt3 surface expression was determined by flow cytometry. Histograms are representative of three independent experiments. Symbols represent individual mice. Bars are mean ± SD, unpaired t-test. **** P <0.0001 (D) Splenic DCs were isolated and stimulated for 0, 3 or 16 hours with CpG 1668 ODN (0.5 μM) at 37°C. Cell lysates were examined by immunoblotting and probing with anti-Flt3 (A2F10) or anti-tubulin (DM1A) antibodies. Blot is from one experiment. (E) Splenic DCs were isolated and stimulated overnight with (+) or without (–) CpG 1668 ODN (0.5 μM) at 37°C. (F) Mice were injected intravenously with PBS (-CpG) or CPG 1668 ODN (0.2 μM) and spleens were harvested one day later or (G) at indicated times. (E-G) Surface expression of Flt3 was determined by flow cytometry. Histograms show representative surface expression. Symbols represent individual mice. (E, F) Data is from at least 3 independent experiments with the gMFI signal normalized to the maximum gMFI signal. Bars

are mean ± SD, unpaired t-test, **** P <0.0001. (G) Data is from one experiment. Bars are mean ± SD, one-way ANOVA with Dunnett's multiple comparisons test. *** P <0.001** P <0.01, ns not significant.

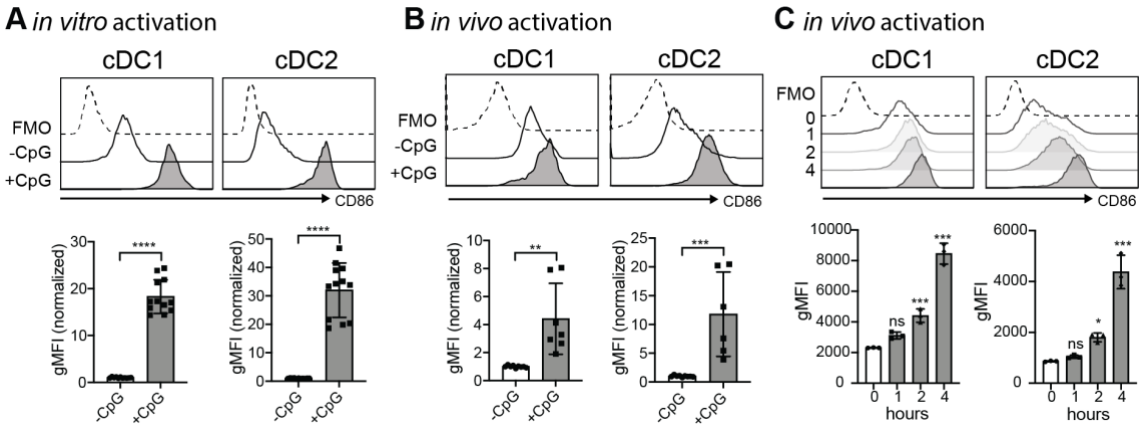


**Figure 2. Splenic DC upregulate CD86 following CpG activation.** (A) Splenic DCs were isolated and stimulated overnight with (+) or without (–) CpG 1668 ODN (0.5 μM) at 37°C. (B) Mice were injected intravenously with PBS (-CpG) or CPG 1668 ODN (0.2 μM). Spleens were harvested one day later. (C) Mice were injected intravenously with PBS or CPG 1668 ODN (0.2 μM). (A-C) Cell surface expression of CD86 was determined by flow cytometry. Histograms are representative cell surface expression. (A-B) Data is from at least 2 independent experiments; symbols represent individual mice. Bars are mean ±SD, unpaired t-test. ****P <0.0001 ***P <0.001 **P <0.01. (C) Data is from one experiment. Bars are mean ± SD, one-way ANOVA with Dunnett's multiple comparisons test. *** P <0.001 *P <0.05, ns not significant.

## Flt3-ITD expands canonical and noncanonical splenic DC populations.

DC populations were analyzed in $Flt3^{+/+}$ and $Flt3^{ITD/ITD}$ littermates. Canonical cDC1 and cDC2 were analyzed in addition to cDC1 subpopulations including noncanonical cDC1 identified as $CD103^{-}$ $CD86^{-}$ (hereafter referred to as NC) (142) and two populations of canonical cDC1; $CD103^{+}$ $CD86^{+}$ ("DP cDC1") and $CD103^{-}$ $CD86^{+}$ ("SP cDC1"). All DCs were significantly increased in $Flt3^{ITD/ITD}$ mice, in agreement with previous studies (35). Specifically, $Flt3^{ITD/ITD}$ cDC1, cDC2 and pDC were expanded 8.3, 4.1 and 4.2-fold

respectively. For $Flt3^{ITD/ITD}$ cDC1 populations, a 12.8-fold increase in NC cells, 14.8-fold increase in DP cDC1 and 2.7-fold increase in SP cDC1 was observed (**Figure 3A**).

A gene-dosage dependent decrease in surface Flt3 was detected for $Flt3^{ITD/ITD}$ cDC1, cDC2 and pDC (35, 152) (**Figure 3B**). Total Flt3 protein and Flt3 tyrosine phosphorylation status was examined following *in vitro* Flt3L (100 ng/mL) stimulation and Flt3 immunoprecipitation. Unlike $Flt3^{+/+}$ DC, only lower MW (intracellular) Flt3 was detected in $Flt3^{ITD/ITD}$ cDC. Increased Flt3 tyrosine phosphorylation was observed for surface (higher MW) $Flt3^{+/+}$, while $Flt3^{+/ITD}$ and $Flt3^{ITD/ITD}$ DCs exhibited ligand-independent tyrosine phosphorylation of intracellular (lower MW) Flt3. Surface Flt3 in heterozygous $Flt3^{+/ITD}$ DCs was still responsive to Flt3L, with delayed phosphorylation (**Figure 3C**).

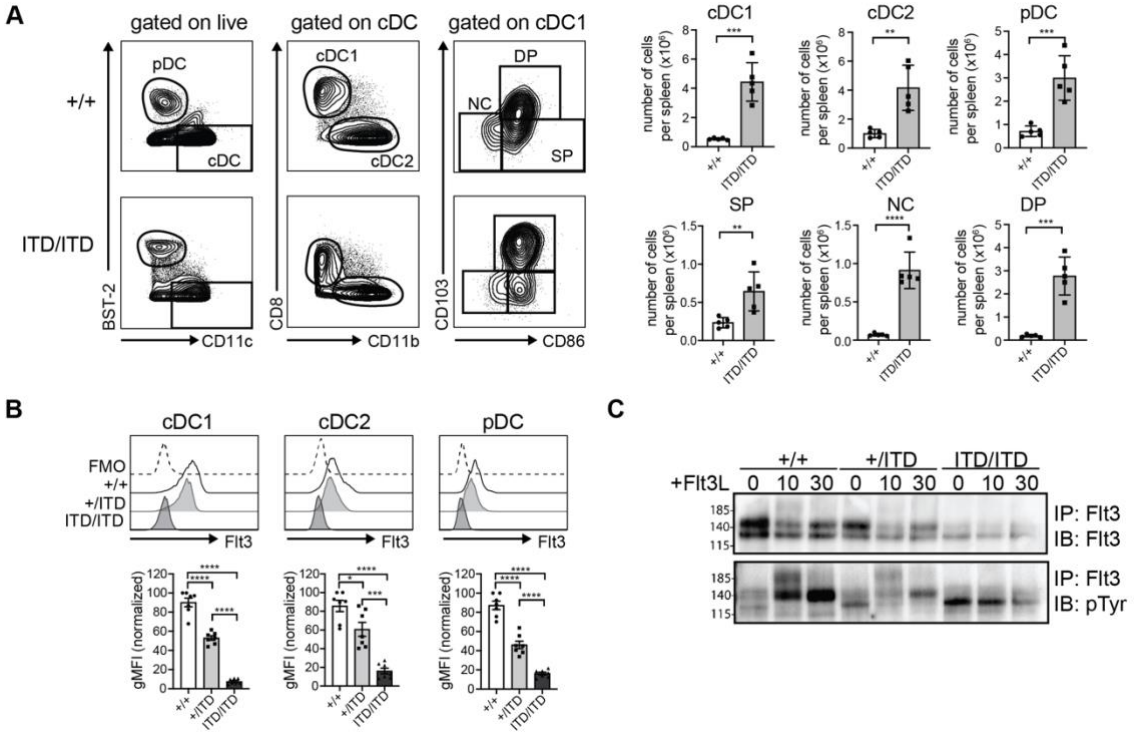


**Figure 3. Flt3-ITD expands splenic DC populations.** (A) Representative gating used to identify $Flt3^{+/+}$ and $Flt3^{ITD/ITD}$ splenic pDC (BST-$2^{+}$ $CD11c^{int}$), cDC1 ($CD11c^{+}$ $CD8^{+}$ $CD11b^{-}$), cDC2 ($CD11c^{+}$ $CD8^{-}$ $CD11b^{+}$), DP cDC1 ($CD11c^{+}$ $CD8^{+}$ $CD11b^{-}$ $CD103^{+}$ $CD86^{+}$), NC cDC1 ($CD11c^{+}$ $CD8^{+}$ $CD11b^{-}$ $CD103^{-}$ $CD86^{-}$) and SP cDC1 ($CD11c^{+}$ $CD8^{+}$ $CD11b^{-}$ $CD103^{-}$ $CD86^{+}$). Quantification of $Flt3^{+/+}$ and $Flt3^{ITD/ITD}$ splenic DC populations. Symbols represent individual mice; data is from one experiment. Bars represent mean ± SEM, unpaired t test, **** P <0.0001*** P <0.001** P <0.01. (B) Splenic DC were isolated from $Flt3^{+/+}$, $Flt3^{+/ITD}$ and $Flt3^{ITD/ITD}$ littermates and surface Flt3 expression was determined by flow cytometry. Data is pooled from 2 independent experiments, with symbols representing individual mice. gMFI has been normalized to the maximum signal for each cell type. Bars represent mean ± SEM, one-way ANOVA with Dunnett's multiple comparisons test, **** P <0.0001*** P <0.001* P <0.05. (C) Spleens from $Flt3^{+/+}$, $Flt3^{+/ITD}$ and $Flt3^{ITD/ITD}$ littermates were harvested and cDCs isolated. Cells were stimulated with Flt3L (100 ng/mL) for the indicated times at 37ºC. Cells were lysed and Flt3 was subsequently immunoprecipitated using anti-Flt3 antibody (A2F10). Immunoprecipitates were analyzed by immunoblot probed with anti-Flt3 (A2F10) or anti-phospho-tyrosine (4G10) antibodies. Blot is representative of 2 independent repeats.

**Flt3-ITD alters the cell surface phenotype of splenic DCs.**

To characterize how Fl3-ITD impacts DC function, cell surface levels of classical DC markers were investigated. Integrins or adhesion molecules (CD11c, CD11b, CD103, CD24), phenotypic molecules (CD8), inhibitory receptors (signal-regulatory protein α, SIRPα), MHC molecules (MHC I and II), costimulatory molecules (CD86, CD80, CD40 and CD24), co-inhibitory molecules (PD-L1), chemokine receptors (XCR1) and endocytic receptors (DEC205, Clec9A, Clec12A) were analyzed. Significantly increased surface expression of MHC I, MHC II, CD103 was observed on most $Flt3^{ITD/ITD}$ DC subsets. This was accompanied by lower CD11c, CD8, Clec9A, DEC205 and PD-L1 and varied expression of Clec12A. While $Flt3^{+/+}$ cDC2 do not express Clec12A, it was detected at the surface of $Flt3^{ITD/ITD}$ cDC2. Confirming genetic profiling of $Flt3^{+/+}$ NC DCs (142), these cells had reduced surface CD103, DEC205 and CD86, in addition to reduced Clec9A, MHC II and CD40 in comparison to other $Flt3^{+/+}$ DC subsets (**Figure 4**).

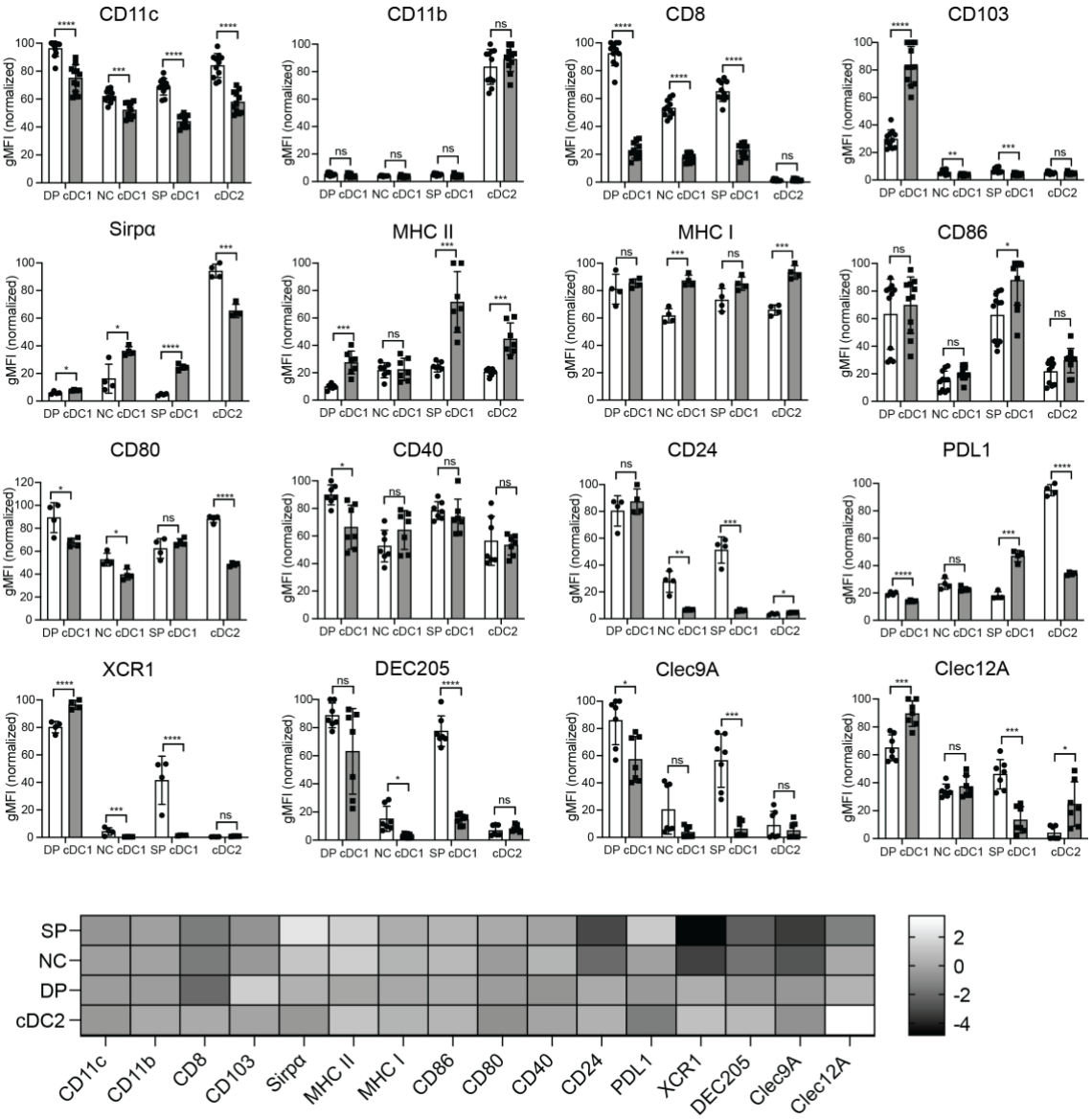


**Figure 4. Flt3-ITD alters splenic DC surface expression.** $Flt3^{+/+}$ (white bars) and $Flt3^{ITD/ITD}$ (grey bars) splenic DCs were stained for surface markers and analyzed by flow cytometry. gMFI has been normalized to the maximum gMFI signal. Data is pooled from at least 2 independent experiments, with symbols representing individual mice. Bars are mean ± SD, multiple unpaired t-tests with Holm-Sidak multiple comparisons test. **** P <0.0001*** P <0.001** P <0.01 * P <0.05, ns not significant. Heat map of surface marker expression of spleen cDC1 or cDC2 isolated from $Flt3^{+/+}$ and $Flt3^{ITD/ITD}$ mice. The log2 ratio of mean gMFI of $Flt3^{ITD/ITD}$ cells relative to mean gMFI of $Flt3^{+/+}$ cells is shown. Data pooled from at least 2 independent experiments.

**Flt3-ITD impacts DC antigen uptake and proteolysis.**

$Flt3^{ITD/ITD}$ DC antigen uptake, endosomal pH and proteolysis were assessed. Ideally, DP, NC and SP cDC1 would be isolated for both $Flt3^{+/+}$ and $Flt3^{ITD/ITD}$ mice, however the low number of cDC1 subpopulations in $Flt3^{+/+}$ mice meant this was not feasible. Therefore, $Flt3^{ITD/ITD}$ DP, NC and SP cDC1 were compared to $Flt3^{+/+}$ cDC1, while $Flt3^{ITD/ITD}$ were compared to $Flt3^{+/+}$ cDC2.

First antigen uptake was examined. DCs were incubated with ovalbumin (OVA)-Cy5 for 15 and 90 mins or dextran-A647 for 15 mins and the intracellular fluorescence was determined by flow cytometry. Overall, similar uptake of either OVA protein or dextran was observed for $Flt3^{+/+}$ and $Flt3^{ITD/ITD}$ cDC1 populations, although $Flt3^{ITD/ITD}$ DP cDC1 showed a trend towards reduced uptake compared to the other subsets (**Figure 5A**). In contrast, OVA protein and dextran uptake by $Flt3^{ITD/ITD}$ cDC2 was significantly elevated compared to $Flt3^{+/+}$ cDC2 at all time points (**Figure 5B**). To investigate $Flt3^{ITD/ITD}$ cDC2 in more detail, their ability to undertake antigen proteolysis was examined using a self-quenched form of OVA which fluoresces as it degrades (DQ-OVA). Purified DCs were pulsed with DQ-OVA, excess antigen removed and DCs examined by flow cytometry at the indicated time points. OVA-Cy5 was used to normalize for the increased uptake of DQ-OVA by $Flt3^{ITD/ITD}$ cDC2 compared to $Flt3^{+/+}$ cDC2. $Flt3^{ITD/ITD}$ cDC2 showed more rapid DQ-OVA proteolysis with the signal plateauing at 30 mins as compared to 60 or 90 mins for $Flt3^{+/+}$ cDC2 (**Figure 5C**). This was accompanied by reduced endosomal pH for $Flt3^{ITD/ITD}$ cDC2 as detected by the pH sensitive probe, dextran-pHrodo which increases fluorescence as the pH decreases.

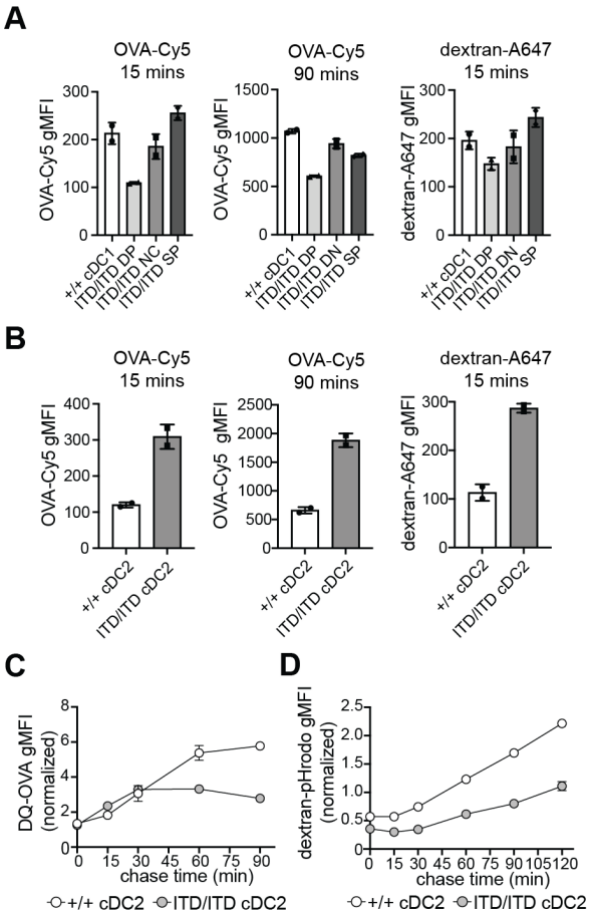


**Figure 5. Flt3-ITD impacts splenic DC antigen uptake and proteolysis.** Purified $Flt3^{+/+}$ and $Flt3^{ITD/ITD}$ (A) cDC1 and (B) cDC2 populations were incubated at 37ºC with 50 μg/mL OVA-Cy5 or 20 μg/mL Dextran-A647 for the indicated times. Cells were washed and the intracellular fluorescence was determined by flow cytometry. Data is representative of two independent experiments, each carried out in technical duplicate. Bars are mean ± SD. (C-D) Purified $Flt3^{+/+}$ and $Flt3^{ITD/ITD}$ cDC2 were pulsed with **(C)** 20 μg/mL DQ-OVA or (D) 20 μg/mL Dextran-pHrodo for 15 mins at 37ºC. Cells were washed before being chased for the indicated times at 37ºC. DQ-OVA and Dextran-pHrodo gMFI was determined by flow cytometry. The gMFI signal for DQ-OVA or Dextran-pHrodo is normalized to the OVA-Cy5 or Dextran-A647 gMFI for the pulse time (15 mins). Data is representative of two independent experiments, each carried out in technical duplicate. Error bars are ± SD. (A-D) Second biological replicate shown in Supplementary Figure 2A-D.

**Flt3-ITD DCs have altered cytokine secretion.**

To assess cytokine secretion by $Flt3^{+/+}$ and $Flt3^{ITD/ITD}$ DCs, cells were sorted to purity and equal numbers of DC populations incubated with CpG and inflammatory cytokines IFNγ and GM-CSF, conditions that elicit maximal DC IL-12 production (153). Supernatants were harvested after 18 hours and concentrations of IL-6, IL-10, IL-12p70, TNF-α and MCP-1 measured using the BD Cytometric Bead Array Assay. IL-10 and MCP-1 were not detected by cDC1 or cDC2, and IL-12 was only detected for cDC1. Robust cytokine secretion was observed for $Flt3^{+/+}$ cDC1 and $Flt3^{ITD/ITD}$ DP cDC1. In contrast, $Flt3^{ITD/ITD}$ NC cDC1 produced significantly reduced IL-6, TNF-α and IL-12 in comparison to other DC subsets. Similarly, $Flt3^{ITD/ITD}$ SP cDC1 produced reduced amounts of TNF-α and IL-12 (**Figure 6A**). For cDC2, $Flt3^{ITD/ITD}$ DCs produced increased amounts of IL-6 and similar amounts of TNF-α in comparison to $Flt3^{+/+}$ DC (**Figure 6B**).

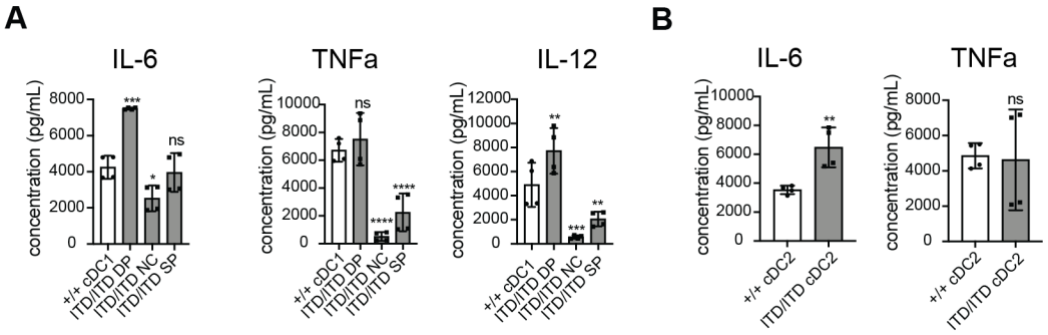


**Figure 6. Flt3-ITD impacts splenic DC cytokine secretion.** $Flt3^{+/+}$ and $Flt3^{ITD/ITD}$ splenic cDC1 (A) and cDC2 (B) populations were isolated and cell sorted to purity. Equal number of cells were incubated with 0.5 μM CpG, 50 ng/mL IFNγ and 20 ng/mL GM-CSF. Supernatants were collected 18 hours later, and cytokine secretion determined using BD™ Cytometric Bead Array (CBA) Mouse Inflammation Kit. Data is pooled from two independent experiments, carried out in duplicate. Bars are mean ± SD, one-way ANOVA with Dunnett's multiple comparisons test. **** P <0.0001*** P <0.001** P <0.01 * P <0.05, ns not significant.

**Flt3-ITD impacts DC antigen presentation.**

Next the antigen presenting capabilities of $Flt3^{ITD/ITD}$ DC subsets were investigated. Due to the expansion of DCs (**Figure 3**) and regulatory T cells in $Flt3^{+/ITD}$ mice (35) *in vitro* antigen presentation assays were performed with direct comparisons of equal numbers of $Flt3^{+/+}$ versus $Flt3^{ITD/ITD}$ DCs. Spleens were harvested and DCs isolated by sorting to purity by flow cytometry. DCs were incubated with CellTrace-Violet (CTV)-labelled OT-I (**Figure 7A)** or OT-II (**Figure 7B)** cells in the presence of cell-associated ovalbumin (OVA) (splenocytes pulsed with OVA protein) or OVA protein alone. T cell proliferation was determined three days later. cDC1 subsets cross-present cell-associated OVA (154) whereas both cDC1 and cDC2 are capable of cross-presenting soluble ovalbumin *in vitro* (155). A significant defect in cross-presentation of cell-associated OVA was observed for $Flt3^{ITD/ITD}$ NC cDC1 in comparison to $Flt3^{+/+}$ cDC1, while only minor changes were observed for MHC I presentation of OVA protein (**Figure 6A**). In contrast, Flt3-ITD largely improved MHC II antigen presentation for both antigens tested, with increased OT-II T cell proliferation observed for $Flt3^{ITD/ITD}$ NC, SP and cDC2 in response to cell-associated OVA, and increased presentation of OVA protein by $Flt3^{ITD/ITD}$ NC and SP DCs (**Figure 7B**). Together, this data demonstrates that the Flt3-ITD mutation alters antigen presentation by both MHC I and MHC II.

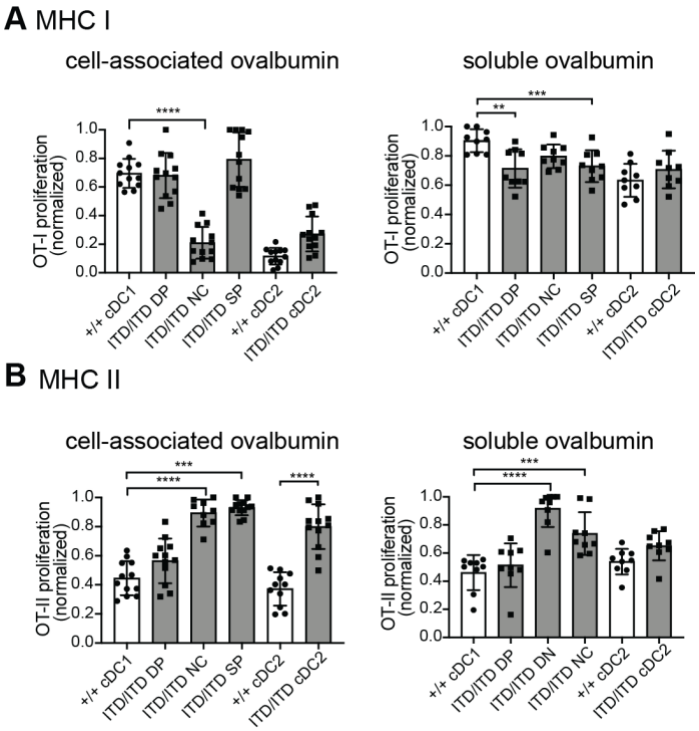


**Figure 7. Flt3-ITD impacts DC antigen presentation.** Equal numbers of purified $Flt3^{+/+}$ and $Flt3^{ITD/ITD}$ DC populations were incubated with purified CellTrace Violet (CTV)-labelled OT-I **(A)** or **(B)** OT-II cells in the presence of ovalbumin (OVA)-coated splenocytes (OCS) or 100 μg/mL OVA. Three days later, antigen presentation capacity was assessed by flow cytometric analysis. T cell proliferation was normalized to the maximum proliferation. Each symbol represents an individual mouse with data pooled from at least two independent experiments, displayed as mean ± SEM. **** P <0.0001*** P <0.001** P <0.01, one-way ANOVA with Dunnett's multiple comparisons test.

# DISCUSSION

Flt3 is one of the most common mutations in hematological malignancies, with Flt3-ITD representing the most common form of the mutation. In addition to being expressed in leukemia blasts, Flt3-ITD is expressed in DCs of AML patients and is correlated with poor prognosis (156, 157). The impact of this mutation in DC has remained unclear. In this study we investigated the expression pattern of Flt3 in DCs and determined the impact of Flt3-ITD on DC number, phenotype and function.

In agreement with previous studies (10, 27), we identified Flt3 expression by WT splenic cDC and pDC populations. For the first time, we have shown cell surface and total Flt3 protein in primary cDC1, cDC2 and pDC. Interestingly, surface Flt3 in pDC migrates slower than in cDC1 and cDC2. There are no described isoforms for murine Flt3, therefore it unlikely that pDC express an alternative Flt3. Flt3 is N-linked glycosylated (151, 152) and the larger form observed in pDC likely represents Flt3 that is more heavily decorated with carbohydrate moieties. Future experiments are required to fully characterize Flt3 biochemistry in pDC. Here we show Flt3 expression is regulated during splenic DC activation, with upregulation of surface Flt3 once activated *in vitro*. In contrast, surface Flt3 is reduced when splenic cDCs are activated by inflammatory stimuli *in vivo*. It is likely that the *in vivo* reduction of DC surface Flt3 is due Flt3L being released from immune cells in response to TLR stimulation. Previous studies have showed increased serum Flt3L in this scenario (158) that would engage and downregulate Flt3. Flt3/Flt3L signaling promotes survival of terminally differentiated DCs, with increased apoptosis observed in BMDC treated with Flt3 tyrosine-kinase inhibitors (159). Therefore, upregulation of surface Flt3 during inflammation, as evidenced under *in vitro*

conditions, could increase DC responsiveness to Flt3L, and promote their survival and immunogenic potential *in vivo*.

In mice harboring the Flt3-ITD mutation, reduced surface Flt3 expression by splenic DCs was observed, accompanied by reduced Flt3L responsiveness. This is in agreement with previous studies demonstrating reduced Flt3L responsiveness in $Flt3^{+/ITD}$ and $Flt3^{ITD/ITD}$ bone marrow cells (35). While less responsive to Flt3L, $Flt3^{ITD/ITD}$ DCs undergo Flt3L-independent Flt3 signaling leading to significantly increased numbers of splenic cDC and pDC populations in $Flt3^{ITD/ITD}$ mice.

Our data demonstrates the Flt3-ITD mutation leads to aberrant splenic DC phenotype and function. Under normal conditions, Flt3 carries out ligand-dependent signaling via STAT3 and PI3K which are critical to DC homeostasis (1, 23, 24). Flt3-ITD, however, is constitutively activated and continuously activates STAT3 (139, 140) and PI3K (136, 138), in addition to unique targets such as STAT5 (135–138). Given homeostasis of DCs is tightly controlled, differences in signaling downstream of Flt3, or its duration, likely leads to atypical DCs. Here, for the first time, we performed functional analysis of $Flt3^{ITD/ITD}$ DC and their capacity to elicit antigen presentation and T cell priming. Flt3-ITD DCs displayed elevated surface MHC I and MHC II, in addition to increased antigen uptake and more rapid antigen proteolysis and lower endosomal pH for $Flt3^{ITD/ITD}$ cDC2. These changes led to improved MHC II presentation of cell-associated antigen by these cells. Flt3-ITD promotes basal autophagy in cancer cell lines (non-DC) and Flt3-$ITD^{+}$ patient samples, while inhibition or knockdown of Flt3-ITD reduces autophagic flux (160). This may account for the elevated $CD4^{+}$ T cell priming since LC3-associated

phagocytosis (LAP) and autophagy contribute to MHC II presentation (161). Future experiments investigating autophagy in $Flt3^{ITD/ITD}$ DCs are of interest. In contrast to MHC II antigen presentation, MHC I cross-presentation of both cell-associated and soluble OVA was largely unchanged and for $Flt3^{ITD/ITD}$ NC cDC1, reduced. Since cytochrome C insensitivity has been previously described for WT NC cDC1 (142), this defect may be cell-intrinsic. Indeed, our data has extended investigations of the functional role of NC cDC1. In humans, these DCs have been shown to stimulate allogenic T cells (144, 145) while in mice it has been suggested they cannot cross-present (142). Here for the first time, we have shown that NC cDC1 cannot cross-present cell-associated OVA but are capable of cross-presenting soluble ovalbumin. Importantly this defect in cell-associated cross presentation, in addition to our observation that Flt3-ITD NC cDC1 have impaired IL-12 production could stem from their reduced DEC205 expression. DCs from mice lacking DEC205 show reduced responsiveness to CpG (162) and as a result have impaired DC maturation and IL-6 and IL-12 secretion.

Importantly, the largest expansion of DCs in Flt3-ITD mice is NC cDC1, in agreement with previous studies (35). This differs to outcomes when Flt3L is administered to $Flt3^{+/+}$ mice, which expands canonical cDC1 populations (35, 142). Given NC cDC1 lack features of canonical cDC1, such as cross-presentation of cell associated antigen and IL-12 production, it is possible that these DCs promote leukemogenesis in Flt3-ITD mice by impairing detection of leukemic cells. Further studies are required to elucidate the biological function of these cells in steady state settings.

In conclusion, we have demonstrated significant changes to the biology of DC expressing Flt3-ITD. Mice expressing Flt3-ITD have expanded numbers of splenic DCs with altered cell surface phenotype, including increased MHC expression. DCs expressing Flt3-ITD have increased pro-inflammatory cytokine secretion and improved MHC II antigen presentation of cell-associated antigen. This data highlights the need to characterize the phenotype and function of human DC in Flt3-ITD$^{+}$ patients to assess their contribution to leukemogenesis.

# Chapter 4 - Uncovering the molecular machinery that regulates Flt3

Sections of this chapter were published in Immunology & Cell Biology (2021). The specific contributions of authors are disclosed in the "Preface" and "Publications arising from this thesis" sections of this thesis. The published manuscript can be found in Appendix 1.

## Introduction

DCs are critical for immunotherapy (7). They have a unique ability to capture, process and present antigen to T cells within the tumor microenvironment and at the draining lymph nodes (37, 38, 40). Whilst DCs are the rarest tumor infiltrating immune cells (37, 38), there is a strong correlation between their abundance (or transcript abundance) and immune outcomes (5, 38, 39). Since the number of DCs at steady state (1–4), and in the tumor microenvironment (5), is reliant on the Flt3/Flt3L signaling cascade, manipulation of this pathway is an attractive solution to increase DC numbers and improve immunotherapy outcomes. Most studies have focused on the administration of Flt3L, however little therapeutic benefit has been observed in clinical trials. In the previous chapter, it was demonstrated that DCs carefully regulate Flt3 expression. Indeed, differences in the expression level of Flt3 were observed between different DC subsets and different DC states (for example, resting and activated). Therefore, an alternative, and largely neglected, approach is to manipulate the regulation of Flt3 itself. For this to occur, however, more knowledge about the regulation of Flt3 is required. In Chapter 4,

this is directly addressed by using CRISPR/Cas9 genome wide screens to elucidate the genes that could be potentially targeted to control Flt3 expression.

**Transcriptional regulation of Flt3**

*Flt3* is regulated by several transcription factors. In DC progenitors, including common myeloid, lymphoid and DC progenitors, the transcription factor PU.1 (*Sfpi1*) promotes *Flt3* expression by directly binding to the *Flt3* promoter (163). As a result, progenitors lacking this transcription factor have reduced DC developmental potential. *Flt3* expression is also enhanced by the transcription factor homeobox A9 (HOXA9), which has been shown to bind directly to the promoter of *Flt3* (164). While mice lacking HOXA9 have reduced $Flt3^+$ progenitors, there are no changes to the DC lineage, indeed the number of bone marrow cDC and plasmacytoid DC (pDC) are unaltered (165). It is unknown if HOXA9 maintains the steady-state level of Flt3 in terminally differentiated DCs. *Flt3* is also enhanced by CCATT/enhancer binding protein alpha (C/EBPα) and Myb in acute myeloid leukemia cells, with their knockdown decreasing *Flt3* expression (166). DC development is dependent on C/EBPα, however, it is not a requirement for survival or function of terminally differentiated DCs. Similarly, Myb regulates hematopoiesis and conditional deletion of this transcription factor in haematopoietic stem cells ablates bone marrow cellularity. Reduced Flt3 on progenitor cells has been observed in *Myb* conditional deletion mice (167). Similar observations of impaired hematopoiesis and reduced Flt3 expression has been observed in mice lacking the transcription factors *Runx1* or its binding partner *Cbfβ* in haematopoietic stem cells (168). It is unclear if C/EBPα, Myb, Runx1 or Cbfβ directly regulate the expression of Flt3 or if the alterations in Flt3 expression are due to reduced progenitors which normally express Flt3. To add to

the complexity, some of the genes described may regulate each other, and as such, their impact on Flt3 is twofold. For example, studies have shown Runx1 binds to the promoter of PU.1 and, depending on the cell type, can promote or repress its expression (169).

In contrast, *Flt3* transcription is repressed by the transcription repressor Hes family BHLH transcription factor 1 (Hes1) which binds to the *Flt3* promoter in HEK293T overexpression studies (170). Mice lacking *Hes1* have impaired T cell development and lack a thymus (171). It is unclear whether Flt3 is regulated by Hes1 in DCs, however, progenitor cells lacking this transcription factor have a developmental bias towards myeloid and DC development (171). *Flt3* suppression also occurs due to paired box protein 5 (Pax5), which binds the *Flt3* promoter in pro-B cells (172). This is critical for B cell development (172). It is unclear whether Pax5 regulates steady-state expression of *Flt3* in DCs.

**Post-transcriptional regulation of Flt3**

Once transcribed and translated the Flt3 receptor behaves like other receptor tyrosine kinases (**Figure 1**). It transits to the cell surface as a monomer which is N-linked glycosylated as confirmed by N-glycosidase F (PNGase F) digestion (151, 152). Once at the cell surface, and bound to the ligand, dimerization occurs. In support of this, when cells are treated with Flt3L, Flt3 can be detected as a species of ~360kDa (representative of 2 monomers bound to the 30kDa Flt3L) (173). Flt3L stimulation promotes Flt3 phosphorylation, indicative of activation (135, 136, 138, 174–178). As shown in the previous chapter, once activated, Flt3 internalizes as quickly as five minutes in DCs.

Internalization of Flt3 from the cell surface is likely regulated by ubiquitination. Much of our current understanding of Flt3 ubiquitination has come from studies in transformed cell lines overexpressing Flt3, with little information for DCs. Nevertheless, these studies have revealed an attractive candidate for Flt3 ubiquitination – the Casitas B-lineage lymphoma (Cbl) family. Cbl was first implicated in Flt3 signaling when their phosphorylation was increased in transformed cell lines stimulated with Flt3L (179, 180). When cells overexpressing Flt3 and c-Cbl are stimulated with Flt3L, the proteins associate (176, 178). In addition, Flt3L stimulation correlates with an increase in Flt3 ubiquitination which is lost when the RING domain of c-Cbl is mutated (176). c-Cbl-dependent ubiquitination of Flt3 is thought to rely on association with adaptor proteins, such as Src-like adaptor protein (SLAP) (181), SLAP2 (182), growth factor receptor-bound protein 2 (GRB2) (179) and SH2B adaptor protein 3 (SH2B3/LNK) (183).

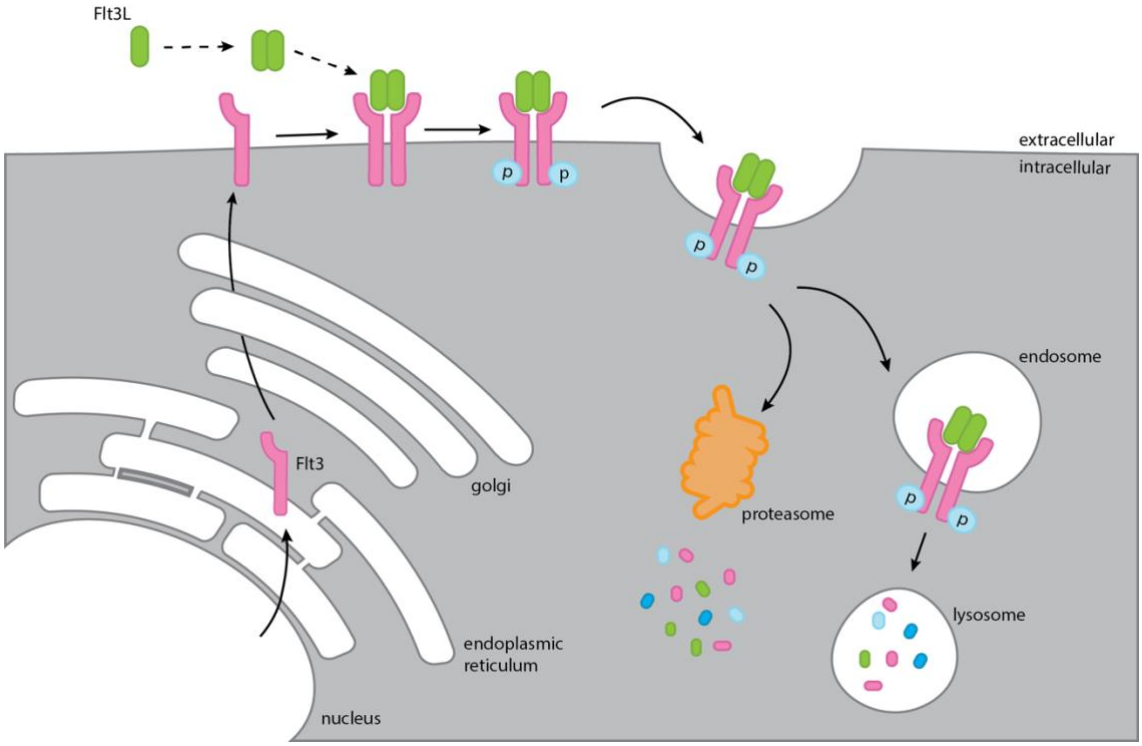


**Figure 1. Schematic of the trafficking of Flt3**. Flt3 is transcribed and translated as a monomer which traffics to the cell surface. During this journey it is glycosylated. Once at the surface, it binds to Flt3L which promotes dimerization and phosphorylation of Flt3. Flt3 internalizes quickly and is degraded by either/or both the lysosomal and proteasomal degradation pathways. Figure from (11).

Studies using c-Cbl and Cbl-b mutant mice have further implicated these E3 ligases in Flt3 regulation. Mice harboring a mutation in the RING domain of c-Cbl (c-Cbl$^{A/-}$) have increased Flt3 expression and signaling in LSK (Lin$^{-}$ SCA-1$^{+}$ c-Kit$^{+}$) cells and develop lethal myeloid leukemia (184). Increased Flt3 expression and signaling is lost when c-Cbl$^{A/-}$ mice are crossed to *Flt3L*$^{-/-}$ mice (184) or are treated with the Flt3 inhibitor AC220 (185). It is currently unclear as to whether the Cbl family regulates DC development and/or Flt3 expression in DCs.

Other E3 ubiquitin ligases, such as suppressor of cytokine signaling 2 (SOCS2) (186) and SOCS6 (187) have also been implicated in Flt3 ubiquitination. Overexpression of SOCS2

or SOCS6 and Flt3 leads to elevated Flt3 ubiquitination and degradation of Flt3 (186, 187). It is unclear if the same occurs with endogenously expressed proteins in DCs.

Deubiquitination of wild type Flt3 is currently unknown, though studies have shown mutated Flt3 (Flt3-ITD) can be deubiquitinated by ubiquitin specific peptidase (USP) 10 (188) and 9 X-linked (USP9X) (189).

Flt3 cell surface expression is also regulated by its phosphorylation status. Phosphorylation is mediated by kinases that attach phosphate groups onto serine, threonine and tyrosine residues (140, 190). The subsequent removal of a phosphate group is facilitated by phosphatases. The modification serves as a docking site for other proteins, such as signaling adaptors, and also allows cross-talk between other post-translational modifications, such as ubiquitination (140, 190). Wild type Flt3 and Flt3-ITD have a number of tyrosine residues that can be targeted by kinases (191, 192). In addition, Flt3 has been shown to interact with a number of phosphatases including DEP-1 (193) SHP-1, PTP-PEST, PTP-1B (152) and SHP-2 (192, 194). Overexpression of these phosphatases along with Flt3 leads to decreased Flt3 phosphorylation and signaling. Importantly, the phosphatases targeting DC Flt3 are currently unknown.

Once internalized, sorting of Flt3 into late endosomes is dependent on late endosomal/lysosomal adaptor and MAPK and mTOR activator 2 (LAMTOR2) (195). As a result, mice lacking LAMTOR2 have increased Flt3 expression and signaling in DCs and increased DC progenitors (195).

In this chapter, the aim was to reveal new genetic machinery responsible for regulating Flt3. The expression of Flt3 was first characterized in the $CD8^+$ DC cell line, MuTu DC1940. After which, this cell line was utilized in two CRISPR/Cas9 genome wide screens to identify positive and negative Flt3 regulators.

# Results

### Characterization of Flt3 expression by MuTu DC1940 cells.

To identify genes that regulate Flt3 expression, a CRISPR/Cas9 genome wide screen utilizing the immortalized murine cDC1 cell line, MuTu DC1940, was carried out. This cell line was chosen as it closely resembles *in vivo* murine cDC1 and is easy to genetically modify (196). However, before commencing the screen, we first confirmed the expression of Flt3 was similar to its *in vivo* counterpart.

Assessment of Flt3 expression by flow cytometry revealed these cells have bimodal expression of Flt3, with some cells expressing high or low cell surface Flt3 (**Figure 2A**). To assist in the characterization of Flt3, a negative control cell line lacking *Flt3* was generated (**Figure 2B**). Two single guide RNAs (gRNAs) Flt3 #1 and Flt3 #2 were designed to target *Flt3* exons three and four, respectively. These gRNAs were cloned into a CFP-expressing vector (123) and lentivirally transduced into Cas9-mCherry expressing MuTu DC1940 cells (previously established by Haiyin Liu, Mintern Lab). gRNA expression was induced for six days with doxycycline. Flow cytometry analysis showed ~30 to 40% transfection efficiency (**Figure 2C**). To generate a homogenous knockout cell line, *ΔFlt3* #2 were cell sorted based on the expression of CFP (**Figure 2D**). As expected, a decrease in the expression of Flt3 was observed in comparison to a negative control cell line that expresses an irrelevant gRNA targeting human *Bim* (*hBim*) (**Figure 2D**). To quantify the insertions and deletions (InDels) present in the knockout cell line, DNA was extracted, and Sanger sequencing was carried out (Australian Genome Research Facility). The trace sequences were analyzed using ICE (Inference of CRISPR

Edits). As shown in **Figure 2E**, ~80% of *ΔFlt3* #2 cells had InDels. This data demonstrates that MuTu DC1940 cells express Flt3, and its expression can be altered by CRISPR/Cas9.

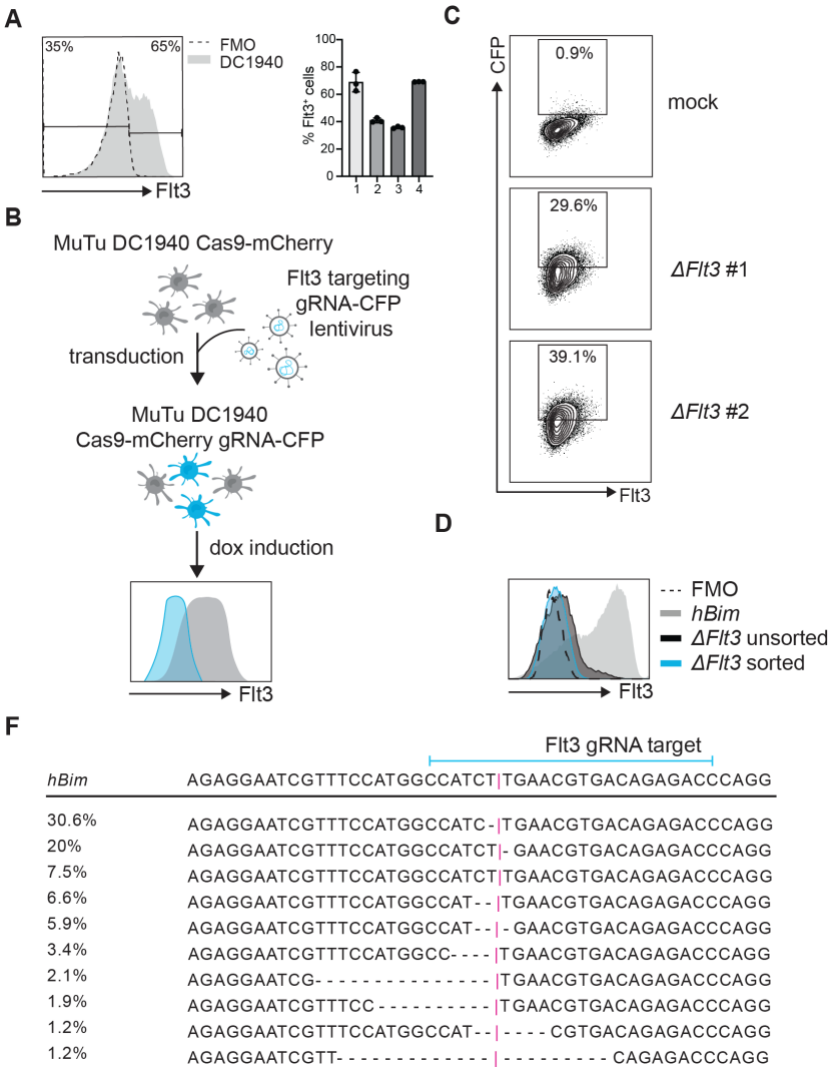


**Figure 2. Generation of ΔFlt3 MuTu DC1940 cells.** (A) Representative Flt3 cell surface expression on MuTu DC1940 cells, as determined by flow cytometry. Bar graph displays the % of Flt3$^+$ cells from four independent experiments (1-4) carried out in triplicate. Bars are mean ± SD. (B) Workflow for generating ΔFlt3 MuTu DC1940 cells. MuTu DC1940 cells expressing Cas9-mCherry were transfected with lentivirus containing Flt3-targeting gRNA in a CFP$^+$ vector. Induction of gRNA was carried out using doxycycline (dox) and the cell surface Flt3 expression was determined by flow cytometry. (C) Transfection efficiency of *ΔFlt3* #1 and #2 MuTu DC1940 cells, as determined by the % of CFP$^+$ cells in comparison to "mock" cells which underwent the same process. (D) *ΔFlt3* #2 was cell-sorted based on CFP expression and the expression of Flt3 was determined by flow cytometry. Representative post-sort histogram is shown. (F) DNA was isolated from *hBim* and *ΔFlt3* cells and Sanger sequencing was carried out before ICE analysis. *hBim* sequence and predicted Cas9 cutting site is indicated in the first row. Top ten trace sequences for ΔFlt3 cells are shown below, with their relative contribution indicated by percentages to the left.

Besides cell surface Flt3, we aimed to investigate total Flt3. To do this, immunoblotting was carried out to detect Flt3 protein levels (**Figure 3A**). Using two antibodies (Clones 8F2 and AF768) two forms of Flt3 were detected, as previously described in non-DC studies (151, 152, 176). The higher molecular weight band has been described as a mature, glycosylated form of Flt3 which sits at the cell surface. The smaller molecular weight band is thought to be a less glycosylated intracellular form of Flt3. To improve the appearance of the blots, different gels and running buffers were trialed, with the optimal conditions determined as 10% Bis-Tris gel with MOPS running buffer (**Figure 3B**). These data demonstrate we can confidently detect protein Flt3 in MuTu DC1940 cells.

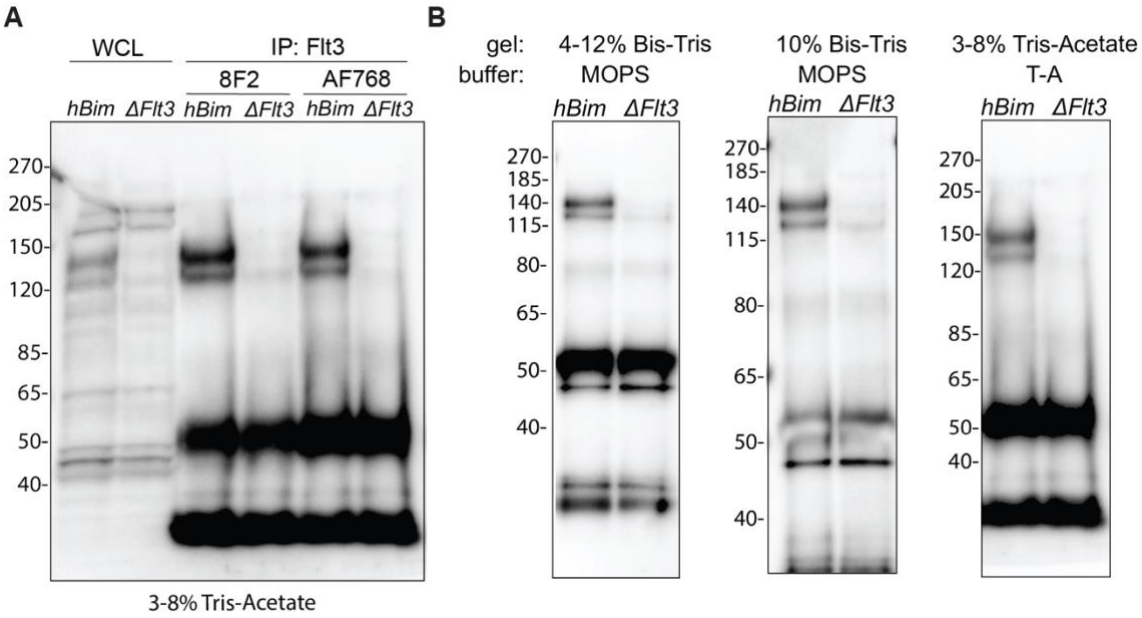


**Figure 3. Detecting protein Flt3.** (A) Equal number of *hBim* and Δ*Flt3* MuTu DC1940 cells were lysed in NP40 lysis buffer. Flt3 was immunoprecipitated using monoclonal rabbit anti-mouse Flt3 (8F2) or goat polyclonal anti-mouse Flt3 (AF768). Proteins were separated by gel electrophoresis and transferred to a PVDF membrane. Flt3 was detected with anti-Flt3 (AF768). (B) Equal numbers of *hBim* and *ΔFlt3* MuTu DC1940 cells were lysed in NP40 lysis buffer. Flt3 was immunoprecipitated using anti-Flt3 (AF768) and the immunoprecipitates were separated by gel electrophoresis using the indicated gels and running buffer before transfer to PVDF membranes. Flt3 was detected using anti-Flt3 (AF768). WCL, whole cell lysate. IP, immunoprecipitate. T-A, Tris-acetate.

We next confirmed that the higher molecular form of Flt3 is in fact at the cell surface. Cell surface proteins were biotinylated and immunoprecipitated using streptavidin agarose (**Figure 4**). After immunoblotting for Flt3 only the higher molecular weight band was detected. This demonstrates the higher molecular weight band is at the cell surface of DCs.

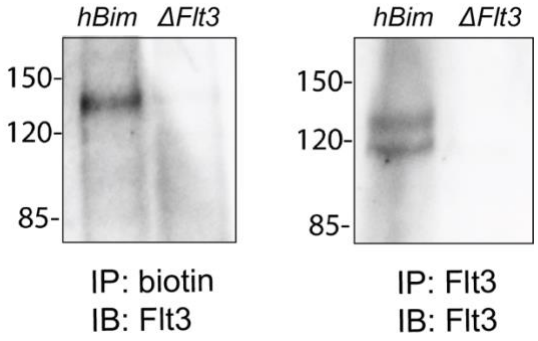


**Figure 4. Higher molecular weight form of Flt3 is at the cell surface.** Cell surface proteins were biotinylated and cells were lysed using NP40 lysis buffer. Biotinylated proteins or Flt3 was immunoprecipitated with streptavidin agarose (Thermo Scientific) or anti-Flt3 (AF768) from an equivalent number of cells. Immunoprecipitates were separated by SDS-PAGE and transferred to a PVDF membrane before Flt3 was detected with anti-Flt3 antibody. Blot is from one experiment.

To confirm that cell surface Flt3 is responsive to Flt3L, MuTu DC1940 cells were stimulated with varying concentrations of Flt3L for 5 – 60 minutes and cell surface expression of Flt3 was determined by flow cytometry (**Figure 5**). Like primary DC (Chapter 3), significant decreases in Flt3 expression were observed for MuTu DC1940 cells in the presence of Flt3L. While the strongest downregulation of Flt3 cell surface expression was observed with cells treated with 1 μg/mL and 0.5 μg/mL Flt3L, this high concentration was not feasible for future experiments, and therefore 0.1 μg/mL Flt3L, which still causes a clear shift in Flt3 expression, was determined as an optimal concentration.

A loss of cell surface Flt3 (higher molecular weight band) was also observed by immunoprecipitating Flt3 from DCs incubated with or without Flt3L (0.1 µg/mL) **(Figure 5B)**. Loss of this Flt3 species correlated with increased phosphorylation of the receptor, indicative of activation. Together, this data demonstrates that MuTu DC1940 cells are responsive to Flt3L.

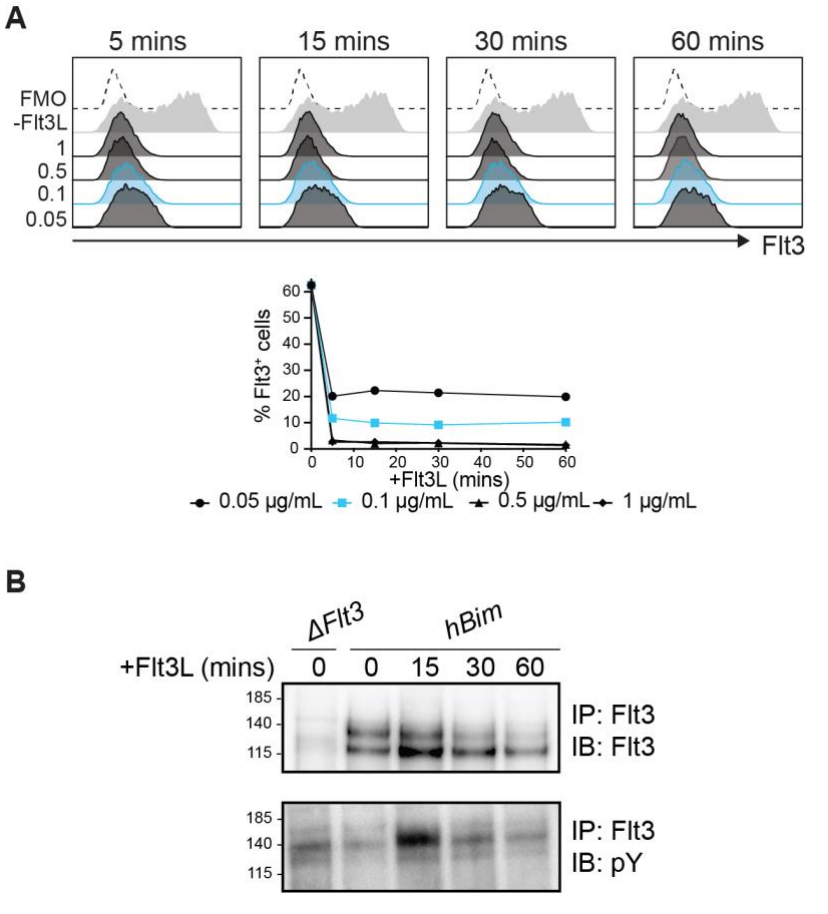


**Figure 5. Impact of Flt3L on Flt3 expression**. (A) Equal number of MuTu DC1940 cells were stimulated with or without Flt3L for the indicated times. Concentration (µg/mL) of Flt3L is indicated by the numbers to the left of the representative histograms. (B) *hBIM* and *ΔFlt3* MuTu DC1940 cells were treated with Flt3L (0.1 µg/mL) for 0 – 60 mins. Equivalent number of cells were lysed in NP40 lysis buffer before Flt3 was immunoprecipitated using anti-Flt3 (AF768). Proteins were separated by gel electrophoresis and transferred to a PVDF membrane. Immunoblotting was carried out using anti-Flt3 (A2F10) or anti-phosphotyrosine (4G10) antibodies.

To quantify the Flt3L-dependent internalization of Flt3 a fluorescently tagged Flt3L was generated, in collaboration with Dr Angus Johnston's lab (Monash University) (125). As shown in **Figure 6A**, the Flt3L sensor comprises Flt3L bound to Cy5 and a *trans*-cyclooctene (TCO) functional group. Cy5 fluorescence is quenched with the addition of a quencher which comprises a tetrazine (Tet) group bound to a dye that absorbs light at the same emission as Cy5 emits. The quencher can quickly and specifically bind to the sensor due to the TCO and Tet clickable groups. For the internalization assay, cells were stained at 4°C for 30 mins with the Flt3L sensor before extensive washing to remove excess ligand (**Figure 6B**). Internalization was then allowed by incubating cells at 37°C. Remaining sensor at the cell surface was then quenched at 4°C. Importantly, the quencher is membrane impermeable ensuring only cell surface signal is quenched. Quantification of the internalization was determined by comparing the Cy5 signal between the samples at 4°C and 37°C. This internalization assay is similar to the commonly used Specific Hybridization Internalization Probe (SHIP) assay which uses Fluorescent Internalization Probe (FIP) sensors (108). Both assays do not affect cell viability or morphology and since the quenchers are specific for the sensors, further phenotype staining can be carried out using other fluorophores. sCy5-TCO, however, is significantly smaller than FIP which makes it ideal for conjugation with small proteins such as Flt3L (~18 kDa).

Before commencing the internalization assays, the specificity of the probe was determined by staining *ΔFlt3* and *hBim* MuTu DC1940 cells with Flt3L-sCy5-TCO (**Figure 6C**). Low fluorescence was observed on cells lacking *Flt3*, confirming the specificity of the probe for Flt3. Next the behavior of the labelled ligand was compared to its unlabeled counterpart (**Figure 6D**). For this, the labeled and unlabeled ligands were

titrated and the loss of Flt3 was measured by flow cytometry. Both ligands behaved similarly with the largest loss of Flt3 observed at ~100 ng/mL. To ensure the Cy5 fluorescence was detectable at this concentration, DCs were stained at 4°C with increasing concentration of Flt3L-sCy5- TCO and the Cy5 fluorescence was detected by flow cytometry (**Figure 6E**). The fluorescence peaked and plateaued at ~50 ng/mL. Based on these assays the optimal concentration for Flt3L-sCy5- TCO was 100 ng/mL. Finally, the internalization of activated Flt3 was determined over a 60-minute period (**Figure 6F**). Flt3 has been described to internalize as quickly as 5 minutes in transformed cell lines (173). In agreement with this, cDC1 and cDC2 began internalizing Flt3 within 5 minutes of incubating at 37°C, with most of the sensor internalized within 20 minutes. cDC1 and cDC2 had the same rate of internalization.

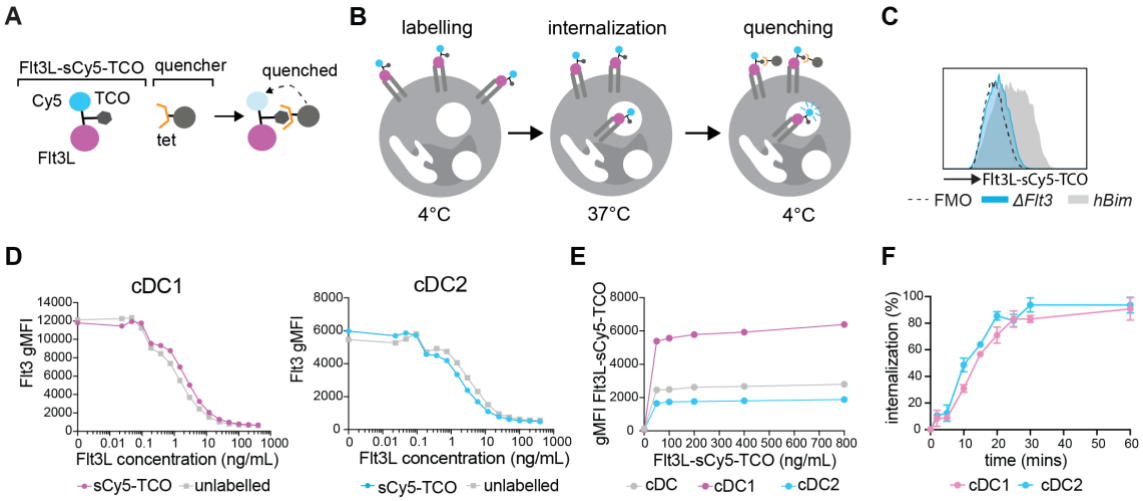


**Figure 6. Quantification of activated Flt3 internalization.** (A) Schematic of the two components in the internalization, adapted from (125). (B) Workflow of internalization assay. Cells are labelled on ice with Flt3L-sCy5-TCO and washed to remove excess ligand. Cells are then incubated at 37°C to allow for internalization. Following internalization, cells are placed at 4°C and quencher is added to quench cell surface fluorescence. (C) *hBim* or *ΔFlt3* MuTu DC1940 cells were labelled with Flt3L-sCy5-TCO and washed extensively before flow cytometry was carried out to determine Cy5 fluorescence. (D) Wild type splenic cDC were isolated and incubated with increasing labeled or unlabeled Flt3L for 60 mins. The expression of Flt3 was determined by flow cytometry. Data is representative of two independent experiments. (E) Wild type DCs were isolated and incubated with increasing labelled Flt3L for 60 mins. The expression of Flt3L-sCy5-TCO was determined by flow cytometry. Data is from one experiment. (F) Primary splenic DCs were isolated and incubated with 100 ng/mL Flt3L-sCy5-TCO for 30 mins. Cells were washed and incubated for increasing amount of time before being stained for cell surface markers. DCs were then treated with or without quencher and flow cytometry was carried out. Data is from one experiment carried out in triplicate. Error bars are ± SEM.

## Identifying genes that regulate Flt3.

To date, not much is known about the intracellular machinery involved in regulating DC Flt3. To address this, two CRISPR/Cas9 genome wide screens were carried out. The workflow for both screens is described in **Figure 7**. First HEK293T cells were co-transfected with plasmid library and lentiviral packaging vectors to produce gRNA library lentivirus supernatant. The supernatant was used to spinfect MuTu DC1940 cells at a low multiplicity of infection (MOI) to ensure only one gRNA was received by each cell. This

resulted in a heterogenous population of cells, each comprising of one single gene knocked out (known as "unsorted"). Since the focus was on genes regulating Flt3 expression, it was reasoned that any cell with a mutation in these genes would have altered Flt3 expression. Genes normally involved in downregulating Flt3, negative regulators, would be enriched in the top 5% of Flt3 expressing cells. Genes that promote Flt3 expression, positive regulators, would be enriched in the bottom 5% of Flt3 expressing cells. Once stained for Flt3, the high and low Flt3 populations were sorted before genomic DNA (gDNA) isolation and Next Generation Sequencing. The genes were then identified by comparing the gRNAs enriched in the sorted populations to the unsorted populations.

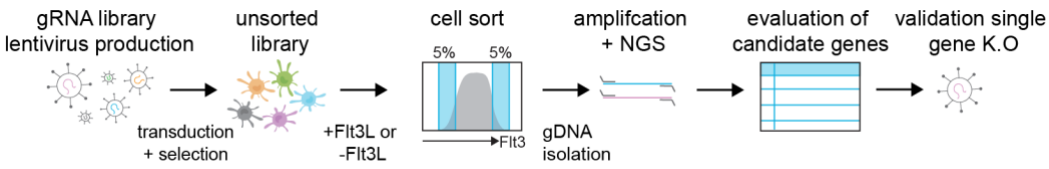


**Figure 7 CRISPR/Cas9 genome wide screen workflow**. Diagram detailing the library screen workflow. First, a gRNA library lentivirus is produced after which MuTu DC1940 cells are transfected and then selected using puromycin. The cells are expanded and then sorted based on their expression of Flt3 (with or without Flt3L). genomic DNA (gDNA) is isolated from the top and bottom 5% of Flt3 expressing cells and the candidate genes are identified by Next Generation Sequencing (NGS, Illumina). Finally, the genes are validated using single gene knockout (K.O) cells.

In the first screen, the aim was to identify genes that regulate activated Flt3. The genome-wide CRISPR-Cas9 knockout (GeCKO) v2 library (126, 127) was utilized. This comprises 67,405 gRNAs that target 20,611 genes in the mouse genome in addition to miRNAs and non-targeting controls. To activate Flt3, the previously determined (**Figure 5A**) optimal concentration of Flt3L (0.1 μg/mL) for 60 minutes was used.

Prior to transfecting the target cells with the library, a puromycin kill curve was carried out to determine the time point at which puromycin selection is complete. An equal number of untransduced MuTu DC1940 cells were incubated with increasing concentrations of puromycin for five days and the optimal timepoint and concentration was determined as three days with 1 μg/mL puromycin (**Figure 8A**, Haiyin Liu, Mintern Lab). Next, the virus was titrated to determine the percentage infection efficiency, which is defined as the number of live cells with selection/the number of live cells without selection x100% (**Figure 8B**). Ideally, an infection efficiency of ~30% is required to decrease the chance of cells infected with multiple gRNA (197). For the virus generated, 20% was required for an infection efficiency of ~34%. The library was used to transfect 72 $x10^6$ MuTu DC1940s, giving ~350x coverage of the library. Puromycin selection was then carried out to generate the unsorted library.

The library strategy in **Figure 8C** was carried out three independent times to generate three biological replicates. In an ideal scenario, cells containing genes that regulate Flt3 would be easily distinguished following Flt3L stimulation (schematic **Figure 8D**). However, given that only a small number of genes are anticipated to regulate Flt3 expression, most knockout cells were able to internalize Flt3 following ligand stimulation. Because of this, the top 5% and bottom 5% Flt3 expressing cells underwent two subsequent sorts to enrich for the relevant genes.

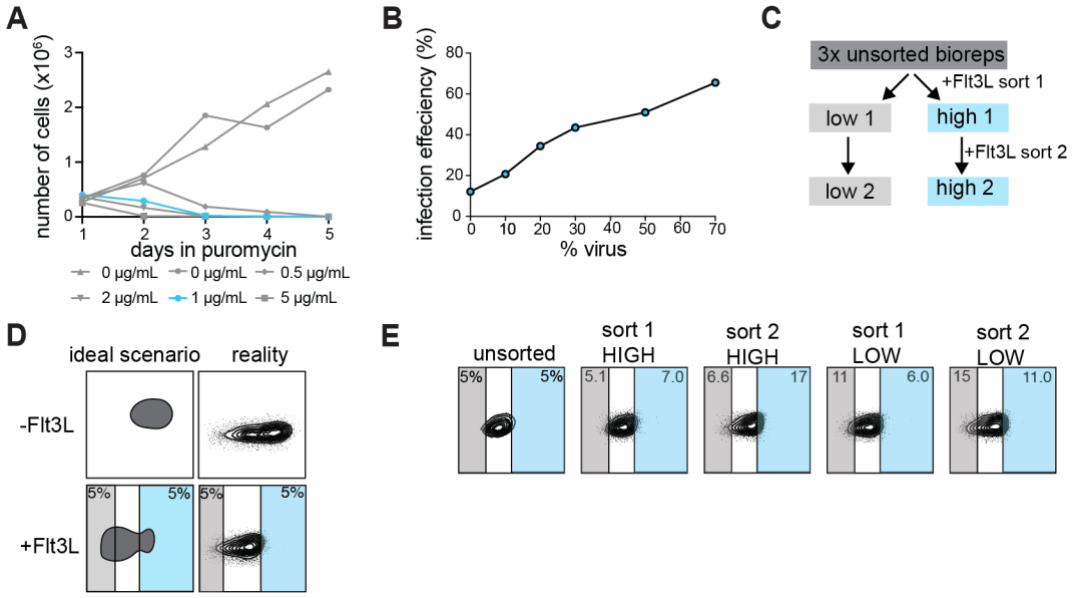


**Figure 8. Preparation for GeCKO CRISPR/Cas9 genome wide screen.** (A) MuTu DC1940 cells were treated with increasing concentration of puromycin for 5 days and the number of live cells was determined by trypan blue exclusion. (B) Infection efficiency. Equal number of MuTu DC1940 cells were seeded and gRNA library lentivirus was added at increasing concentrations. The gRNA-containing cells were then selected for with puromycin (1 µg/mL) for 3 days and the number of cells were determined by bead acquisition on flow cytometry. (C) Sorting scheme. Three biological replicates (bioreps, BR) were produced (BR1US, BR2US, BR3US) and underwent two subsequent sorts to enrich for the high and low Flt3 expressing cells. (D) Schematic detailing ideal Flt3 expression of bulk library following Flt3L stimulation in comparison to the actual expression of Flt3 on the bulk library. (E) Expression of Flt3 one week following subsequent cell sorts for Flt3 high and low expressing cells. Plots are representative of 3 biological replicates.

To generate amplicons for next generation sequencing, DNA was extracted from the unsorted and sorted samples and PCR was carried out. The amplicons were confirmed by gel electrophoresis and purified by magnetic beads (**Figure 4.9A**). Sequencing was carried out using NextSeq platform (carried out by Stephen Wilcox, WEHI Genomics Hub) and ~250 million reads were obtained. Bioinformatic analysis of the screen carried out using MAGeCK software (130). First, the data was cleaned using Cutadapt, to

generate fastq files with the same length reads. The MAGeCK “count” command was then used to normalize read counts across all samples and determine the abundance of guides. Finally, the MAGeCK “test” command was used to determine the gene enrichment. Across the sorted and unsorted samples, a total of 65,619 unique guides were detected representing 97% of the guides from the original library. Most of these guides had 100-1000 reads (**Figure 9B**) and these reads were relatively well distributed across all samples (**Figure 9C**). Together, these data demonstrate that the uniformity of the library was maintained and unbiased. When looking for enrichment between unsorted samples and sorted samples, there were no guides that were differentially abundant after sort 1, therefore gene enrichment analysis was carried out on sort 2 only.

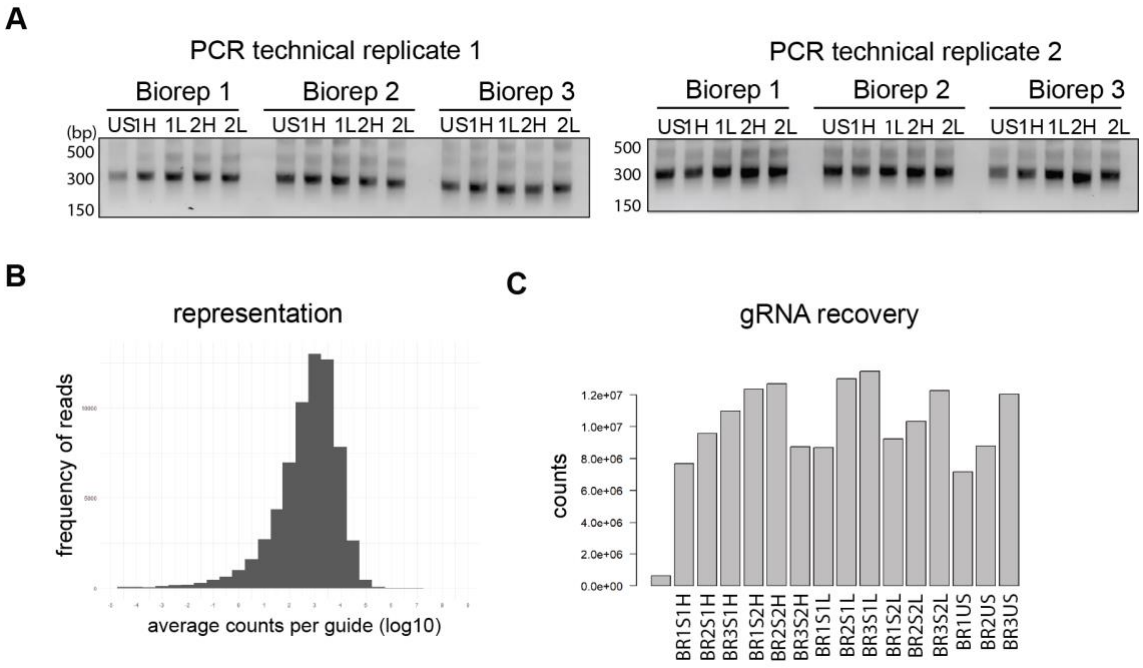


**Figure 9. GeCKO CRISPR/Cas9 genome wide screen quality control.** (A) PCR products following amplification of DNA regions containing gRNA sequences. DNA was run on 2% agarose gel and final product is expected at ~280bp. Two technical replicates are shown. (B) Histogram showing the frequency of reads recovered for each gRNA after sequencing. (C) Pooled counts of all gRNAs recovered in each of the samples.

Genes were considered enriched in the sorted populations compared to the unsorted populations when the gRNA count increased at least two-fold ($log_2$fold>1) with a false discovery ratio of <1% or <5% (FDR <0.01 or <0.05). For the Flt3$^{hi}$ sorted cells, we obtained 5 statistically significant enriched genes - *Mediator Complex Subunit 25 (Med25), Transcription Factor 7-like 2 (Tcfl2), Myc-Associated Factor X (Max), tumor protein p53 (Trp53)* and *Polycomb group RING finger protein 1 (Pcgf1)* (**Figure 10**).

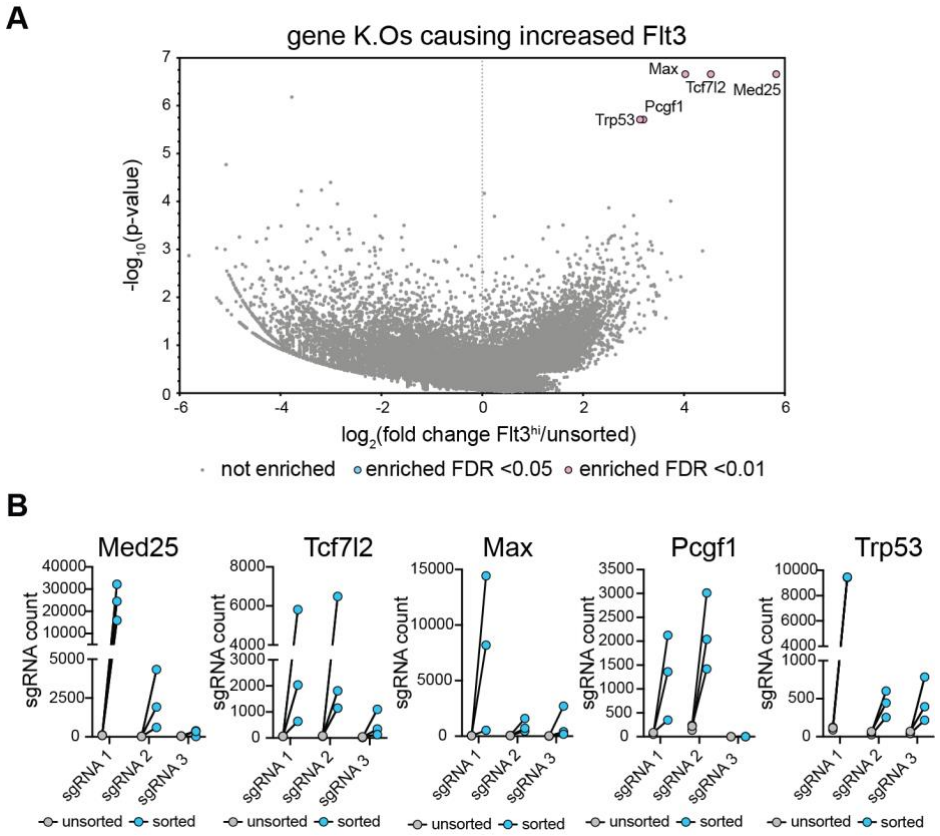


**Figure 10. Gene knockouts causing increased Flt3 in the presence of Flt3L.** (A) Volcano plot for gene hits in $Flt3^{hi}$ sorted populations. X-axis shows $log_2$ fold change to unsorted populations. The y-axis shows the p-value as calculated by MAGeck. Hits with a false discovery rate (FDR) of <0.05 or <0.01 are shown as blue and pink respectively. Genes not enriched are indicated by grey symbols. (B) gRNA count for the three gRNAs targeting each of the significantly enriched genes. Symbols represent the three unsorted (grey) or sorted (blue) populations.

Four statistically significant candidate genes were identified in the $Flt3^{lo}$ populations – *Core-binding factor subunit beta (Cbfβ), runt-related transcription factor 1 (Runx1), CREB binding protein (Crebbp)* and *mesoderm development candidate 2 (Mesdc2)* (**Figure 11**). Importantly, mice lacking *Cbfβ* and *Runx1* in hematopoietic progenitors have reduced Flt3 expressing progenitors and impaired DC development suggesting these genes may regulate the expression of Flt3 (168). It should be noted that *Crebbp* and *Mesdc2* only had one out of three gRNAs statistically enriched (**Figure 11B**). For confidence in the screen, Flt3 should be identified in the $Flt3^{lo}$ cells. When investigating

the abundance of gRNA targeting Flt3 across all samples, it was clear that two out of the three guides were not detected in the unsorted populations suggesting these were simply ineffective (**Figure 11C**). The single guide that was identified did not reach statistical significance.

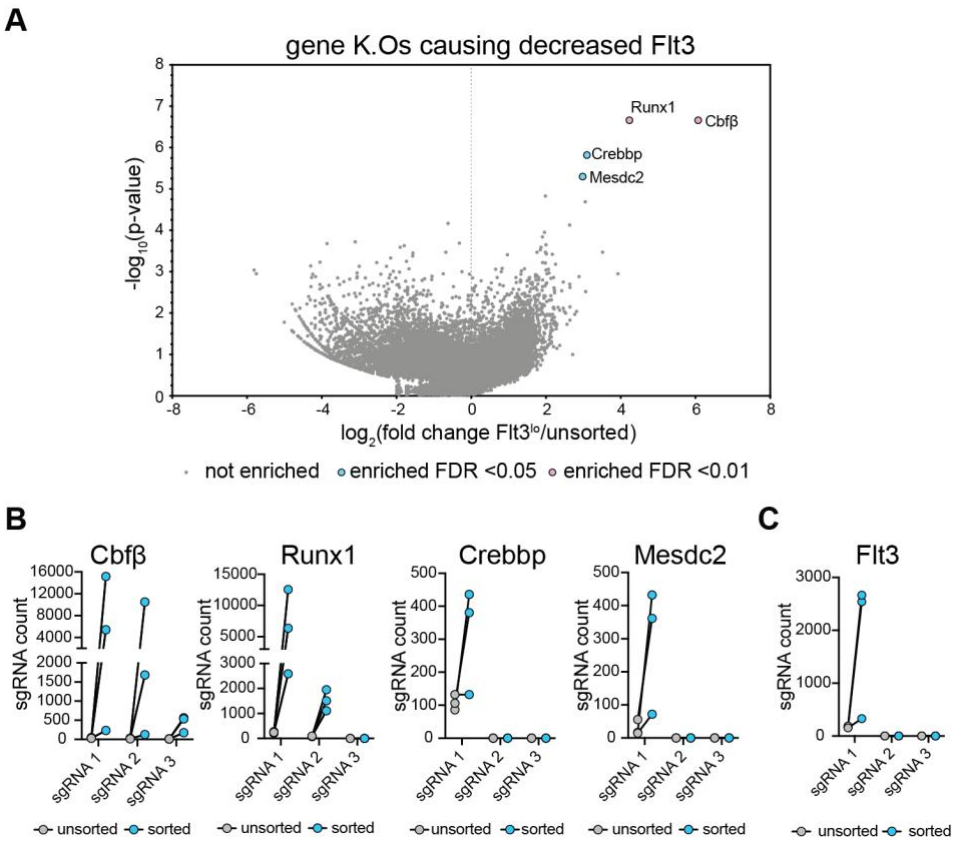


**Figure 11. Gene knockouts enriched in Flt3$^{lo}$ samples in the presence of Flt3L.** (A) Volcano plot for gene hits in Flt3$^{lo}$ sorted populations. X-axis shows $log_2$ fold change to unsorted populations. The y-axis shows the p-value as calculated by MAGeCK. Hits with a false discovery rate (FDR) of <0.05 or <0.01 are shown as blue and pink respectively. Genes not enriched are indicated by grey symbols. (B) gRNA count for the three gRNAs targeting each of the significantly enriched genes. Symbols represent the three unsorted (grey) or sorted (blue) populations. (C) gRNA count for the three gRNAs targeting *Flt3*. Symbols represent three unsorted (grey) or sorted (blue) populations.

To complement the GeCKO v2 Flt3L screen, a second screen was carried out to identify genes that regulate steady-state Flt3. In this screen three improvements were made. First, instead of utilizing GeCKO we used the newer CRISPR/Cas9 library, Brie (122). Brie has improved gRNA design with demonstrated increased on-target and decreased off-

target activity. It also has an increased number of gRNAs (78,637 gRNAs), which target 19,674 genes. Unlike GeCKO which has three gRNAs per gene, Brie has four gRNAs per gene. The second improvement was increasing the number of biological replicates from three to four. Finally, the cell line utilized was improved. In the GeCKO screen, the MuTu DC1940 cells used had varied Flt3 expression which added statistical noise to the analysis. Here, MuTu DC1940 cells with homogenous Flt3 expression were used.

To obtain homogenous expression of Flt3, MuTu DC1940 cells were sorted based on $Flt3^{hi}$ expression (**Figure 12A**). Similar to the previous screen, lentivirus was generated by co-transfecting HEK293T cells with Brie library and lentiviral packaging vectors. The supernatant was then used to transduce at least 131 $x10^6$ cells to achieve ~500x copies of each gRNA. Once transduced, the gRNA-containing cells were selected using 1 μg/mL puromycin for at least 3 days (previously determined in **Figure 8**). To avoid multiple gRNAs in a single cell, the lentivirus was titrated to get an MOI of 0.2. As shown in **Figure 12B**, this required 10% virus supernatant during the transduction. The strategy for the library is detailed in **Figure 12C**. One week after each sort, the cell surface expression of Flt3 was assessed by flow cytometry (**Figure 12D**). Successful enrichment of Flt3 high cells was observed with an increase from 5% in the bulk population to ~20% after the second sort. A similar enrichment was observed for Flt3 low sorted cells (from 5% to ~50%).

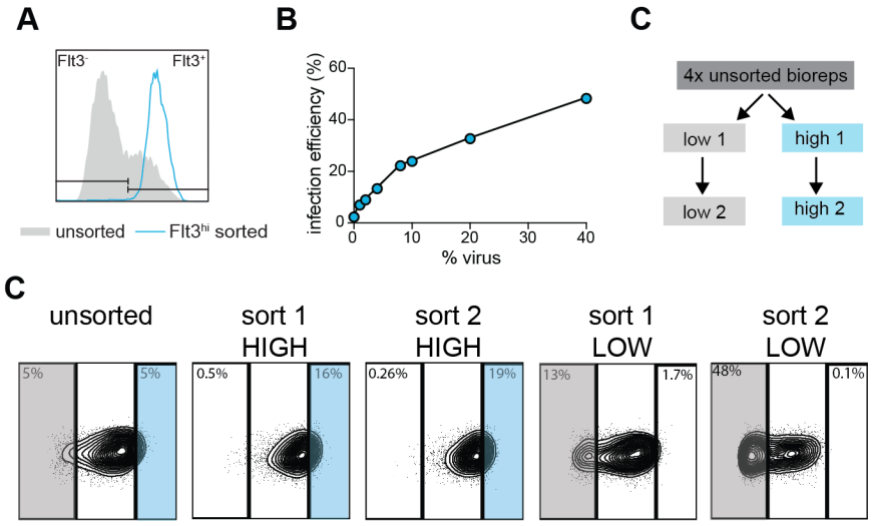


**Figure 12. Brie CRISPR/Cas9 screen to identify genes that regulate steady-state Flt3.** (A) MuTu DC1940 cells were sorted for high Flt3 expression. Representative post-sort histogram shown. (B) Infection efficiency. Equal number of MuTu DC1940 cells were seeded and library lentivirus was added at increasing concentrations. Library-containing cells were then selected for using puromycin (1 μg/mL) for 3 days and the number of cells were determined by bead acquisition on flow cytometry. (C) Sorting scheme. Four biological replicates underwent two subsequent sorts to enrich for the high and low Flt3 expressing cells. (D) Expression of Flt3 one-week post sort. Plots are representative of 4 biological replicates.

To generate amplicons for next generation sequencing, DNA was extracted from the sorted and unsorted samples before PCR was carried out. The amplicons were confirmed by gel electrophoresis and purified by magnetic beads (**Figure 13A**). Sequencing was carried out using NextSeq platform (carried out by Stephen Wilcox, WEHI Genomics Hub) and ~400 million reads were obtained. Bioinformatic analysis of the screen carried out using MAGeCK software (130), as described for the GeCKO screen. Across the sorted and unsorted samples, 78,632 unique gRNAs were detected which represents 99% of gRNAs from the original library. Most guides had 1000-10000 reads (**Figure 13B**) and these reads were evenly distributed across all samples (**Figure 13C**). Together, these data demonstrate that the uniformity of the library was maintained and unbiased.

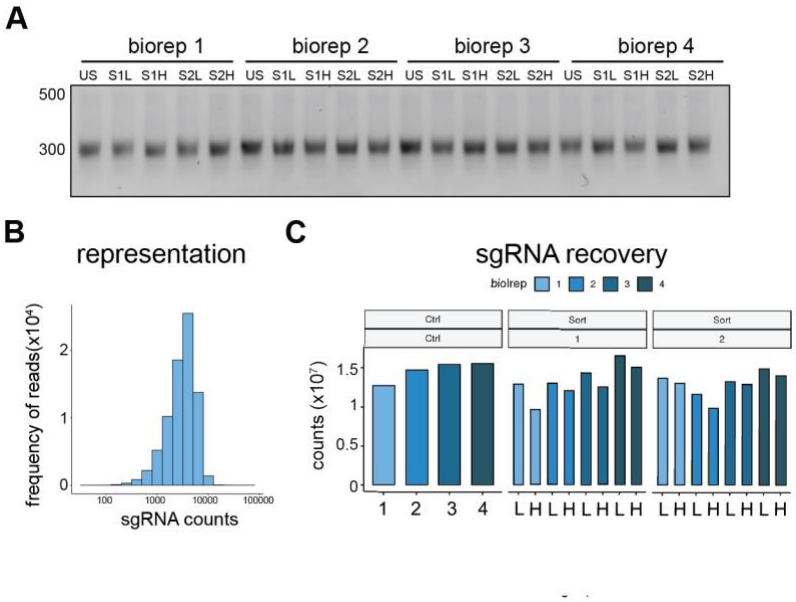


**Figure 13. Brie CRISPR/Cas9 genome-wide screen quality control.** (A) PCR products following amplification of DNA regions containing gRNA sequences. DNA was run on 2% agarose gel and final product is expected at ~280bp (B) Representation of library. Histogram showing the frequency of reads recovered for each gRNA following sequencing. (C) gRNA recovery. Pooled counts of all gRNAs in each sample.

When looking for enrichment between the sorted and unsorted samples (**Table 1**), there were genes enriched in both sort 1 and sort 2. Genes were considered enriched in the sorted populations compared to the unsorted populations when the gRNA count increased at least two-fold ($log_2$fold>1) with a false discovery ratio of <1% or <5% (FDR <0.01 or <0.05).

**Table 1. Brie differential gene enrichment across sorted samples.**

| | Flt3 low | | Flt3 high | |
|---|---|---|---|---|
| Sort | 1 | 2 | 1 | 2 |
| Number of genes enriched | 27 | 22 | 7 | 65 |
| Number of genes found in both sorts | 20 | | 7 | |
| Number of unique genes | 7 | 2 | 0 | 58 |

First, positive regulators were investigated by looking at the gene hits enriched in the Flt3$^{lo}$ population in comparison to the unsorted population and 22 candidate genes were identified (**Figure 14** and **Table 2**). The full list of genes can be found in **Appendix 2 and 3**. These included the positive control *Flt3* in addition to *Cbfβ* and *Runx1* which appeared in the first GeCKO screen and have previously been described to impact Flt3 expression (168). Detection of these genes in the screen demonstrates that the screen is robust in detecting genes that regulate Flt3 expression.

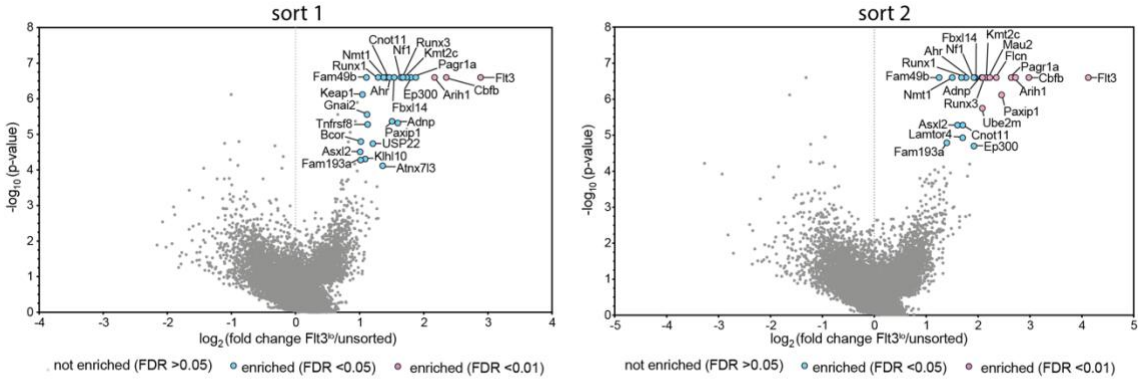


**Figure 14. Volcano plots for gene knockouts causing decreased Flt3 expression.** Volcano plot shows gene hits in first sorted Flt3$^{lo}$ population (left) or second sorted Flt3$^{lo}$ population (right) in comparison to unsorted population. The x-axis shows $\log_2$ fold change enrichment. The y-axis shows the p-value calculated by MAGeCK. Hits with a false discovery rate (FDR) of <0.05 or <0.01 are shown as blue or pink respectively. Genes not enriched in sorted populations are shown as grey symbols.

**Table 2. Brie gene knockouts causing Flt3 downregulation.** Top hits of MAGeCK analysis comparing Flt3$^{lo}$ population to unsorted population. Hits are sorted by log fold change (LFC) with an FDR <0.05 and a cutoff of LFC>1. Sort 1 and Sort 2 refer to the population the gene was enriched in. For genes enriched in both sort 1 and sort 2 the highest LFC and Log P-value are shown.

| LFC | LogP | gene | name | sort 1 | sort 2 |
|---|---|---|---|---|---|
| 4.12 | 6.60 | **Flt3** | FMS-like tyrosine kinase 3 | ✓ | ✓ |
| 2.98 | 6.60 | **Cbfβ** | Core-Binding Factor Subunit Beta | ✓ | ✓ |
| 2.72 | 6.60 | **Arih1** | Ariadne RBR E3 Ubiquitin Protein Ligase 1 | ✓ | ✓ |

| | | | | | |
|---|---|---|---|---|---|
| 2.64 | 6.60 | **Pagr1a** | PAX-Interacting Protein 1 (PAXIP1)-associated glutamate rich protein 1 | ✓ | ✓ |
| 2.45 | 6.12 | **Paxip1** | PAX-Interacting Protein 1 | ✓ | ✓ |
| 2.35 | 6.60 | **Flcn** | Folliculin | ✓ | ✓ |
| 2.23 | 6.60 | **Mau2** | MAU2 chromatid cohesion factor homolog | ✓ | ✓ |
| 2.16 | 6.60 | **Kmt2c** | Lysine Methyltransferase 2C | ✓ | ✓ |
| 2.09 | 6.60 | **Runx3** | Runt-related transcription factor 3 | ✓ | ✓ |
| 2.08 | 5.75 | **Ube2m** | NEDD8-conjugating enzyme Ubc12 | ✓ | ✓ |
| 2.07 | 6.60 | **Adnp** | Activity-dependent neuroprotector homeobox | ✓ | ✓ |
| 1.94 | 6.60 | **Fbxl14** | F-box/LRR-repeat protein 14 | ✓ | ✓ |
| 1.92 | 4.70 | **EP300** | Histone acetyltransferase | ✓ | ✓ |
| 1.92 | 6.60 | **Nf1** | neurofibromin | ✓ | ✓ |
| 1.77 | 6.60 | **Ahr** | aryl hydrocarbon receptor | ✓ | ✓ |
| 1.71 | 5.28 | **Cnot11** | CCR4-NOT transcription complex subunit 11 | ✓ | ✓ |
| 1.70 | 4.93 | **Lamtor4** | Late Endosomal/Lysosomal Adaptor, MAPK And MTOR Activator 4 | | ✓ |
| 1.68 | 6.60 | **Runx1** | Runt-related transcription factor 1 | ✓ | ✓ |
| 1.60 | 5.28 | **Asxl2** | Additional sex combs-like protein 2 | ✓ | ✓ |
| 1.50 | 6.60 | **Nmt1** | N-myristoyltransferase | ✓ | ✓ |
| 1.40 | 4.79 | **Fam193a** | Family with Sequence Similarity 193 Member A | ✓ | ✓ |
| 1.36 | 4.12 | **Atxn7l3** | Ataxin 7 Like 3 | ✓ | |
| 1.25 | 6.60 | **Fam49b** | Family With Sequence Similarity 49 Member b | ✓ | ✓ |
| 1.21 | 4.74 | **Usp22** | Ubiquitin specific peptidase 22 | ✓ | |
| 1.13 | 5.28 | **Tnfrsf8** | TNF Receptor Superfamily Member 8 | ✓ | |
| 1.12 | 5.56 | **Gnai2** | G Protein Subunit Alpha I2 | ✓ | |
| 1.09 | 4.31 | **Klhl10** | Kelch Like Family Member 10 | ✓ | |
| 1.04 | 6.12 | **Keap1** | Kelch-like ECH-associated protein 1 | ✓ | |
| 1.02 | 4.80 | **Bcor** | BCL-6 corepressor | ✓ | |

Further analysis using Cytoscape revealed experimentally determined and predicted interactions and functions of Flt3$^{lo}$ hits (**Figure 15**). Most of the hits are involved in DNA binding and histone modification, suggesting they are involved in the transcriptional regulation of *Flt3*.

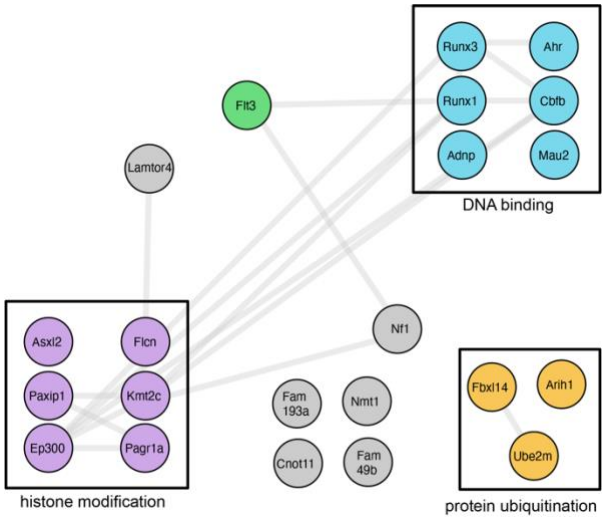


**Figure 15. Protein-protein interactions and functional analysis of Flt3$^{lo}$ hits.** Schematic of experimentally determined and predicted protein interactions and functions as determined using STRING-dp plugin on Cytoscape.

Next, genes enriched in the Flt3$^{hi}$ cells were investigated (i.e. negative regulators). 65 candidate genes across the two sorts were identified (top 20 genes in **Figure 16** and **Table 3**). The full list of genes can be found in **Appendix 4 and 5**.

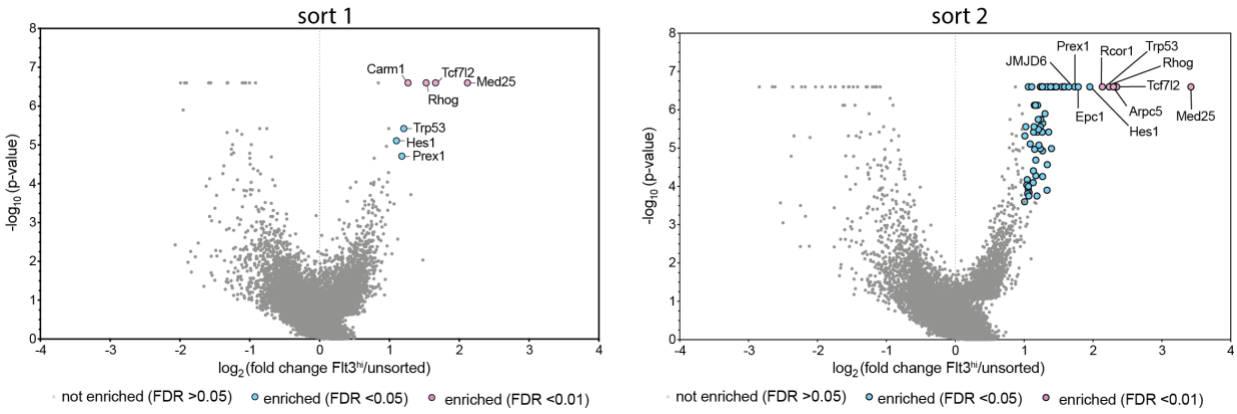


**Figure 16. Volcano plots for gene knockouts causing increased Flt3 expression.** Volcano plot shows gene hits in first sorted Flt3$^{hi}$ population (left) or second sorted Flt3$^{hi}$ population (right) in comparison to unsorted population. The x-axis shows $\log_2$ fold change enrichment. The y-axis shows the p-value calculated by MAGeCK. Hits with a false discovery rate (FDR) of <0.05 or <0.01 are shown as blue or pink respectively. Genes not enriched in sorted populations are shown as grey symbols.

**Table 3. Brie gene knockouts causing Flt3 upregulation.** Top hits of MAGeCK analysis comparing $Flt3^{hi}$ population to unsorted population. Hits are sorted by log fold change (LFC) with an FDR <0.05 and a cutoff of LFC>1. Sort 1 and Sort 2 refer to the population the gene was enriched in. For genes enriched in both sort 1 and sort 2 the highest LFC and Log P-value are shown.

| LFC | Logp | gene | name | sort 1 | sort 2 |
|---|---|---|---|---|---|
| 3.42 | 6.60 | **Med25** | Mediator Complex Subunit 25 | ✓ | ✓ |
| 2.34 | 6.60 | **Tcf7l2** | Transcription Factor 7-like 2 | ✓ | ✓ |
| 2.33 | 6.60 | **Rhog** | Ras homology Growth-related | ✓ | ✓ |
| 2.30 | 6.60 | **Arpc5** | Actin-related protein 2/3 complex subunit 5 | | ✓ |
| 2.24 | 6.60 | **Trp53** | Tumor protein p53 | ✓ | ✓ |
| 2.14 | 6.60 | **Rcor1** | REST corepressor 1 | | ✓ |
| 1.59 | 6.60 | **Carm1** | Coactivator-associated arginine methyltransferase 1 | | ✓ |
| 1.39 | 6.60 | **Dek** | DEK oncogene (DNA binding) | | ✓ |
| 1.28 | 6.60 | **Elf4** | E74-like factor 4 (ets domain transcription factor) | | ✓ |
| 1.79 | 6.60 | **Epc1** | Enhancer of polycomb homolog 1 | | ✓ |
| 1.96 | 6.60 | **Hes1** | Hairy and enhancer of split 1 | ✓ | ✓ |
| 1.65 | 6.60 | **Jmjd6** | Jumonji domain containing 6 | | ✓ |
| 1.11 | 6.60 | **Kmt2d** | Lysine (K)-specific methyltransferase 2D | | ✓ |
| 1.06 | 6.60 | **Marcks** | myristoylated alanine rich protein kinase C substrate | | ✓ |
| 1.57 | 6.60 | **Mbd2** | Methyl-CpG binding domain protein 2 | | ✓ |
| 1.41 | 6.60 | **Mta2** | Metastasis-associated gene family, member 2 | | ✓ |
| 1.25 | 6.60 | **Mxi1** | MAX Interactor 1, Dimerization Protein | | ✓ |
| 1.26 | 6.60 | **Nckap1l** | NCK associated protein 1 like | | ✓ |
| 1.35 | 6.60 | **Pcnxl3** | Pecanex 3 | | ✓ |

Analysis of gene interaction and function using Cytoscape demonstrated that, similar to the $Flt3^{lo}$ hits, the majority of the genes enriched in the $Flt3^{hi}$ samples regulate transcription (**Figure 17**).

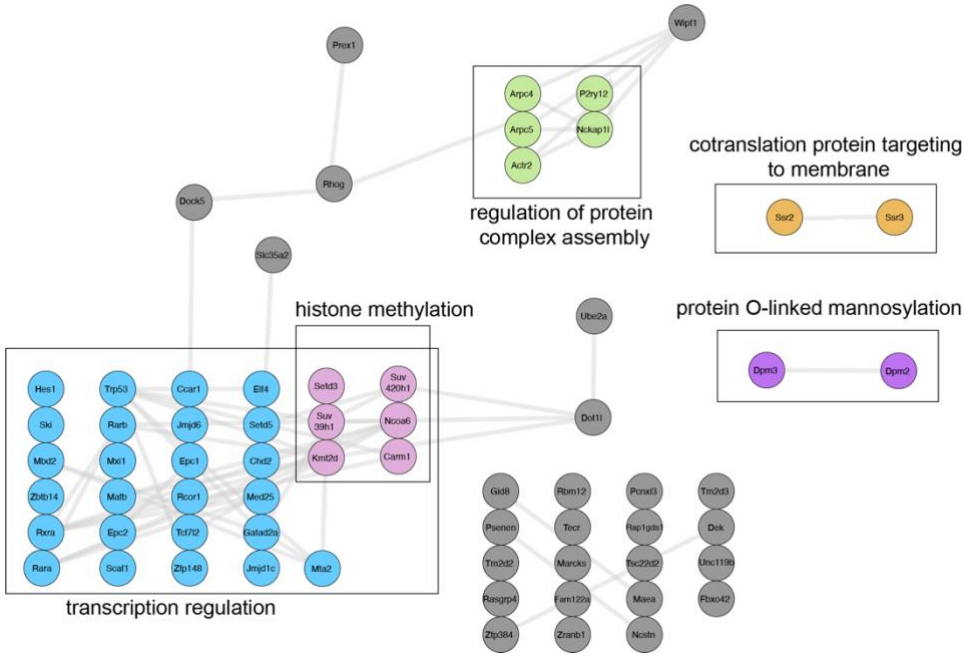


**Figure 17. Protein-protein interactions and functional analysis of Flt3$^{hi}$ hits.** Schematic of experimentally determined and predicted protein interactions and functions as determined using STRING-db plugin on Cytoscape.

Altogether, these data demonstrate we can utilize CRISPR/Cas9 genome wide screens to identify novel regulators of Flt3.

## Validating novel Flt3 regulators.

To narrow the focus, four Flt3$^{hi}$ hits (Med25, Tcf7l2, RhoG and Hes1) and four Flt3$^{lo}$ hits (Ups22, KMT2C, EP300 and ARIH1) were chosen for validation. Flt3 was used as a positive control. These genes were chosen for further validation based on the rationale described in **Table 4**.

**Table 4. Genes chosen for further investigation.**

| gene | regulation | rationale |
|---|---|---|
| ***Med25*** | negative | Most significantly enriched gene in both screens. Described as transcriptional activator in Mediator complex. Not described in DCs. |
| ***Tcf7l2*** | negative | Significantly enriched in both screens. Previously identified as a DC regulator, however, the mechanism is unclear. |
| ***Rhog*** | negative | GTPase with described role in membrane trafficking. Potential post-translational Flt3 regulator. |
| ***Hes1*** | negative | Transcriptional repressor shown to bind to *Flt3* promoter in non-DC cells. |
| ***Flt3*** | positive | Positive control |
| ***KMT2C*** | positive | One of four COMPASS subunits identified in the screen, suggesting COMPASS regulates *Flt3*. |
| ***EP300*** | positive | One of four COMPASS subunits identified in the screen. In addition, has independent roles with other identified hits (for example, Runx1). |
| ***ARIH1*** | positive | E3 ubiquitin ligase. Potentially regulating Flt3 through post-translational mechanism. |
| ***Usp22*** | positive | Binding partner (ATXN7L3) also significantly enriched. Demonstrated role in immune regulation. Undescribed role in DCs. |

To validate the hits, single gene knockouts were generated. To bypass the time-consuming cloning and lentivirus generation that was previously required to generate knockouts, we used synthetic Alt-R CRISPR-Cas9 crRNA and tracrRNA. In addition to being faster, synthetic crRNA is degraded within three-five days. This is particularly useful when it comes to reintroducing the wild type gene at later stages. One caveat is that there is no selection marker for successful transfectants. To generate the knockouts, crRNA specific to each gene and tracrRNA was delivered to cells via lipofection. For a negative control, cells were transfected with a computationally designed non-targeting crRNA. One week following transfection, cell surface Flt3 was assessed by flow cytometry (**Figure 18A**). Clear shifts in the expression of Flt3 were observed in knockout cells in comparison to the negative control. To generate more homogenous populations, the knockout cell lines were sorted for high or low Flt3 expression. Cell surface (**Figure 18B**) Flt3 expression was determined by flow cytometry. This data validates the CRISPR/Cas9 screen hits as genes that regulate Flt3 expression.

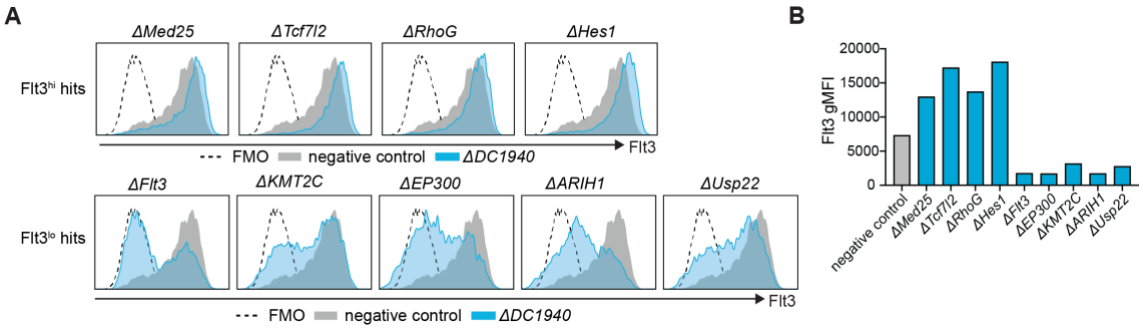


**Figure 18. Flt3 expression on single gene knockouts.** MuTu DC1940 cells were transfected with the crRNA targeting the indicated genes. One week later, cells were stained for Flt3 and analyzed by flow cytometry. (A) Representative cell surface expression. (B) Quantification of (A). Data is representative of at least two independent repeats.

Two of the hits, Med25 and USP22, were then chosen for further characterization. Med25 was selected as it was the most significantly enriched gene for Flt3$^{hi}$ samples in both screens. It has also been identified in a screen for genes that regulate MHC II (Haiyin Liu, Mintern Lab), which indicates it could be a currently unknown master regulator of cDC1 transcription. USP22 was chosen as its binding partner, ATXN7L3, was also a hit in the library. In addition, studies in T and B cells have demonstrated the importance of USP22 in immunity (198, 199), which makes it particularly interesting to study in the context of DC biology.

Before characterizing the role of these genes in Flt3 expression, single cell clones were generated (**Figure 19**) from the single gene knockouts previously engineered (**Figure 18**). For each of the cell lines, 288 clones were generated, expanded and those which survived were genotyped by Sanger sequencing and ICE analysis. From here, eight *ΔFlt3*, nine *ΔMed25* and six *ΔUSP22* clones were confirmed.

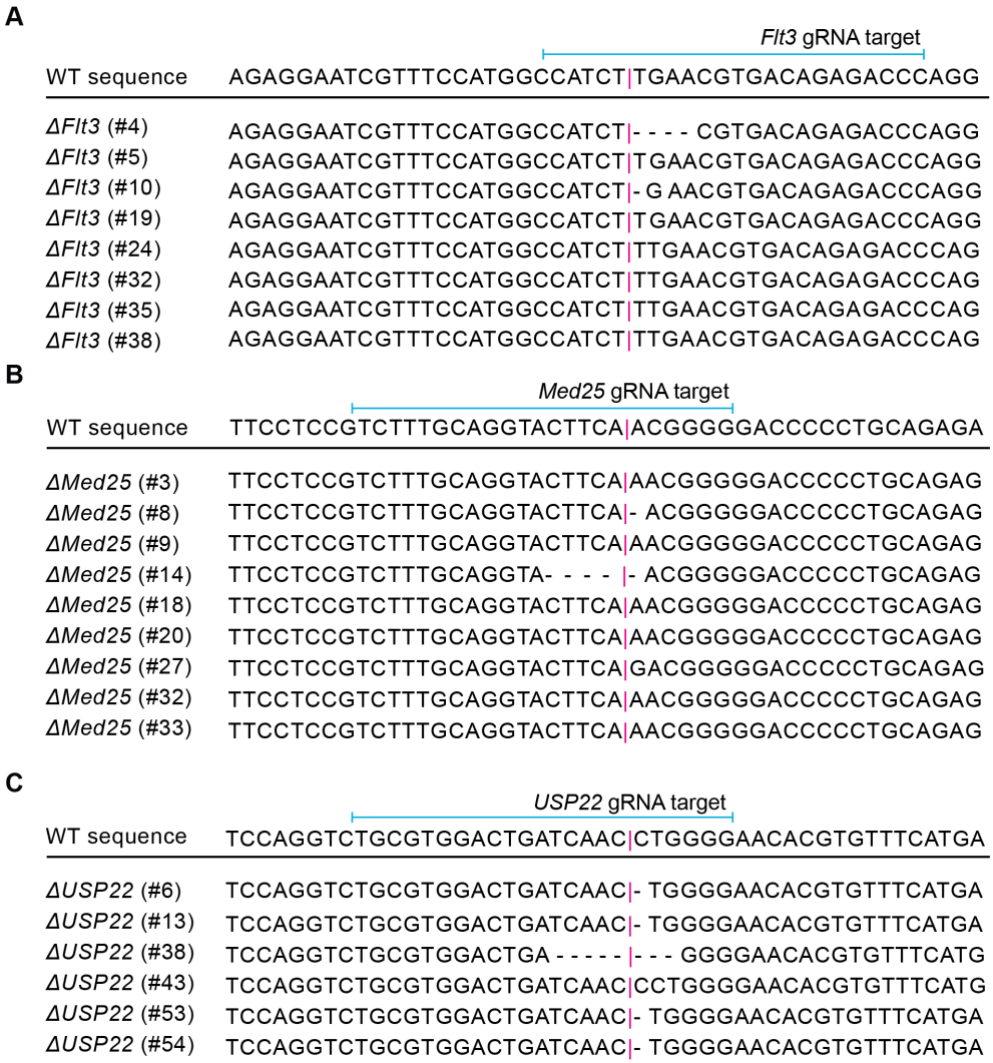


**Figure 19. ICE analysis of *ΔFlt3, ΔMed25* and *ΔUSP22* clones.** Genomic DNA was purified from wild type or single cell sorted (A) *ΔFlt3*, (B) *ΔMed25* and (C) *ΔUSP22* cell lines and the gRNA targeted region was amplified by PCR and sequenced by Sanger sequencing. Formation of insertions and deletions was analyzed by ICE analysis. gRNA target for each gene is indicated by the blue line. Predicted cut site is indicated by the pink line.

The validated clones were used in subsequent experiments. First, the expression of cell surface molecules was analyzed by flow cytometry (**Figure 20A**). In agreement with our previous data, loss of *Med25* led to increased Flt3 cell surface expression, whereas loss of *USP22* reduced Flt3 cell surface expression. Notably, the loss of *USP22* led to a significant reduction in CD24 and small reductions in CD40 and DEC205. In addition to Flt3, the loss of *Med25* lead to a small decrease in MHC II expression. The latter was

expected given Med25 was a hit in a screen for genes that regulate MHC II cell surface expression (Haiyin Liu, Mintern Lab).

Med25 deficient cells have elevated Flt3 cell surface expression and therefore it is important to determine if the receptor is responsive to Flt3L. Given *ΔUSP22* clones lack Flt3, they were not included in this assay. To test Flt3L responsiveness, Med25 deficient cells and WT cells were stimulated with 100 ng/mL Flt3L for 30 minutes and the cell surface expression of Flt3 was determined by flow cytometry (**Figure 20B**). A significant reduction in the expression of Flt3 was observed in *ΔMed25* clones in comparison to WT clones, this is unsurprising given the steady-state expression of Flt3 is higher on *ΔMed25* cells. This data confirms that *ΔMed25* cell surface Flt3 is responsive to Flt3L.

.

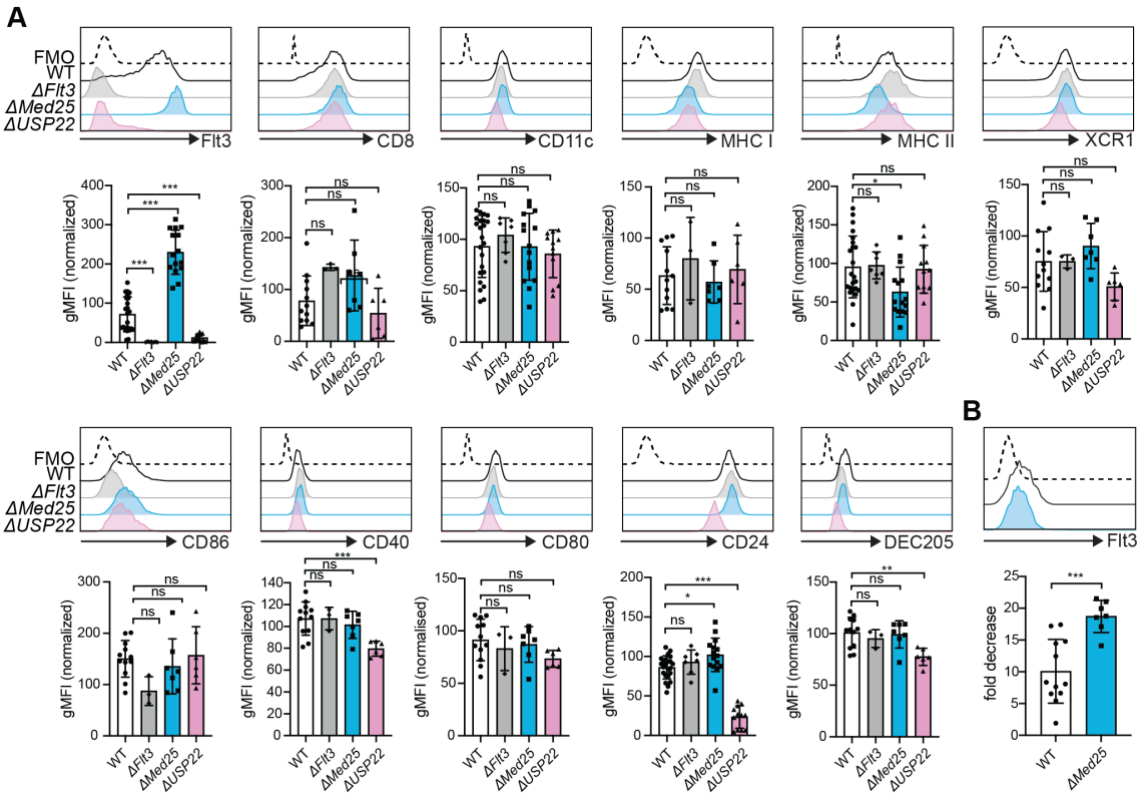


**Figure 20. Impact of the loss of *Flt3, Med25 and USP22* on DC cell surface expression.** (A) Wild type (WT), *ΔFlt3*, *ΔMed25*, *ΔUSP22* MuTuDC1940 cells were stained with antibodies against Flt3, CD8, CD11c, MHC I, CD80, XCR1, CD86, CD40, MHC II, CD24 and DEC205 before analysis by flow cytometry. Data is pooled from one or two experiments. gMFI has been normalized to the average WT gMFI. Symbols represent individual knockout clones. (B) WT (solid black line) and *ΔMed25* (filled blue line) MuTuDC1940 cells were stimulated with 100 ng/mL Flt3L for 30 mins. Cells were washed extensively prior to staining for Flt3 and analysis by flow cytometry. Data is from one experiment. Statistical analysis was performed with a one-way ANOVA with Dunnett's multiple comparisons test. Symbols represent individual clones. Ns not significant, * P<0.033, ** P<0.002, *** P<0.001

Changes in Flt3 cell surface expression could be due to altered *Flt3* transcription or Flt3 trafficking. To investigate the former, qPCR and immunoblotting were carried out on the knockout clones (**Figure 21**). Elevated *Flt3* expression (**Figure 21A**) and protein Flt3 (**Figure 21B**) was observed in cells lacking *Med25*. This suggests transcriptional changes are responsible for the observed increase in Flt3 cell surface expression. In contrast, the loss of *USP22* resulted in reduced *Flt3* mRNA expression (**Figure 21A**) and reduced total

Flt3 expression (**Figure 21B**), indicating the reduced Flt3 cell surface expression in these cells is likely due to reduced *Flt3* transcription.

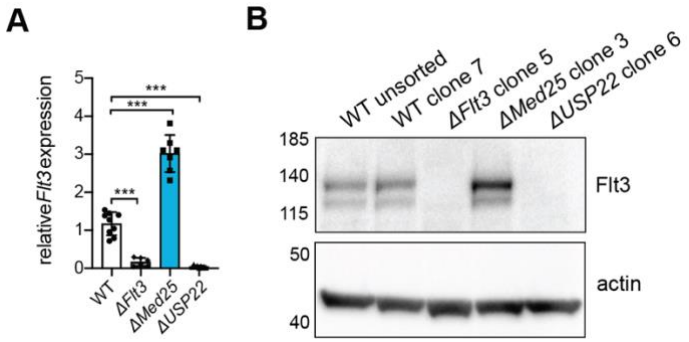


**Figure 21. Flt3 expression in knockout cells.** (A) *Flt3* mRNA expression. RNA was extracted from equivalent number of MuTu DC1940 cells using RNeasy Mini Kit before genomic DNA was removed with DNAse I. cDNA was synthesized using SensiFAST cDNA synthesis kit and qPCR was performed using Taqman Fast system and Taqman probes specific for Flt3 and HPRT. The relative *Flt3* expression was normalized to HPRT and calculated using the ddCt method. (B) Wild type (WT) unsorted and WT and knockout clonal cells were lysed in NP40 lysis buffer. Equivalent to 2 x $10^5$ cells/lane were separated by gel electrophoresis and transferred to a PVDF membrane. Blots were probed for Flt3 or actin.

Altogether, these data demonstrate we have identified Med25 and Usp22 as two previously unknown regulators of *Flt3* expression.

# Discussion

In this chapter, CRISPR/Cas9 genome-wide screens were used to uncover genes that regulate Flt3 in DCs. Prior to carrying out the screens, we characterized the expression of Flt3 in the $CD8^+$ MuTu DC1940 cell line and confirmed it behaved the same as its *in vivo* counterpart. Indeed, both intracellular and cell-surface Flt3 were easily detected, and the latter was responsive to Flt3L. Notably, the regulation of wild type DC Flt3 has been neglected until now, with this chapter being the first to use a screen to identify wild type Flt3 regulators.

Flt3L-stimulated screen vs steady-state screen

In the first screen, cells were stimulated with Flt3L prior to cell sorting to elucidate the genes that regulate activated Flt3. Internalization of cell surface Flt3 is thought to be mediated by phosphorylation and ubiquitination of the receptor, and as such we predicted phosphorylation and ubiquitination machinery genes to be enriched. Surprisingly, we did not identify any known Flt3 phosphatases, ubiquitin ligases and deubiquitinating enzymes. While it is possible that the screen was simply not sensitive enough to identify these genes, the more likely scenario is that the genes that regulate activated Flt3 are functionally redundant. Indeed, in non-DC lines, overexpressed Flt3 has been shown to interact with numerous phosphatases (152, 192–194) and E3 ligases (176, 178). Therefore, alternative phosphatases, E3 ligases or deubiquitinases could compensate for the loss of a single gene. Given the screens were specifically designed such that every cell only received one gRNA, any gene that could be compensated for by others would not be identified. Further studies will therefore be required to investigate the post-translational modifiers of Flt3. One method which would allow for the identification of

proteins that preferentially bind to activated Flt3 is co-immunoprecipitation of Flt3 from DCs stimulated with or without Flt3L followed by mass spectrometry.

It is less surprising that Flt3-specific phosphatases or ubiquitin E3 ligases were not identified in the steady-state Flt3 screen, given these genes would only impact the expression of activated Flt3 (not steady-state). Indeed, overexpression studies have showed interactions between cell surface Flt3 and c-Cbl are enhanced upon Flt3L stimulation (176, 178). Other genes expected to appear in the screens were PU.1 (*Sfpi1*), homeobox protein Hox-A9 (HOXA9) and the negative regulator LAMTOR2. It is possible that these genes were missed in both screens due to the 5% sorting gates that were used which may have been too stringent to capture genes that have a mild effect on Flt3 expression. In addition, it is possible that alternate pathways regulate Flt3 expression in DC1940 cell line. In future, these limitations could be circumvented by increasing the sorting gates (from 5% to 10%) and using $Cas9^{+}$ bone marrow cells (200).

In the steady-state Flt3 screen, 22 potential positive regulators and 65 potential negative regulators of Flt3 were identified. The high number of Flt3 negative regulators suggests uncontrolled upregulation of Flt3 may be detrimental to DCs and hematopoietic progenitors. In line with this, overexpression of wild type *Flt3* is observed in some patients with AML and is correlated with reduced prognosis and overall survival (201). Elevated Flt3 is correlated with autophosphorylation of the receptor (201) likely due to increased Flt3L binding due to a proposed compensatory feedback loop (202). This is supported by studies showing elevated serum Flt3L in mice with increased DC Flt3 cell surface expression due to absence of LAMTOR2 (195). It is tempting to speculate that

multilayered negative regulation of Flt3 is necessary to prevent excessive Flt3 signaling and unchecked cell proliferation and survival.

Flt3 positive regulators

The most significantly enriched potential positive Flt3 regulator was *Flt3* itself. In addition to this, *runt-related transcription factor- 1(Runx1), -3 (Runx3)* and *Core-binding factor subunit beta (Cbfβ)* were significantly enriched. Runx proteins are transcription factors whose binding to DNA is improved by forming heterodimers with Cbfβ (203, 204). Runx1 and Cbfβ are required for the development of DCs and their progenitors, with reduced DCs observed in the spleens of lethally irradiated mice reconstituted with bone marrow cells lacking *Runx1* or *Cbfβ* (168). Mice lacking either of these genes in $CD11c^+$ cells had reduced Flt3 expressing progenitors, suggesting these genes may regulate Flt3 expression in addition to DC development (168), though this has not been shown in DCs as yet. *Flt3* does not have a Runx binding motif so Runx proteins and/or Cbfβ would have to indirectly regulate *Flt3* expression by promoting transcription of a Flt3 positive regulator. An example of this would be Runx1 binding directly to the PU.1 locus and promoting PU.1 expression (169), which would then promote Flt3 expression (163). These genes were not followed up with in this study due to their already well-described roles in hematopoiesis, however, future experiments could validate their role in Flt3 regulation by generating single gene knockouts. In addition, chromatin-immunoprecipitation (ChIP) using antibodies for Runx1, Runx3 or Cbfβ followed by DNA sequencing (ChIP-seq) could be used to identify the genes they regulate in primary cDC1.

Out of the remaining Flt3 positive regulators, *lysine Methyltransferase 2C (KMT2C), E1A Binding Protein P300 (EP300), Ariadne RBR E3 ubiquitin ligase (ARIH1) and ubiquitin specific peptidase 22 (USP22)* were chosen for further investigations.

Flt3 positive regulators: COMPASS

*KMT2C* and *EP300* were chosen as they are known to associate in the large protein complex COMPASS (Complex of Proteins Associated with SET1). Importantly, two other members of COMPASS were significantly enriched in the $Flt3^{lo}$ samples: *PAX Interacting Protein 1 (PAXIP1)* and *PAXIP1-associated glutamate-rich protein 1A* (PAGR1A) (Figure 22). The appearance of four members of COMPASS strongly implicates this complex in the regulation of Flt3. COMPASS plays a critical role in regulating gene expression by post-translationally modifying histones (205). KMT2C is responsible for the monomethylation of histone (H) 3 lysine (K) 4 (H3K4me1) (206), whereas EP300 acetylates histones H3K27 (207, 208). PAXIP1 is required for the recruitment of COMPASS members to the target gene and also regulates histone methylation (209, 210). PAGR1A directly binds to PAXIP1(210) . These modifications allow for chromatin relaxation and promote gene transcription. Individual knockouts of *KMT2C* and *EP300* in MuTu DC1940 showed reduced Flt3 cell surface expression and confirmed the genes are positive regulator of Flt3. While the role of COMPASS has not been described in DC, it is hypothesized that COMPASS promotes the transcription of *Flt3* by modifying chromatin at the Flt3 locus. To validate this, future experiments could use ChIP-seq to confirm where in the genome these proteins bind. In addition, co-immunoprecipitation of the proteins could confirm that they are in fact acting together in COMPASS. This is particularly important given that some members of COMPASS are

known to perform COMPASS-independent functions. For example, EP300 and one of its binding partners CBP, can acetylate non-histone proteins (211).

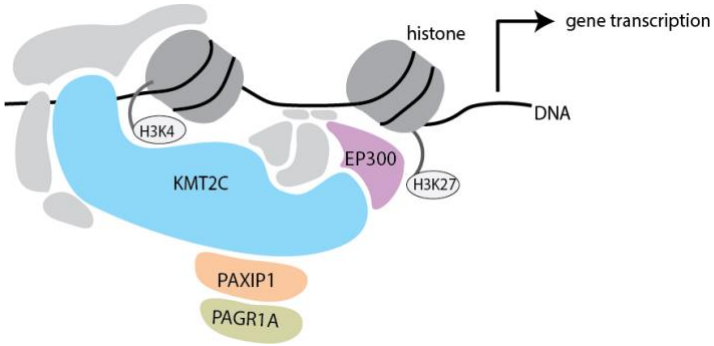


**Figure 22. COMPASS regulates *Flt3* transcription.** Diagram depicting the potential role of COMPASS in the regulation of *Flt3* transcription. Colored components, including KMT2C, PAXIP1, PAGR1A and EP300, were identified in the screen. Shaded components were not identified in the screen.

Flt3 positive regulators: ARIH1

*ARIH1* encodes a Really Interesting New Gene (RING)-in-between-RING (RBR) E3 ubiquitin ligase. ARIH1 ubiquitinates target proteins with the assistance of its cognate E2 ubiquitin-conjugating enzyme, ubiquitin-conjugating enzyme E2 L3 (UBCH7/UBE2L3) (212–214). Unlike standard E3 ubiquitin ligases, ARIH1 is autoinhibited and requires the assistance of neddylated Cullin RING E3 ligases (CRLs) for activation (Figure 23). As such, ARIH1 has been shown to bind to the majority of Cullins (213, 214). This association activates it and promotes monoubiquitination of target proteins (213, 214). Once the target is monoubiquitinated, it can be further polyubiquitinated by the CRL (214).

There are currently no studies investigating the role of ARIH1 in DCs. If ARIH1 was ubiquitinating Flt3 directly, we would expect elevated Flt3 in its absence. Given we see

the opposite, it is likely that ARIH1, in combination with a CRL, ubiquitinates a Flt3 repressor. An appealing candidate is Hes1 - a negative Flt3 regulator identified in this screen and previously shown to repress Flt3-ITD in cancer cells by binding directly to the Flt3 promoter (170). This is particularly attractive given that FBXL14, a CRL substrate receptor, which was also identified as a positive Flt3 regulator in this screen, has been shown to bind to Hes1 and promote its ubiquitin-dependent degradation in non-DC lines (215). It will be interesting to investigate the Hes1 ubiquitination status and protein expression level in cells lacking *ARIH1* and *FBXL14*. If these genes do indirectly regulate Flt3 via Hes1, reduced Hes1 ubiquitination and elevated Hes1 protein expression would be expected in their absence.

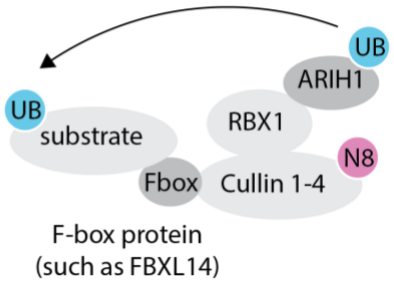


**Figure 23. ARIH1 regulates Flt3.** Diagram depicting the potential role of ARIH1 in the post-translational regulation of Flt3. ARIH1 binds to Cullin RING E3 ligases via RBX1 (RING-box protein 1) and adds the first ubiquitin to the target substrate. Recognition of the substrate is carried out by Fbox proteins, such as FBXL14 which was identified in the screen. Given loss of ARIH1 leads to reduced Flt3 expression, it is hypothesized that ARIH1 promotes the ubiquitination of a Flt3 repressor, such as HES1.

Flt3 positive regulators: USP22

*USP22* was the final positive regulator the analysis was extended to. USP22 forms part of the death-from-cancer gene signature (216), with elevated expression correlating with

poor prognosis of solid tumors (217). USP22 is a deubiquitinating enzyme in the deubiquitination module (DUBm) of the Spt-Ada-Gcn5 acetyltransferase (SAGA) complex (218–221). SAGA also comprises a histone acetyltransferase (HAT) module, which along with the DUBm, allows it to coordinate chromatin modifications and regulate gene transcription (222). Additional members of the DUBm include USP22 cofactors Ataxin 7-like 3 (ATXN7L3) (221, 223, 224) and enhancer of yellow 2 homology (ENY2) (221, 225). Importantly, the former was also identified in the screen which strongly implicates the SAGA DUBm in the regulation of *Flt3*.

As a deubiquitinase, USP22 deubiquitinates H2A monobuqitination (H2Aub1) (226) and H2Bub1 (218, 219) which promotes gene transcription (Figure 24A). After confirming the role of USP22 in Flt3 regulation by generating *ΔUSP22* MuTu DC1940 cells, this gene was selected for extended analysis using single cell sorting as it has not been described in DCs, yet numerous studies have underscored its important role in other aspects of immunity. In Tregs, USP22 and ATXN7L3 are positive regulators of the transcription factor *Foxp3* (198). Tregs lacking *USP22* display elevated H2Aub1 and H2Bub1 and reduced Foxp3 expression. Ultimately, these changes lead to Tregs that are unable to suppress immune responses to the same extent as wild type Tregs which improves antitumor responses but exacerbates autoimmunity (198). In B cells, the loss of *USP22* again leads to elevated H2Bub1. This impacts non-homologous end joining repeats which leads to defective class-switch recombination, IgG responses and B cell development (199). Mice lacking *USP22* in hematopoietic cells have elevated H2Bub1 and have a skewed differentiation towards myeloid cells with impaired B cell development observed (227). Gene expression analysis on hematopoietic stem cells

revealed a lack of USP22 leads to elevated inflammation and immunity-related gene expression, particularly with interferon-stimulated genes (227). Given we observe reduced *Flt3* in *ΔUSP22* MuTu DC1940 cells, if the same occurs in DC progenitors, it is possible that altered DC development would also occur in these mice. Unfortunately, however, the authors failed to investigate the DC compartment. Given mice lacking Flt3 or Flt3L lack DCs, if USP22 does regulate Flt3 expression, reduced DC differentiation would be expected in its absence.

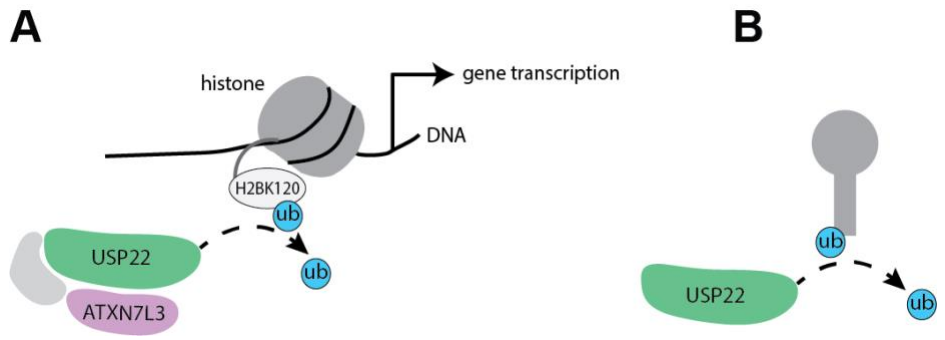


**Figure 24. USP22 regulates Flt3.** Diagram depicting the potential ways in which USP22, and ATXN7L3, may regulate Flt3 expression. (A) In the DUB module of the SAGA complex, USP22 and ATXN7L3 may deubiquitinate histones and promote the transcription of *Flt3* or a Flt3 positive regulator. (B) Independent of SAGA, USP22 may deubiquitinate non-histone proteins, such as Flt3 negative regulator.

Notably, USP22 can also deubiquitinate non-histone proteins independent of SAGA (Figure 24B). Indeed, Cortez and associates demonstrated that besides regulating *Foxp3* transcription, USP22 interacts with Foxp3 in primary murine Tregs. When USP22, Foxp3 and ubiquitin are overexpressed in HEK293T cells, reduced Foxp3 ubiquitination is observed (198). Similar results are observed when USP22 and the transcription factor PU.1 are overexpressed in HEK293T cells (228). These interactions could be artefacts of overexpression. Indeed, myeloid progenitor cells lacking USP22 have a similar expression of PU.1 as wild type progenitor cells (228). USP22 deubiquitination of non-

histone proteins is, however, more convincing in cancer cells. In liver (229) and lung cancer cells (230) USP22 interacts with PD-L1, with elevated PD-L1 ubiquitination and degradation observed in the absence of USP22 (229, 230). Given the co-inhibitory role of PD-L1, mice harboring *USP22* knockout tumor cells have increased tumor infiltrating lymphocytes and improved tumor clearance in comparison to mice harboring wild type tumor cells (229, 230). Similarly, in colorectal carcinoma cells, USP22 interacts with Sirt1 (231). Loss of USP22 increases Sirt1 ubiquitination and degradation (231). It is unclear if the same interactions occur in wild type cells with endogenous protein expression. While it is possible that USP22 is regulating Flt3 post-translationally, transcriptional regulation is more likely given USP22s cofactor, ATXN7L3, was a hit in the screen in addition to reduced *Flt3* mRNA observed in *ΔUSP22* MuTu DC1940 cells. Besides regulating *Flt3* transcription directly, it is possible that USP22 indirectly regulates *Flt3* by promoting the transcription of a Flt3 positive regulator. While beyond the scope of this project, ChIP-qPCR will be useful in determining if USP22 is directly regulating histone ubiquitination at the *Flt3* locus. In addition, to identify all DC genes regulated by USP22, ChIP-seq could be carried out. In combination with RNA-sequencing of wild type versus USP22 knockout cells, this could reveal the full extent of USP22 regulation in DCs. Given *ΔUSP22* MuTu DC1940 cells have reduced expression of CD40, CD24, and DEC205 in addition to Flt3, ChIP-seq and RNA-seq may reveal USP22 regulates the transcription of these individual genes or alternatively acts as a master regulator of DC transcription.

It is unlikely that the responsibility of *Flt3* promotion is due to one single transcriptional pathway (for example Runx/Cbf*β*, COMPASS or SAGA). Instead, a combination of

transcription factors and chromatin modifiers is likely at play. This would allow DCs, and other immune cells, to fine tune their expression of *Flt3*. In support of this idea, EP300 has been shown to bind to (232, 233) and acetylate (234) Runx1. This increases the DNA-binding affinity of Runx1 and potentiates Runx1-dependent transcription.

Flt3 negative regulators

In regard to Flt3 negative regulators, *hairy and enhancer of split-1 (Hes1), transcription factor 7 like 2 (TCF7L2), Ras homology Growth-related (RhoG)* and *Mediator 25 (Med25)* were chosen for further investigations.

Flt3 negative regulators: Hes1

*Hes1* encodes a transcriptional repressor (Figure 25) that plays an important role in Notch signaling. In particular, it has well-described roles in T cell development, and is often upregulated in cancer (reviewed in (235)). Hematopoietic cells lacking *Hes1* have impaired T cell development (171, 236, 237) and a skew towards myeloid cell and DC development (171). This phenotype is rescued with the deletion of CCAAT/enhancer-binding protein alpha (C/EBPα) (171), a transcription factor essential for the development of DCs (238). Hes1 can bind to the promoter of C/EBPα (171, 239) and therefore likely represses the expression of C/EBPα directly to allow for the development of non-DC lineages. Loss of C/EBPα in common myeloid progenitor cells leads to reduced PU.1 expression (238), which, as previously mentioned, promotes *Flt3* expression (163). It is possible that the same mechanism occurs in DCs given we observed reduced Flt3 expression in MuTu DC1940 cells lacking *Hes1*. To investigate this, ChIP assays along with RNA-seq will essential.

Notably, Hes1 has been shown to bind directly to the promoter of Flt3 and repress the transcription of Flt3-ITD in cancer cells (170). It is possible that Hes1 performs the same function in healthy DC, though this does assume the transcription factor is performing the same in healthy and malignant settings. This not always the case, especially for transcription factors which are often dysregulated in cancer to confer growth and/or survival advantages (240).

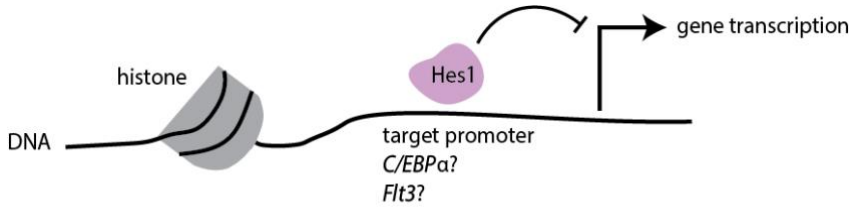


**Figure 25. Hes1 regulates *Flt3*.** Diagram depicting the potential role of Hes1 in the regulation of Flt3. As a corepressor, Hes1 binds to target gene promoters and represses the transcription of genes. Hes1 can indirectly repress Flt3 by repressing Flt3 positive regulators, such as C/EBPα or alternatively Hes1 can directly repress the transcription of Flt3.

Flt3 negative regulators: TCF7L2

*TCF7L2* was significantly enriched in the $Flt3^{hi}$ sorted samples in both the GeCKO and Brie screens which gave confidence it was a genuine Flt3 regulator. TCF7L2 is one of four transcription factors in the TCF/LEF (T cell factor/lymphoid enhancer factor) family. TCF/LEF proteins act downstream of Wnt signaling to regulate gene expression (241). In the absence of Wnt ligands, TCF/LEFs repress transcription of genes by binding DNA and corepressors. In the presence of Wnt ligands and signaling, TCF/LEFs promote gene transcription due to β-catenin associating and displacing corepressors whilst recruiting coactivators (241) (Figure 26). Often corepressors and coactivators are involved in

histone modification (242). Surprisingly, one chromatin modifying enzyme identified in this screen, jumonji domain-containing protein 6 (JMJD6), has been shown to impact TCF7L2 expression in glioma stem cells (243). It is unclear if it performs the same function in healthy DCs. The role of TCF7L2 in immune cells is elusive given most studies have focused on its role in β cells. This is due to large-scale genome-wide association studies identifying small nucleotide polymorphisms (SNPs) within the *TCF7L2* locus as the most significant signal for diabetes mellitus type 2 (244). Importantly, RNA-seq analysis from the Immunological Genome Project shows *TCF7L2* is highly expressed in DC and macrophages (245), with little expression observed in B or T cells. Further to this, a large-scale phenotypic and transcriptional analysis of human blood, spleen and thymus cDC1 ($CD141^+$), cDC2 ($CDc1^+$) and pDC ($CD303^+$) revealed TCF7L2 as a potential $CD141^+$ DC transcriptional regulator, though the authors were unclear of the mechanism (246). Along with the increased Flt3 expression observed in *ΔTCF7L2* MuTu DC1940, this data provides a strong basis for further investigations into the role of DC TCF7L2.

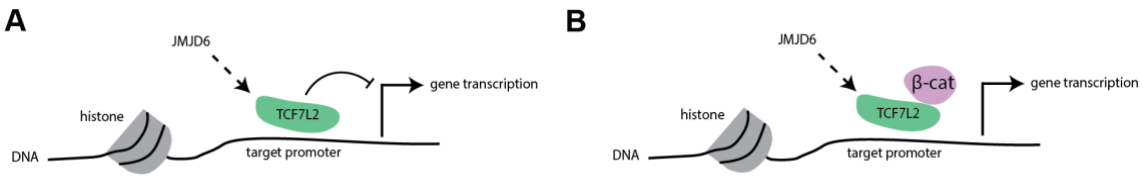


**Figure 26. TCF7L2 regulates *Flt3*.** Diagram depicting the potential role of TCF7L2 in the regulation of Flt3. (A) In the absence of Wnt ligands, TCF/LEFs repress transcription of genes by binding DNA and corepressors. (B) In the presence of Wnt ligands and signaling, TCF/LEFs promote gene transcription due to β-catenin associating and displacing corepressors whilst recruiting coactivators. JMJD6, a hit in the screen, has been shown to promote TCF7L2 expression.

Flt3 negative regulators: RhoG

*RhoG* was another gene identified. RhoG belongs to the Rac subfamily of the Rho GTPases. As a GTPase, it cycles between an "off" and "on" state to regulate signaling pathways (Figure 27). In the off state, GTPases are bound to GDP and are often sequestered by guanine nucleotide dissociation inhibitors (GDI) in the cytoplasm. Once a guanine nucleotide exchange factor (GEF) exchanges GDP for GTP, the GTPase changes conformation and can interact with downstream effectors which have significant impacts on immunity, such as toll-like receptor signaling, chemotaxis and endocytosis (247). GTPases are returned to their inactive state when GTP is hydrolyzed by GTPase activating proteins (GAPs). Importantly, this screen also identified *$PIP_3$-dependent Rac exchange factor-1* (*P-rex1)*, a known RhoG GEF in neutrophils (248). This suggests that activated RhoG regulates Flt3 expression in DCs. RhoG has not been extensively studied in DCs, however, it has been shown to play an important role in exocytosis (249), phagocytosis (250–252), macropinocytosis (253), trogocytosis (254), and receptor internalization (254) in natural killer cells, $CD8^+$ T cells, B cells, macrophages and fibroblasts. It is currently unclear how RhoG impacts Flt3 expression in DCs, though it is likely an inadvertent effect of RhoG's control over membrane trafficking. To confirm this, the internalization of Flt3 in wild type and *$RhoG^{-/-}$* DC should be investigated, with reduced Flt3 internalization expected in the latter. In addition, the transcription of *Flt3* is expected to remain unchanged in the absence of RhoG. While beyond the scope of this study, investigations into the role of RhoG in DC endocytosis, which is critical for DC antigen presentation and immunity, will be particularly intriguing given the role it plays in other immune cells.

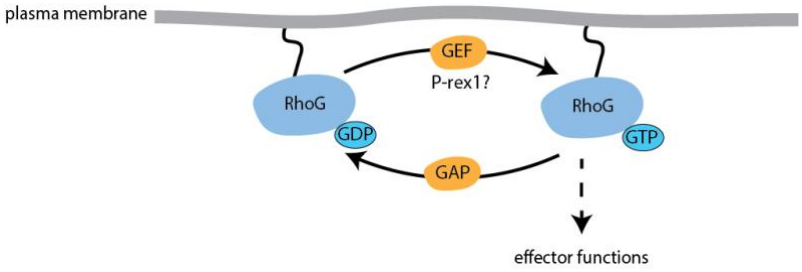


**Figure 27. RhoG is a GTPase with pleiotropic effects.** Diagram depicting RhoG activation and the potential involvement of P-rex1. As a GTPase, RhoG is bound to GDP in an "off" state until guanine nucleotide exchange factors (GEFs), such as P-rex1, exchange GDP for GTP. Once bound to GTP, RhoG is active and can carry out its effector functions, which include receptor internalization, exocytosis, phagocytosis and micropinocytosis. RhoG is returned to its inactive state by guanine activating proteins (GAPs).

## Flt3 negative regulators: Med25

The final gene hit investigated was *Med25*. Med25 is a subunit of the Mediator Complex, which comprises of approximately thirty subunits in humans (255). These subunits are assembled into four modules termed the "head", "middle", "tail" and the cyclin-dependent kinase (CDK8) (256). Mediator is required for the transcription of all RNA polymerase II (Pol II)-dependent genes (255). It performs this function by bridging gene-specific transcription factors, initiation factors and elongation factors with Pol II (257) (Figure 28). Not all subunits are required for transcription of all genes. The loss of one subunit tends to impact specific pathways, depending on the transcription factors it binds to (257). Med25 resides in the tail module and regulates the transcription of specific genes by binding to gene-specific transcription factors, such as ETV1, 4 and 5 (258), JUN/FOS (258), SRY-Box transcription factor 9 (SOX9) (259), Hepatocyte Nuclear Factor 4 α (HNF4α) (260), estrogen receptor α (ERα) (261) and retinoic acid (RA)- bound retinoic

acid receptor (RAR) (262). Interactions with these transcription factors promote the transcription of genes. It's role in DCs is undescribed but given *ΔMed25* MuTu DC1940 cells exhibit elevated cell surface Flt3 which corresponds to elevated *Flt3* transcription it is likely that Med25 promotes the transcription of a Flt3 negative regulator. For example, Med25 could bind to the transcription factor SOX9 (259), which in turn could bind to the promoter of Hes1 (263). As previously mentioned, Hes1 can bind to the promoter of *Flt3* in leukemia cells and repress *Flt3* transcription (170). As mentioned for other transcription factors identified in this screen, future studies will have to rely on ChiP-seq and RNA-seq to identify where Med25 binds and which genes it is regulates. In addition, co-immunoprecipitation and mass spectrometry will be useful for revealing the transcription factors it binds to. Interestingly, Med25 has appeared in two other screens that investigated genes that regulate MHC II and PD-L1 (Haiyin Liu and Christophe Macri, Mintern Lab). In corroboration with the former, this chapter showed reduced MHC II expression in *ΔMed25* MuTu DC1940 cells. Together, this suggests that Med25 may play an important role as a master regulator of DC function, regulating the expression of genes that are essential for survival and antigen presentation.

An important question is why other Mediator subunits were not detected in the screen. One reason for this is that the complete loss of Mediator would lead to a widespread reduction in gene transcription and cell death. As such, any gene that impacts the structure or function of Mediator would not be detected in the screen. Given Med25 sits at the tail of Mediator and is only implicated in specific pathways, it is unlikely that it impacts the widespread transcription of genes in Mutu DC1940 cells and as a result cells lacking this gene were viable.

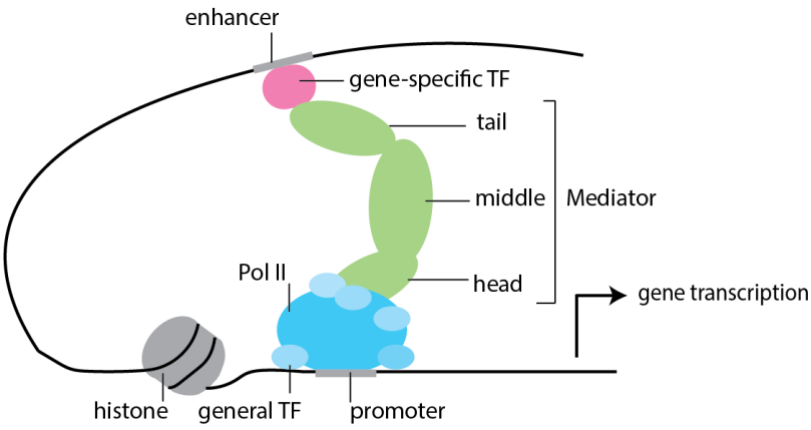


**Figure 28. Med25 is a component of Mediator and controls transcription.** Diagram depicting the role of Mediator in gene regulation. Mediator promotes the transcription of genes by bridging gene-specific transcription factors (TFs), general TFs, initiation factors and RNA polymerase II (Pol II). Med25 is a nonessential component that resides in the tail of Mediator and connects it to gene-specific TFs.

## Future prospects

Moving forward, it will be essential to examine if manipulation of the genes identified in this chapter can improve immune outcomes. First, the proliferation and survival of the knockout cells need to be assessed *in vitro*. This can be done by quantitating cell growth over a certain number of days, in addition to looking at BrdU incorporation, Ki67 and/or CFSE/cell trace violet staining. To determine the impact on DC development, each gene can be knocked out in $Cas9^{+}$ bone marrow cells by transducing the cells with gRNA. The impact of the loss of the gene on DC development can then be assessed *in vitro* or *in vivo* (264). It is expected that the loss of positive regulators, which have reduced Flt3 expression, will lead to reduced DC developmental potential. Conversely, loss of negative regulators should increase differentiation of DCs. The impact on antigen presentation can also be assessed *in vitro* by incubating knockout MuTu DC1940 cells with ovalbumin antigen and cell-trace violet labelled T cells specific for OVA-antigen on MHC I or MHC II (OT cells). Some genes, such as Med25 (265), have specific inhibitors which can be

utilized *in vitro* and *in vivo*. These could be useful for assessing the impact of the gene on Flt3 expression and immune responses *in vivo*. Finally, the function of these genes on Flt3 expression and DC function *in vivo* can be assessed with knockout mice. Importantly, the loss of several of the genes discussed in this chapter leads to unviable mice. Therefore, mice which allow targeted ablation of the gene in cDC1 (*XCR1*-cre), DCs (*Zbtb46*-cre or -DTR) and hematopoietic progenitors (*Vav1*-cre) should be used.

# Chapter 5 - Publication: MHC II ubiquitination regulates dendritic cell function and immunity.

This chapter was published in The Journal of Immunology (2021). The specific contributions of authors are disclosed in the "Preface" and "Publications arising from this thesis" sections of this thesis. The published manuscript can be found in Appendix 6.

## ABSTRACT

Major histocompatibility class II (MHC II) antigen presentation by dendritic cells (DCs) is critical for $CD4^+$ T cell immunity. Cell surface levels of MHC II loaded with peptide is controlled by ubiquitination. Here we have examined how MHC II ubiquitination impacts immunity, using *MHC IIKR*$^{KI/KI}$ mice expressing mutant MHC II molecules that are unable to be ubiquitinated. Numbers of conventional DC (cDC)1, cDC2 and plasmacytoid DC (pDC) were significantly reduced in *MHC IIKR*$^{KI/KI}$ spleen, with the remaining *MHC IIKR*$^{KI/KI}$ DC expressing an altered surface phenotype. While antigen uptake, endosomal pH, and cathepsin protease activity were unaltered, *MHC IIKR*$^{KI/KI}$ cDC1 produced increased inflammatory cytokines and possessed defects in antigen proteolysis. Immunization of *MHC IIKR*$^{KI/KI}$ mice identified impairments in MHC II and MHC I presentation of soluble, cell-associated and/or DC-targeted ovalbumin via mAb specific for DC surface receptor Clec9A (anti-Clec9A-OVA mAb). Reduced T cell responses and impaired cytotoxic T lymphocyte killing was observed in *MHC IIKR*$^{KI/KI}$ mice following immunization with cell-associated and anti-Clec9A-OVA and immunization of *MHC IIKR*$^{KI/KI}$ mice failed to elicit significant follicular T helper ($T_{FH}$)

cell responses and generated barely detectable antibody to anti-Clec9A mAb-targeted antigen. In summary, MHC II ubiquitination in DCs impacts the homeostasis, phenotype, cytokine production and antigen proteolysis by DCs with significant consequences for antigen presentation, T cell and antibody-mediated immunity.

# INTRODUCTION

Major histocompatibility class II molecules (MHC II) present peptide antigens derived from the endosomal pathway to $CD4^+$ T cells. This is essential for T cell activation during immune responses, but also in thymic T cell selection and T cell maintenance in peripheral lymphoid organs. The stability and abundance of peptide-loaded MHC II (pMHC II) at the cell surface of antigen presenting cells is regulated by ubiquitination. Ubiquitination occurs on lysine 225 (K225) in the β chain of MHC II (89–91). The E3 ligase responsible for pMHC II ubiquitination in hematopoietic cells, including B cells and dendritic cells (DCs), is membrane associated RING-CH-type finger 1 (MARCH1) (92, 93, 95, 99) while MARCH8 is responsible for ubiquitination in thymic epithelial cells (95, 106, 107) and type II alveolar epithelial cells (95). Ubiquitination targets pMHC II for lysosomal degradation (100). As a result, DCs from mice lacking MARCH1 (*Marchf1*$^{-/-}$) (92, 95) or expressing MHC II molecules with Lys225 mutated to Arg (*MHC IIKR*$^{KI/KI}$), which cannot be ubiquitinated, have increased surface MHC II expression (94). Despite surface MHC II being critical for T cell development, mice that lack MHC II ubiquitination have only minor alterations in their T cell compartments. We and others reported reduced regulatory T cells (Tregs) (12, 13, 14), but there is little impact on steady state conventional T cell populations (110). The functional consequences for immunity are unclear though, as little analysis has been carried out to address this question. This is surprising given the important role of antigen presenting cells, particularly DCs, in initiating immunity.

An appealing hypothesis is that MHC II ubiquitination limits antigen presentation to prevent detrimental outcomes. *In vitro* antigen presentation assays that investigate this

scenario are inconclusive, showing increased (100), unaltered (112) or reduced (115–117) $CD4^+$ T cell priming in response to *MHC IIKR*$^{KI/KI}$ DC antigen presentation. This inconsistency may be due to differences in cell types with some studies using bone marrow-derived DC (100, 112, 116) and others bulk $CD11c^+$ DC (115, 117). Moreover, the impact of MHC II ubiquitination on MHC I presentation has largely been ignored. We have previously described that a lack of MHC II ubiquitination reduces MHC I surface expression and impairs cross-presentation *in vitro* (109). From these studies it is clear that an in-depth *in vivo* investigation is required to fully elucidate the impact of MHC II ubiquitination on DC antigen presentation and immunity.

In this study, we have systematically investigated the role of MHC II ubiquitination on primary DC function and *in vivo* immune outcomes. We have identified that in mice lacking MHC II ubiquitination there is a significant decrease in the number of splenic DCs. The remaining DCs have an altered surface phenotype accompanied by defects in antigen proteolysis and cytokine secretion. Functionally, these changes reduce *in vivo* $CD4^+$ and $CD8^+$ T cell priming in response to soluble, cell-associated and DC-targeted antigen. Importantly, *ex vivo* T cell priming revealed these changes were not simply due to reduced DC numbers but an intrinsic defect in DC function. Additionally, significant impairment in cytotoxic T lymphocyte (CTL) killing, $T_{FH}$ cell generation and antibody responses were observed in *MHC IIKR*$^{KI/KI}$ mice following immunization. Our results demonstrate the importance of DC MHC II ubiquitination for effective immunity.

# MATERIALS AND METHODS

## Mice

C57BL/6, *MHC IIKR*$^{KI/KI}$ (94), *IA*$\alpha^{-/-}$ (148), OT-II x Ly5.1 and OT-I x Ly5.1 mice were used at 6 - 12 weeks of age. All mice were bred and maintained in specific pathogen–free conditions at the Melbourne Bioresources Platform at Bio21 Molecular Science and Biotechnology Institute. Experimental procedures were approved by the Animal Ethics Committee of the University of Melbourne (1714375).

## Isolation of immune cells

Primary splenic or thymic DCs were isolated as previously described (120). Splenic cDCs were stained with mAbs specific for CD11c (N418), CD8α (53-6.7) and CD11b (M1/70) (all BioLegend). pDC preparations were stained with BST-2 (927) and Siglec-H (551) (both BioLegend). Thymus DCs were identified with mAbs specific for CD11c (N418), CD8α (53-6.7), CD11b (M1/70), B220 (RA3-6B2), Sirpα (all BioLegend) and NK1.1 (PK136, BD Biosciences). In some experiments, cDC1 ($CD11c^+$ $CD8^+$ $CD11b^-$) and cDC2 ($CD11c^+$ $CD8^-$ $CD11b^+$) were sorted to purity by flow cytometry on a Becton Dickinson Influx (Murdoch Children's Research Institute Flow Cytometry and Imaging facility). To obtain absolute cell numbers, an internal microsphere counting standard (BD Biosciences) was used.

For determining the expression of cell surface markers, single cell suspensions were generated. Splenocytes were either treated with red blood cell removal buffer, or light cells were separated by density gradient separation in 1.077 g/cm3 Nycodenz (Nycomed

Pharma). Cells were stained with mAbs specific for CD3 (KT3-1.1), CD8α (53-6.7), CD11b (M1/70), CD11c (N418), CD19 (6D5), CD24 (M1/69), CD40 (FGK45.5), CD45R/B220 (RA3-6B2), CD80 (16-10A1), CD86 (GL1), CD135/Flt3 (A2F10), CD172 (Sirpα), CD205/DEC205 (NLDC-145), CD274/PD-L1 (10F.9G2), CD317/BST2 (927), CD370/Clec9A (7H11), H-2Kb (AF6-8815), IgD (11-26c.2a), IgM (RMM-1), SiglecH (551), XCR1 (ZET) (all BioLegend), Ly6C.2 (5075-3.6) or Ly6G (1A8) (Walter and Eliza Hall antibody facility). Stained cells were acquired on the LSRFortessa (BD Biosciences) flow cytometer and analyzed on FlowJo software (Tree Star) with exclusion of cell doublets and dead cells in all cases, identified based on forward and side scatter (FSC and SSC), as well as staining with PI or DAPI. Statistical analysis was performed with Prism software.

**Cytokines**

Splenic cDC1 and cDC2 were isolated and sorted to purity. 1 x $10^5$ DCs were cultured in completed medium (RPMI 1640 medium supplemented with 10% heat-inactivated FCS, 1% penicillin/streptomycin, 50 nM 2-ME and 1% GlutaMAX) with or without 0.5 μM phosphorothioated CpG 1668 (Bioneer), 50 ng/mL interferon gamma (IFN)-γ (Peprotech) and 20 ng/mL granulocyte-macrophage colony-stimulating factor (Peprotech) or 0.5 μM CpG alone. Supernatants were collected 18 hours later and stored at -20°C. Cytokine secretion was determined using the BD Cytometric Bead Array Mouse Inflammation kit according to the manufacturer's instructions (BD Biosciences).

**Antigen uptake, proteolysis and endosomal pH analyses**

To assess antigen uptake, 5 x $10^4$ purified cDC1 or cDC2 were incubated with 50 µg/mL ovalbumin-Cy5 in complete medium for 0 – 90 minutes at 37°C. DCs were washed twice and the fluorescence was measured by flow cytometry. As a control, DCs were pulsed with ovalbumin-Cy5 for 90 min at 4°C. To assess antigen proteolysis and endosomal pH, 2.5 x $10^5$ purified DCs were incubated with 20 µg/mL DQ-OVA (Life Technologies) or with 20 µg/mL dextran-pHrodo (Life Technologies) for 15 min at 37°C. Cells were washed twice, resuspended in complete medium and chased for the indicated time. At each time point, cells were kept on ice and the fluorescence was measured by flow cytometry. As a control, DCs were pulsed with DQ-OVA or dextran-pHrodo for 15 min at 4°C, washed twice and analyzed by flow cytometry. The signal was calculated for the 37°C chase time point by subtracting the gMFI at 4°C. To normalize for dextran-pHrodo internalization, we simultaneously measured uptake of dextran-A647.

***In vivo* antigen presentation assays**

Single cell suspensions were generated from lymph nodes of OT-I x Ly5.1 or OT-II x Ly5.1 mice. Cells were stained with rat anti-mouse mAbs specific for: CD11b (M1/70), F4/80 (F4/80), red blood cells (TER119), Ly6G/-Ly6C (RB68C5), MHCII (M5/114), CD45R (RA36B2) and CD4 (GK1.5) for OT-I T cells or CD8α (53-6.7) for OT-II cells. Cells were washed and incubated with BioMag anti-rat IgG-coupled magnetic beads (Qiagen). After magnetic depletion, the $CD4^+$ or $CD8^+$ T cell-enriched supernatant was recovered. Cells were washed with phosphate-buffered saline (PBS) supplemented with 0.1% bovine serum albumin (BSA) and labelled with CellTrace Violet (CTV, Thermo Fisher). To enable accurate quantification of the number of OT-II or OT-I cells, mice also

received transfer of a control population of carboxyfluorescein succinimidyl ester (CFSE, Thermo Fisher)-labelled splenocytes. Single cell suspensions were treated with red blood cell removal buffer. Cells were washed with PBS 0.1% BSA and labelled with CFSE. Equal numbers of CTV-labelled OT-II or OT-I cells and CFSE-labelled splenocytes were pooled and resuspended in RPMI 2% FCS at 1 x $10^7$ cells/mL respectively and injected intravenously. 24 hours later, mice received 50 µg (for OT-II transferred mice) or 25 µg (for OT-I transferred mice) soluble ovalbumin (sOVA; Sigma-Aldrich), 20 x $10^6$ OVA-coated splenocytes or 0.2 µg anti-Clec9A-OVA mAb (266) via intravenous injection. For OVA-coated splenocytes, single cell suspensions were generated from spleens of C57BL/6 mice, treated with red blood cell removal buffer, washed and incubated with 10 mg/mL OVA protein (Sigma) in FCS-free RPMI at 37°C. 64 hours after immunization, spleens were harvested, single cell suspensions generated, and red blood cells lysed. Cells were stained with mAbs specific for CD8α (53-6.7, BioLegend) or CD4 (GK1.5; Walter and Eliza Hall Antibody Facility) and Ly5.1 (A20; BioLegend). The number of divided OT-II and OT-I was determined as the number of $CD4^+$ or $CD8^+$ $Ly5.1^+$ cells that had undergone CTV dilution. The number of cells was normalized to the number of CFSE-labelled splenocytes recovered.

### *Ex vivo* antigen presentation assays

Mice were immunized intravenously with 1 µg anti-Clec9A-OVA mAb (266). One day later, spleens were harvested, and DC were isolated as previously described before sorting to purity. Sorted cDC1 ($CD11c^+$ $CD8^+$ $CD11b^-$) or cDC2 ($CD11c^+$ $CD8^-$ $CD11b^+$) (numbers indicated in figures) were cultured *in vitro* with 2.5 x $10^4$ CTV-labelled OT-II

or OT-I cells in complete medium. Four or five days later the number of divided OT cells was determined.

**In vitro antigen presentation assays**

DCs were isolated as previously described and cDC1 ($CD11c^+$ $CD8^+$ $CD11b^-$) and cDC2 ($CD11c^+$ $CD8^-$ $CD11b^+$) sorted to purity. 2.5 x $10^4$ sorted cDC1 or cDC2 were cultured *in vitro* with 2.5 x $10^4$ CTV-labelled OT-II cells and $OVA_{323-339}$ peptide. 68 hours later, the number of divided OT-II cells was determined by flow cytometry.

**Cytotoxic T lymphocyte (CTL) assays**

Mice were injected with 2 x $10^7$ OVA-coated splenocytes (prepared as previously described) or 1 mg anti-Clec9A-OVA mAb, both with 1 mg LPS as adjuvant. Six days later, single cell suspensions of target cells (splenocytes) were prepared from spleens of WT mice. Half of the suspension ($OVA^+$ $CTV^{hi}$) was pulsed and labelled with 1 mg $OVA_{257-264}$ (Worthington) and 5 mM of CTV (Thermo Fischer). The other half of the suspension ($OVA^-$ $CTV^{lo}$) was labelled with 0.5 mM CTV only. Equal number of $OVA^+$ $CTV^{hi}$ and $OVA^-$ $CTV^{lo}$ were pooled and 10 x $10^6$ target cells were injected intravenously. 36-42 hours later spleens were harvested and the % of OVA-specific lysis was determined as follows:

$$R = (\%\ CTV^{lo} / \%\ CTV^{hi})$$

$$\%\ \text{OVA-specific lysis} = [1-(r_{unprimed}/r_{primed}) \times 100$$

**T cell characterization**

1 x $10^4$ OT-II x Ly5.1 or OT-I x Ly5.1 were adoptively transferred into WT and *MHC IIKR*$^{KI/KI}$ mice. One day later, mice were immunized with 1 µg anti-Clec9A-OVA mAb and 1 µg LPS. Seven days later, spleens were harvested, single cell suspensions generated, and red blood cells lysed. Splenocytes were stained with mAbs specific for TCR Vα2 (B20.1; Walter and Eliza Hall Antibody Facility), Ly5.1 (A20) PD-1 (29F.1A12), CD44 (IM7) and CD62L (MEL-14) (all BioLegend). For IFNg analysis, splenocytes were incubated with 1 mg/ml of $OVA_{257-264}$ in the presence of BD Golgi Plug™ for five hours at 37ºC. For intracellular staining of IFNg and T-bet, splenocytes were permeabilized and fixed with BD Cytofix/Cytoperm™ Kit or eBioscience™ Foxp3/Transcription Factor Staining Buffer Set. Cells were stained for IFNg (XMG1.2) or T-bet (REA102, Miltenyi Biotec).

**Induction and detection of antibody responses**

For $T_{FH}$ induction, 1 x $10^6$ OT-II x Ly5.1 cells were adoptively transferred into mice. One day later, mice were immunized with 0.5 µg anti-Clec9A-OVA mAb or PBS (no antigen control). Six days later, spleens were harvested, single cell suspensions generated, and red blood cells lysed. Cells were stained with mAbs specific for CD4 (GK1.5; Walter and Eliza Hall Antibody Facility), Ly5.1 (A20), PD-1 (29F.1A12), CD44 (IM7) (all BioLegend) and CXCR5 (2G8, BD Biosciences). The number of OT-II and $T_{FH}$ cells was determined as the number of $CD4^+$ $Ly5.1^+$ cells or $CD4^+$ $Ly5.1^+CXCR5^+$ $PD\text{-}1^+$. For anti-rat Ig response, mice were injected intravenously with 2 µg of rat anti-Clec9A mAb (10B4) and serum samples obtained at 2 weeks post injection. Anti-rat Ig reactivity was determined by enzyme-linked immunosorbent assay (ELISA). Nunc MaxiSorp™

(Thermo Fisher Scientific) plates were coated overnight at 4°C with 1.5 μg/mL of rat GL117 mAb (Walter and Eliza Hall antibody facility). Unbound antibody was removed by washing with PBS + 0.05% Tween-20, PBS, and MilliQ water. Serum samples were serially diluted in 5% skim milk powder in PBS and incubated at 4°C overnight. Captured mouse anti–rat Ig antibodies were detected using anti-mouse IgG-HRP and visualized using 1-Step Ultra 3,3′,5,5′-Tetramethylbenzidine (TMB) ELISA Substrate (Thermo Scientific). Absorbance at 440 nm was detected with a ClarioSTAR plate reader (BMG LABTECH). Titers were considered positive when the absorbance was above 0.1 compared to blank.

**Protease activity assay and cystatin C immunoblot**

To generate a large number of DCs, WT and *MHC IIKR*$^{KI/KI}$ mice were injected subcutaneously with 5 x $10^6$ Flt3L secreting B16 melanoma cells (267). Nine days later, spleens were harvested and DCs isolated as previously described (120). cDC1 and cDC2 were further separated by positive selection using MACS magnetic separation (Miltenyi Biotec). >90% purity was determined by flow cytometry. Cells were lysed in PBS 0.1% Triton X-100 on ice for 20 minutes. Post-nuclear supernatants equivalent to 80 μg of protein were acidified by adding 10x citrate buffer (final concentrations: 50 mM Citrate, pH 5.5, 0.5% 3- ((3-Cholamidopropyl) dimethylammonio)-1-Propanesulfonic Acid (CHAPS), 0.1% Triton X-100, 4 mM Dithiothreitol (DTT). Where indicated, lysates were pre-incubated with the pan-cysteine cathepsin inhibitor E-64 (25 μM; Sigma-Aldrich) or DMSO vehicle at 37˚C. 1 μM BMV109, a fluorescently quenched pan-cysteine cathepsin activity-based probe, was added and lysates were incubated at 37˚C. Labeling reactions were stopped by addition of 5x sample buffer (50% glycerol, 200 mM Tris-Cl, pH 6.8,

10% SDS, 0.05% bromophenol blue, 6.25% beta-mercaptoethanol) followed by heating at 95˚C for 5 minutes. Proteins were resolved on a 15% SDS-PAGE gel and the gel was scanned for Cy5 fluorescence using a Typhoon flatbed laser scanner (GE Healthcare). For cystatin C immunoblots, proteins were transferred to nitrocellulose membranes and probed with goat anti-cystatin C (R&D) and rabbit anti-actin (Sigma-Aldrich) antibodies. After washing with PBS + 0.05% Tween-20, blots were incubated with donkey anti-goat HRP (Novex Life Tech) and goat anti-rabbit IRDye 800CW (Li-Cor). IRDye 800CW immunoblots were scanned using Typhoon, and HRP labelling was visualized on a ChemiDoc MP imager (Bio-Rad) with the use of Amersham ECL Western blotting reagents (GE). Protease activity and cystatin C (band intensity) were measured by densitometry using ImageJ. Values were normalized to actin (band intensity). Statistical analyses were performed using GraphPad Prism 8.

# RESULTS

**The inability to ubiquitinate MHC II impacts DC number and surface phenotype.**

To investigate the impact of MHC II ubiquitination on DC biology, we used mice harboring a mutant MHC II unable to undergo ubiquitination (*MHC IIKR*$^{KI/KI}$) (94). First, we analyzed the number of splenic DCs. Conventional DC 1 (cDC1), 2 (cDC2) and plasmacytoid DCs (pDCs) were enriched by DNAse/collagenase digestion followed by density centrifugation. A reduction in the number of cDC1 (61% decrease), cDC2 (50% decrease) and pDC (30% decrease) was detected in *MHC IIKR*$^{KI/KI}$ mice compared to wild type (WT) mice (**Figure 1A**). The decreased cell number was specific for splenic cDC and pDC, with no significant changes observed for splenic B cells (**Figure 1A**) or thymic cDC1 and cDC2 (**Figure 1B**).

Remaining cDC in *MHC IIKR*$^{KI/KI}$ spleen were profiled for their surface expression of characteristic DC markers (**Figure 1C, Figure 2**). As expected, significantly increased MHC II expression was observed on *MHC IIKR*$^{KI/KI}$ cDC1 (3.4-fold increase) and cDC2 (2.4-fold increase) while no changes were observed in CD86, a well-known MARCH1 substrate (94, 112, 115). Increased MHC II expression was accompanied by significant decreases in MHC I, CD24 and CD8, which we and others have previously reported as being reduced in the absence of MHC II ubiquitination (109, 113, 115). In addition, we detected previously undescribed reductions in CD11b, Sirpα, CD40, CD80, Flt3, XCR1 and DEC205. The only molecule besides MHC II to show increased expression was CD11c, most notably for *MHC IIKR*$^{KI/KI}$ cDC1 (**Figure 1C, Figure 2**). Similar patterns were observed in splenic B cells, with increased MHC II expression correlating with

small, but significant, decreases in the surface expression of IgM, PD-L1, CD19 and CD40 (**Figure 2**). These results indicate that impaired MHC II ubiquitination was sufficient to alter a variety of surface molecules including integrins, chemokine receptors and C-type lectin receptors.

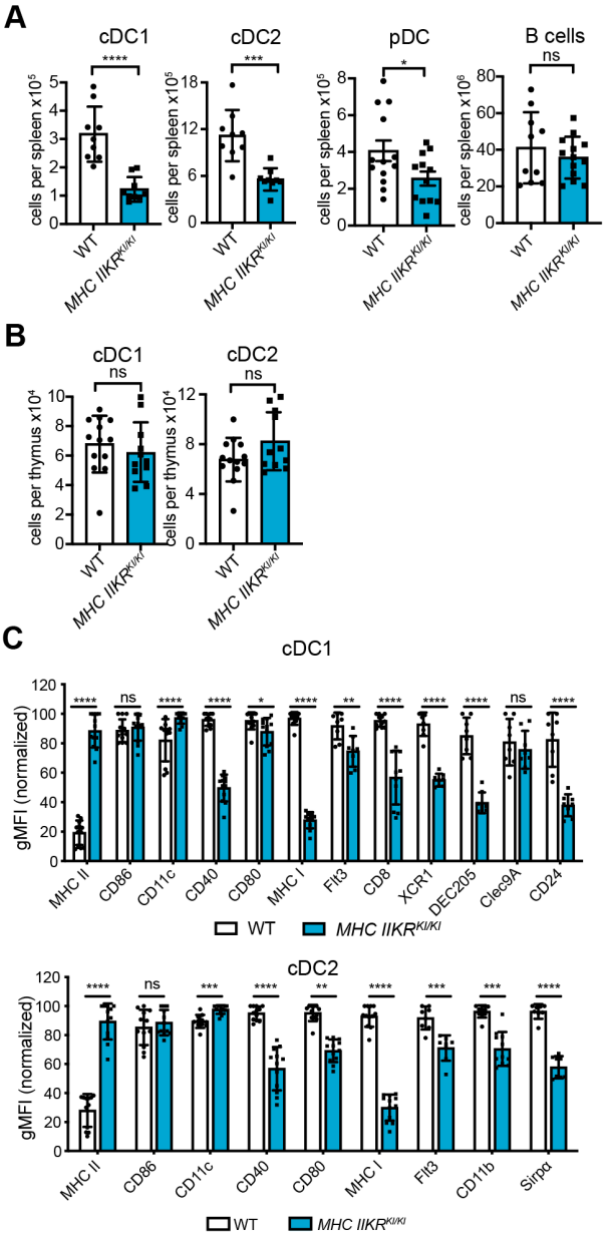


**Figure 1. MHC II ubiquitination controls splenic DC number and cell-surface phenotype.** Quantification of (A) splenic cDC1 ($CD11c^+$ $CD8^+$ $CD11b^-$), cDC2 ($CD11c^+$ $CD8^-$ $CD11b^+$), pDC (BST-$2^+$ Siglec-$H^+$), B cells ($CD19^+$ $B220^+$) and (B) thymic cDC1 ($XCR1^+$ $Sirp\alpha^-$) and cDC2 ($XCR1^-$ $Sirp\alpha^+$). Absolute numbers were determined as described in Materials and Methods. (C) WT and *MHC IIKR$^{KI/KI}$* splenic cDC1 and cDC2 cell-surface marker expression determined by flow cytometry. gMFI has been normalized to the maximum gMFI signal. (A) and (B) Symbols represent individual mice, with data pooled from a minimum of 2 independent experiments, displayed as mean ± SD. **** P <0.0001*** P <0.001** P <0.01 * P <0.05, ns not significant, unpaired t test.

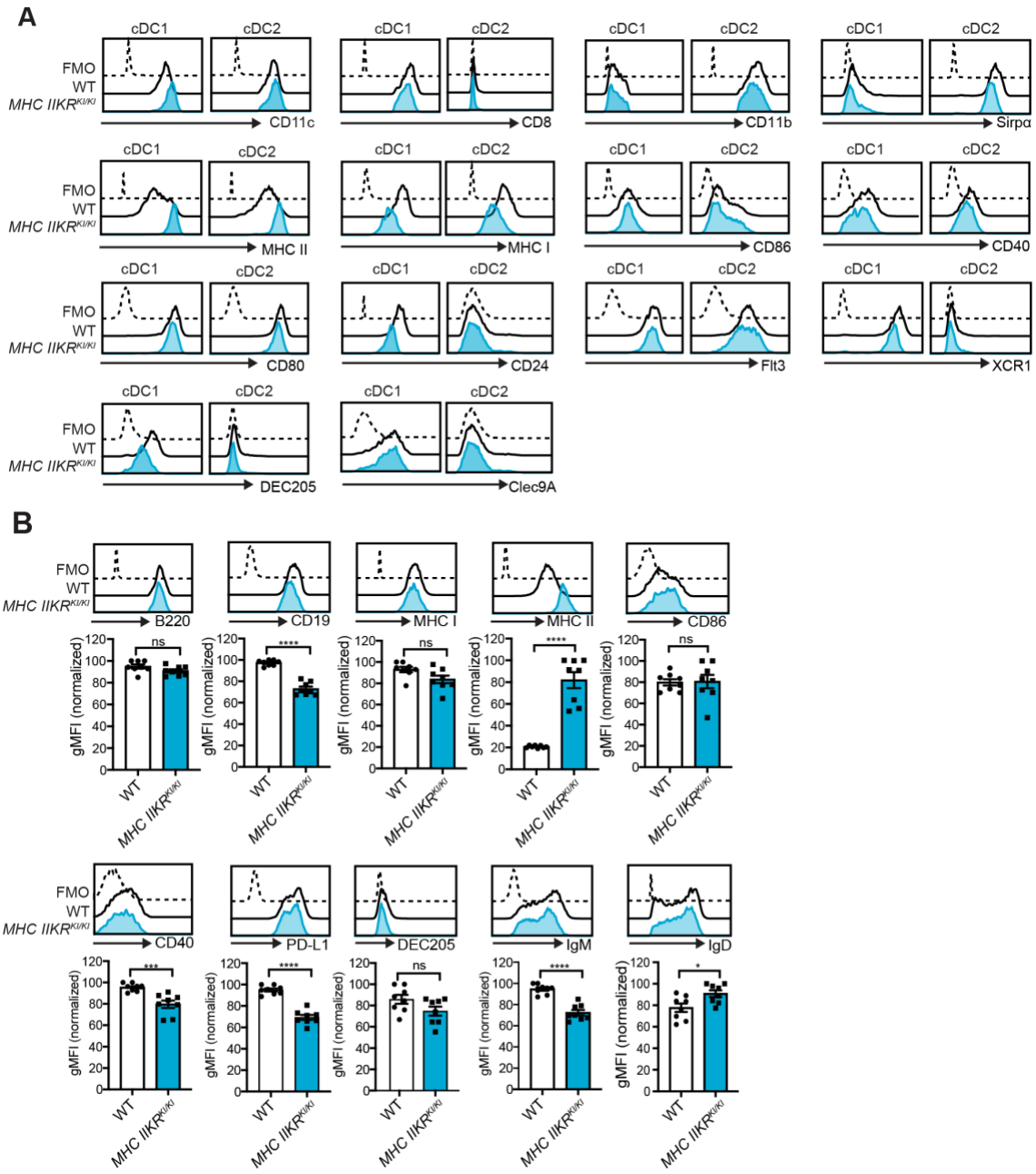


**Figure 2. Lack of MHC II ubiquitination alters splenic DC and B cell cell-surface phenotype.** WT and *MHC IIKR*$^{KI/KI}$ splenic (A) DC or (B) B cell surface marker expression determined by flow cytometry. Representative histograms are shown for fluorescence minus one (FMO, dashed line), WT (black line) and *MHC IIKR*$^{KI/KI}$ (blue filled). gMFI for B cell markers has been quantified by normalizing the gMFI signal to the maximum gMFI signal. Symbols represent individual mice, with data pooled from a minimum of 2 independent experiments, displayed as mean ± SD. **** P <0.0001*** P <0.001 * P <0.05, ns not significant, unpaired t test.

**An inability to ubiquitinate MHC II impacts dendritic cell function.**

For productive T cell activation, T cells require three signals from DCs – antigen presentation, costimulation and inflammatory cytokines. Given that we observed reduced costimulatory molecule expression (CD40 and CD80) on *MHC IIKR*$^{KI/KI}$ DCs we aimed to next assess other parameters of antigen presentation. For efficient presentation by DCs, antigen must undergo endocytic uptake and proteolytic degradation. First, we measured ovalbumin protein (OVA) uptake. WT and *MHC IIKR*$^{KI/KI}$ cDC were purified and incubated with fluorescent soluble OVA-Cy5 (OVA-Cy5). In agreement with previous studies (154), we found cDC1 and cDC2 captured similar amounts of OVA. Similar uptake was observed by *MHC IIKR*$^{KI/KI}$ and WT cDC, demonstrating a lack of MHC II ubiquitination does not alter uptake of OVA (**Figure 3A**).

Once internalized, antigen is degraded and loaded onto MHC molecules. To investigate if antigen proteolysis was impacted by a loss of MHC II ubiquitination, we utilized DQ-OVA, a self-quenched form of ovalbumin which fluoresces once degraded. *MHC IIKR*$^{KI/KI}$ cDC1 and cDC2 were sorted to purity and equal numbers of DCs were incubated with DQ-OVA. After antigen pulsing, excess DQ-OVA was removed by washing and assessment of DQ-OVA fluorescence over time, as a read out of OVA proteolysis, was assessed by flow cytometry. In comparison to WT cDC1, *MHC IIKR*$^{KI/KI}$ cDC1, and to some extent cDC2, displayed significantly reduced DQ-OVA proteolysis (**Figure 3B**). The defect was specific to OVA, given that DQ-BSA, a self-quenched form of bovine-serum albumin underwent similar proteolysis in *MHC IIKR*$^{KI/KI}$ DC as in WT DC (**Figure 3C**). Impaired proteolysis of DQ-OVA could result from alterations in the endosomal environment in *MHC IIKR*$^{KI/KI}$ cDC. To investigate this, we assessed endosomal pH using

dextran-pHrodo. This is a pH sensitive probe where fluorescence is only detected once the probe enters an acidic environment. Purified WT and *MHC IIKR*$^{KI/KI}$ cDC1 and cDC2 were pulsed with dextran-pHrodo and chased for 120 minutes (**Figure 3D**). As expected, fluorescence increased with time, indicative of dextran-pHrodo accessing an acidic environment. No difference was observed between *MHC IIKR*$^{KI/KI}$ and WT cDC indicating no significant changes to endosomal pH in the absence of MHC II ubiquitination.

To examine protease activity, a fluorescently quenched activity-based probe, BMV109, was used to measure the activity of four cysteine cathepsins, which are key antigen-degrading enzymes (268, 269). BMV109 irreversibly binds to cathepsins in an activity-dependent manner, giving rise to Cy5 fluorescence upon release of a QSY21 quenching group. As the binding is covalent, cathepsin binding can be detected by in-gel fluorescence as a surrogate measure of protease activity. A pan-cysteine cathepsin inhibitor, E-64, was first used to confirm the specificity of BMV109 for active papain-fold cysteine proteases. As expected, BMV109 did not bind cathepsins in the presence of E-64, confirming its specificity (**Figure 4A**). In agreement with previous studies (270), cysteine protease inhibitor cystatin C (CTS3) could only be detected in cDC1 (**Figure 4B**). Next, cysteine cathepsin protease activity was compared between *MHC IIKR*$^{KI/KI}$ DC and WT DC and no significant differences were observed (**Figure 3E**).

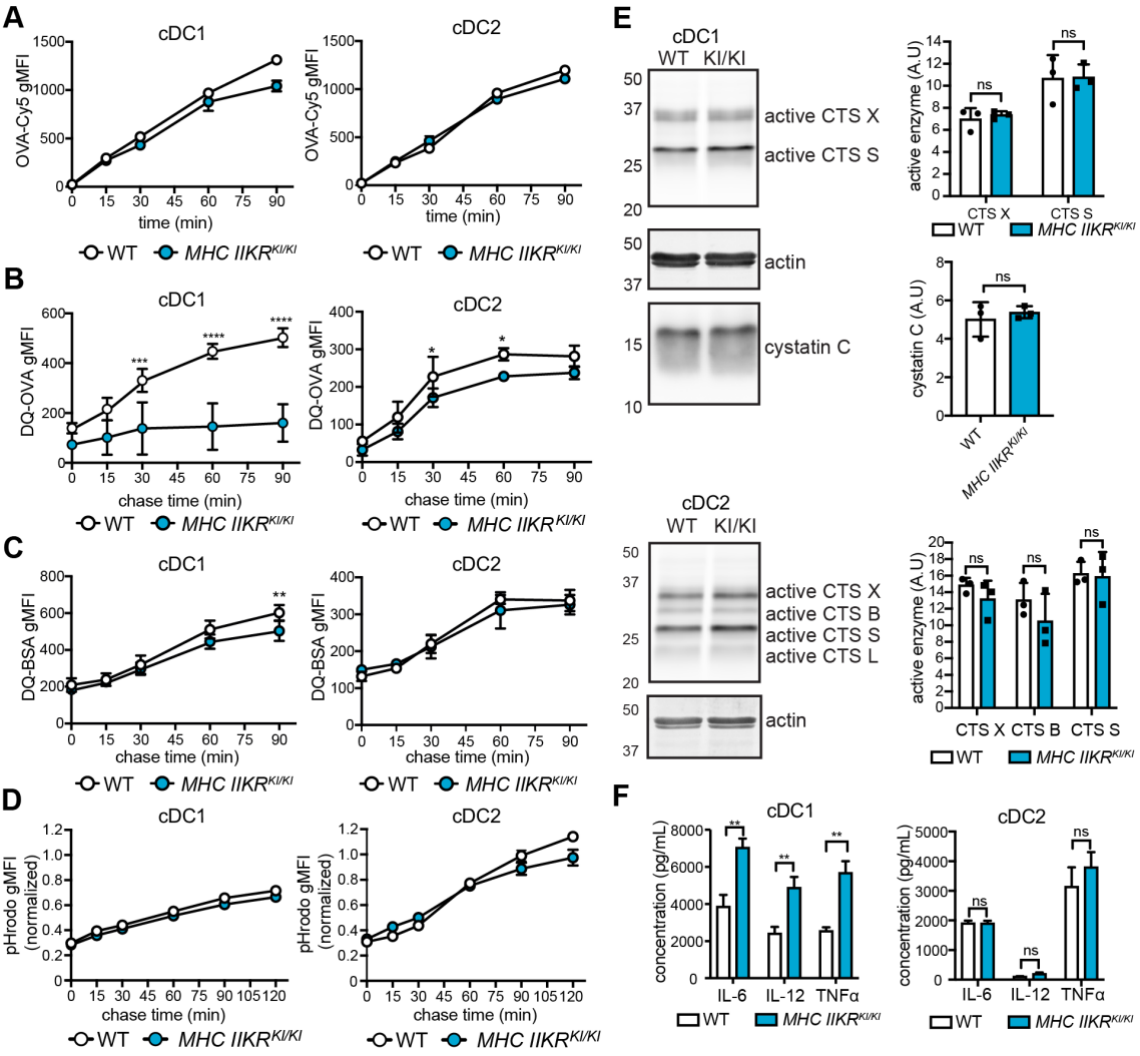


**Figure 3. Lack of MHC II ubiquitination impairs antigen proteolysis and cytokine secretion without impacting antigen uptake, endosomal pH or protease activity.** (A) *MHC IIKR*$^{KI/KI}$ and WT cDC1 and cDC2 were sorted to purity and incubated at 37ºC with 50 μg/mL OVA-Cy5 for the indicated times. Cells were washed before the Cy5 fluorescence was determined by flow cytometry. Data are from one experiment, carried out in technical triplicate. (B and C) *MHC IIKR*$^{KI/KI}$ and WT cDC1and cDC2 were sorted to purity and pulsed with 20 μg/mL (B) DQ-OVA or (C) DQ-BSA for 15 min at 37ºC. Cells were washed and chased for the indicated time before the DQ signal was measured by flow cytometry. **** P <0.0001*** P <0.001* P <0.05, 2-way ANOVA with Bonferroni's test for multiple comparisons. (D) *MHC IIKR*$^{KI/KI}$ and WT cDC1and cDC2 were sorted to purity and pulsed with 20 μg/mL Dextran-pHrodo or Dextran-A647 for 15 min at 37ºC. Cells were washed and Dextran-pHrodo or Dextran-A647 signal was measured by flow cytometry at different chase time points. To account for any changes in uptake, the

Dextran-pHrodo gMFI was normalized to the Dextran-A647. Data are from one experiment, carried out in technical triplicate. (E) cDC1 (top panel) and cDC2 (lower panel) protease activity analysis. DC were isolated as described in Materials and Methods. Cells were lysed before incubation with the pan cathepsin (CTS) protease activity-based probe BMV109 (1 μM). Proteins were resolved on SDS-PAGE gel and Cy5 fluorescence was determined. Representative in-gel fluorescence of three independent experiments for WT or *MHC IIKR*$^{KI/KI}$ is shown. Quantification of protease activity or total protein expression is normalized to actin, displayed as mean ± SD. For Cystatin C expression, blots were probed with goat anti-cystatin C and rabbit anti-actin (Sigma-Aldrich) antibodies. Data are representative of three biological replicates. Ns not significant, unpaired Welch's t test. (F) Cytokine secretion. cDC1 and cDC2 were sorted to purity and incubated with 0.5 μM CpG, 50 ng/mL IFNγ and 20 ng/mL GM-CSF. Supernatants were collected 18 hours later, and cytokine secretion was determined using BD™ Cytometric Bead Array (CBA) Mouse Inflammation Kit. Bars display mean ± SD from two independent experiments with cells pooled from 8 mice. ** P <0.01, ns not significant, unpaired t test with Holm-Sidak correction for multiple comparisons.

Given the cathepsin activity was normal in *MHC IIKR*$^{KI/KI}$ DC, the reduction in antigen proteolysis, together with altered cell surface phenotype, suggest that a lack of MHC II ubiquitination could impact endocytic events. Since the production of cytokines is dependent on the endosomal trafficking of toll-like receptors (TLRs) and their recognition of toll-like receptor ligands, we next investigated the capacity of *MHC IIKR*$^{KI/KI}$ DC to produce inflammatory cytokines. Splenic cDC1 and cDC2 were sorted to purity and equal numbers were incubated in the presence of TLR9 ligand, CpG and inflammatory cytokines interferon gamma (IFN)-γ and granulocyte-macrophage colony-stimulating factor (GM-CSF), conditions that elicit maximal IL-12 production (153). Supernatants were harvested after 18 hours and the presence of IL-6, IL-10, IL-12p70, TNF-α and monocyte chemoattractant protein-1 (MCP-1) measured using BD Cytometric Bead Array Assay. IL-10 and MCP-1 were not produced by either cDC1 or cDC2. *MHC IIKR*$^{KI/KI}$ cDC1 produced significantly increased amounts of IL-6, IL-12 and TNFα

compared to WT cDC1, while the cytokine production of *MHC IIKR*$^{KI/KI}$ cDC2 was unaltered (**Figure 3F**). Similar patterns, albeit at lower concentrations, were observed when DCs were treated with CpG alone (**Figure 4C**).

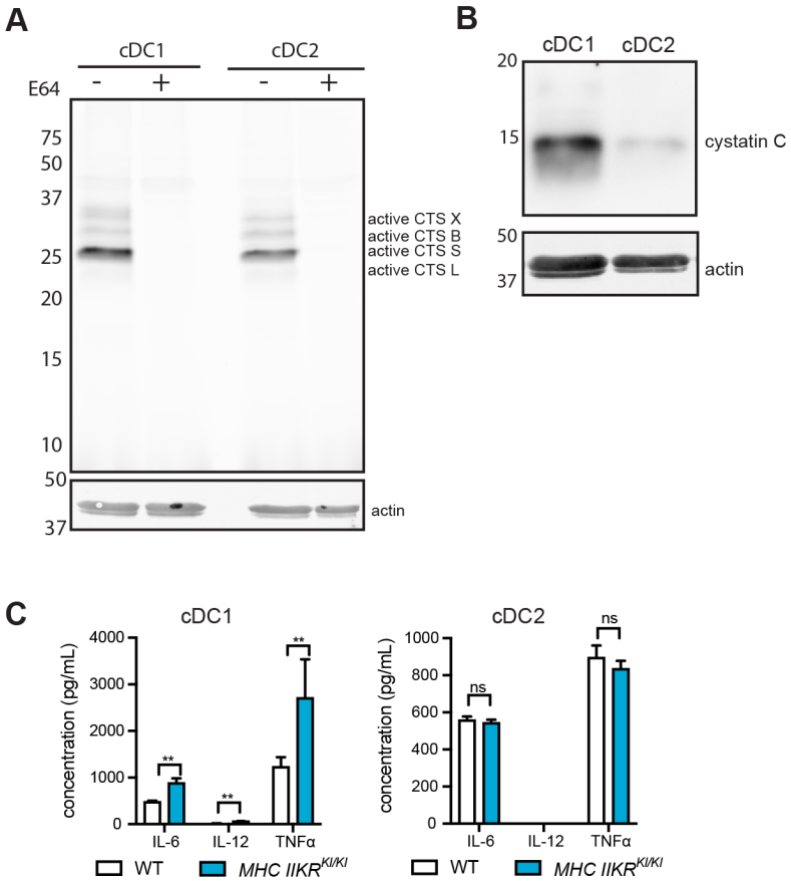


**Figure 4. Protease activity and cytokine secretion.** (A) WT cDC1 and cDC2 were isolated and lysed before being treated with (+) ir without (-) cysteine protease inhibitor, E64 (25 µM). They lysates were labelled with BMV109 (1 µM). Labelling of active cathepsins are shown by in-gel fluorescence. Immunoblot is from one experiment. (B) WT cDC1 and cDC2 were isolated and lysed. Proteins were resolved on SDS-PAGE and western transferred. Immunoblots were probed with goat anti-cystatin C and rabbit anti-actin (Sigma-Aldrich) antibodies. (C) DCs were isolated, sorted to purity and incubated with 0.5 µM CpG. Supernatants were collected 18 hours later, and cytokine secretion was determined using BD Cytometric Bead Array (CBA) Mouse Inflammation Kit. Bars display mean ± SD from two experiments with cells pooled from eight mice. ** P <0.01 ns not significant, unpaired t test with Holm-Sidak correction for multiple comparisons.

In summary, an inability to ubiquitinate MHC II reduces DC numbers, alters their surface phenotype, reduces proteolysis of some forms of antigen and enhances cytokine production, in particular for the cDC1 subset, but does not impact DC endosomal pH or cysteine cathepsin protease activity.

MHC II expression levels *per se*, rather than the extent of its ubiquitination, may regulate endosomal functions. If this were the case, such functions might also be affected in cells deficient in MHC II expression. To address this, we analyzed DC from $IA\alpha^{-/-}$ mice. First, the cell surface phenotype was investigated. In contrast to the *MHC IIKR*$^{KI/KI}$ DC, no significant alterations were observed except for a slight increase in CD80 (**Figure 5A**). Next, we investigated the cytokine secretion of $IA\alpha^{-/-}$ cDC1 and cDC2 (**Figure 5B**). In agreement with previous studies (52), DC lacking MHC II produced slightly less IL-6, IL-12 and TNFα than WT DC. Finally, we investigated antigen proteolysis using DQ-OVA, which proceeded similarly in WT and $IA\alpha^{-/-}$ DC (**Figure 5C**). Overall, the impact of MHC II deficiency was negligible compared to that caused by lack of MHC II ubiquitination, suggesting that the altered phenotype of *MHC IIKR*$^{KI/KI}$ DC is due to changes in MHC II trafficking rather than to altered MHC II surface expression.

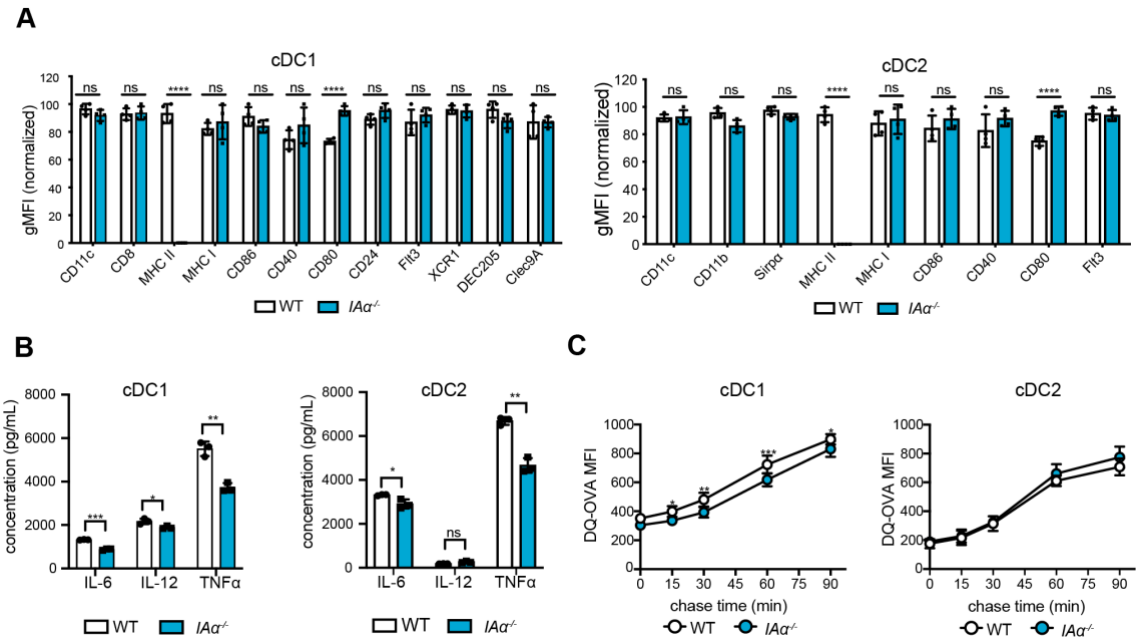


**Figure 5. DC lacking MHC II have altered function.** (A) WT and *IAα*$^{-/-}$ splenic cDC1 and cDC2 cell-surface marker expression determined by flow cytometry. gMFI has been normalized to the maximum gMFI signal. Symbols represent individual mice, bars display mean ± SD. Data are from one experiment. **** P <0.0001 ns, not significant, unpaired t test. (B) WT and *IAα*$^{-/-}$ splenic cDC1 and cDC2 cytokine secretion. DC were sorted to purity and incubated with 0.5 µM CpG, 50 ng/mL IFNγ and 20 ng/mL GM-CSF. Supernatants were collected 18 hours later, and cytokine secretion was determined using BD Cytometric Bead Array (CBA) Mouse Inflammation Kit. Bars display mean ± SD from two experiments with cells pooled from eight mice, *** P <0.001 ** P <0.01 * P <0.05, ns not significant, unpaired t test. (C) WT and *IAα*$^{-/-}$ splenic cDC1 and cDC2 were isolated, sorted to purity and pulsed with 20 µg/mL DQ-OVA for 15 min. Cells were washed twice and DQ-OVA signal was measured by flow cytometry at different chase time points. **** P <0.0001 *** P <0.001 * P <0.05, two-way ANOVA with Bonferroni's test for multiple comparisons.

## An inability to ubiquitinate MHC II in antigen presenting cells impairs MHC II antigen presentation *in vivo*.

Given the important role of MHC II in B cell and T cell immunity (271) and the dysregulation in antigen processing observed in *MHC IIKR*$^{KI/KI}$ DC, we next investigated

the impact of MHC II ubiquitination on adaptive immunity. To investigate antigen presentation in a physiologically relevant setting, WT or *MHC IIKR*$^{KI/KI}$ mice were injected intravenously with CellTrace Violet-labelled OT-II or OT-I. The following day, mice were immunized intravenously with one of three different forms of the model of antigen, ovalbumin (OVA): (i) OVA protein, (ii) cell-associated (splenocytes pre-incubated *in vitro* with OVA protein); (iii) OVA protein genetically fused to mAb against Clec9A (anti-Clec9A-OVA) (266). Clec9A was chosen as a receptor to measure receptor-mediated antigen uptake as it is highly expressed by cDC1 (272) and is not altered in DC with impaired MHC II ubiquitination (**Figure 1C**). T cell priming with OCS (273) and anti-Clec9A-OVA (143) is cDC1-dependent. The number of dividing OT-II and OT-I cells in spleen was determined by flow cytometry three days following intravenous immunization. For all antigens tested, *MHC IIKR*$^{KI/KI}$ mice displayed a significant reduction in the number of dividing OT-II and OT-I cells (**Figure 6A**). Therefore, a lack of MHC II ubiquitination impacts both MHC II and MHC I antigen presentation of soluble, cell-associated, and DC-targeted antigen *in vivo*.

Changes in *in vivo* T cell priming could be due to intrinsic alterations in DC function and/or the observed reduction in DC numbers (**Figure 1A**). To control for the latter, *ex vivo* antigen presentation assays were performed using equivalent numbers of isolated WT and *MHC IIKR*$^{KI/KI}$ DC. In this case, WT or *MHC IIKR*$^{KI/KI}$ mice were immunized with anti-Clec9A-OVA (266) and 22 hours later, spleens were harvested and cDC1 sorted to purity before equal number of cells were incubated with CTV-labelled OT-II or OT-I cells. Proliferation was determined four or three days later for OT-II or OT-I respectively. In agreement with *in vivo* analysis, reduced OT-II and OT-I priming was observed for

*MHC IIKR*$^{KI/KI}$ cDC1 (**Figure 6B**). Second, we tested the capacity of WT and *MHC IIKR*$^{KI/KI}$ cDC1 to present ovalbumin peptide *in vitro*. WT and *MHC IIKR*$^{KI/KI}$ DC were incubated with $OVA_{323-339}$ peptide and $IA^b$-$OVA_{323-339}$-specific OT-II T cells for 3 days. No significant change in OT-II proliferation was observed *in-vitro* (**Figure 7**). Previously, we have demonstrated reduced OT-I proliferation when *MHC IIKR*$^{KI/KI}$ DC are pulsed with $OVA_{254-267}$ peptide (109). Together, these data demonstrate that a lack of MHC II ubiquitination causes DC-intrinsic impairments in antigen presentation.

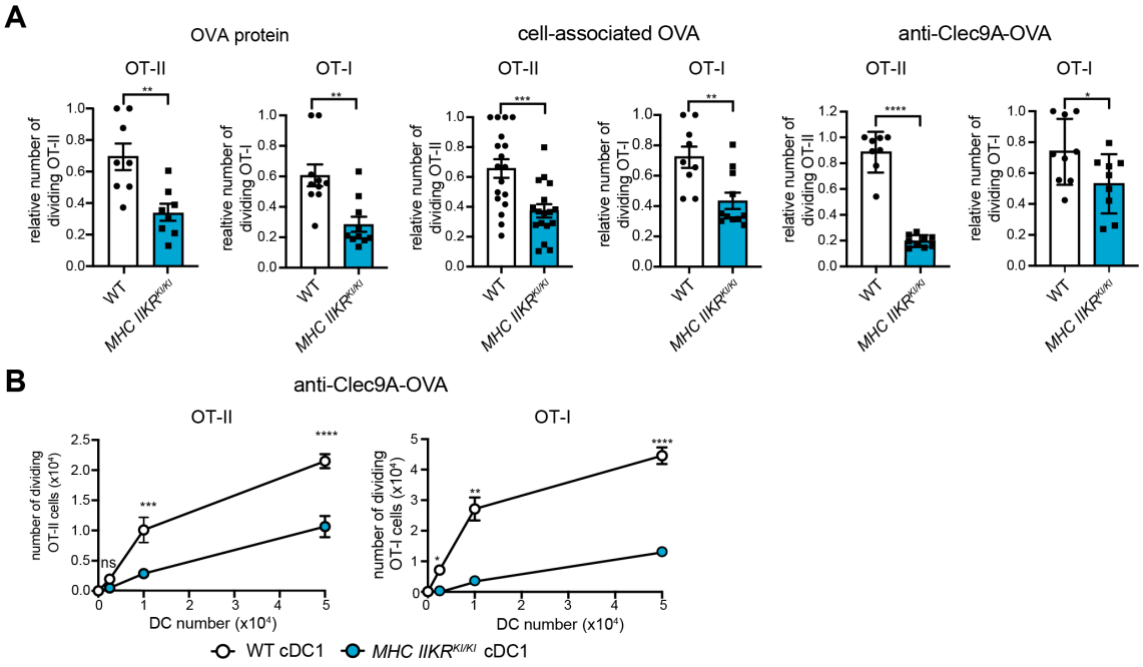


**Figure 6. Lack of MHC II ubiquitination impairs DC antigen presentation *in vivo* and *ex vivo*.** (A) Purified CellTrace Violet (CTV)-labelled OT-II or OT-I cells and CFSE-labelled BL6 mouse splenocytes were adoptively transferred into *MHC IIKR*$^{KI/KI}$ and WT mice. 24 hours later, mice were injected with 50 µg (OT-II), 25 µg (OT-I) soluble ovalbumin (OVA protein), 20 x $10^6$ OVA-coated splenocytes (cell-associated OVA) or 0.2 µg anti-Clec9A-OVA mAb via intravenous injection (anti-Clec9A-OVA). Spleens were harvested 64 hours later and antigen presentation capacity was assessed by flow cytometry as described in Materials and Methods. Each symbol represents an individual mouse with data pooled from at least two independent experiments, displayed as mean ± SD. (B) WT and *MHC IIKR*$^{KI/KI}$ mice were intravenously injected with 1 µg of anti–Clec9A-OVA. 22 hours later, spleen cDC1 were isolated and cell-

sorted to purity. DCs were cultured *ex vivo* with 2.5 × $10^4$ OT-I for 64h, or OT-II for 84h and divided OT-I cells were quantified by flow cytometry. Data are pooled from 2 independent experiments and graphs show mean ± SD. **** P <0.0001 *** P <0.001 ** P <0.01 * P <0.05, ns not significant, 2-way ANOVA with Bonferroni's test for multiple comparisons.

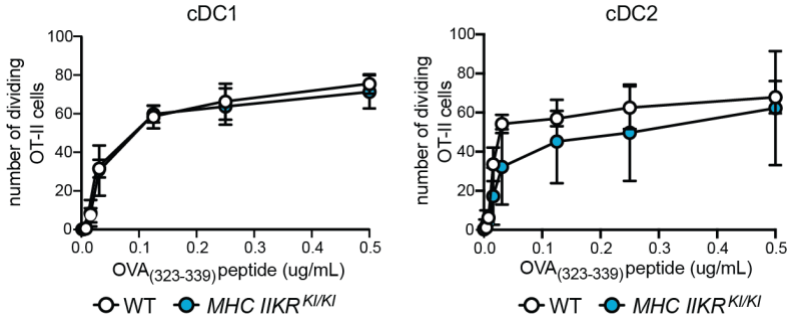


**Figure 7. MHC II ubiquitination does not impact *in vitro* presentation of $OVA_{323-339}$ peptide.** 2.5 x $10^4$ sorted WT and *MHC IIKR$^{KI/KI}$* cDC1 and cDC2 were incubated with increasing concentration of $OVA_{323-339}$ peptide and 2.5 x $10^4$ OT-II cells. 65 hours later, the number of divided OT cells was determined as described in Materials and Methods. Data is pooled from two independent experiments.

## An inability to ubiquitinate MHC II impairs CTL immune responses.

We investigated if a lack of MHC II ubiquitination alters generation of effector cytotoxic lymphocytes (CTLs). WT and *MHC IIKR$^{KI/KI}$* mice were immunized with cell-associated OVA or anti-Clec9A-OVA, with LPS used as an adjuvant. Six days later, mice were injected with target cells which comprised of an equal mix of syngeneic splenocytes pulsed with $OVA_{257-264}$ peptide (labelled with high concentration of CTV, "$CTV^{hi}$") or without peptide (labelled with low concentration of CTV, "$CTV^{lo}$"). Robust CTL responses were observed in WT mice immunized with cell-associated OVA (274) or anti-Clec9A OVA mAb (266). In contrast, significantly reduced CTL killing was observed in *MHC IIKR$^{KI/KI}$* mice in response to both immunogens (**Figure 8**).

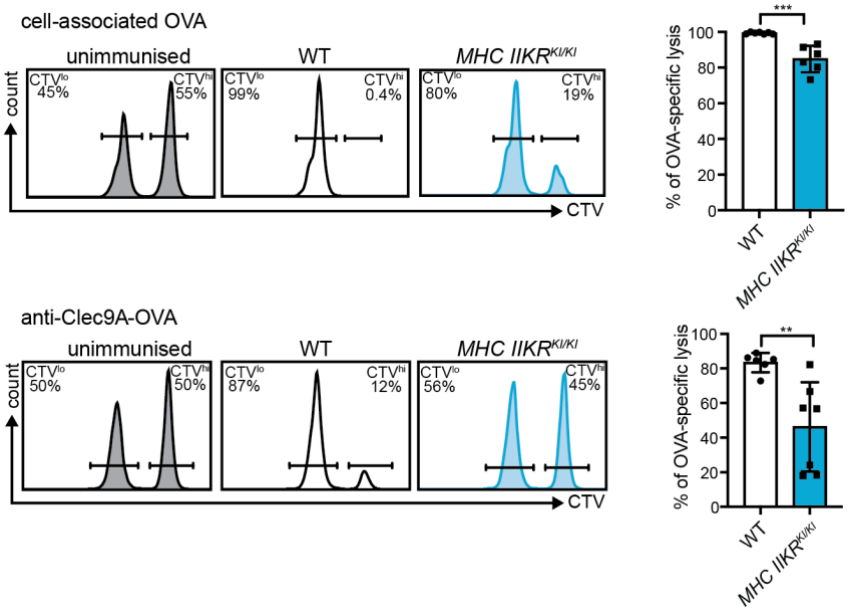


**Figure 8. Lack of MHC II ubiquitination impairs cytotoxic T cell responses.** *MHC IIKR$^{KI/KI}$* and WT mice were immunized intravenously with 2.5 × $10^7$ OVA-coated splenocytes (cell-associated OVA) or 1 µg anti-Clec9A-OVA mAb (anti-Clec9A-OVA) in the presence of lipopolysaccharide (LPS). 6 days later, mice were challenged with equal number of CTV$^{hi}$ ($OVA_{257-264}^+$) and CTV$^{lo}$ ($OVA^-$) target cells. 36-42 hours later the spleens were harvested and the percentage lysis of CTV$^{hi}$ cells was determined by flow cytometry as described in Materials and Methods. Histograms are representative of killing in each group, including no antigen (unimmunized) negative control. Bars show mean ± SD and are data pooled from two independent experiments, with symbols representing individual mice. *** P <0.001 ** P <0.01, unpaired t test.

To further investigate T cell responses in *MHC IIKR$^{KI/KI}$* mice OT-II or OT-I cells were transferred into WT and *MHC IIKR$^{KI/KI}$* mice before immunization with anti-Clec9A-OVA, together with LPS as an adjuvant. Six days later, their number and phenotype were examined (**Figure 9**). In response to immunization, *MHC IIKR$^{KI/KI}$* mice had significantly reduced numbers of OT-II cells accompanied by reduced PD-1 expression, a marker expressed by activated T cells (275), and a reduction in the percentage of $CD62L^-CD44^+$ OT-II cells. Expression of T-bet, indicative of Th1 differentiation, was unaltered (**Figure**

**9A**). Significantly reduced OT-I numbers were also observed in *MHC IIKR*$^{KI/KI}$ mice following immunization. These cells expressed lower PD-1, but did not differ in their expression of CD62L and CD44, or IFNg production when re-stimulated with antigen (**Figure 9B**).

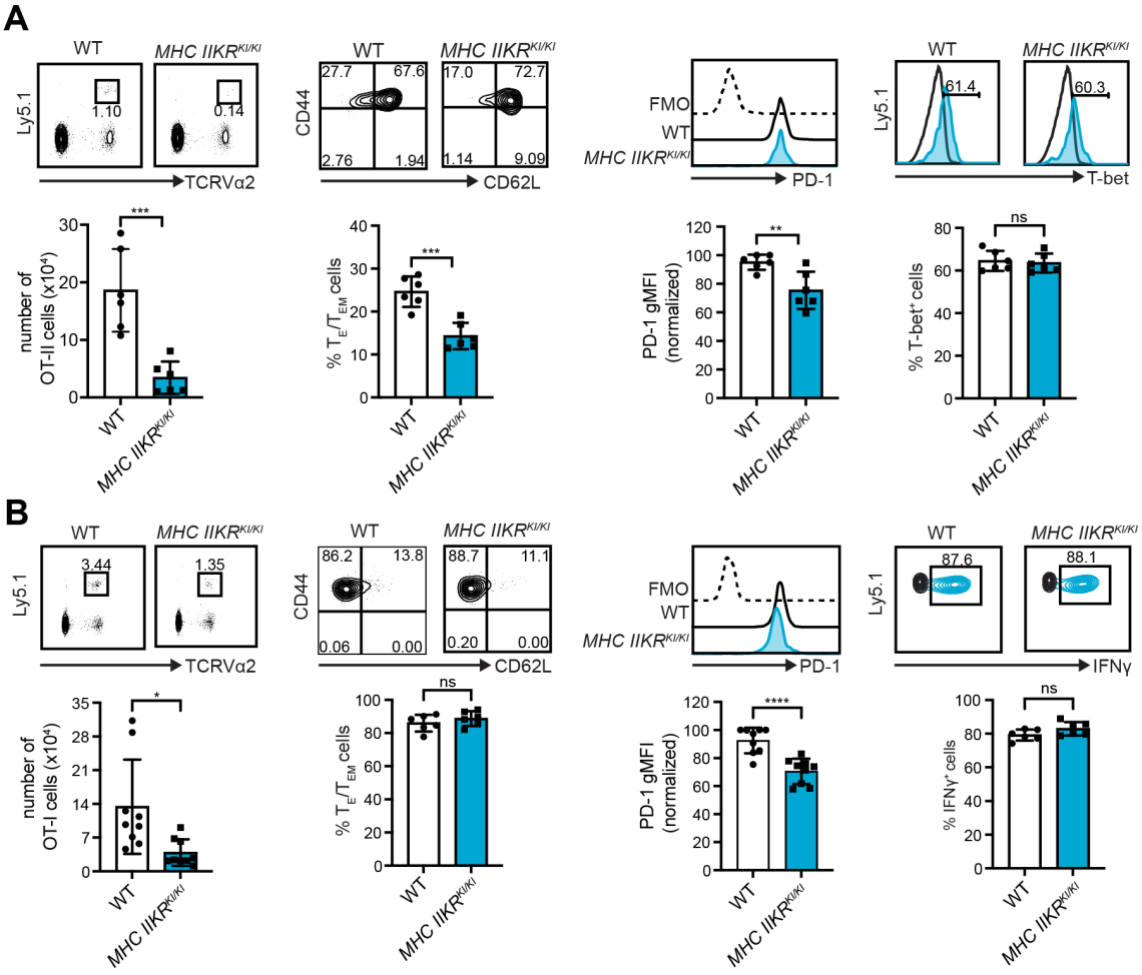


**Figure 9. Lack of MHC II ubiquitination impairs CD4$^+$ and CD8$^+$ T cell responses.** 1 x 10$^4$ OT-II (A) or OT-I (B) were adoptively transferred into *MHC IIKR*$^{KI/KI}$ and WT mice. One day later, mice were immunized with 1 µg anti-Clec9A-OVA mAb and 1 µg LPS. Seven days later, spleens were harvested, and the number of OT-II and OT-I cells, surface PD-1, CD44 and CD62L and intracellular IFNγ and T-bet expression determined. For IFNγ analysis, cells were incubated with 1 µg/ml of $OVA_{257-264}$ in the presence of BD Golgi Plug$^{TM}$ for five hours at 37ºC before intracellular staining as described in Materials and Methods. Data are from two independent experiments with symbols representing individual mice. **** P <0.0001 *** P <0.001 ** P <0.01 * P <0.05, ns not significant, unpaired t test.

**An inability to ubiquitinate MHC II impairs antibody responses.**

Finally, a role for MHC II ubiquitination in humoral immunity was assessed. WT and *MHC IIKR*$^{KI/KI}$ mice were immunized with rat anti-mouse Clec9A mAb which elicits anti-rat Ig reactive antibodies (266, 272). Generating germinal centers and antibody responses requires CD4$^{+}$ follicular T helper ($T_{FH}$) cells. To investigate $T_{FH}$ cell induction, OT-II cells were transferred into WT and *MHC IIKR*$^{KI/KI}$ mice, and 1 day later mice were immunized with anti-Clec9A-OVA mAb. Six days later we examined production of $T_{FH}$, which upregulate PD-1 and CXCR5. WT mice injected with anti-Clec9A-OVA mAb had robust expansion of OT-II cells with increased PD-1 and CXCR5 expression (266, 276). In contrast, significantly reduced $T_{FH}$ cells were detected in *MHC IIKR*$^{KI/KI}$ mice (**Figure 10A**). The reduction in $T_{FH}$ cells was associated with a barely detectable antibody response. While a robust anti-rat Ig response was detected in WT mice, *MHC IIKR*$^{KI/KI}$ mice failed to generate significant serum anti-rat Ig in response to anti-Clec9A (**Figure 10B**). Therefore, *MHC IIKR*$^{KI/KI}$ mice display significant impairments in humoral immunity.

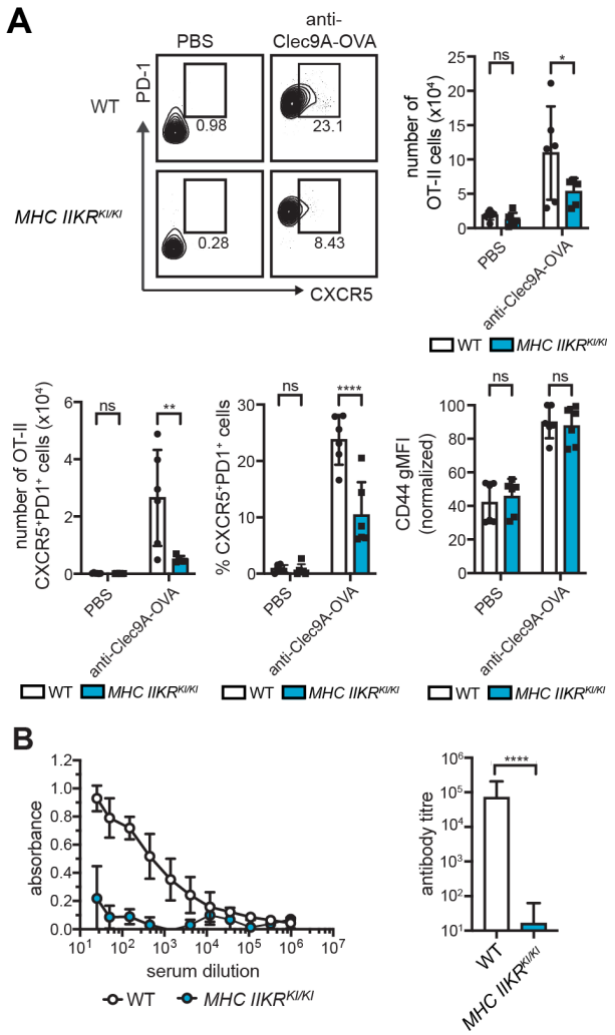


**Figure 10. Lack of MHC II ubiquitination impairs antibody responses.** (A) $T_{FH}$ induction. 1 x $10^6$ OT-II x Ly5.1 cells were adoptively transferred into *MHC IIKR$^{KI/KI}$* and WT mice. 24 hours later, mice were injected with PBS (no antigen) or 1 μg anti-Clec9A-OVA mAb (αClec9A-OVA). 6 days later, spleens were harvested and the number of OT-II cells and OT-II CXCR5$^+$ PD1$^+$ ($T_{FH}$) cells was determined. The activation status of OT-II cells was assessed by staining for CD44. gMFI has been normalized to the maximum gMFI signal. Data are from 2 independent experiments with n = 6 mice. **** P <0.0001 ** P <0.01 * P <0.05, ns not significant, 2-way ANOVA with Sidak's test for multiple comparisons. (B) Antibody production. WT and *MHC IIKR$^{KI/KI}$* mice were injected intravenously with 2 μg anti-Clec9A mAb (10B4), and serum anti-rat reactivity was measured by ELISA 14 days after injection. Representative anti-rat Ig response is shown (left). Bars show mean titers ± SD with n = 10 mice, data are pooled from two independent experiments performed in duplicate. **** p <0.0001, Mann-Whitney test.

# Discussion

Ubiquitination of MHC II plays an important role in regulating cell surface MHC II; however, the biological consequences of this post-translational modification are unclear. Here we conduct the first comprehensive analysis *in vivo* and show that an absence of MHC II ubiquitination reduces splenic DC numbers, alters DC cytokine production, impairs DC antigen proteolysis, and ultimately reduces *in vivo* antigen presentation, cytotoxic T cell and humoral immunity.

Previously, different *in vitro* antigen presentation studies have yielded disparate outcomes and have focused on $CD4^+$ T cell priming only (100, 109, 112, 115–117). Here, for the first time, we demonstrate a significant reduction in MHC II and MHC I antigen presentation in response to soluble, cell-associated and anti-Clec9A mAb-targeted antigen following immunization of *MHC IIKR*$^{KI/KI}$ mice. This data is in agreement with a recent study identifying *MHC IIKR*$^{KI/KI}$ mice have reduced $CD4^+$ T cell priming following immunization with OVA in the presence of CFA (117). Our study extends this work to different forms of antigen including soluble, cell associated and Clec9A-targeted antigen, demonstrating that MHC II ubiquitination impacts MHC II presentation of antigen acquired via different intracellular routes. In addition, we have demonstrated for the first time that MHC II ubiquitination impacts MHC I presentation *in vivo*. Reduced splenic DC numbers may contribute to this impairment, and in addition, *ex vivo* antigen presentation assays demonstrate a cell-intrinsic defect in DC function. In agreement with this, *MHC IIKR*$^{KI/KI}$ DC isolated from mixed bone marrow chimeric mice generated from *MHC IIKR*$^{KI/KI}$ bone marrow have reduced *in vitro* $CD4^+$ T cell priming in comparison to the WT DC from the same mouse (117). Several parameters of DC biology are likely

involved including reduced costimulatory molecule and MHC I cell surface expression, altered cytokine secretion and altered antigen proteolysis. Altered cell surface phenotype has previously been observed in cells lacking MHC II ubiquitination. Indeed, altered expression of CD80, CD40, CD71, PD-L1 ICOS-L (95), CD4 and CD8 (115) is detected on APCs lacking *Marchf1* and *MHC IIKR*$^{KI/KI}$ bone marrow derived DCs (BMDC) have reduced tetraspanin expression (113).

Elevated IL-6, IL-12 and TNF-α secretion described here is in contrast to other studies demonstrating *MHC IIKR*$^{KI/KI}$ and *Marchf1*$^{-/-}$ DC have reduced IL-12 and TNF-α production (115, 117). This difference is likely due to differences in stimuli tested, with CpG (TLR9 agonist), IFN-γ and GM-CSF used here in contrast to LPS (TLR4 agonist). This study also shows that *MHC IIKR*$^{KI/KI}$ cDC1 have reduced OVA degradation, but overall *MHC IIKR*$^{KI/KI}$ cDC1 or cDC2 do not exhibit a global antigen proteolysis defect. BSA degradation was similar to WT and likewise no defects in endosomal acidification or cathepsin activity were detected.

Impairments in DC antigen presentation in the absence of MHC II ubiquitination are likely due to excessive MHC II accumulation on the plasma membrane, which disrupt plasma membrane and lipid raft structure (113). Lipid rafts are important for antigen presentation, and if disrupted can lead to reduced APC: T cell conjugate formation and reduced T cell activation (277, 278). In agreement with this, *Marchf1* deficient and *MHC IIKR*$^{KI/KI}$ BMDC engage thymocytes at a lower frequency (113) and when pulsed with OVA, *Marchf1* deficient and *MHC IIKR*$^{KI/KI}$ spleen CD11c$^{+}$ DC are unable to form stable conjugates with CD4$^{+}$ T cells to the same extent as WT DC (117). Altered MHC II

trafficking in the absence of its ubiquitination has been previously described with reduced pMHC II degradation (100), MHC II internalization (109, 110) and increased recycling (100). The downstream consequences for T cell priming were examined and reduced numbers and impaired phenotype of $CD4^+$ (OT-II) and $CD8^+$ (OT-I) T cells following Clec9A-OVA immunization was identified. This likely accounts for impaired CTL immunity following immunization with cell-associated or Clec9A-targeted antigen and similarly, poor antibody responses. Indeed, we also observe reduced induction of $CD4^+$ follicular T helper ($T_{FH}$) cells in *MHC IIKR*$^{KI/KI}$ mice, in accordance with longer TCR:pMHC II interactions being required to promote their differentiation (279, 280).

*MHC IIKR*$^{KI/KI}$ mice failed to generate antibody responses to DC-targeted antigen. This is in conflict to previous studies that show normal antibody responses for *MHC IIKR*$^{KI/KI}$ mice (112). The discrepancy could stem from the different mouse models, with *MHC IIKR*$^{KI/KI}$ mice used here as opposed to *MHC IIKR-GFP* mice, or differences in immunization timing and antigen. Our study immunized with rat anti-Clec9A mAb which specifically relies on cDC1 presentation, whereas the previous analysis used protein (OVA and HEL) and influenza A virus infection, all of which will engage other DC subsets, including cDC2, that we show here are less impacted by a lack of MHC II ubiquitination. Importantly, changes in antibody production could also be due to alterations in B cell biology. Indeed, MHC II is regulated by MARCH1-mediated ubiquitination in B cells. In germinal center B cells in particular, MHC II expression is dynamically regulated by ubiquitination as the cells cycle between the light and dark zones (281). A lack of MHC II ubiquitination in germinal center B cells leads to prolonged peptide presentation which may impact the presented peptide repertoire and in

turn delay affinity maturation (281). Therefore, it is possible that this too contributes to the decreased antibody production observed in *MHC IIKR*$^{KI/KI}$ mice.

Here we identify the importance of MHC II ubiquitination in DC, T cell and B cell responses. Evolutionary conservation of MARCH ligases and the target residue of ubiquitination in MHC II (Lys225), may therefore have been driven not by a simple requirement to regulate MHC II surface expression, but to prevent secondary effects induced by the excessive deposition of MHC II on the cell surface.

# Chapter 6 - Final discussion

This thesis has interrogated two key molecules necessary for the generation and function of dendritic cells (DCs) – FMS-like tyrosine kinase 3 (Flt3) and major histocompatibility complex class II (MHC II). The main aim was to increase the understanding of DC biology such that DCs can be more easily manipulated to improve immune responses to vaccines against infection and cancer.

It is becoming increasingly apparent that DCs play a critical role in immunotherapy. cDC1 are required for tumor rejection (38, 39, 273), and expression of cDC1-related genes correlates with improved overall survival (5, 282). Additionally, cDC1 are required for efficient adoptive T cell therapy (39). Recently it has been demonstrated that cDC2 are required for anti-tumoral $CD4^+$ T cell responses (283). Manipulation of the number of DCs via Flt3/Flt3L signaling cascade improves tumor clearance (41, 42, 284, 285). Currently, clinical strategies rely upon administration of Flt3L, however, improved understanding of the expression and regulation of Flt3 could lead to more sophisticated and long-lasting approaches.

In this thesis we have demonstrated that splenic cDC1, cDC2 and pDC express both surface and intracellular Flt3 and regulate its expression at the cell surface. Expression of the receptor varies between the subsets, with pDC expressing a larger form of Flt3 at the cell surface. Flt3 is N-linked glycosylated (151, 152) and the larger form observed in pDC likely represents Flt3 that is more heavily decorated with carbohydrate moieties. Flt3 glycosylation has not been studied in DCs yet, in fact, this thesis is the first study to

demonstrate different forms of Flt3 in DC subsets. Given glycosylation impacts the trafficking, interactions, ligand binding, internalization and signaling of receptors (286), if the glycosylation status of Flt3 differs in pDC it is possible that these aspects of Flt3 biology are also altered. Further experiments will be necessary to investigate not only the glycosylation status of Flt3 in DC subsets but also the immunological impact on DC function. These studies may be difficult to perform with primary cDC1 and pDC given their rarity, though this could be overcome with the use of bone marrow-derived DCs, assuming the same pattern of Flt3 expression is observed.

Differences in Flt3 expression suggest differential requirements for Flt3/Flt3L signaling in DC subsets. In line with this hypothesis, cDC2-produced Flt3L is essential for the maintenance of splenic cDC2 suggesting that this DC subset requires preferential autocrine access to Flt3L and as a result, Flt3 signaling (20). While it is well known that Flt3 signaling regulates cDC and pDC development, the role for Flt3 in terminally differentiated DC is less clear. It has been suggested that Flt3 signaling regulates the division of terminally differentiated peripheral cDC, with *Flt3*$^{-/-}$ cDC incorporating less BrdU in comparison to wildtype cDC (3). In contrast, *Flt3*$^{-/-}$ pDC proliferate to the same extent as their wild type counterpart (3). This again hints towards differential requirements of Flt3 signaling in DC subsets. Further to this, when bone marrow-derived DCs are treated with a Flt3 tyrosine kinase inhibitor (CEP-701) they undergo apoptosis to a greater extent than untreated DCs (159). This suggesting Flt3 promotes the survival of differentiated DCs, though further experiments are required to assess the impact on primary cDC and pDC. Therefore, the differences in Flt3 expression we observed in this thesis may allow DCs to finetune signaling and regulate DC numbers in the periphery.

Besides differential Flt3 expression at steady state, our work also indicates Flt3 is regulated during DC activation. DC undergo many changes during their activation to promote relevant antigen peptide presentation and T cell activation (9). It is possible that changes in Flt3 expression could increase DC responsiveness to Flt3L which could promote their survival and T cell priming potential. In support of this, increased Flt3L responsiveness has been observed in $Flt3^{+}$ and $Flt3^{-}$ progenitor cells overexpressing Flt3 (1). Similarly, when Flt3 signaling is inhibited reduced T cell stimulation is observed in mixed leukocyte reactions (159).

At the time of writing this, 7 clinical trials utilizing Flt3L were underway (as registered on ClinicalTrials.gov). Despite the strong interest in exploiting the Flt3/Flt3L signaling pathway for immunotherapy and vaccination, the regulation of Flt3 in DCs has largely been neglected. Besides characterizing the expression of Flt3, this thesis used CRISPR/Cas9 genome-wide screens to identify novel Flt3 regulators. These regulators could be targeted to finetune Flt3 expression and potentially increase the efficacy of Flt3L treatment or alternatively decrease the impact of Flt3 signaling. The former will be particularly helpful where a boost in DC numbers is required to improve immune outcomes, such as patients with solid tumors. In support of this, improved tumor clearance is observed in advanced stages of indolent non-Hodgkin's lymphoma patients treated with Flt3L, radiotherapy and poly I:C (40). Similarly, improved tumor clearance has been demonstrated in tumor bearing mice treated with Flt3L-secreting CAR-T cells (41). On the other hand, reducing Flt3 signaling may be useful where a reduction in DC numbers is required, for example in autoimmune diseases where elevated DCs are observed at sites

of inflammation, such as rheumatoid arthritis (287, 288). Indeed, mice with reduced Flt3 signaling (due to a lack of *Flt3L*) are better protected from collagen-induced arthritis, a model for rheumatoid arthritis (289). Similarly, mice with experimental autoimmune encephalomyelitis (a model for multiple sclerosis) have reduced disease progression when treated with a Flt3 tyrosine kinase inhibitor (159).

It is currently unclear how the new Flt3 regulators identified here impact Flt3 expression. Since Med25 has a described role in the Mediator Complex and USP22, along with ATXN7L3, are part of the SAGA complex, it is likely these two proteins regulate Flt3 at the transcriptional level. In agreement with this, we observed altered *Flt3* mRNA in cells lacking *Med25* or *USP22*. However, several questions remain to be answered: do Med25 and USP22 regulate *Flt3* transcription directly or indirectly? Which transcription factors recruit them to DNA? Given that we observe changes in other immunoreceptors in their absence, are they so-called "master regulators" of DC function? Since we observed changes in Flt3 expression during DC activation, do the expression of these genes differ during DC activation? Finally, the most important question remaining is the function of these genes in immunity. It is unlikely that the altered Flt3 expression observed in *Med25* and *USP22* knockout DCs will impact DC function *in vitro* given *Flt3*$^{-/-}$ cDC1 and cDC2 prime CD8$^{+}$ T cells to a similar extent as wild type DCs (290). It has recently been demonstrated that Flt3 signaling promotes the expression of activation related genes in tumor-infiltrating cDC1 (291). This is thought to improve cDC1 and CD8$^{+}$ T cell infiltration and anti-tumor responses (291). Therefore, future studies exploring the role of Med25 and USP22 should rely not only on *in vitro* assays but also on *in vivo* assays in conditional knockout mice to fully elucidate the role of these genes in T cell priming and

anti-tumor responses. Together, these studies could reveal novel tools for the manipulation of DCs.

*Flt3* mutations occur in ~30% of acute myeloid leukemia (AML) patients, making it one of the most common perturbations in hematological malignancies (6). The most common mutation is Flt3-internal tandem duplication (ITD). Flt3-ITD$^{+}$ patients have poorer prognosis, overall survival, and increased risk of relapse in comparison to AML patients without the mutation (6). This suggests the mutation confers a leukemogenic advantage to cells. In cancer, DC function is usually altered to allow for immune evasion (7) therefore the impact of Flt3-ITD on DC function was investigated. We demonstrated elevated number of DCs in mice harboring Flt3-ITD, in agreement with previous studies (35). This is in contrast to studies which have demonstrated AML patients have reduced number of blood DC at diagnosis, though increased numbers are observed following remission (292). It has been suggested that Flt3-ITD promotes DC tolerance, due to Flt3-ITD$^{+}$ DCs inducing strong allogeneic T cell proliferation in addition to the elevated Tregs observed in Flt3-ITD bearing mice (35). To further investigate the impact of Flt3-ITD on DC function, we extended the analysis of previous studies to assess the ability of Flt3-ITD expressing DC to stimulate antigen-specific T cells. This is particularly important given improved outcomes are correlated with increased leukemia-associated antigen specific CD8$^{+}$ T cells in AML (293). We found the mutation does not impact MHC I cross presentation of soluble or cell associated antigen. It does, however, significantly improve MHC II antigen presentation of soluble and cell-associated antigen. One caveat to this analysis is that due to rarity of WT cDC1, we were unable to compare WT cDC1 subsets with Flt3-ITD cDC1 subsets. Therefore, we cannot directly delineate differences

that are due to the Flt3-ITD mutation from inherent differences in cDC1 subsets. One potential way to circumvent this issue in future, is to treat WT mice with Flt3L prior to isolating DCs. However, given Flt3L does not expand NC cDC1 to the same extent as Flt3-ITD it is unclear if similar numbers would be achievable. Furthermore, assessment of antigen presentation in this study was carried out *in vitro* and as such may not reflect *in vivo* immune responses. Future experiments could benefit from using a more relevant setting. For example, AML development requires two mutations and therefore DC function could be investigated in mice harboring Flt3-ITD in addition to a second mutation such as the AML/ETO fusion protein (294). Even better would be the characterization of Flt3-ITD$^+$ DCs from AML patients in remission.

Together, this will improve our understanding of how Flt3-ITD impacts DC function and assist in the therapeutically exploiting DCs for immunotherapy.

Our investigations also led to new insights about the recently discovered noncanonical cDC1, also known as "$CX_3CR1^+$ $CD8^+$" (35, 142), "CD8 look-alike"(143), "$Axl^+$ $Siglec6^+$ (AS DC/DC5)" (144, 295), "pre-DC" (145), and more recently "transitional DCs (tDCs)" (296). Gene expression analysis has demonstrated noncanonical cDC1 share features with both pDC and cDC (142, 144, 145, 295, 296). In this study, and in others (35), it was shown that noncanonical cDC1 are significantly expanded in Flt3-ITD mice. This presented us with the opportunity to extend their characterization. We found noncanonical cDC1 are unable to produce IL-12, in accordance with previous studies

(142, 296). In addition, for the first time, we demonstrated noncanonical cDC1 have reduced capacity to produce TNFα and IL-6 in comparison to canonical cDC1. Previous studies have shown noncanonical cDC1 are robust at stimulating allogeneic $CD4^+$ T cell proliferation (142, 144, 145, 296), however, their role in antigen-specific T cell priming was unclear. Here, we show noncanonical cDC1 have elevated MHC II antigen presentation and while they can cross present soluble antigen, they have impaired cross presentation of cell-associated antigen.

Given their recent discovery, the immunological function of noncanonical DCs remains elusive. It was initially suggested that noncanonical DCs are progenitor DCs (145), however, more recent analysis has demonstrated this is unlikely due to their dissimilarity with described progenitors in addition to their lymphoid features (296). It has been demonstrated that along with pDC, noncanonical DC accumulate in influenza-infected lungs (296). This, in addition to their unique phenotype, has led to the hypothesis that they may cooperate with pDC in antiviral immunity (296). Further work, possibly with mouse models specifically lacking noncanonical DC (296), is required to fully elucidate the function of these cells in immunity. This may reveal a new DC subset that can be targeted and manipulated for improved immunity.

An alternative angle for DC manipulation is to target DC function. Given the central role of cross-presenting cDC1 in tumor clearance, it is unsurprising that most work has focused on MHC I-dependent $CD8^+$ T cell priming. However, it is becoming increasingly apparent that effective immunotherapy also requires MHC II-dependent $CD4^+$ T cell priming (297, 298). In contrast with its immunoprotective role, MHC II is also implicated

in autoimmunity (299, 300). In this thesis, the impact of MHC II ubiquitination on DC function and immunity was investigated. It is well known that the surface expression of MHC II in DCs is regulated by MARCH1-mediated ubiquitination (90, 93, 94, 100), therefore manipulation of this pathway could potentially alter immunity.

Prior to this study, the impact of MHC II ubiquitination on immunity was controversial. We, and others, demonstrated MHC II ubiquitination impacts Treg development (110, 113, 114) however conventional T cell are unaffected (110). *In vitro* antigen presentation studies had disparate outcomes and only focused on $CD4^+$ T cell priming (100, 112, 115–117). An irregular cell surface phenotype was observed in DCs lacking MHC II ubiquitination (95, 109, 115), which hinted these DCs may have an altered function. At the time of publishing this study, DCs lacking MHC II ubiquitination (*MHC IIKR*$^{KI/KI}$) were reported to have impaired function (117). Kim et al., demonstrated reduced MHC II *in vivo* antigen presentation in response to OVA-CFA immunization, in addition to altered cytokine secretion (117). Importantly, this study did not investigate other aspects of DC biology, such as antigen uptake or proteolysis. Further to this, it was unclear if the defect in $CD4^+$ T cell priming was specific to one form of antigen (OVA-CFA), or if there was a global defect in antigen presentation which affects all forms of antigen presentation to $CD4^+$ and $CD8^+$ T cells.

In this thesis, we showed that *MHC IIKR*$^{KI/KI}$ mice have impaired $CD4^+$ and $CD8^+$ T cell priming to soluble, cell-associated, and DC-targeted antigen. In addition, we demonstrated that mice lacking MHC II ubiquitination have reduced CTL killing, follicular T helper ($T_{FH}$) cell generation and antibody responses. This failed immunity

likely stems from *MHC IIKR*$^{KI/KI}$ mice having a reduced number of DCs which exhibit a dysfunctional phenotype. Indeed, in this thesis we showed altered cell surface phenotype, defective antigen proteolysis and cytokine secretion. Altered gene expression profile has also recently been demonstrated (117). We suggest these changes may be due to the excessive accumulation of MHC II at the cell surface, which leads to the disruption of plasma membrane and lipid raft structures (113), which are known to be important for antigen presentation (277, 278). Impaired immune responses could also be amplified by impaired B cell function, given B cell MHC II is also regulated by MARCH1 (92). Furthermore, while not yet investigated, it is possible that the *MHC IIKR*$^{KI/KI}$ exhibit defects in antigen turnover or exchange which could contribute to impaired antigen presentation. While the mechanism behind these abnormalities remains to be uncovered, these studies demonstrate the importance of MHC II ubiquitination in regulating DC homeostasis. A therapeutic agent capable of interfering with MHC II ubiquitination might recapitulate the effects described in *MHC IIKR*$^{KI/KI}$ mice and dampen autoimmunity. Importantly, given *MHC IIKR*$^{KI/KI}$ mice have altered MHC I expression and function, it suggests that in addition to directly regulating MHC II, MARCH1 also indirectly regulates MHC I – a hypothesis we previously proposed (109). Therefore, any therapy targeting MHC II may also impact MHC I induced immunity.

The concept of targeting the ubiquitin system to alter immunity is not new. In fact, numerous molecules that target the proteasome, E1 ubiquitin-activating enzymes, E2 ubiquitin-conjugating enzymes, E3 ubiquitin ligases and deubiquitinating enzymes (DUBs) are in development or in use already (301, 302). For example, lenalidomide is a drug that has been approved for the treatment of multiple myeloma (303). It binds to and

activates cereblon (CRBN) E3 ligase complex (304), which targets transcription factors to the proteasome and promotes multiple myeloma cell cytotoxicity (305, 306). Interestingly, lenalidomide has been implicated in the regulation of MARCH1 in DCs (307). Monocyte-derived DCs generated in the presence of the drug have elevated MHC II and CD86 in addition to reduced *Marchf1* transcription (307). This phenotype leads to reduced T cell proliferation in mixed leukocyte reactions, similar to the reduced T cell priming we observed in this thesis with *MHC IIKR*$^{KI/KI}$ DC. Due to its pleiotropic effects, lenalidomide may not be the best drug to specifically target MHC II ubiquitination, however, it does clearly illustrate the therapeutic potential of targeting ubiquitination for immunity.

In conclusion, this thesis has utilized biochemical, immunological and advanced genomic analyses to advance the understanding of DC biology. We have characterized the expression of Flt3 and Flt3-ITD and have demonstrated the latter alters DC function. In addition, novel genetic machinery responsible for regulating Flt3 expression was identified. Finally, using mice lacking MHC II ubiquitination, we clearly demonstrated that MHC II ubiquitination controls DC function and shapes immune responses. Together this work will assist in the manipulation of DCs in vaccines for infection and cancer.

# References

1. Onai, N., A. Obata-Onai, R. Tussiwand, A. Lanzavecchia, and M. G. Manz. 2006. Activation of the Flt3 signal transduction cascade rescues and enhances type I interferon–producing and dendritic cell development. *J. Exp. Med.* 203: 227–238.

2. Maraskovsky, E., K. Brasel, M. Teepe, E. R. Roux, S. D. Lyman, K. Shortman, H. J. McKenna, P. Online, S. Info, M. Genetics, I. Corporation, T. Walter, E. Maraskovsky, K. Brasel, M. Teepe, E. R. Roux, S. D. Lyman, K. Shortman, and H. J. McKenna. 1996. Dramatic increase in the numbers of functionally mature dendritic cells in Flt3 ligand-treated mice: multiple dendritic cell subpopulations identified. *J. Exp. Med.* 184: 1953–1962.

3. Waskow, C., K. Liu, G. Darrasse-Jèze, P. Guermonprez, F. Ginhoux, M. Merad, T. Shengelia, K. Yao, and M. Nussenzweig. 2008. The receptor tyrosine kinase Flt3 is required for dendritic cell development in peripheral lymphoid tissues. *Nat. Immunol.* 9: 676–683.

4. Karsunky, H., M. Merad, A. Cozzio, I. L. Weissman, and M. G. Manz. 2003. Flt3 Ligand Regulates Dendritic Cell Development from Flt3+ Lymphoid and Myeloid-committed Progenitors to Flt3+ Dendritic Cells In Vivo. *J. Exp. Med.* 198: 305–313.

5. Barry, K. C., J. Hsu, M. L. Broz, F. J. Cueto, M. Binnewies, A. J. Combes, A. E. Nelson, K. Loo, R. Kumar, M. D. Rosenblum, M. D. Alvarado, D. M. Wolf, D. Bogunovic, N. Bhardwaj, A. I. Daud, P. K. Ha, W. R. Ryan, J. L. Pollack, B. Samad, S. Asthana, V. Chan, and M. F. Krummel. 2018. A natural killer–dendritic cell axis defines checkpoint therapy–responsive tumor microenvironments. *Nat. Med.* 24: 1178–1191.

6. Daver, N., R. F. Schlenk, N. H. Russell, and M. J. Levis. 2019. Targeting FLT3 mutations in AML: review of current knowledge and evidence. *Leukemia* 33: 299–312.

7. Wculek, S. K., F. J. Cueto, A. M. Mujal, I. Melero, M. F. Krummel, and D. Sancho. 2020. Dendritic cells in cancer immunology and immunotherapy. *Nat. Rev. Immunol.* 20: 7–24.

8. Steinman, R. M., and Z. A. Cohn. 1973. Identification of a novel cell type in peripheral lymphoid organs of mice. I. Morphology, quantitation, tissue distribution. *J. Exp. Med.* 137: 1142–62.

9. Reis e Sousa, C. 2006. Dendritic cells in a mature age. *Nat. Rev. Immunol.* 6: 476–483.

10. Miller, J. C., B. D. Brown, T. Shay, E. L. Gautier, V. Jojic, A. Cohain, G. Pandey, M. Leboeuf, K. G. Elpek, J. Helft, D. Hashimoto, A. Chow, J. Price, M. Greter, M. Bogunovic, A. Bellemare-Pelletier, P. S. Frenette, G. J. Randolph, S. J. Turley, M. Merad, C. Jakubzick, A. J. Best, J. Knell, A. Goldrath, D. Koller, N. Cohen, P. Brennan, M. Brenner, A. Regev, A. Fletcher, D. Malhotra, R. Jianu, D. Laidlaw, J. Collins, K. Narayan, K. Sylvia, J. Kang, R. Gazit, D. J. Rossi, F. Kim, T. N. Rao, A. Wagers, S. A. Shinton, R. R. Hardy, P. Monach, N. A. Bezman, J. C. Sun, C. C. Kim, L. L. Lanier, T. Heng, T. Kreslavsky, M. Painter, J. Ericson, S. Davis, D. Mathis, and C. Benoist. 2012. Deciphering the transcriptional network of the dendritic cell lineage. *Nat. Immunol.* 13: 888–899.

11. Wilson, K. R., J. A. Villadangos, and J. D. Mintern. 2021. Dendritic cell Flt3 – regulation, roles and repercussions for immunotherapy. *Immunol. Cell Biol.* imcb.12484.

12. Lyman, S. D., L. James, L. Johnson, K. Brasel, P. De Vries, S. S. Escobar, H.

Downey, R. R. Splett, M. P. Beckmann, H. J. Mckenna, B. S. D. Lyman, L. James, L. Johnson, K. Brasel, P. De Vries, S. S. Escobar, H. Downey, R. R. Splett, M. P. Beckmann, H. J. Mckenna, S. D. Lyman, L. James, L. Johnson, K. Brasel, P. De Vries, S. S. Escobar, H. Downey, R. R. Splett, M. P. Beckmann, and H. J. Mckenna. 1994. Cloning of the human homologue of the murine flt3 ligand: a growth factor for early hematopoietic progenitor cells. *Blood* 83: 2795–2802.

13. Hannum, C., J. Culpepper, D. Campbell, T. McClanahan, S. Zurawsk, J. F. Bazan, R. Kastelein, S. Hudak, J. Wagner, J. Mattson, J. Luh, G. Duda, N. Nartina, D. Peterson, S. Menon, a Shanafelt, M. Muench, G. Kelner, R. Namikawa, D. Rennick, M.-G. Roncarolo, a Zlotnik, O. Rosnet, P. Dubreuil, D. Birnbaum, and F. Lee. 1994. Ligand for FLT3/FLK2 receptor tyrosine kinase regulates grouth of haematopoietic stem cells and is encoded by variant RNAs. *Nature* 368: 643–648.

14. Lyman, S. D., L. James, T. V. Bos, P. de Vries, K. Brasel, B. Gliniak, L. T. Hollingsworth, K. S. Picha, H. J. McKenna, R. R. Splett, F. a. Fletcher, E. Maraskovsky, T. Farrah, D. Foxworthe, D. E. Williams, and M. P. Beckmann. 1993. Molecular cloning of a ligand for the flt3/flk-2 tyrosine kinase receptor: A proliferative factor for primitive hematopoietic cells. *Cell* 75: 1157–1167.

15. Lyman, S. D., L. James, S. Escobar, H. Downey, P. De Vries, I. Brasel, K. Stocking, M. P. Beckmann, N. G. Copeland, L. S. Cleveland, N. A. Jenkins, J. W. Belmont, and B. L. Davison. 1995. Identification of soluble and membrane-bound isoforms of the murine flt3 ligand generated by alternative splicing of mRNAs. *Oncogene* 10: 149–157.

16. Chklovskaia, E., W. Jansen, C. Nissen, S. D. Lyman, C. Rahner, L. Landmann, A. Wodnar-filipowicz, E. Chklovskaia, W. Jansen, C. Nissen, S. D. Lyman, C. Rahner, L. Landmann, and A. Wodnar-filipowicz. 1999. Mechanism of flt3 Ligand Expression in

Bone Marrow Failure: Translocation From Intracellular Stores to the Surface of T Lymphocytes After Chemotherapy-Induced Suppression of Hematopoiesis. *Blood* 93: 2595–2604.

17. Saito, Y., C. S. Boddupalli, C. Borsotti, and M. G. Manz. 2013. Dendritic cell homeostasis is maintained by nonhematopoietic and T-cell-produced Flt3-ligand in steady state and during immune responses. *Eur. J. Immunol.* 43: 1651–1658.

18. Chklovskaia, E., C. Nissen, L. Landmann, C. Rahner, O. Pfister, and A. Wodnar-Filipowicz. 2001. Cell-surface trafficking and release of flt3 ligand from T lymphocytes is induced by common cytokine receptor y-chain signaling and inhibited by cyclosporin A. *Blood* 97: 1027–1034.

19. Horiuchi, K., H. Morioka, H. Takaishi, H. Akiyama, C. P. Blobel, and Y. Toyama. 2009. Ectodomain shedding of FLT3 ligand is mediated by TACE. *J. Immunol.* 182: 7408–14.

20. Fujita, K., S. Chakarov, T. Kobayashi, K. Sakamoto, B. Voisin, K. Duan, T. Nakagawa, K. Horiuchi, M. Amagai, F. Ginhoux, and K. Nagao. 2019. Cell-autonomous FLT3L shedding via ADAM10 mediates conventional dendritic cell development in mouse spleen. *Proc. Natl. Acad. Sci.* 116: 14714–14723.

21. Durai, V., P. Bagadia, C. G. Briseño, D. J. Theisen, A. Iwata, J. T. Davidson, M. Gargaro, D. H. Fremont, T. L. Murphy, K. M. Murphy, J. T. D. Iv, M. Gargaro, D. H. Fremont, T. L. Murphy, and K. M. Murphy. 2018. Altered compensatory cytokine signaling underlies the discrepancy between Flt3 –/– and Flt3l –/– mice. *J. Exp. Med.* 215: 1–19.

22. Zhang, S., C. Mantel, and H. E. Broxmeyer. 1999. Flt3 signaling involves tyrosyl-phosphorylation of SHP-2 and SHIP and their association with Grb2 and Shc in

Baf3/Flt3 cells. *J. Leukoc. Biol.* 65: 372–380.

23. Sathaliyawala, T., W. E. O'Gorman, M. Greter, M. Bogunovic, V. Konjufca, Z. E. Hou, G. P. Nolan, M. J. Miller, M. Merad, and B. Reizis. 2010. Mammalian target of rapamycin controls dendritic cell development downstream of Flt3 ligand signaling. *Immunity* 33: 597–606.

24. Laouar, Y., T. Welte, X. Y. Fu, and R. A. Flavell. 2003. STAT3 Is Required for Flt3L-Dependent Dendritic Cell Differentiation. *Immunity* 19: 903–912.

25. Naik, S. H., L. Perié, E. Swart, C. Gerlach, N. Van Rooij, R. J. De Boer, and T. N. Schumacher. 2013. Diverse and heritable lineage imprinting of early haematopoietic progenitors. *Nature* 496: 229–232.

26. D'Amico, A., and L. Wu. 2003. The Early Progenitors of Mouse Dendritic Cells and Plasmacytoid Predendritic Cells Are within the Bone Marrow Hemopoietic Precursors Expressing Flt3. *J. Exp. Med.* 198: 293–303.

27. Audiger, C., and S. Lesage. 2020. FLT3 Ligand Is Dispensable for the Final Stage of Type 1 Conventional Dendritic Cell Differentiation. *J. Immunol.* 205: 2117–2127.

28. Ginhoux, F., K. Liu, J. Helft, M. Bogunovic, M. Greter, D. Hashimoto, J. Price, N. Yin, J. Bromberg, S. A. Lira, E. R. Stanley, M. Nussenzweig, and M. Merad. 2009. The origin and development of nonlymphoid tissue CD103+ DCs. *J. Exp. Med.* 206: 3115–3130.

29. Maraskovsky, E., E. Daro, E. Roux, M. Teepe, C. R. Maliszewski, J. Hoek, D. Caron, M. E. Lebsack, and H. J. McKenna. 2000. In vivo generation of human dendritic cell subsets by Flt3 ligand. *Blood* 96: 878–884.

30. Mackarehtschian, K., J. D. Hardin, K. A. Moore, S. Boast, S. P. Goff, and I. R. Lemischka. 1995. Targeted disruption of the flk2/flt3 gene leads to deficiencies in

primitive hematopoietic progenitors. *Immunity* 3: 147–161.

31. McKenna, H. J., K. L. Stocking, R. E. Miller, K. Brasel, T. De Smedt, E. Maraskovsky, C. R. Maliszewski, D. H. Lynch, J. Smith, B. Pulendran, E. R. Roux, M. Teepe, S. D. Lyman, and J. J. Peschon. 2000. Mice lacking flt3 ligand have deficient hematopoiesis affecting hematopoietic progenitor cells, dendritic cells, and natural killer cells. *Blood* 95: 3489–3497.

32. Swee, L. K., N. Bosco, B. Malissen, R. Ceredig, A. Rolink, and W. Dc. 2009. Expansion of peripheral naturally occurring T regulatory cells by Fms-like tyrosine kinase 3 ligand treatment. *Blood* 113: 6277–6287.

33. Darrasse-Jèze, G., S. Deroubaix, H. Mouquet, G. D. Victora, T. Eisenreich, K. Yao, R. F. Masilamani, M. L. Dustin, A. Rudensky, K. Liu, and M. C. Nussenzweig. 2009. Feedback control of regulatory T cell homeostasis by dendritic cells in vivo. *J. Exp. Med.* 206: 1853–1862.

34. Klein, O., L. M. Ebert, D. Zanker, K. Woods, B. S. Tan, J. Fucikova, A. Behren, I. D. Davis, E. Maraskovsky, W. Chen, and J. Cebon. 2013. Flt3 ligand expands CD4+ FoxP3+ regulatory T cells in human subjects. *Eur. J. Immunol.* 43: 533–539.

35. Lau, C. M., S. A. Nish, N. Yogev, A. Waisman, S. L. Reiner, and B. Reizis. 2016. Leukemia-associated activating mutation of Flt3 expands dendritic cells and alters T cell responses. *J. Exp. Med.* 213: 415–431.

36. Guermonprez, P., J. Helft, C. Claser, S. Deroubaix, H. Karanje, A. Gazumyan, G. Darasse-Jèze, S. B. Telerman, G. Breton, H. A. Schreiber, N. Frias-Staheli, E. Billerbeck, M. Dorner, C. M. Rice, A. Ploss, F. Klein, M. Swiecki, M. Colonna, A. O. Kamphorst, M. Meredith, R. Niec, C. Takacs, F. Mikhail, A. Hari, D. Bosque, T. Eisenreich, M. Merad, Y. Shi, F. Ginhoux, L. Rénia, B. C. Urban, and M. C.

Nussenzweig. 2013. Inflammatory Flt3l is essential to mobilize dendritic cells and for T cell responses during Plasmodium infection. *Nat. Med.* 19: 730–738.

37. Salmon, H., J. Idoyaga, A. Rahman, M. Leboeuf, R. Remark, S. Jordan, M. Casanova-Acebes, M. Khudoynazarova, J. Agudo, N. Tung, S. Chakarov, C. Rivera, B. Hogstad, M. Bosenberg, D. Hashimoto, S. Gnjatic, N. Bhardwaj, A. K. Palucka, B. D. Brown, J. Brody, F. Ginhoux, and M. Merad. 2016. Expansion and Activation of CD103+ Dendritic Cell Progenitors at the Tumor Site Enhances Tumor Responses to Therapeutic PD-L1 and BRAF Inhibition. *Immunity* 44: 924–938.

38. Broz, M. L., M. Binnewies, B. Boldajipour, A. E. Nelson, J. L. Pollack, D. J. Erle, A. Barczak, M. D. Rosenblum, A. Daud, D. L. Barber, S. Amigorena, L. J. van'tVeer, A. I. Sperling, D. M. Wolf, and M. F. Krummel. 2014. Dissecting the Tumor Myeloid Compartment Reveals Rare Activating Antigen-Presenting Cells Critical for T Cell Immunity. *Cancer Cell* 26: 638–652.

39. Spranger, S., D. Dai, B. Horton, and T. F. Gajewski. 2017. Tumor-Residing Batf3 Dendritic Cells Are Required for Effector T Cell Trafficking and Adoptive T Cell Therapy. *Cancer Cell* 31: 711-723.e4.

40. Hammerich, L., T. U. Marron, R. Upadhyay, J. Svensson-Arvelund, M. Dhainaut, S. Hussein, Y. Zhan, D. Ostrowski, M. Yellin, H. Marsh, A. M. Salazar, A. H. Rahman, B. D. Brown, M. Merad, and J. D. Brody. 2019. Systemic clinical tumor regressions and potentiation of PD1 blockade with in situ vaccination. *Nat. Med.* 25: 814–824.

41. Lai, J., S. Mardiana, I. G. House, K. Sek, M. A. Henderson, L. Giuffrida, A. X. Y. Chen, K. L. Todd, E. V Petley, J. D. Chan, E. M. Carrington, A. M. Lew, B. J. Solomon, J. A. Trapani, K. Kedzierska, M. Evrard, S. J. Vervoort, J. Waithman, P. K. Darcy, and P. A. Beavis. 2020. Adoptive cellular therapy with T cells expressing the

dendritic cell growth factor Flt3L drives epitope spreading and antitumor immunity. *Nat. Immunol.* 1–13.

42. Esche, C., V. M. Subbotin, C. Maliszewski, M. T. Lotze, and M. R. Shurin. 1998. FLT3 ligand administration inhibits tumor growth in murine melanoma and lymphoma. *Cancer Res.* 58: 380–383.

43. Sánchez-Paulete, A. R., F. J. Cueto, M. Martínez-López, S. Labiano, A. Morales-Kastresana, M. E. Rodríguez-Ruiz, M. Jure-Kunkel, A. Azpilikueta, M. A. Aznar, J. I. Quetglas, D. Sancho, and I. Melero. 2016. Cancer immunotherapy with immunomodulatory anti-CD137 and anti–PD-1 monoclonal antibodies requires BATF3-dependent dendritic cells. *Cancer Discov.* 6: 71–79.

44. Anandasabapathy, N., R. Feder, S. Mollah, S.-W. Tse, M. P. Longhi, S. Mehandru, I. Matos, C. Cheong, D. Ruane, L. Brane, A. Teixeira, J. Dobrin, O. Mizenina, C. G. Park, M. Meredith, B. E. Clausen, M. C. Nussenzweig, and R. M. Steinman. 2014. Classical Flt3L-dependent dendritic cells control immunity to protein vaccine. *J. Exp. Med.* 211: 1875–1891.

45. Bedoui, S., S. Prato, J. Mintern, T. Gebhardt, Y. Zhan, A. M. Lew, W. R. Heath, J. A. Villadangos, and E. Segura. 2009. Characterization of an Immediate Splenic Precursor of CD8+ Dendritic Cells Capable of Inducing Antiviral T Cell Responses. *J. Immunol.* 182: 4200–4207.

46. Beshara, R., V. Sencio, D. Soulard, A. Barthélémy, J. Fontaine, T. Pinteau, L. Deruyter, M. B. Ismail, C. Paget, J.-C. Sirard, F. Trottein, and C. Faveeuw. 2018. Alteration of Flt3-Ligand-dependent de novo generation of conventional dendritic cells during influenza infection contributes to respiratory bacterial superinfection. *PLOS Pathog.* 14: e1007360.

47. Saevarsdottir, S., T. A. Olafsdottir, E. V. Ivarsdottir, G. H. Halldorsson, K. Gunnarsdottir, A. Sigurdsson, A. Johannesson, J. K. Sigurdsson, T. Juliusdottir, S. H. Lund, A. O. Arnthorsson, E. L. Styrmisdottir, J. Gudmundsson, G. M. Grondal, K. Steinsson, L. Alfredsson, J. Askling, R. Benediktsson, R. Bjarnason, A. J. Geirsson, B. Gudbjornsson, H. Gudjonsson, H. Hjaltason, A. B. Hreidarsson, L. Klareskog, I. Kockum, H. Kristjansdottir, T. J. Love, B. R. Ludviksson, T. Olsson, P. T. Onundarson, K. B. Orvar, L. Padyukov, B. Sigurgeirsson, V. Tragante, K. Bjarnadottir, T. Rafnar, G. Masson, P. Sulem, D. F. Gudbjartsson, P. Melsted, G. Thorleifsson, G. L. Norddahl, U. Thorsteinsdottir, I. Jonsdottir, and K. Stefansson. 2020. FLT3 stop mutation increases FLT3 ligand level and risk of autoimmune thyroid disease. *Nature* 584.

48. Dehlin, M., M. Bokarewa, R. Rottapel, S. J. Foster, M. Magnusson, L. E. Dahlberg, and A. Tarkowski. 2008. Intra-articular fms-like tyrosine kinase 3 ligand expression is a driving force in induction and progression of arthritis. *PLoS One* 3: e3633.

49. Klein, L., B. Kyewski, P. M. Allen, and K. A. Hogquist. 2014. Positive and negative selection of the T cell repertoire: What thymocytes see (and don't see). *Nat. Rev. Immunol.* 14: 377–391.

50. Audiger, C., M. J. Rahman, T. J. Yun, K. V. Tarbell, and S. Lesage. 2017. The Importance of Dendritic Cells in Maintaining Immune Tolerance. *J. Immunol.* 198: 2223–2231.

51. Al-Daccak, R., N. Mooney, and D. Charron. 2004. MHC class II signaling in antigen-presenting cells. *Curr. Opin. Immunol.* 16: 108–13.

52. Liu, X., Z. Zhan, D. Li, L. Xu, F. Ma, P. Zhang, H. Yao, and X. Cao. 2011. Intracellular MHC class II molecules promote TLR-triggered innate immune responses by maintaining activation of the kinase Btk. *Nat. Immunol.* 12: 416–424.

53. Stern, L. J., J. H. Brown, T. S. Jardetzky, J. C. Gorga, R. G. Urban, J. L. Strominger, and D. C. Wiley. 1994. Crystal structure of the human class II MHC protein HLA-DR1 complexed with an influenza virus peptide. *Nature* 368: 215–221.

54. Brown, J. H., T. S. Jardetzky, J. C. Gorga, L. J. Stern, R. G. Urban, J. L. Strominger, and D. C. Wiley. 1993. Three-dimensional structure of the human class II histocompatibility antigen HLA-DR1. *Nature* 364: 33–39.

55. Reith, W., S. LeibundGut-Landmann, and J. M. Waldburger. 2005. Regulation of MHC class II gene expression by the class II transactivator. *Nat. Rev. Immunol.* 5: 793–806.

56. LeibundGut-Landmann, S., J. M. Waldburger, M. Krawczyk, L. A. Otten, T. Suter, A. Fontana, H. Acha-Orbea, and W. Reith. 2004. Specificity and expression of CIITA, the master regulator of MHC class II genes. *Eur. J. Immunol.* 34: 1513–1525.

57. Anderson, M. S., and J. Miller. 1992. Invariant chain can function as a chaperone protein for class II major histocompatibility complex molecules. *Proc. Natl. Acad. Sci. U. S. A.* 89: 2282–2286.

58. Roche, P. A., and P. Cresswell. 1990. Invariant chain association with HLA-DR molecules inhibits immunogenic peptide binding. *Nature* 345: 615–8.

59. Bakke, O., and B. Dobberstein. 1990. MHC class II-associated invariant chain contains a sorting signal for endosomal compartments. *Cell* 63: 707–716.

60. Lotteau, V., L. Teyton, A. Peleraux, T. Nilsson, L. Karlsson, S. L. Schmid, V. Quaranta, and P. A. Peterson. 1990. Intracellular transport of class II MHC molecules directed by invariant chain. *Nature* 348: 600–605.

61. Bénaroch, P., M. Yilla, G. Raposo, K. Ito, K. Miwa, H. J. Geuze, and H. L. Ploegh. 1995. How MHC class II molecules reach the endocytic pathway. *EMBO J.* 14: 37–49.

62. McCormick, P. J., J. A. Martina, and J. S. Bonifacino. 2005. Involvement of clathrin and AP-2 in the trafficking of MHC class II molecules to antigen-processing compartments. *Proc. Natl. Acad. Sci. U. S. A.* 102: 7910–7915.

63. Dugast, M., H. Toussaint, C. Dousset, and P. Benaroch. 2005. AP2 clathrin adaptor complex, but not AP1, controls the access of the major histocompatibility complex (MHC) class II to endosomes. *J. Biol. Chem.* 280: 19656–19664.

64. Roche, P. A., and P. Cresswell. 1991. Proteolysis of the class II-associated invariant chain generates a peptide binding site in intracellular HLA-DR molecules. *Proc. Natl. Acad. Sci. U. S. A.* 88: 3150–3154.

65. Villadangos, J. A., R. J. Riese, C. Peters, H. A. Chapman, and H. L. Ploegh. 1997. Degradation of mouse invariant chain: Roles of cathepsins S and D and the influence of major histocompatibility complex polymorphism. *J. Exp. Med.* 186: 549–560.

66. Riese, R. J., P. R. Wolf, D. Brömme, L. R. Natkin, J. A. Villadangos, H. L. Ploegh, and H. A. Chapman. 1996. Essential role for cathepsin S in MHC class II-associated invariant chain processing and peptide loading. *Immunity* 4: 357–366.

67. Denzin, L. K., and P. Cresswell. 1995. HLA-DM induces clip dissociation from MHC class II αβ dimers and facilitates peptide loading. *Cell* 82: 155–165.

68. Sloan, V. S., P. Cameron, G. Porter, M. Gammon, M. Amaya, and D. M. Zaller. 1995. Mediation by HLA-DM of dissociation of peptides from HLA-DR. *Nature* 375: 802–806.

69. Sherman, M. A., D. A. Weber, and P. E. Jensen. 1995. DM enhances peptide binding to class II MHC by release of invariant chain-derived peptide. *Immunity* 3: 197–205.

70. Morris, P., J. Shaman, M. Attaya, M. Amaya, S. Goodman, C. Bergman, J. J.

Monaco, and E. Mellins. 1994. An essential role for HLA-DM in antigen presentation by class II major histocompatibility molecules. *Nature* 368: 551–554.

71. Guce, A. I., S. E. Mortimer, T. Yoon, C. A. Painter, W. Jiang, E. D. Mellins, and L. J. Stern. 2013. HLA-DO acts as a substrate mimic to inhibit HLA-DM by a competitive mechanism. *Nat. Struct. Mol. Biol.* 20: 90–8.

72. Lancien, M., G. Bienvenu, S. Salle, L. Gueno, M. Feyeux, E. Merieau, S. Remy, A. Even, A. Moreau, A. Molle, C. Fourgeux, F. Coulon, G. Beriou, L. Bouchet-Delbos, E. Chiffoleau, P. Kirstetter, S. Chan, S. M. Kerfoot, S. Abdu Rahiman, V. De Simone, G. Matteoli, G. Boncompain, F. Perez, R. Josien, J. Poschmann, M. C. Cuturi, and C. Louvet. 2021. Dendritic Cells Require TMEM176A/B Ion Channels for Optimal MHC Class II Antigen Presentation to Naive CD4 + T Cells . *J. Immunol.* 207: 421–435.

73. Sercarz, E. E., and E. Maverakis. 2003. MHC-guided processing: Binding of large antigen fragments. *Nat. Rev. Immunol.* 3: 621–629.

74. Chow, A., D. Toomre, W. Garrett, and I. Mellman. 2002. Dendritic cell maturation triggers retrograde MHC class II transport from lysosomes to the plasma membrane. *Nature* 418: 988–994.

75. Anderson, H. A., and P. A. Roche. 2015. MHC Class II Association with Lipid Rafts on the Antigen Presenting Cell Surface. *Biochim. Biophys. Acta* 1853: 775–780.

76. Cella, M., A. Engering, V. Pinet, J. Pieters, and A. Lanzavecchia. 1997. Inflammatory stimuli induce accumulation of MHC class II complexes on dendritic cells. *Nature* 388: 782–7.

77. Pinet, V., M. Vergelli, R. Marting, O. Bakke, and E. O. Long. 1995. Antigen presentation mediated by recycling of surface HLA-DR molecules. *Nature* 375: 603–606.

78. Reid, P. A., and C. Watts. 1990. Cycling of cell-surface MHC glycoproteins through promaquine-sensitive intracellular compartments. *Nature* 346: 655–657.

79. Reid, P. A., and C. Watts. 1992. Constitutive endocytosis and recycling of major histocompatibility complex class II glycoproteins in human B-lymphoblastoid cells. *Immunology* 77: 539–42.

80. Machy, P., J. P. Bizozzero, H. Reggio, and L. Leserman. 1990. Endocytosis and recycling of MHC-encoded class II molecules by mouse B lymphocytes. *J. Immunol.* 145: 1350–1355.

81. Sinnathamby, G., and L. C. Eisenlohr. 2003. Presentation by Recycling MHC Class II Molecules of an Influenza Hemagglutinin-Derived Epitope That Is Revealed in the Early Endosome by Acidification. *J. Immunol.* 170: 3504–3513.

82. Kleijmeer, M., G. Ramm, D. Schuurhuis, J. Griffith, M. Rescigno, P. Ricciardi-Castagnoli, A. Y. Rudensky, F. Ossendorp, C. J. M. Melief, W. Stoorvogel, and H. J. Geuze. 2001. Reorganization of multivesicular bodies regulates MHC class II antigen presentation by dendritic cells. *J. Cell Biol.* 155: 53–63.

83. Wilson, N. S., D. El-Sukkari, and J. A. Villadangos. 2004. Dendritic cells constitutively present self antigens in their immature state in vivo and regulate antigen presentation by controlling the rates of MHC class II synthesis and endocytosis. *Immunobiology* 103: 2187–2195.

84. Rescigno, M., S. Citterio, C. Thery, M. Rittig, D. Medaglini, G. Pozzi, S. Amigorena, and P. Ricciardi-Castagnoli. 1998. Bacteria-induced neo-biosynthesis, stabilization, and surface expression of functional class I molecules in mouse dendritic cells. *Proc. Natl. Acad. Sci.* 95: 5229–5234.

85. Landmann, S., A. Mühlethaler-Mottet, L. Bernasconi, T. Suter, J. M. Waldburger,

K. Masternak, J. F. Arrighi, C. Hauser, A. Fontana, and W. Reith. 2001. Maturation of dendritic cells is accompanied by rapid transcriptional silencing of class II transactivator (CIITA) expression. *J. Exp. Med.* 194: 379–391.

86. West, M. A., A. R. Prescott, E. L. Eskelinen, A. J. Ridley, and C. Watts. 2000. Rac is required for constitutive macropinocytosis by dendritic cells but does not control its downregulation. *Curr. Biol.* 10: 839–848.

87. Garrett, W. S., L. M. Chen, R. Kroschewski, M. Ebersold, S. Turley, S. Trombetta, J. E. Galán, and I. Mellman. 2000. Developmental control of endocytosis in dendritic cells by Cdc42. *Cell* 102: 325–334.

88. Moser, M. 2003. Dendritic cells in immunity and tolerance - Do they display opposite functions? *Immunity* 19: 5–8.

89. Ohmura-Hoshino, M., Y. Matsuki, M. Aoki, E. Goto, M. Mito, M. Uematsu, T. Kakiuchi, H. Hotta, and S. Ishido. 2006. Inhibition of MHC class II expression and immune responses by c-MIR. *J. Immunol.* 177: 341–354.

90. Shin, J. S., M. Ebersold, M. Pypaert, L. Delamarre, A. Hartley, and I. Mellman. 2006. Surface expression of MHC class II in dendritic cells is controlled by regulated ubiquitination. *Nature* 444: 115–118.

91. van Niel, G., R. Wubbolts, T. ten Broeke, S. I. Buschow, F. A. Ossendorp, C. J. Melief, G. Raposo, B. W. van Balkom, and W. Stoorvogel. 2006. Dendritic Cells Regulate Exposure of MHC Class II at Their Plasma Membrane by Oligoubiquitination. *Immunity* 25: 885–894.

92. Matsuki, Y., M. Ohmura-Hoshino, E. Goto, M. Aoki, M. Mito-Yoshida, M. Uematsu, T. Hasegawa, H. Koseki, O. Ohara, M. Nakayama, K. Toyooka, K. Matsuoka, H. Hotta, A. Yamamoto, and S. Ishido. 2007. Novel regulation of MHC class II

function in B cells. *EMBO J.* 26: 846–854.

93. De Gassart, A., V. Camosseto, J. Thibodeau, M. Ceppi, N. Catalan, P. Pierre, and E. Gatti. 2008. MHC class II stabilization at the surface of human dendritic cells is the result of maturation-dependent MARCH I down-regulation. *Proc. Natl. Acad. Sci. U. S. A.* 105: 3491–3496.

94. Walseng, E., K. Furuta, B. Bosch, K. A. Weih, Y. Matsuki, O. Bakke, S. Ishido, and P. A. Roche. 2010. Ubiquitination regulates MHC class II-peptide complex retention and degradation in dendritic cells. *Proc. Natl. Acad. Sci. U. S. A.* 107: 20465–70.

95. Schriek, P., H. Liu, A. C. Ching, P. Huang, N. Gupta, K. R. Wilson, M. Tsai, Y. Yan, C. F. Macri, L. F. Dagley, G. Infusini, A. I. Webb, H. McWilliam, S. Ishido, J. D. Mintern, and J. A. Villadangos. 2021. Physiological Substrates and Ontogeny-Specific Expression of the Ubiquitin Ligases MARCH1 and MARCH8. *bioRxiv* 2021.04.15.439921.

96. Walseng, E., K. Furuta, R. S. Goldszmid, K. A. Weih, A. Sher, and P. A. Roche. 2010. Dendritic Cell Activation Prevents MHC Class II Ubiquitination and Promotes MHC Class II Survival Regardless of the Activation Stimulus. *J. Biol. Chem.* 285: 41749–41754.

97. Kaul, S., S. K. Mittal, and P. A. Roche. 2018. A major isoform of the E3 ubiquitin ligase March-I in antigen-presenting cells has regulatory sequences within its gene. *J. Biol. Chem.* 293: 4478–4485.

98. Bourgeois-Daigneault, M.-C., and J. Thibodeau. 2012. Autoregulation of MARCH1 Expression by Dimerization and Autoubiquitination. *J. Immunol.* 188: 4959–4970.

99. Young, L. J., N. S. Wilson, P. Schnorrer, A. Proietto, T. ten Broeke, Y. Matsuki, A. M. Mount, G. T. Belz, M. O'Keeffe, M. Ohmura-Hoshino, S. Ishido, W. Stoorvogel, W.

R. Heath, K. Shortman, and J. A. Villadangos. 2008. Differential MHC class II synthesis and ubiquitination confers distinct antigen-presenting properties on conventional and plasmacytoid dendritic cells. *Nat. Immunol.* 9: 1244–1252.

100. Cho, K.-J., E. Walseng, S. Ishido, and P. A. Roche. 2015. Ubiquitination by March-I prevents MHC class II recycling and promotes MHC class II turnover in antigen-presenting cells. *Proc. Natl. Acad. Sci. U. S. A.* 112: 10449–54.

101. Thibodeau, J., M. C. Bourgeois-Daigneault, G. Huppé, J. Tremblay, A. Aumont, M. Houde, E. Bartee, A. Brunet, M. E. Gauvreau, A. de Gassart, E. Gatti, M. Baril, M. Cloutier, S. Bontron, K. Früh, D. Lamarre, and V. Steimle. 2008. Interleukin-10-induced MARCH1 mediates intracellular sequestration of MHC class II in monocytes. *Eur. J. Immunol.* 38: 1225–1230.

102. Mittal, S. K., K. J. Cho, S. Ishido, and P. A. Roche. 2015. Interleukin 10 (IL-10)-mediated Immunosuppression March-i induction regulates antigen presentation by macrophages but not Dendritic cells. *J. Biol. Chem.* 290: 27158–27167.

103. Tze, L. E., K. Horikawa, H. Domaschenz, D. R. Howard, C. M. Roots, R. J. Rigby, D. A. Way, M. Ohmura-hoshino, S. Ishido, C. E. Andoniou, M. A. Degli-esposti, and C. C. Goodnow. 2011. CD83 increases MHC II and CD86 on dendritic cells by opposing IL-10 – driven MARCH1-mediated ubiquitination and degradation. *J. Exp. Med.* 208: 149–165.

104. Chattopadhyay, G., and E. M. Shevach. 2013. Antigen-Specific Induced T Regulatory Cells Impair Dendritic Cell Function via an IL-10/MARCH1–Dependent Mechanism. *J. Immunol.* 191: 5875–5884.

105. Galbas, T., V. Steimle, R. Lapointe, S. Ishido, and J. Thibodeau. 2012. MARCH1 down-regulation in IL-10-activated B cells increases MHC class II expression. *Cytokine*

59: 27–30.

106. Liu, H., R. Jain, J. Guan, V. Vuong, S. Ishido, N. L. La Gruta, D. H. Gray, J. A. Villadangos, and J. D. Mintern. 2016. Ubiquitin ligase MARCH 8 cooperates with CD83 to control surface MHC II expression in thymic epithelium and CD4 T cell selection. *J. Exp. Med.* 213: 1695–1703.

107. von Rohrscheidt, J., E. Petrozziello, J. Nedjic, C. Federle, L. Krzyzak, H. L. Ploegh, S. Ishido, A. Steinkasserer, and L. Klein. 2016. Thymic CD4 T cell selection requires attenuation of March8-mediated MHCII turnover in cortical epithelial cells through CD83. *J. Exp. Med.* 213: 1685–1694.

108. Liu, H., and A. P. R. Johnston. 2013. A programmable sensor to probe the internalization of proteins and nanoparticles in live cells. *Angew. Chemie - Int. Ed.* 52: 5744–5748.

109. Wilson, K. R., H. Liu, G. Healey, V. Vuong, S. Ishido, M. J. Herold, J. A. Villadangos, and J. D. Mintern. 2018. MARCH1-mediated ubiquitination of MHC II impacts the MHC I antigen presentation pathway. *PLoS One* 13: 1–16.

110. Liu, H., K. R. Wilson, P. Schriek, C. Macri, A. B. Blum, L. Francis, M. Heinlein, C. Nataraja, J. Harris, S. A. Jones, D. H. D. Gray, J. A. Villadangos, and J. D. Mintern. 2020. Ubiquitination of MHC Class II Is Required for Development of Regulatory but Not Conventional CD4 + T Cells. *J. Immunol.* 205: 1207–1216.

111. Oh, J., and J.-S. Shin. 2015. Molecular mechanism and cellular function of MHCII ubiquitination. *Immunol. Rev.* 266: 134–144.

112. McGehee, A. M., K. Strijbis, E. Guillen, T. Eng, O. Kirak, and H. L. Ploegh. 2011. Ubiquitin-dependent control of class II MHC localization is dispensable for antigen presentation and antibody production. *PLoS One* 6.

113. Oh, J., J. S. A. A. Perry, H. Pua, N. Irgens-Möller, S. Ishido, C.-S. S. Hsieh, and J.-S. S. Shin. 2018. MARCH1 protects the lipid raft and tetraspanin web from MHC II proteotoxicity in dendritic cells. *J. Cell Biol.* 217: 1395–1410.

114. Oh, J., N. Wu, G. Baravalle, B. Cohn, J. Ma, B. Lo, I. Mellman, S. Ishido, M. Anderson, and J.-S. Shin. 2013. MARCH1-mediated MHCII ubiquitination promotes dendritic cell selection of natural regulatory T cells. *J. Exp. Med.* 210: 1069–77.

115. Ohmura-Hoshino, M., Y. Matsuki, M. Mito-Yoshida, E. Goto, M. Aoki-Kawasumi, M. Nakayama, O. Ohara, and S. Ishido. 2009. Cutting edge: requirement of MARCH-I-mediated MHC II ubiquitination for the maintenance of conventional dendritic cells. *J. Immunol.* 183: 6893–7.

116. Ishikawa, R., M. Kajikawa, and S. Ishido. 2014. Loss of MHC II ubiquitination inhibits the activation and differentiation of CD4 T cells. *Int. Immunol.* 26: 283–9.

117. Kim, H. J., J. Bandola-Simon, S. Ishido, N. W. Wong, V. N. Koparde, M. Cam, and P. A. Roche. 2020. Ubiquitination of MHC Class II by March-I Regulates Dendritic Cell Fitness. *J. Immunol.* 206: ji2000975.

118. Szöllósi, J., V. Horejsí, L. Bene, P. Angelisová, and S. Damjanovich. 1996. Supramolecular complexes of MHC class I, MHC class II, CD20, and tetraspan molecules (CD53, CD81, and CD82) at the surface of a B cell line JY. *J. Immunol.* 157: 2939–2946.

119. Jenei, A., S. Varga, L. Bene, L. Mátyus, A. Bodnár, Z. Bacsó, C. Pieri, R. Gáspár, T. Farkas, and S. Damjanovich. 1997. HLA class I and II antigens are partially co-clustered in the plasma membrane of human lymphoblastoid cells. *Proc. Natl. Acad. Sci. U. S. A.* 94: 7269–74.

120. Vremec, D. 2010. The isolation of mouse dendritic cells from lymphoid tissues and

the identification of dendritic cell subtypes by mutliparameter flow cytometry. *Methods Mol. Biol.* 595: 205–209.

121. Steiner, Q. G., L. A. Otten, M. J. Hicks, G. Kaya, F. Grosjean, E. Saeuberli, C. Lavanchy, F. Beermann, K. L. McClain, and H. Acha-Orbea. 2008. In vivo transformation of mouse conventional CD8α+ dendritic cells leads to progressive multisystem histiocytosis. *Blood* 111: 2073–2082.

122. Doench, J. G., N. Fusi, M. Sullender, M. Hegde, E. W. Vaimberg, K. F. Donovan, I. Smith, Z. Tothova, C. Wilen, R. Orchard, H. W. Virgin, J. Listgarten, and D. E. Root. 2016. Optimized sgRNA design to maximize activity and minimize off-target effects of CRISPR-Cas9. *Nat. Biotechnol.* 34: 184–191.

123. Aubrey, B. J., G. L. Kelly, A. J. Kueh, M. S. Brennan, L. O'Connor, L. Milla, S. Wilcox, L. Tai, A. Strasser, and M. J. Herold. 2015. An Inducible Lentiviral Guide RNA Platform Enables the Identification of Tumor-Essential Genes and Tumor-Promoting Mutations InVivo. *Cell Rep.* 10: 1422–1432.

124. Hsiau, T., T. Maures, K. Waite, J. Yang, R. Kelso, K. Holden, and R. Stoner. 2018. Inference of CRISPR Edits from Sanger Trace Data. *bioRxiv* 1–14.

125. Selby, L. I., L. Aurelio, D. Yuen, B. Graham, and A. P. R. Johnston. 2018. Quantifying Cellular Internalization with a Fluorescent Click Sensor. *ACS Sensors* 3: 1182–1189.

126. Shalem, O., N. E. Sanjana, E. Hartenian, X. Shi, D. A. Scott, T. S. Mikkelsen, D. Heckl, B. L. Ebert, D. E. Root, J. G. Doench, and F. Zhang. 2014. Genome-Scale CRISPR-Cas9 Knockout Screening in Human Cells. *Science* 343: 84–88.

127. Sanjana, N. E., O. Shalem, and F. Zhang. 2014. Improved vectors and genome-wide libraries for CRISPR screening. *Nat. Methods* 11: 783–784.

128. Laird, C. D. 1971. Chromatid structure: relationship between DNA content and nucleotide sequence diversity. *Chromosoma* 32: 378–406.

129. Robinson, M. D., D. J. McCarthy, and G. K. Smyth. 2009. edgeR: A Bioconductor package for differential expression analysis of digital gene expression data. *Bioinformatics* 26: 139–140.

130. Liu, X. S., F. Zhang, R. A. Irizarry, T. Xiao, L. Cong, M. I. Love, W. Li, H. Xu, J. S. Liu, and M. Brown. 2014. MAGeCK enables robust identification of essential genes from genome-scale CRISPR/Cas9 knockout screens. *Genome Biol.* 15: 1–12.

131. Martin, M. 2013. Cutadapt removes adapter sequences from high-throughput sequencing reads. *EMBnet.journal* 7: 2803–2809.

132. Pulendran, B., J. Banchereau, S. Burkeholder, E. Kraus, E. Guinet, C. Chalouni, D. Caron, C. Maliszewski, J. Davoust, J. Fay, and K. Palucka. 2000. Flt3-Ligand and Granulocyte Colony-Stimulating Factor Mobilize Distinct Human Dendritic Cell Subsets In Vivo. *J. Immunol.* 165: 566–572.

133. Nakao, M., S. Yokota, T. Iwai, H. Kaneko, S. Horiike, K. Kashima, Y. Sonoda, T. Fujimoto, and S. Misawa. 1996. Internal tandem duplication of the flt3 gene found in acute myeloid leukemia. *Leukemia* 10: 1911–1918.

134. Schnittger, S., C. Schoch, and M. Dugas. 2002. Analysis of FLT3 length mutations in 1003 patients with acute myeloid leukemia: correlation to cytogenetics, FABsubtype, and prognosis in theAMLCGstudy and usefulness as a marker for the detection of minimal residual disease. *Blood* 100: 59–67.

135. Hayakawa, F., M. Towatari, H. Kiyoi, M. Tanimoto, T. Kitamura, H. Saito, and T. Naoe. 2000. Tandem-duplicated Flt3 constitutively activates STAT5 and MAP kinase and introduces autonomous cell growth in IL-3-dependent cell lines. *Oncogene* 19:

624–31.

136. Mizuki, M., R. Fenski, H. Halfter, I. Matsumura, R. Schmidt, C. Müller, W. Grüning, K. Kratz-Albers, S. Serve, C. Steur, T. Büchner, J. Kienast, Y. Kanakura, W. E. Berdel, and H. Serve. 2000. Flt3 mutations from patients with acute myeloid leukemia induce transformation of 32D cells mediated by the Ras and STAT5 pathways. *Blood* 96: 3907–14.

137. Kiyoi, H., R. Ohno, R. Ueda, H. Saito, and T. Naoe. 2002. Mechanism of constitutive activation of FLT3 with internal tandem duplication in the juxtamembrane domain. *Oncogene* 21: 2555–2563.

138. Choudhary, C., J. Schwäble, C. Brandts, L. Tickenbrock, B. Sargin, T. Kindler, T. Fischer, W. E. Berdel, C. Müller-Tidow, and H. Serve. 2005. AML-associated Flt3 kinase domain mutations show signal transduction differences compared with Flt3 ITD mutations. *Blood* 106: 265–273.

139. Mead, A. J., S. Kharazi, D. Atkinson, I. Macaulay, C. Pecquet, S. Loughran, M. Lutteropp, P. Woll, O. Chowdhury, S. Luc, N. Buza-Vidas, H. Ferry, S. A. Clark, N. Goardon, P. Vyas, S. N. Constantinescu, E. Sitnicka, C. Nerlov, and S. E. W. Jacobsen. 2013. FLT3-ITDs Instruct a Myeloid Differentiation and Transformation Bias in Lymphomyeloid Multipotent Progenitors. *Cell Rep.* 3: 1766–1776.

140. Schmidt-Arras, D., S. A. Bohmer, S. Koch, J. P. Müller, L. Blei, H. Cornils, R. Bauer, S. Korasikha, C. Thiede, and F. D. Böhmer. 2009. Anchoring of FLT3 in the endoplasmic reticulum alters signaling quality. *Blood* 113: 3568–3576.

141. Lee, B. H., Z. Tothova, R. L. Levine, K. Anderson, N. Buza-Vidas, D. E. Cullen, E. P. McDowell, J. Adelsperger, S. Fröhling, B. J. P. Huntly, M. Beran, S. E. Jacobsen, and D. G. Gilliland. 2007. FLT3 Mutations Confer Enhanced Proliferation and Survival

Properties to Multipotent Progenitors in a Murine Model of Chronic Myelomonocytic Leukemia. *Cancer Cell* 12: 367–380.

142. Bar-On, L., T. Birnberg, K. L. Lewis, B. T. Edelson, D. Bruder, K. Hildner, J. Buer, K. M. Murphy, B. Reizis, and S. Jung. 2010. CX3CR1+ CD8 + dendritic cells are a steady-state population related to plasmacytoid dendritic cells. *Proc. Natl. Acad. Sci.* 107: 14745–14750.

143. Caminschi, I., D. Vremec, F. Ahmet, M. H. Lahoud, J. A. Villadangos, K. M. Murphy, W. R. Heath, and K. Shortman. 2012. Antibody responses initiated by Clec9A-bearing dendritic cells in normal and Batf3-/-mice. *Mol. Immunol.* 50: 9–17.

144. Villani, A.-C., R. Satija, G. Reynolds, S. Sarkizova, K. Shekhar, J. Fletcher, M. Griesbeck, A. Butler, S. Zheng, S. Lazo, L. Jardine, D. Dixon, E. Stephenson, E. Nilsson, I. Grundberg, D. McDonald, A. Filby, W. Li, P. L. De Jager, O. Rozenblatt-Rosen, A. A. Lane, M. Haniffa, A. Regev, and N. Hacohen. 2017. Single-cell RNA-seq reveals new types of human blood dendritic cells, monocytes, and progenitors. *Science* 356.

145. See, P., C.-A. Dutertre, J. Chen, P. Günther, N. McGovern, S. E. Irac, M. Gunawan, M. Beyer, K. Händler, K. Duan, H. R. Bin Sumatoh, N. Ruffin, M. Jouve, E. Gea-Mallorquí, R. C. M. Hennekam, T. Lim, C. C. Yip, M. Wen, B. Malleret, I. Low, N. B. Shadan, C. F. S. Fen, A. Tay, J. Lum, F. Zolezzi, A. Larbi, M. Poidinger, J. K. Y. Chan, Q. Chen, L. Rénia, M. Haniffa, P. Benaroch, A. Schlitzer, J. L. Schultze, E. W. Newell, and F. Ginhoux. 2017. Mapping the human DC lineage through the integration of high-dimensional techniques. *Science* 356.

146. Barnden, M. J., J. Allison, W. R. Heath, and F. R. Carbone. 1998. Defective TCR expression in transgenic mice constructed using cDNA- based α- and β-chain genes

under the control of heterologous regulatory elements. *Immunol. Cell Biol.* 76: 34–40.

147. Hogquist, K. A., S. C. Jameson, W. R. Heath, J. L. Howard, M. J. Bevan, and F. R. Carbone. 1994. T cell receptor antagonist peptides induce positive selection. *Cell* 76: 17–27.

148. Köntgen, F., G. Süss, C. Stewart, M. Steinmetz, and H. Bluethmann. 1993. Targeted disruption of the MHC class II Aa gene in C57BL/6 mice. *Int. Immunol.* 5: 957–964.

149. Teshima, T., P. Reddy, K. P. Lowler, M. A. KuKuruga, C. Liu, K. R. Cooke, and J. L. M. Ferrara. 2002. Flt3 ligand therapy for recipients of allogeneic bone marrow transplants expands host CD8α+ dendritic cells and reduces experimental acute graft-versus-host disease. *Blood* 99: 1825–1832.

150. O'Keeffe, M., T. C. Brodnicki, B. Fancke, D. Vremec, G. Morahan, E. Maraskovsky, R. Steptoe, L. C. Harrison, and K. Shortman. 2005. Fms-like tyrosine kinase 3 ligand administration overcomes a genetically determined dendritic cell deficiency in NOD mice and protects against diabetes development. *Int. Immunol.* 17: 307–314.

151. Lyman, S. D., L. James, J. Zappone, P. R. Sleath, M. P. Beckmann, and T. Bird. 1993. Characterization of the protein encoded by the flt3 (flk2) receptor-like tyrosine kinase gene. *Oncogene* 8: 815–822.

152. Schmidt-Arras, D.-E., A. Bohmer, B. Markova, C. Choudhary, H. Serve, and F.-D. Bohmer. 2005. Tyrosine Phosphorylation Regulates Maturation of Receptor Tyrosine Kinases. *Mol. Cell. Biol.* 25: 3690–3703.

153. Hochrein, H., M. O'Keeffe, T. Luft, S. Vandenabeele, R. J. Grumont, E. Maraskovsky, and K. Shortman. 2000. Interleukin (IL)-4 is a major regulatory cytokine

governing bioactive IL-12 production by mouse and human dendritic cells. *J. Exp. Med.* 192: 823–33.

154. Schnorrer, P., G. M. N. N. Behrens, N. S. Wilson, J. L. Pooley, C. M. Smith, D. El-Sukkari, G. Davey, F. Kupresanin, M. Li, E. Maraskovsky, G. T. Belz, F. R. Carbone, K. Shortman, W. R. Heath, and J. A. Villadangos. 2006. The dominant role of CD8+ dendritic cells in cross-presentation is not dictated by antigen capture. *Proc. Natl. Acad. Sci. U. S. A.* 103: 10729–10734.

155. Theisen, D. J., J. T. Davidson, C. G. Briseño, M. Gargaro, E. J. Lauron, Q. Wang, P. Desai, V. Durai, P. Bagadia, J. R. Brickner, W. L. Beatty, H. W. Virgin, W. E. Gillanders, N. Mosammaparast, M. S. Diamond, L. D. Sibley, W. Yokoyama, R. D. Schreiber, T. L. Murphy, and K. M. Murphy. 2018. WDFY4 is required for cross-presentation in response to viral and tumor antigens. *Science* 362: 694–699.

156. Rickmann, M., J. Krauter, K. Stamer, M. Heuser, G. Salguero, E. Mischak-Weissinger, A. Ganser, and R. Stripecke. 2011. Elevated frequencies of leukemic myeloid and plasmacytoid dendritic cells in acute myeloid leukemia with the FLT3 internal tandem duplication. *Ann. Hematol.* 90: 1047–1058.

157. Rickmann, M., L. Macke, M. Heuser, J. Krauter, A. Ganser, and R. Stripecke. 2013. Monitoring dendritic cell and cytokine biomarkers during remission prior to relapse in patients with FLT3-ITD acute myeloid leukemia. *Ann. Hematol.* 92: 1079–1090.

158. Eidenschenk, C., K. Crozat, P. Krebs, R. Arens, D. Popkin, C. N. Arnold, A. L. Blasius, C. a Benedict, E. M. Y. Moresco, Y. Xia, and B. Beutler. 2010. Flt3 permits survival during infection by rendering dendritic cells competent to activate NK cells. *Proc. Natl. Acad. Sci. U. S. A.* 107: 9759–64.

159. Whartenby, K. A., P. A. Calabresi, E. McCadden, B. Nguyen, D. Kardian, T. Wang, C. Mosse, D. M. Pardoll, and D. Small. 2005. Inhibition of FLT3 signaling targets DCs to ameliorate autoimmune disease. *Proc. Natl. Acad. Sci.* 102: 16741–16746.

160. Heydt, Q., C. Larrue, E. Saland, S. Bertoli, J. E. Sarry, A. Besson, S. Manenti, C. Joffre, and V. Mansat-De Mas. 2018. Oncogenic FLT3-ITD supports autophagy via ATF4 in acute myeloid leukemia. *Oncogene* 37: 787–797.

161. Roche, P. A., and K. Furuta. 2015. The ins and outs of MHC class II-mediated antigen processing and presentation. *Nat. Rev. Immunol.* 15: 203–216.

162. Lahoud, M. H., F. Ahmet, J.-G. Zhang, S. Meuter, A. N. Policheni, S. Kitsoulis, C.-N. Lee, M. O'Keeffe, L. C. Sullivan, A. G. Brooks, R. Berry, J. Rossjohn, J. D. Mintern, J. Vega-Ramos, J. A. Villadangos, N. A. Nicola, M. C. Nussenzweig, K. J. Stacey, K. Shortman, W. R. Heath, and I. Caminschi. 2012. DEC-205 is a cell surface receptor for CpG oligonucleotides. *Proc. Natl. Acad. Sci.* 109: 16270–16275.

163. Carotta, S., A. Dakic, A. D'Amico, S. H. M. Pang, K. T. Greig, S. L. Nutt, and L. Wu. 2010. The transcription factor PU.1 controls dendritic cell development and Flt3 cytokine receptor expression in a dose-dependent manner. *Immunity* 32: 628–641.

164. Gwin, K., E. Frank, A. Bossou, and K. L. Medina. 2010. Hoxa9 Regulates Flt3 in Lymphohematopoietic Progenitors. *J. Immunol.* 185: 6572–6583.

165. Gwin, K. A., M. B. Shapiro, J. J. Dolence, Z. L. Huang, and K. L. Medina. 2013. Hoxa9 and Flt3 Signaling Synergistically Regulate an Early Checkpoint in Lymphopoiesis. *J. Immunol.* 191: 745–754.

166. Volpe, G., D. S. Walton, W. Del Pozzo, P. Garcia, E. Dassé, L. P. O'Neill, M. Griffiths, J. Frampton, and S. Dumon. 2013. C/EBPα and MYB regulate FLT3

expression in AML. *Leukemia* 27: 1487–1496.

167. Volpe, G., M. Clarke, P. Garcìa, D. S. Walton, A. Vegiopoulos, W. Del Pozzo, L. P. O'Neill, J. Frampton, and S. Dumon. 2015. Regulation of the flt3 gene in haematopoietic stem and early progenitor cells. *PLoS One* 10: 1–18.

168. Satpathy, A. T., C. G. Briseno, X. Cai, D. G. Michael, C. Chou, S. Hsiung, D. Bhattacharya, N. A. Speck, and T. Egawa. 2014. Runx1 and Cbf regulate the development of Flt3+ dendritic cell progenitors and restrict myeloproliferative disorder. *Blood* 123: 2968–2977.

169. Huang, G., P. Zhang, H. Hirai, S. Elf, X. Yan, Z. Chen, S. Koschmieder, Y. Okuno, T. Dayaram, J. D. Growney, R. A. Shivdasani, D. G. Gilliland, N. A. Speck, S. D. Nimer, and D. G. Tenen. 2008. PU.1 is a major downstream target of AML1 (RUNX1) in adult mouse hematopoiesis. *Nat. Genet.* 40: 51–60.

170. Kato, T., M. Sakata-Yanagimoto, H. Nishikii, M. Ueno, Y. Miyake, Y. Yokoyama, Y. Asabe, Y. Kamada, H. Muto, N. Obara, K. Suzukawa, Y. Hasegawa, I. Kitabayashi, K. Uchida, A. Hirao, H. Yagita, R. Kageyama, and S. Chiba. 2015. Hes1 suppresses acute myeloid leukemia development through FLT3 repression. *Leukemia* 29: 576–585.

171. De Obaldia, M. E., J. J. Bell, X. Wang, C. Harly, Y. Yashiro-Ohtani, J. H. Delong, D. A. Zlotoff, D. A. Sultana, W. S. Pear, and A. Bhandoola. 2013. T cell development requires constraint of the myeloid regulator C/EBP-α by the Notch target and transcriptional repressor Hes1. *Nat. Immunol.* 14: 1277–1284.

172. Holmes, M. L., S. Carotta, L. M. Corcoran, and S. L. Nutt. 2006. Repression of Flt3 by Pax5 is crucial for B-cell lineage commitment. *Genes Dev.* 20: 933–938.

173. Turner, A. M., N. L. Lin, S. Issarachai, S. D. Lyman, and V. C. Broudy. 1996. FLT3 Receptor Expression on the Surface of Normal and Malignant Human

Hematopoietic Cells. *Blood* 88: 3383–390.

174. Zhang, S., and H. E. Broxmeyer. 1999. p85 subunit of PI3 kinase does not bind to human Flt3 receptor, but associates with SHP2, SHIP, and a tyrosine-phosphorylated 100-kDa protein in Flt3 ligand-stimulated hematopoietic cells. *Biochem. Biophys. Res. Commun.* 254: 440–445.

175. Spiekermann, K., K. Bagrintseva, R. Schwab, and K. Schmieja. 2003. Overexpression and Constitutive Activation of FLT3 Induces STAT5 Activation in Primary Acute Myeloid Leukemia Blast Cells Overexpression and Constitutive Activation of FLT3 Induces STAT5 Activation in Primary Acute Myeloid Leukemia Blast Cells 1. *Clin. Cancer Res.* 9: 2140–2150.

176. Sargin, B., C. Choudhary, N. Crosetto, M. H. H. Schmidt, R. Grundler, M. Rensinghoff, C. Thiessen, L. Tickenbrock, J. Schwäble, C. Brandts, B. August, S. Koschmieder, S. R. Bandi, J. Duyster, W. E. Berdel, C. Müller-Tidow, I. Dikic, and H. Serve. 2007. Flt3-dependent transformation by inactivating c-Cbl mutations in AML. *Blood* 110: 1004–1012.

177. Oshikawa, G., T. Nagao, N. Wu, T. Kurosu, and O. Miura. 2011. c-Cbl and Cbl-b ligases mediate 17-allylaminodemethoxygeldanamycin-induced degradation of autophosphorylated Flt3 kinase with internal tandem duplication through the ubiquitin proteasome pathway. *J. Biol. Chem.* 286: 30263–30273.

178. Reindl, C., H. Quentmeier, K. Petropoulos, P. A. Greif, T. Benthaus, B. Argiropoulos, G. Mellert, S. Vempati, J. Duyster, C. Buske, S. K. Bohlander, K. R. Humphries, W. Hiddemann, and K. Spiekermann. 2009. CBL Exon 8/9 Mutants Activate the FLT3 Pathway and Cluster in Core Binding Factor/11q Deletion Acute Myeloid Leukemia/Myelodysplastic Syndrome Subtypes. *Clin. Cancer Res.* 15: 2238–

2247.

179. Lavagna-Sévenier, C., S. Marchetto, D. Birnbaum, and O. Rosnet. 1998. FLT3 signaling in hematopoietic cells involves CBL, SHC and an unknown P115 as prominent tyrosine-phosphorylated substrates. *Leukemia* 12: 301–310.

180. Lavagna-Sévenier, C., S. Marchetto, D. Birnbaum, and O. Rosnet. 1998. The CBL-related protein CBLB participates in FLT3 and interleukin-7 receptor signal transduction in pro-B cells. *J. Biol. Chem.* 273: 14962–14967.

181. Kazi, J. U., and L. Rönnstrand. 2012. Src-Like Adaptor Protein (SLAP) Binds to the Receptor Tyrosine Kinase Flt3 and Modulates Receptor Stability and Downstream Signaling. *PLoS One* 7.

182. Moharram, S. A., R. A. Chougule, X. Su, T. Li, J. Sun, H. Zhao, L. Rönnstrand, and J. U. Kazi. 2016. Src-like adaptor protein 2 (SLAP2) binds to and inhibits FLT3 signaling. *Oncotarget* 7: 57770–57782.

183. Lin, D. C., T. Yin, M. Koren-Michowitz, L. W. Ding, S. Gueller, S. Gery, T. Tabayashi, U. Bergholz, J. U. Kazi, L. Rönnstrand, C. Stocking, and H. P. Koeffler. 2012. Adaptor protein Lnk binds to and inhibits normal and leukemic FLT3. *Blood* 120: 3310–3317.

184. Rathinam, C., C. B. F. Thien, R. A. Flavell, and W. Y. Langdon. 2010. Myeloid leukemia development in c-Cbl RING finger mutant mice is dependent on FLT3 signaling. *Cancer Cell* 18: 341–352.

185. Taylor, S. J., S. A. Dagger, C. B. F. Thien, M. E. Wikstrom, and W. Y. Langdon. 2012. Flt3 inhibitor AC220 is a potent therapy in a mouse model of myeloproliferative disease driven by enhanced wild-type Flt3 signaling. *Blood* 120: 4049–4057.

186. Kazi, J. U., and L. Rönnstrand. 2013. Suppressor of cytokine signaling 2 (SOCS2)

associates with FLT3 and negatively regulates downstream signaling. *Mol. Oncol.* 7: 693–703.

187. Kazi, J. U., J. Sun, B. Phung, F. Zadjali, A. Flores-Morales, and L. Rönnstrand. 2012. Suppressor of cytokine signaling 6 (SOCS6) negatively regulates Flt3 signal transduction through direct binding to phosphorylated tyrosines 591 and 919 of Flt3. *J. Biol. Chem.* 287: 36509–36517.

188. Weisberg, E. L., N. J. Schauer, J. Yang, I. Lamberto, L. Doherty, S. Bhatt, A. Nonami, C. Meng, A. Letai, R. Wright, H. Tiv, P. C. Gokhale, M. S. Ritorto, V. De Cesare, M. Trost, A. Christodoulou, A. Christie, D. M. Weinstock, S. Adamia, R. Stone, D. Chauhan, K. C. Anderson, H. S. Seo, S. Dhe-Paganon, M. Sattler, N. S. Gray, J. D. Griffin, and S. J. Buhrlage. 2017. Inhibition of USP10 induces degradation of oncogenic FLT3. *Nat. Chem. Biol.* 13: 1207–1215.

189. Akiyama, H., Y. Umezawa, S. Ishida, K. Okada, A. Nogami, and O. Miura. 2019. Inhibition of USP9X induces apoptosis in FLT3-ITD-positive AML cells cooperatively by inhibiting the mutant kinase through aggresomal translocation and inducing oxidative stress. *Cancer Lett.* 453: 84–94.

190. Hunter, T. 1995. Protein Kinases and Phosphatases : The Yin and Yang of Protein Phosphorylation and Signaling. 80: 225–236.

191. Razumovskaya, E., K. Masson, R. Khan, S. Bengtsson, and L. Rönnstrand. 2009. Oncogenic Flt3 receptors display different specificity and kinetics of autophosphorylation. *Exp. Hematol.* 37: 979–989.

192. Heiss, E., K. Masson, C. Sundberg, M. Pedersen, J. Sun, S. Bengtsson, and L. Rönnstrand. 2006. Identification of Y589 and Y599 in the juxtamembrane domain of Flt3 as ligand-induced autophosphorylation sites involved in binding of Src family

kinases and the protein tyrosine phosphatase SHP2. *Blood* 108: 1542–1550.

193. Arora, D., S. Stopp, S. A. Böhmer, J. Schons, R. Godfrey, K. Masson, E. Razumovskaya, L. Rönnstrand, S. Tänzer, R. Bauer, F. D. Böhmer, and J. P. Mü Ller. 2011. Protein-tyrosine phosphatase DEP-1 controls receptor tyrosine kinase FLT3 signaling. *J. Biol. Chem.* 286: 10918–10929.

194. Müller, J. P., C. Schönherr, B. Markova, R. Bauer, C. Stocking, and F. D. Böhmer. 2008. Role of SHP2 for FLT3-dependent proliferation and transformation in 32D cells. *Leukemia* 22: 1945–1948.

195. Scheffler, J. M., F. Sparber, C. H. Tripp, C. Herrmann, A. Humenberger, J. Blitz, N. Romani, P. Stoitzner, and L. A. Huber. 2014. LAMTOR2 regulates dendritic cell homeostasis through FLT3-dependent mTOR signalling. *Nat. Commun.* 5: 5138.

196. Fuertes Marraco, S. A., F. Grosjean, A. Duval, M. Rosa, C. Lavanchy, D. Ashok, S. Haller, L. A. Otten, Q. G. Steiner, P. Descombes, C. A. Luber, F. Meissner, M. Mann, L. Szeles, W. Reith, and H. Acha-Orbea. 2012. Novel murine dendritic cell lines: A powerful auxiliary tool for dendritic cell research. *Front. Immunol.* 3.

197. Joung, J., S. Konermann, J. S. Gootenberg, O. O. Abudayyeh, R. J. Platt, M. D. Brigham, N. E. Sanjana, and F. Zhang. 2017. Genome-scale CRISPR-Cas9 knockout and transcriptional activation screening. *Nat. Protoc.* 12: 828–863.

198. Cortez, J. T., E. Montauti, E. Shifrut, J. Gatchalian, Y. Zhang, O. Shaked, Y. Xu, T. L. Roth, D. R. Simeonov, Y. Zhang, S. Chen, Z. Li, J. M. Woo, J. Ho, I. A. Vogel, G. Y. Prator, B. Zhang, Y. Lee, Z. Sun, I. Ifergan, F. Van Gool, D. C. Hargreaves, J. A. Bluestone, A. Marson, and D. Fang. 2020. CRISPR screen in regulatory T cells reveals modulators of Foxp3. *Nature* .

199. Li, C., T. Irrazabal, C. C. So, M. Berru, L. Du, E. Lam, A. K. Ling, J. L.

Gommerman, Q. Pan-Hammarström, and A. Martin. 2018. The H2B deubiquitinase Usp22 promotes antibody class switch recombination by facilitating non-homologous end joining. *Nat. Commun.* 9.

200. Parnas, O., M. Jovanovic, T. M. Eisenhaure, R. H. Herbst, A. Dixit, C. J. Ye, D. Przybylski, R. J. Platt, I. Tirosh, N. E. Sanjana, O. Shalem, R. Satija, R. Raychowdhury, P. Mertins, S. A. Carr, F. Zhang, N. Hacohen, and A. Regev. 2015. A Genome-wide CRISPR Screen in Primary Immune Cells to Dissect Regulatory Networks. *Cell* 162: 675–686.

201. Ozeki, K., H. Kiyoi, Y. Hirose, M. Iwai, M. Ninomiya, Y. Kodera, S. Miyawaki, K. Kuriyama, C. Shimazaki, H. Akiyama, M. Nishimura, T. Motoji, K. Shinagawa, A. Takeshita, R. Ueda, R. Ohno, N. Emi, and T. Naoe. 2004. Biologic and clinical significance of the FLT3 transcript level in acute myeloid leukemia. *Blood* 103: 1901–1908.

202. Stirewalt, D. L., and J. P. Radich. 2003. The role of FLT3 in haematopoietic malignancies. *Nat. Rev. Cancer* 3: 650.

203. Tahirov, T. H., T. Inoue-Bungo, H. Morii, A. Fujikawa, M. Sasaki, K. Kimura, M. Shiina, K. Sato, T. Kumasaka, M. Yamamoto, S. Ishhi, and K. Ogata. 2001. Structural Analyses of DNA Recognition by the AML1/Runx-1 Runt Domain and Its Allosteric Control by CBFβ. *Cell* 105: 291.

204. Bartfeld, D., L. Shimon, G. C. Couture, F. Frolow, D. Levanon, Y. Groner, and Z. Shakked. 2002. DNA recognition by the RUNX1 transcription factor is mediated by an allosteric transition in the RUNT domain and by DNA bending. *Structure* 10: 1395–1407.

205. Fagan, R. J., and A. K. Dingwall. 2019. COMPASS Ascending: Emerging clues

regarding the roles of MLL3/KMT2C and MLL2/KMT2D proteins in cancer. *Cancer Lett.* 458: 56–65.

206. Hu, D., X. Gao, M. A. Morgan, H.-M. Herz, E. R. Smith, and A. Shilatifard. 2013. The MLL3/MLL4 Branches of the COMPASS Family Function as Major Histone H3K4 Monomethylases at Enhancers. *Mol. Cell. Biol.* 33: 4745–4754.

207. Ogryzko, V. V., R. L. Schiltz, V. Russanova, B. H. Howard, and Y. Nakatani. 1996. The transcriptional coactivators p300 and CBP are histone acetyltransferases. *Cell* 87: 953–959.

208. Bannister, A. J., and T. Kouzarides. 1996. The CBP co-activator is a histone acetyltransferase. *Nature* 384: 641–643.

209. Muñoz, I. M., and J. Rouse. 2009. Control of histone methylation and genome stability by PTIP. *EMBO Rep.* 10: 239–245.

210. Cho, Y., T. Hong, S. Hong, H. Guo, H. Yu, D. Kim, T. Guszczynski, G. R. Dressler, T. D. Copeland, M. Kalkum, and K. Ge. 2007. PTIP Associates with MLL3- and MLL4-containing Histone H3 Lysine 4 Methyltransferase Complex. *J. Biol. Chem.* 282: 20395–20406.

211. Weinert, B. T., T. Narita, S. Satpathy, B. Srinivasan, B. K. Hansen, C. Schölz, W. B. Hamilton, B. E. Zucconi, W. W. Wang, W. R. Liu, J. M. Brickman, E. A. Kesicki, A. Lai, K. D. Bromberg, P. A. Cole, and C. Choudhary. 2018. Time-Resolved Analysis Reveals Rapid Dynamics and Broad Scope of the CBP/p300 Acetylome. *Cell* 174: 231-244.e12.

212. Wenzel, D. M., A. Lissounov, P. S. Brzovic, and R. E. Klevit. 2011. UBCH7 reactivity profile reveals parkin and HHARI to be RING/HECT hybrids. *Nature* 474: 105–108.

213. Kelsall, I. R., D. M. Duda, J. L. Olszewski, K. Hofmann, A. Knebel, F. Langevin, N. Wood, M. Wightman, B. A. Schulman, and A. F. Alpi. 2013. TRIAD1 and HHARI bind to and are activated by distinct neddylated Cullin-RING ligase complexes. *EMBO J.* 32: 2848–2860.

214. Scott, D. C., D. Y. Rhee, D. M. Duda, I. R. Kelsall, J. L. Olszewski, J. A. Paulo, A. de Jong, H. Ovaa, A. F. Alpi, J. W. Harper, and B. A. Schulman. 2016. Two Distinct Types of E3 Ligases Work in Unison to Regulate Substrate Ubiquitylation. *Cell* 166: 1198–1214.

215. Chen, F., C. Zhang, H. Wu, Y. Ma, X. Luo, X. Gong, F. Jiang, Y. Gui, H. Zhang, and F. Lu. 2017. The E3 ubiquitin ligase SCFFBXL14 complex stimulates neuronal differentiation by targeting the Notch signaling factor HES1 for proteolysis. *J. Biol. Chem.* 292: 20100–20112.

216. Glinsky, G. V., O. Berezovska, and A. B. Glinskii. 2005. Microarray analysis identifies a death-from-cancer signature predicting therapy failure in patients with multiple types of cancer. *J. Clin. Invest.* 115: 1503–1521.

217. Yang, X., H. Zang, Y. Luo, J. Wu, Z. Fang, W. Zhu, and Y. Li. 2018. High expression of USP22 predicts poor prognosis and advanced clinicopathological features in solid tumors: A meta-analysis. *Onco. Targets. Ther.* 11: 3035–3046.

218. Henry, K. W., A. Wyce, W. S. Lo, L. J. Duggan, N. C. T. Emre, C. F. Kao, L. Pillus, A. Shilatifard, M. A. Osley, and S. L. Berger. 2003. Transcriptional activation via sequential histone H2B ubiquitylation and deubiquitylation, mediated by SAGA-associated Ubp8. *Genes Dev.* 17: 2648–2663.

219. Daniel, J. A., M. S. Torok, Z. W. Sun, D. Schieltz, C. D. Allis, J. R. Yates, and P. A. Grant. 2004. Deubiquitination of Histone H2B by a Yeast Acetyltransferase

Complex Regulates Transcription. *J. Biol. Chem.* 279: 1867–1871.

220. Zhang, X., M. Varthi, S. M. Sykes, C. Phillips, C. Warzecha, W. Zhu, A. Wyce, A. W. Thorne, S. L. Berger, and S. B. McMahon. 2008. The Putative Cancer Stem Cell Marker USP22 Is a Subunit of the Human SAGA Complex Required for Activated Transcription and Cell-Cycle Progression. *Mol. Cell* 29: 102–111.

221. Zhao, Y., G. Lang, S. Ito, J. Bonnet, E. Metzger, S. Sawatsubashi, E. Suzuki, X. Le Guezennec, H. G. Stunnenberg, A. Krasnov, S. G. Georgieva, R. Schüle, K. I. Takeyama, S. Kato, L. Tora, and D. Devys. 2008. A TFTC/STAGA Module Mediates Histone H2A and H2B Deubiquitination, Coactivates Nuclear Receptors, and Counteracts Heterochromatin Silencing. *Mol. Cell* 29: 92–101.

222. Koutelou, E., C. L. Hirsch, and S. Y. R. Dent. 2010. Multiple faces of the SAGA complex. *Curr. Opin. Cell Biol.* 22: 374–382.

223. Lee, K. K., L. Florens, S. K. Swanson, M. P. Washburn, and J. L. Workman. 2005. The Deubiquitylation Activity of Ubp8 Is Dependent upon Sgf11 and Its Association with the SAGA Complex. *Mol. Cell. Biol.* 25: 1173–1182.

224. Ingvarsdottir, K., N. J. Krogan, N. C. T. Emre, A. Wyce, N. J. Thompson, A. Emili, T. R. Hughes, J. F. Greenblatt, and S. L. Berger. 2005. H2B Ubiquitin Protease Ubp8 and Sgf11 Constitute a Discrete Functional Module within the Saccharomyces cerevisiae SAGA Complex . *Mol. Cell. Biol.* 25: 1162–1172.

225. Köhler, A., P. Pascual-García, A. Llopis, M. Zapater, F. Posas, E. Hurt, and S. Rodríguez-Navarro. 2006. The mRNA Export Factor Sus1 Is Involved in Spt/Ada/Gcn5 Acetyltransferase-mediated H2B Deubiquitinylation through Its Interaction with Ubp8 and Sgf11. *Mol. Biol. Cell* 17: 4228–4236.

226. Zhang, X., H. Pfeiffer, A. Thorne, and S. B. McMahon. 2008. USP22, an hSAGA

subunit and potential cancer stem cell marker, reverses the polycomb-catalyzed ubiquitylation of histone H2A. *Cell Cycle* 7: 1522–1524.

227. Dietlein, N., X. Wang, E. R. Correa, B. Erbil, D. B. Lipka, Y. Begus-nahrmann, R. L. Kosinsky, S. A. Johnsen, and H. Thomas. 2021. Loss of Usp22 enhances histone H2B monoubiquitination and stimulates intracellular and systemic interferon immunity Nikolaus. *bioRxiv* .

228. Melo-Cardenas, J., Y. Xu, J. Wei, C. Tan, S. Kong, B. Gao, E. Montauti, G. Kirsammer, J. D. Licht, J. Yu, P. Ji, J. D. Crispino, and D. Fang. 2018. USP22 deficiency leads to myeloid leukemia upon oncogenic Kras activation through a PU.1-dependent mechanism. *Blood* 132: 423–434.

229. Huang, X., Q. Zhang, Y. Lou, J. Wang, X. Zhao, L. Wang, X. Zhang, S. Li, Y. Zhao, Q. Chen, T. Liang, and X. Bai. 2019. USP22 deubiquitinates CD274 to suppress anticancer immunity. *Cancer Immunol. Res.* 7: 1580–1590.

230. Wang, Y., Q. Sun, N. Mu, X. Sun, Y. Wang, S. Fan, L. Su, and X. Liu. 2020. The deubiquitinase USP22 regulates PD-L1 degradation in human cancer cells. *Cell Commun. Signal.* 18: 1–13.

231. Lin, Z., H. Yang, Q. Kong, J. Li, S. M. Lee, B. Gao, H. Dong, J. Wei, J. Song, D. D. Zhang, and D. Fang. 2012. USP22 Antagonizes p53 Transcriptional Activation by Deubiquitinating Sirt1 to Suppress Cell Apoptosis and Is Required for Mouse Embryonic Development. *Mol. Cell* 46: 484–494.

232. Kitabayashi, I., A. Yokoyama, K. Shimizu, and M. Ohki. 1998. Interaction and functional cooperation of the leukemia-associated factors AML1 and p300 in myeloid cell differentiation. *EMBO J.* 17: 2994–3004.

233. Pencovich, N., R. Jaschek, J. Dicken, A. Amit, J. Lotem, A. Tanay, and Y. Groner.

2013. Cell-Autonomous Function of Runx1 Transcriptionally Regulates Mouse Megakaryocytic Maturation. *PLoS One* 8: 1–11.

234. Yamaguchi, Y., M. Kurokawa, Y. Imai, K. Izutsu, T. Asai, M. Ichikawa, G. Yamamoto, E. Nitta, T. Yamagata, K. Sasaki, K. Mitani, S. Ogawa, S. Chiba, and H. Hirai. 2004. AML1 Is Functionally Regulated through p300-mediated Acetylation on Specific Lysine Residues. *J. Biol. Chem.* 279: 15630–15638.

235. Rani, A., R. Greenlaw, R. A. Smith, and C. Galustian. 2016. HES1 in immunity and cancer. *Cytokine Growth Factor Rev.* 30: 113–117.

236. Wendorff, A. A., U. Koch, F. T. Wunderlich, S. Wirth, C. Dubey, J. C. Brüning, H. R. MacDonald, and F. Radtke. 2010. Hes1 is a critical but context-dependent mediator of canonical notch signaling in lymphocyte development and transformation. *Immunity* 33: 671–684.

237. Tomita, K., M. Hattori, E. Nakamura, S. Nakanishi, N. Minato, and R. Kageyama. 1999. The bHLH gene Hes1 is essential for expansion of early T cell precursors. *Genes Dev.* 13: 1203–1210.

238. Welner, R. S., D. Bararia, G. Amabile, A. Czibere, T. Benoukraf, C. Bach, K. D. S. A. Wansa, M. Ye, H. Zhang, T. Iino, C. J. Hetherington, K. Akashi, and D. G. Tenen. 2013. C/EBPA is required for development of dendritic cell progenitors. *Blood* 121: 4073–4081.

239. Klinakis, A., C. Lobry, O. Abdel-Wahab, P. Oh, H. Haeno, S. Buonamici, I. van De Walle, S. Cathelin, T. Trimarchi, E. Araldi, C. Liu, S. Ibrahim, M. Beran, J. Zavadil, A. Efstratiadis, T. Taghon, F. Michor, R. L. Levine, and I. Aifantis. 2011. A novel tumour-suppressor function for the Notch pathway in myeloid leukaemia. *Nature* 473: 230–233.

240. Lee, T. I., and R. A. Young. 2013. Transcriptional regulation and its misregulation in disease. *Cell* 152: 1237–1251.

241. Cadigan, K. M., and M. L. Waterman. 2012. TCF/LEFs and Wnt Signaling in the Nucleus. *Cold Spring Harb. Perspect. Biol.* 4: a007906–a007906.

242. Mosimann, C., G. Hausmann, and K. Basler. 2009. β-Catenin hits chromatin: Regulation of Wnt target gene activation. *Nat. Rev. Mol. Cell Biol.* 10: 276–286.

243. Zhou, D. X., D. Zhou, S. Q. Zhan, P. Wang, K. Qin, W. Gan, and X. F. Lin. 2017. Inhibition of JMJD6 expression reduces the proliferation, migration and invasion of neuroglioma stem cells. *Neoplasma* 64: 700–708.

244. Grant, S. F. A. 2019. The TCF7L2 locus: A genetic window into the pathogenesis of type 1 and type 2 diabetes. *Diabetes Care* 42: 1624–1629.

245. Heng, T. S. P., M. W. Painter, T. Immunological, and G. Project. 2008. The Immunological Genome Project: networks of gene expression in immune cells. *Nat. Immunol.* 9: 1091–1094.

246. Heidkamp, G. F., J. Sander, C. H. K. Lehmann, L. Heger, N. Eissing, A. Baranska, J. J. Lühr, A. Hoffmann, K. C. Reimer, A. Lux, S. Söder, A. Hartmann, J. Zenk, T. Ulas, N. McGovern, C. Alexiou, B. Spriewald, A. Mackensen, G. Schuler, B. Schauf, A. Forster, R. Repp, P. A. Fasching, A. Purbojo, R. Cesnjevar, E. Ullrich, F. Ginhoux, A. Schlitzer, F. Nimmerjahn, J. L. Schultze, and D. Dudziak. 2016. Human lymphoid organ dendritic cell identity is predominantly dictated by ontogeny, not tissue microenvironment. *Sci. Immunol.* 1: 40–50.

247. Bokoch, G. M. 2005. Regulation of innate immunity by Rho GTPases. *Trends Cell Biol.* 15: 163–171.

248. Damoulakis, G., L. Gambardella, K. L. Rossman, C. D. Lawson, K. E. Anderson,

Y. Fukui, H. C. Welch, C. J. Der, L. R. Stephens, and P. T. Hawkins. 2014. P-Rex1 directly activates RhoG to regulate GPCR-driven Rac signalling and actin polarity in neutrophils. *J. Cell Sci.* 127: 2589–2600.

249. Kalinichenko, A., G. Perinetti Casoni, L. Dupré, L. Trotta, J. Huemer, D. Galgano, Y. German, B. Haladik, J. Pazmandi, M. Thian, Ö. Yüce Petronczki, S. C. Chiang, M. Taskinen, A. Hekkala, S. Kauppila, O. Lindgren, T. Tapiainen, M. J. Kraakman, K. Vettenranta, A. J. Lomakin, J. Saarela, M. R. J. Seppänen, Y. T. Bryceson, and K. Boztug. 2021. RhoG deficiency abrogates cytotoxicity of human lymphocytes and causes hemophagocytic lymphohistiocytosis. *Blood* 137: 2033–2045.

250. Martínez-Riaño, A., E. R. Bovolenta, P. Mendoza, C. L. Oeste, M. J. Martín-Bermejo, P. Bovolenta, M. Turner, N. Martínez-Martín, and B. Alarcón. 2018. Antigen phagocytosis by B cells is required for a potent humoral response. *EMBO Rep.* 19: 1–15.

251. Tzircotis, G., V. M. M. Braga, and E. Caron. 2011. Rhog is required for both fccr- and cr3-mediated phagocytosis. *J. Cell Sci.* 124: 2897–2902.

252. deBakker, C. D., L. B. Haney, J. M. Kinchen, C. Grimsley, M. Lu, D. Klingele, P.-K. Hsu, B.-K. Chou, L.-C. Cheng, A. Blangy, J. Sondek, M. O. Hengartner, Y.-C. Wu, and K. S. Ravichandran. 2004. Phagocytosis of Apoptotic Cells Is Regulated by a UNC-73/TRIO-MIG-2/RhoG Signaling Module and Armadillo Repeats of CED-12/ELMO. *Curr. Biol.* 14: 2208–2216.

253. Ellerbroek, S. M., K. Wennerberg, W. T. Arthur, J. M. Dunty, D. R. Bowman, K. A. DeMali, C. Der, and K. Burridge. 2004. SGEF, a RhoG Guanine Nucleotide Exchange Factor that Stimulates Macropinocytosis. *Mol. Biol. Cell* 15: 3309–3319.

254. Martínez-Martín, N., E. Fernández-Arenas, S. Cemerski, P. Delgado, M. Turner, J.

Heuser, D. J. Irvine, B. Huang, X. R. Bustelo, A. Shaw, and B. Alarcón. 2011. T Cell Receptor Internalization from the Immunological Synapse Is Mediated by TC21 and RhoG GTPase-Dependent Phagocytosis. *Immunity* 35: 208–222.

255. Soutourina, J. 2018. Transcription regulation by the Mediator complex. *Nat. Rev. Mol. Cell Biol.* 19: 262–274.

256. Abdella, R., A. Talyzina, S. Chen, C. J. Inouye, R. Tjian, and Y. He. 2021. Structure of the human Mediator-bound transcription preinitiation complex. *Science* 372: 52–56.

257. Allen, B. L., and D. J. Taatjes. 2015. The Mediator complex: A central integrator of transcription. *Nat. Rev. Mol. Cell Biol.* 16: 155–166.

258. Currie, S. L., J. J. Doane, K. S. Evans, N. Bhachech, B. J. Madison, D. K. W. Lau, L. P. McIntosh, J. J. Skalicky, K. A. Clark, and B. J. Graves. 2017. ETV4 and AP1 Transcription Factors Form Multivalent Interactions with three Sites on the MED25 Activator-Interacting Domain. *J. Mol. Biol.* 429: 2975–2995.

259. Nakamura, Y., K. Yamamoto, X. He, B. Otsuki, Y. Kim, H. Murao, T. Soeda, N. Tsumaki, J. M. Deng, Z. Zhang, R. R. Behringer, B. de Crombrugghe, J. H. Postlethwait, M. L. Warman, T. Nakamura, and H. Akiyama. 2011. Wwp2 is essential for palatogenesis mediated by the interaction between Sox9 and mediator subunit 25. *Nat. Commun.* 2: 251.

260. Han, E. H., G. B. Rha, and Y.-I. Chi. 2012. MED25 Is a Mediator Component of HNF4α-Driven Transcription Leading to Insulin Secretion in Pancreatic Beta-Cells. *PLoS One* 7: e44007.

261. Shi, Z., W. Yang, J. A. Goldstein, and S.-Y. Y. Zhang. 2014. Med25 is required for estrogen receptor alpha (ERα)-mediated regulation of human CYP2C9 expression.

*Biochem. Pharmacol.* 90: 425–431.

262. Lee, H. K., U. H. Park, E. J. Kim, and S. J. Um. 2007. MED25 is distinct from TRAP220/MED1 in cooperating with CBP for retinoid receptor activation. *EMBO J.* 26: 3545–3557.

263. Liang, E., Y. Lu, Y. Shi, Q. Zhou, and F. Zhi. 2020. MYEOV increases HES1 expression and promotes pancreatic cancer progression by enhancing SOX9 transactivity. *Oncogene* 39: 6437–6450.

264. Tian, L., S. Tomei, J. Schreuder, T. S. Weber, D. Amann-Zalcenstein, D. S. Lin, J. Tran, C. Audiger, M. Chu, A. Jarratt, T. Willson, A. Hilton, E. S. Pang, T. Patton, M. Kelly, S. Su, Q. Gouil, P. Diakumis, M. Bahlo, T. Sargeant, L. M. Kats, P. D. Hodgkin, M. O'Keeffe, A. P. Ng, M. E. Ritchie, and S. H. Naik. 2021. Clonal multi-omics reveals Bcor as a negative regulator of emergency dendritic cell development. *Immunity* 1–14.

265. Garlick, J. M., S. M. Sturlis, P. A. Bruno, J. A. Yates, A. L. Peiffer, Y. Liu, L. Goo, L. Bao, S. N. De Salle, G. Tamayo-Castillo, C. L. Brooks Iii, S. D. Merajver, and A. K. Mapp. 2021. Norstictic acid is a selective allosteric transcriptional regulator. *bioRxiv* 2021.03.26.437253.

266. Lahoud, M. H., F. Ahmet, S. Kitsoulis, S. S. Wan, D. Vremec, C.-N. C.-N. C.-N. Lee, B. Phipson, W. Shi, G. K. Smyth, A. M. Lew, Y. Y. Y. Y. Kato, S. N. Mueller, G. M. Davey, W. R. Heath, K. Shortman, and I. Caminschi. 2011. Targeting Antigen to Mouse Dendritic Cells via Clec9A Induces Potent CD4 T Cell Responses Biased toward a Follicular Helper Phenotype. *J. Immunol.* 187: 842–850.

267. Mach, N., S. Gillessen, S. B. Wilson, C. Sheehan, M. Mihm, and G. Dranoff. 2000. Differences in dendritic cells stimulated in vivo by tumors engineered to secrete granulocyte-macrophage colony-stimulating factor or Flt3-ligand. *Cancer Res.* 60:

3239–3246.

268. Verdoes, M., K. Oresic Bender, E. Segal, W. A. van der Linden, S. Syed, N. P. Withana, L. E. Sanman, and M. Bogyo. 2013. Improved Quenched Fluorescent Probe for Imaging of Cysteine Cathepsin Activity. *J. Am. Chem. Soc.* 135: 14726–14730.

269. Edgington-Mitchell, L. E., M. Bogyo, and M. Verdoes. 2017. Live Cell Imaging and Profiling of Cysteine Cathepsin Activity Using a Quenched Activity-Based Probe. In *Activity-Based Proteomics: Methods and Protocols* H. S. Overkleeft, and B. I. Florea, eds. Springer New York, New York, NY. 145–159.

270. El-Sukkari, D., N. S. Wilson, K. Hakansson, R. J. Steptoe, A. Grubb, K. Shortman, and J. A. Villadangos. 2003. The Protease Inhibitor Cystatin C Is Differentially Expressed among Dendritic Cell Populations, but Does Not Control Antigen Presentation. *J. Immunol.* 171: 5003–5011.

271. Cosgrove, D., D. Gray, A. Dierich, J. Kaufman, M. Lemeur, C. Benoist, and D. Mathis. 1991. Mice lacking MHC class II molecules. *Cell* 66: 1051–1066.

272. Caminschi, I., A. I. Proietto, F. Ahmet, S. Kitsoulis, J. S. Teh, J. C. Y. Lo, A. Rizzitelli, L. Wu, D. Vremec, S. L. H. Van Dommelen, I. K. Campbell, E. Maraskovsky, H. Braley, G. M. Davey, P. Mottram, N. Van De Velde, K. Jensen, A. M. Lew, M. D. Wright, W. R. Heath, K. Shortman, and M. H. Lahoud. 2008. The dendritic cell subtype-restricted C-type lectin Clec9A is a target for vaccine enhancement. *Blood* 112: 3264–3273.

273. Hildner, K., B. T. Edelson, W. E. Purtha, M. Diamond, H. Matsushita, M. Kohyama, B. Calderon, B. U. Schraml, E. R. Unanue, M. S. Diamond, R. D. Schreiber, T. L. Murphy, and K. M. Murphy. 2008. Batf3 Deficiency Reveals a Critical Role for CD8 + Dendritic Cells in Cytotoxic T Cell Immunity. *Science* 322: 1097–1100.

274. Carbone, F. R., and M. J. Bevan. 1990. Class I-restricted processing and presentation of exogenous cell-associated antigen in vivo. *J. Exp. Med.* 171: 377–387.

275. Sharpe, A. H., and K. E. Pauken. 2018. The diverse functions of the PD1 inhibitory pathway. *Nat. Rev. Immunol.* 18: 153–167.

276. Kato, Y., A. Zaid, G. M. Davey, S. N. Mueller, S. L. Nutt, D. Zotos, D. M. Tarlinton, K. Shortman, M. H. Lahoud, W. R. Heath, and I. Caminschi. 2015. Targeting Antigen to Clec9A Primes Follicular Th Cell Memory Responses Capable of Robust Recall. *J. Immunol.* 195: 1006–1014.

277. Hiltbold, E. M., N. J. Poloso, and P. A. Roche. 2003. MHC Class II-Peptide Complexes and APC Lipid Rafts Accumulate at the Immunological Synapse. *J. Immunol.* 170: 1329–1338.

278. Anderson, H. A., E. M. Hiltbold, and P. A. Roche. 2000. Concentration of MHC class II molecules in lipid rafts facilitates antigen presentation. *Nat. Immunol.* 1: 156–162.

279. Tubo, N. J., A. J. Pagán, J. J. Taylor, R. W. Nelson, J. L. Linehan, J. M. Ertelt, E. S. Huseby, S. S. Way, and M. K. Jenkins. 2013. Single Naive CD4+ T Cells from a Diverse Repertoire Produce Different Effector Cell Types during Infection. *Cell* 153: 785–796.

280. Benson, R. A., M. K. L. Macleod, B. G. Hale, A. Patakas, P. Garside, and J. M. Brewer. 2015. Antigen presentation kinetics control T cell/dendritic cell interactions and follicular helper T cell generation in vivo. *Elife* 4: 1–16.

281. Bannard, O., S. J. McGowan, J. Ersching, S. Ishido, G. D. Victora, J. S. Shin, and J. G. Cyster. 2016. Ubiquitin-mediated fluctuations in MHC class II facilitate efficient germinal center B cell responses. *J. Exp. Med.* 213: 993–1009.

282. Böttcher, J. P., E. Bonavita, P. Chakravarty, H. Blees, M. Cabeza-Cabrerizo, S. Sammicheli, N. C. Rogers, E. Sahai, S. Zelenay, and C. Reis e Sousa. 2018. NK Cells Stimulate Recruitment of cDC1 into the Tumor Microenvironment Promoting Cancer Immune Control. *Cell* 172: 1022-1037.e14.

283. Binnewies, M., A. M. Mujal, J. L. Pollack, A. J. Combes, E. A. Hardison, K. C. Barry, J. Tsui, M. K. Ruhland, K. Kersten, M. A. Abushawish, M. Spasic, J. P. Giurintano, V. Chan, A. I. Daud, P. Ha, C. J. Ye, E. W. Roberts, and M. F. Krummel. 2019. Unleashing Type-2 Dendritic Cells to Drive Protective Antitumor CD4 + T Cell Immunity. *Cell* 177: 556-571.e16.

284. Lynch, D. H., A. Andreasen, E. Maraskovsky, J. Whitmore, R. E. Miller, and J. C. Schuh. 1997. Flt3 ligand induces tumor regression and antitumor immune responses in vivo. *Nat. Med.* 3: 625–31.

285. Wang, H., J. Dai, S. Hou, W. Qian, B. Li, J. Ma, X. Fan, J. Zhao, S. Yang, H. Sang, Q. Yang, R. Wang, and Y. Guo. 2005. Treatment of hepatocellular carcinoma with adenoviral vector-mediated Flt3 ligand gene therapy. *Cancer Gene Ther.* 12: 769–777.

286. Pucci, M., G. Venturi, N. Malagolini, M. Chiricolo, and F. Dall'Olio. 2018. Glycosylation as a Main Regulator of Growth and Death Factor Receptors Signaling. *Int. J. Mol. Sci.* 19: 580.

287. Jongbloed, S. L., M. C. Lebre, A. R. Fraser, J. A. Gracie, R. D. Sturrock, P. P. Tak, and I. B. McInnes. 2005. Enumeration and phenotypical analysis of distinct dendritic cell subsets in psoriatic arthritis and rheumatoid arthritis. *Arthritis Res. Ther.* 8: 1–13.

288. Lutzky, V., S. Hannawi, and R. Thomas. 2007. Cells of the synovium in rheumatoid arthritis. Dendritic cells. *Arthritis Res. Ther.* 9: 1–12.

289. Ramos, M. I. P., O. N. Karpus, P. Broekstra, S. Aarrass, S. E. Jacobsen, P. P. Tak, and M. C. Lebre. 2015. Absence of Fms-like tyrosine kinase 3 ligand (Flt3L) signalling protects against collagen-induced arthritis. *Ann. Rheum. Dis.* 74: 211–219.

290. Durai, V., P. Bagadia, C. G. Briseño, D. J. Theisen, A. Iwata, J. T. Davidson, M. Gargaro, D. H. Fremont, T. L. Murphy, and K. M. Murphy. 2018. Altered compensatory cytokine signaling underlies the discrepancy between Flt3–/– and Flt3l–/– mice. *J. Exp. Med.* 215: 1417–1435.

291. Cueto, F. J., C. del Fresno, P. Brandi, A. J. Combes, E. Hernández-García, A. R. Sánchez-Paulete, M. Enamorado, C. P. Bromley, M. J. Gomez, R. Conde-Garrosa, S. Mañes, S. Zelenay, I. Melero, S. Iborra, M. F. Krummel, and D. Sancho. 2021. DNGR-1 limits Flt3L-mediated antitumor immunity by restraining tumor-infiltrating type I conventional dendritic cells. *J. Immunother. Cancer* 9: e002054.

292. Hsu, J. L., C. E. Bryant, M. S. Papadimitrious, B. Kong, R. E. Gasiorowski, D. Orellana, H. M. McGuire, B. F. de S. Groth, D. E. Joshua, P. J. Ho, S. Larsen, H. J. Iland, J. Gibson, G. J. Clark, P. D. Fromm, and D. N. J. Hart. 2018. A blood dendritic cell vaccine for acute myeloid leukemia expands anti-tumor T cell responses at remission. *Oncoimmunology* 7: e1419114.

293. Tian, Y., H. Yu, S. Hu, and Y. Zhang. 2020. *Advanced Concepts in Human Immunology: Prospects for Disease Control*, (P. Jain, and L. C. Ndhlovu, eds). Springer International Publishing, Cham.

294. Deguchi, K., and D. G. Gilliland. 2002. Cooperativity between mutations in tyrosine kinases and in hematopoietic transcription factors in AML. *Leukemia* 16: 740–744.

295. Alcántara-Hernández, M., R. Leylek, L. E. Wagar, E. G. Engleman, T. Keler, M.

P. Marinkovich, M. M. Davis, G. P. Nolan, and J. Idoyaga. 2017. High-Dimensional Phenotypic Mapping of Human Dendritic Cells Reveals Interindividual Variation and Tissue Specialization. *Immunity* 47: 1037-1050.e6.

296. Leylek, R., M. Alcántara-Hernández, Z. Lanzar, A. Lüdtke, O. A. Perez, B. Reizis, and J. Idoyaga. 2019. Integrated Cross-Species Analysis Identifies a Conserved Transitional Dendritic Cell Population. *Cell Rep.* 29: 3736-3750.e8.

297. Borst, J., T. Ahrends, N. Bąbała, C. J. M. Melief, and W. Kastenmüller. 2018. CD4+ T cell help in cancer immunology and immunotherapy. *Nat. Rev. Immunol.* 18: 635–647.

298. Melssen, M., and C. L. Slingluff. 2017. Vaccines targeting helper T cells for cancer immunotherapy. *Curr. Opin. Immunol.* 47: 85–92.

299. Jones, E. Y., L. Fugger, J. L. Strominger, and C. Siebold. 2006. MHC class II proteins and disease: A structural perspective. *Nat. Rev. Immunol.* 6: 271–282.

300. Matzaraki, V., V. Kumar, C. Wijmenga, and A. Zhernakova. 2017. The MHC locus and genetic susceptibility to autoimmune and infectious diseases. *Genome Biol.* 18.

301. Wu, H. Q., D. Baker, and H. Ovaa. 2020. Small molecules that target the ubiquitin system. *Biochem. Soc. Trans.* 48: 479–497.

302. Liu, J., Y. Cheng, M. Zheng, B. Yuan, Z. Wang, X. Li, J. Yin, M. Ye, and Y. Song. 2021. Targeting the ubiquitination/deubiquitination process to regulate immune checkpoint pathways. *Signal Transduct. Target. Ther.* 6: 28.

303. Wang, H., Y. Halida, and T. X. Wu. 2011. Lenalidomide plus dexamethasone for relapsed or refractory multiple myeloma: A systemic review. *Chinese J. Evidence-Based Med.* 11: 187–194.

304. Ito, T., H. Ando, T. Suzuki, T. Ogura, K. Hotta, Y. Imamura, Y. Yamaguchi, and H. Handa. 2010. Identification of a primary target of thalidomide teratogenicity. *Science* 327: 1345–1350.

305. Lu, G., R. E. Middleton, H. Sun, M. V. Naniong, C. J. Ott, C. S. Mitsiades, K. K. Wong, J. E. Bradner, and W. G. Kaelin. 2014. The myeloma drug lenalidomide promotes the cereblon-dependent destruction of ikaros proteins. *Science* 343: 305–309.

306. Kronke, J., N. D. Udeshi, A. Narla, P. Grauman, S. N. Hurst, M. McConkey, T. Svinkina, D. Heckl, E. Comer, X. Li, C. Ciarlo, E. Hartman, N. Munshi, M. Schenone, S. L. Schreiber, S. A. Carr, and B. L. Ebert. 2014. Lenalidomide Causes Selective Degradation of IKZF1 and IKZF3 in Multiple Myeloma Cells. *Science* 343: 301–305.

307. López-Relaño, J., B. Martín-Adrados, I. Real-Arévalo, J. Lozano-Bartolomé, B. Abós, S. Sánchez-Ramón, B. Alonso, M. G. del Moral, and E. Martínez-Naves. 2018. Monocyte-derived dendritic cells differentiated in the presence of lenalidomide display a semi-mature phenotype, enhanced phagocytic capacity, and Th1 polarization capability. *Front. Immunol.* 9: 1–14.

# Appendix 1

Article type : Review

Article type: Review

# Dendritic cell Flt3 – regulation, roles and repercussions for immunotherapy

Kayla R Wilson[1], Jose A Villadangos[1, 2], Justine D Mintern[1]

[1] Department of Biochemistry and Molecular Biology, The University of Melbourne, Bio21 Molecular Science and Biotechnology Institute, 30 Flemington Rd, Parkville, VIC 3010, Australia.

[2] Department of Microbiology and Immunology, Peter Doherty Institute for Infection and Immunity, The University of Melbourne, Parkville, VIC 3010, Australia.

Corresponding Authors: j.villadangos@unimelb.edu.au, jmintern@unimelb.edu.au

Running title: Dendritic cell Flt3

Keywords: Flt3, dendritic cells, immunity

## Abstract

Dendritic cells (DCs) are essential for initiating immune responses. Depending on the environment, the type of DC and the way in which it interacts with T cells; these immune responses can be beneficial or detrimental. DCs can be exploited as cellular vectors for vaccines against infection and cancer. The development and maintenance of DCs is dependent on the FMS-like tyrosine kinase 3 (Flt3)/Flt3 ligand (Flt3L) signaling cascade. Flt3 is also one of the most commonly mutated genes in leukemia and as such represents an attractive drug target. In this review, Flt3 is discussed with a particular

focus on DCs. We detail the lifecycle of Flt3, from transcription to degradation, and interrogate recent studies as to how this pathway can be manipulated for immunotherapy, vaccination and treatment of autoimmune disease.

**Introduction**

An exciting advance to immunotherapy against infection, cancer and autoimmunity is to exploit the biology of dendritic cells (DCs).[1] DCs are unrivalled in their ability to acquire, process and present antigenic peptide to T cells. Discovered in 1973,[2] they are a functionally and phenotypically heterogenous population of cells that are widely distributed throughout the body. Under steady state conditions, DCs are well-equipped at acquiring and processing antigen but poor at inducing immunity. Interactions between immature DCs and naïve T cells can lead to tolerance, are important in shaping T cell development in the thymus and maintaining T cell populations in the peripheral lymphoid organs. Upon encounter with inflammatory stimuli DCs undergo maturation. Inflammatory stimuli include pathogen associated molecular patterns (PAMPs) which are recognized by pattern recognition receptors (PRRs) on DCs in addition to inflammatory cytokines.[3] Mature DCs have elevated MHC, costimulatory molecules and inflammatory cytokines and migrate to T cell zones of secondary lymphoid organs where they can initiate immune responses. DC interaction with T cells can be a double-edged sword, with DCs capable of not only initiating immune responses against non-self but also initiating autoimmunity.

To manipulate DCs in clinical settings, it is important to understand the major signaling cascade that generates these cells - FMS-like tyrosine kinase 3 (Flt3)/Flt3 ligand (Flt3L). Indeed, years of studies into Flt3 have revealed it is essential in DC development and maintenance and is a tool commonly employed to manipulate the number of DCs *in vitro* and *in vivo*. More recently, focus has shifted to how this pathway can be manipulated for effective immunotherapy. In this review, we discuss the lifecycle of Flt3, including its transcription, intracellular trafficking, signaling and degradation. Understanding the biology of Flt3/Flt3L is important to create new avenues for the clinical manipulation of this pathway and exploitation of DCs. Finally, we highlight recent efforts that exploit Flt3 in immunotherapy and vaccination.

**FMS-like tyrosine kinase 3 (Flt3) receptor**

The *Flt3* gene encodes a type III receptor tyrosine kinase in the same family as macrophage colony-stimulating factor (M-CSF) receptor (M-CSFR), mast/stem cell growth factor receptor (SCFR/c-KIT/CD117) and platelet-derived growth factor receptors A and B (PDGFR-A and -B). These receptors share a similar structure with five extracellular immunoglobulin-like domains, one transmembrane domain, one juxtamembrane domain and two tyrosine kinase domains (**Figure 1**). Flt3 expression is restricted to hematopoietic stem cells and DCs.[4]

**Flt3 ligand (Flt3L)**

The ligand for Flt3 is Flt3 ligand (Flt3L), a type I transmembrane protein in the same family as the ligands for SCFR and M-CSFR. It comprises five extracellular domains, a transmembrane domain and a cytosolic tail (**Figure 1**). There are three main isoforms of Flt3L. The first isoform, found in both humans[5,6] and mice,[7] is cleavable membrane-bound Flt3L which can form soluble Flt3L. Flt3L can also be generated as a soluble protein which lacks a membrane anchor.[5–7] This occurs due to an early stop-codon which is introduced into Flt3L due to exon skipping. The last isoform is membrane-tethered and cannot be cleaved.[8] Similar to soluble Flt3L, membrane-tethered Flt3L occurs due to alternative splicing and results in a protein that lacks the cleavage site. While all forms are biologically active, the abundance of each differs between species. In humans, the most common form is the cleavable membrane-bound Flt3L,[8] whereas in mice the most common form is the membrane-tethered Flt3L.[5,8] It is currently unclear whether the different isoforms perform different functions.

In contrast to the Flt3 receptor, Flt3L mRNA is expressed by most hematopoietic and non-hematopoietic tissues.[5,7] Even so, in healthy individuals serum Flt3L levels are low.[9] The non-hematopoietic sources have not been studied extensively; however, for the hematopoietic source it has been shown that $CD4^+$ T cells secrete Flt3L.[10] When lethally irradiated $Flt3L^{-/-}$ mice are reconstituted with bone marrow from mice lacking T cells ($CD3\varepsilon^{-/-}$) there is a significant reduction in serum Flt3L in comparison to $Flt3L^{-/-}$ mice reconstituted with wild type bone marrow.[10] In particular, $CD4^+$ T cells were found to

secrete higher amounts of Flt3L than $CD8^+$ T cells when stimulated *ex vivo* with anti-CD3ε and anti-CD28 antibodies.[10] In T cells, Flt3L is stored intracellularly and colocalizes with Golgi-resident proteins.[9,11] Trafficking to the cell surface can be induced by cytokines which signal through the common γ receptor chain though the mechanism involved is unclear.[11] The metalloprotease TNFα converting enzyme (TACE/ADAM17) cleaves membrane-bound Flt3L to soluble Flt3L.[12]

Recently, there has been evidence of additional hematopoietic sources of Flt3L during steady-state conditions. Whilst not as highly expressed as in T cells, *Flt3L* is detected in conventional DC (cDC) subset 2 (cDC2) with low levels of soluble Flt3L detected in primary murine cDC2 cultures. The metalloprotease responsible for cleaving cDC2 Flt3L is a disintegrin and metalloproteinase 10 (ADAM10).[13] Mice lacking ADAM10 specifically in DCs have increased surface cDC2 Flt3L, reduced serum Flt3L and significantly reduced splenic cDC2 (defined as $CD11b^+$ $CD4^+$ $ESAM^+$).[13] This is the first paper to provide evidence for differential roles of Flt3L isoforms, with cleaved soluble Flt3L, not membrane-bound or tethered, required for the development and maintenance of $ESAM^+$ cDC2. It is currently unclear why splenic cDC2 preferentially require soluble Flt3L, though it has been suggested this improves accessibility of the ligand.[13]

**The lifecycle of Flt3**

Transcription

*Flt3* is regulated by a number of transcription factors. In DC progenitors, including common myeloid, lymphoid and DC progenitors, the transcription factor PU.1 (*Sfpi1*) promotes *Flt3* expression by directly binding to the *Flt3* promoter.[14] As a result, progenitors lacking this transcription factor have reduced DC developmental potential. *Flt3* expression is also enhanced by the transcription factor homeobox A9 (HOXA9), which has been shown to bind directly to the promoter of *Flt3*.[15] While mice lacking HOXA9 have reduced $Flt3^+$ progenitors, there are no changes to the DC lineage, indeed the number of bone marrow cDC and plasmacytoid DC (pDC) are unaltered.[16] It is unknown if HOXA9 maintains the steady-state level of Flt3 in terminally differentiated DCs. *Flt3* is also enhanced by CCATT/enhancer binding protein alpha (C/EBPα) and Myb in acute myeloid leukemia cells, with their knockdown decreasing *Flt3* expression. [17] DC

development is dependent on C/EBPα; however, it is not a requirement for survival or function of terminally differentiated DCs. Similarly, Myb regulates hematopoiesis and conditional deletion of this transcription factor in haematopoietic stem cells ablates bone marrow cellularity. Reduced *Flt3* on progenitor cells has been observed in *Myb* conditional deletion mice.[18] It is unclear whether C/EBPα and Myb regulate *Flt3* in DCs. In contrast, *Flt3* transcription is repressed by the transcription repressor Hes family BHLH transcription factor 1 (Hes1) which binds to the *Flt3* promoter.[19] Mice lacking Hes1 have impaired T cell development and lack a thymus.[20] It is unclear whether Flt3 is regulated by Hes1 in DCs; however, progenitor cells lacking this transcription factor have a developmental bias towards myeloid and DC development.[20] *Flt3* suppression also occurs due to paired box protein 5 (Pax5), which binds the *Flt3* promoter in pro-B cells.[21] This is critical for B cell development.[21] It is unclear whether Pax5 regulates steady-state expression of *Flt3* in DCs.

Trafficking to the cell surface

Given that endogenous expression of Flt3 in terminally differentiated cells is restricted to DCs, surprisingly little is known about its intracellular biology in this cell type. Most of these studies have been carried out in irrelevant cell lines, often over expressing *Flt3*. Nevertheless, once transcribed and translated the Flt3 receptor behaves similar to other receptor tyrosine kinases (**Figure 2**). It transits to the cell surface as a monomer which is N-linked glycosylated as confirmed by N-glycosidase F (PNGase F) digestion.[22] Once at the cell surface, and bound to the ligand, dimerization occurs. In support of this, when cells are treated with Flt3L, Flt3 can be detected as a species of ~360kDa (representative of 2 monomers bound to the 30kDa Flt3L).[23] Flt3L stimulation promotes Flt3 phosphorylation, indicative of activation.[24]

Flt3/Flt3L signaling

Once activated, Flt3 signals via mitogen-activated protein kinase (MAPK), phosphatidylinositol 3 kinase (PI3K) and signal transducers and activators of transcription 3 (STAT3) pathways (**Figure 3**). Flt3 signaling is also implicated in the indirect regulation of other signaling pathways given that in the absence of Flt3, DCs and their progenitors are more responsive to other growth factors (such as M-CSF and stem cell factor) and can activate additional pathways.[25] The MAPK pathway is implicated in Flt3 signaling in

different cell lines overexpressing wild type Flt3. Once stimulated with Flt3L, increased activation of SHC adaptor protein 1 (SHC) and extracellular signal-related kinase (ERK)1/2 is observed.[26] While this likely occurs in DCs, it has yet to be shown. The PI3K pathway is also implicated in Flt3 signaling. Flt3-mediated PI3K activation has been demonstrated in DCs.[27] Indeed, *in vivo* administration of Flt3L leads to increased phosphorylation of ribosomal protein S6 kinase beta-1 (S6K) in splenic cDCs. Congruent to this, global or DC-specific deletion of phosphatase and tensin homolog (PTEN), an inhibitor of AKT and downstream of PI3K signaling, leads to an increase in the number of DCs suggesting an important role of Flt3L-induced PI3K signaling in DC regulation.[27] Finally, activation of STAT3 is critical for DC development and occurs following Flt3L stimulation.[28] Consequently, mice lacking STAT3 in hematopoietic cells have fewer DCs which cannot be rescued by Flt3L treatment.[28] Similarly, forced expression of STAT3 leads to increased DC developmental potential.[29]

Flt3 degradation

Once activated, Flt3 internalizes and degrades as quickly as 5 and 20 minutes respectively.[23] Internalization of Flt3 from the cell surface is likely regulated by ubiquitination. Much of our current understanding of Flt3 ubiquitination has come from studies in transformed cell lines overexpressing Flt3, with little information for DCs. Nevertheless, these studies have revealed an attractive candidate for Flt3 ubiquitination – the Casitas B-lineage lymphoma (Cbl) family. Cbl was first implicated in Flt3 signaling when their phosphorylation was increased in transformed cell lines stimulated with Flt3L.[30] Studies using c-Cbl and Cbl-b mutant mice have further implicated these E3 ligases in Flt3 regulation. Mice harboring a mutation in the RING domain of c-Cbl (c-Cbl$^{A/-}$) have increased Flt3 expression and signaling in LSK (Lin$^{-}$ SCA-1$^{+}$ c-Kit$^{+}$) cells and develop lethal myeloid leukemia.[31] Increased Flt3 expression and signaling is lost when c-Cbl$^{A/-}$ mice are crossed to Flt3L$^{-/-}$ mice.[31] It is currently unclear as to whether the Cbl family regulates DC development and/or Flt3 expression in DCs. Once internalized, sorting of Flt3 into late endosomes is dependent on late endosomal/lysosomal adaptor and MAPK and mTOR activator 2 (LAMTOR2).[32] As a result, mice lacking LAMTOR2 have increased Flt3 expression and signaling in DCs and increased DC progenitors.[32]

**Flt3 and DC development**

Single cell analysis has revealed the development of terminally differentiated DCs is a continuous process whereby progenitor cells progressively differentiate.[33] DC development is dependent on Flt3/Flt3L signaling. As such, all cells that differentiate into cDCs and pDCs express Flt3.[34,35] Surface expression of Flt3 differs, with the highest expression observed for splenic cDC1 and the lowest for pre-cDC1 and pre-cDC2.[36] It should be noted that not all DCs rely on Flt3. Indeed, Langerhans cells, an epidermal-resident DC, are unaffected by loss of Flt3 signalling,[37] indicating their establishment and maintenance is Flt3-independent. The critical role of Flt3 in cDC and pDC development has been reinforced by studies overexpressing Flt3.[29] Onai and colleagues showed $Flt3^-$ hematopoietic progenitors, such as the megakaryocyte erythrocyte progenitor, MEP, cannot produce cDC or pDC irrespective of Flt3L stimulation. However, upon *Flt3* introduction, these progenitors can give rise to cDC and pDC.[29] Further to this, lethally irradiated mice have reduced cDCs and pDCs following reconstitution with $Flt3L^{-/-}$ bone marrow. Similarly, lethally irradiated $Flt3L^{-/-}$ mice reconstituted with wild type bone marrow have reduced cDCs and pDCs.[10] This not only demonstrates the importance of Flt3 signaling in DC development but also highlights the importance of hematopoietic sources of Flt3L, particularly $CD4^+$ T cells. Further evidence of the critical role of Flt3 in haematopoietic development comes from studies showing an increase in DC and progenitor number when Flt3L is administered to mice[35,38,39] or humans.[40] Other growth factors, such as granulocyte colony-stimulating factor (G-CSF) increase DC numbers; however, they are incapable of expanding DCs to the same extent as Flt3L.[38] Although increased cellularity is not observed in the bone marrow of Flt3L treated mice, there is an increase in the number of B cell and DC precursors and their mobilization.[39] In support of this, when Flt3L-treated and untreated splenocytes are depleted of cDCs and transferred into irradiated recipients there is an increase in DCs originating from Flt3L-treated splenocytes.[39] This is indicative of increased DC progenitors in Flt3L-treated spleens.

A greater understanding of Flt3 signaling on hematopoiesis has been gained from mice lacking *Flt3* (*$Flt3^{-/-}$*)[41] or *Flt3L* (*$Flt3L^{-/-}$*).[42] Initially $Flt3^{-/-}$ mice were described to have no changes in cellularity with the exception of reduced bone marrow B cell progenitors.[41] However, more recent analysis using complex multicolor immunophenotyping has

revealed additional decreases in lymphoid[39] and nonlymphoid[37] DCs. A similar, albeit more severe, phenotype is observed in Flt3L$^{-/-}$ mice. Mice lacking Flt3L$^{-/-}$ have reduced DC progenitors.[42] In addition, significant reductions in lymphoid[25,39,42] and non-lymphoid DCs[37] are observed. Flt3L$^{-/-}$ mice also have reduced natural killer (NK) cells.[42] This indicates Flt3 signaling regulates early progenitor cells involved in the differentiation of a number of lineages. In competitive bone marrow transplantation experiments Flt3$^{-/-}$ bone marrow cells are unable to reconstitute DCs[39] and other lineages[39,41] to the same extent as wild type bone marrow. In addition, by assessing bromodeoxyuridine (BrdU) incorporation into Flt3$^{-/-}$ and wild type splenic DCs, Waskow *et al*. demonstrated that Flt3$^{-/-}$ DCs in the periphery are unable to proliferate to the same extent as their wild type counterparts.[39] Therefore, Flt3 signaling regulates not only the differentiation and mobilization of progenitor DCs, but also plays a role in the homeostatic division of cDCs in peripheral lymphoid organs. More recent analysis suggests that while the earlier stages of cDC1 development require Flt3 signalling, the final stage is independent of this pathway.[36] Similar proportions of cDC1 are generated when purified splenic pre-cDCs (CD11c$^{+}$ MHC II$^{int}$ Flt3+ SiRPα$^{int}$) were cultured *in vitro* with feeder cells with and without Flt3L. This is in contrast to cDC2, that are significantly reduced in the absence of Flt3L.[36] This is surprising given cDC1 express higher Flt3 than cDC2,[36] and suggests Flt3 may play other important roles in cDC1.

**Flt3 and immune responses**

Flt3-mediated DC homeostasis is important for regulating normal immune responses, mainly due to its indirect effect on T cell homeostasis. DC numbers highly correlate with regulatory T cell (Treg) numbers. Flt3L administration increases Tregs and Flt3 depletion reduces Tregs.[43,44] This relationship is observed in humans, with Flt3L treatment causing significant expansion of Tregs.[45] Alterations to T cell compartments are independent of thymic Treg production as Flt3L administration increases splenic Tregs in thymectomized mice.[43] DCs regulate Treg proliferation in the periphery.[43–45] Given the relationship between DCs and Tregs, aberrant DC Flt3 signaling may alter immunosurveillance in cancer.[46]

Serum Flt3L levels, and as a result DC and T cell numbers, vary during different diseased states. Dramatic increases in serum Flt3L is often observed in conditions of decreased progenitors, for example patients undergoing high-dose chemotherapy.[9] Increased Flt3L is also evident at inflammation sites, such as following *Plasmodium* infection.[47] While $CD4^+$ T cells and cDC2 may be responsible for steady-state levels of Flt3L, this may not be the case in the presence of reduced hematopoietic progenitors, inflammation or infection. Indeed, mast cells, not $CD4^+$ T cells, are a major source of Flt3L during *Plasmodium* infection.[47] Similarly, in cancer, natural killer (NK) cells produce Flt3L at the tumor site.[48] Increases in Flt3L during infection and cancer play important protective roles by expanding DCs capable of presenting exogenous antigen by MHC I (cross-presenting cDC1) and improving $CD8^+$ T cell responses.

**Exploiting Flt3/Flt3L signaling in immunotherapy and vaccination**

There is significant interest in exploiting DCs in tumor immunotherapy. This is because of their excellent ability to capture and present antigen, in addition to trafficking to T cell zones. Unfortunately, harnessing the power of DCs has proved difficult due to their rare number in healthy and malignant tissues. Indeed, assessment of tumor infiltrating immune cells shows DCs to be the rarest cell type.[49,50] Whilst the number of tumor infiltrating DCs (TIDs) may be small, the role they play in tumor clearance is anything but. Cross-presenting cDC1 ($CD141^+$/$BDCA3^+$ in humans and $CD103^+$ in mice) are essential in solid tumor clearance. Mice lacking cross-presenting DCs (*Batf3*$^{-/-}$) have decreased $CD8^+$ T cell recruitment and increased tumor burden following tumor inoculation.[50,51] Similarly, high expression of $BDCA3^+$-related gene expression in melanoma correlates with increased overall patient survival.[48] This dramatic phenotype is due to an increase in $CD8^+$ T cell activation and infiltration.[51] Indeed, while a number of tumor-infiltrating immune cells, such as macrophages, can capture tumor-associated antigen, only cross-presenting TIDs are able to traffic to, and activate, $CD8^+$ T cells in the tumor and at tumor draining lymph nodes.[49,50] The normal number of TIDs is reliant on Flt3L production by NK cells, with a decrease in cross-presenting TIDs in mice lacking NK cells.[48] In agreement with this, the number of NK cells correlates with *Flt3L* gene expression and $BDCA3^+$ DC numbers in human melanoma.[48]

The Flt3/Flt3L signaling cascade is being targeted to manipulate the number of cross-presenting TIDs to improve anti-tumor immune responses. Administration of Flt3L to mice and humans significantly expands cross-presenting TIDs and their progenitors.[49,50,52,53] This promotes anti-tumor immunity in mice with solid tumors.[53,54] Improved outcomes occur when Flt3L is used together with a stimulatory agent and checkpoint inhibitors. Mice treated with Flt3L in combination with poly I:C (TLR3 agonist), mAb specific for programmed cell death-1 (PD1) with and without irradiation have significantly reduced primary and secondary tumor growth and increased survival.[49,52,55] This phenotype is reliant on cross-presenting $CD103^+$ DC and $CD8^+$ T cells.[49,52] The former is essential for anti-PD1 therapy.[55] Including Flt3L in combination therapy appears promising in clinical trials, with increased tumor regression in B cell lymphoma patients treated with Flt3L, irradiation and poly I:C.[52]

Adoptive T cell transfer (ACT) is an immunotherapy where patients are infused with T cells that are expanded *in vitro*. Importantly, these T cells can be genetically modified to improve their anti-cancer efficacy. For example, chimeric antigen receptor (CAR) T cells are engineered to express receptors specific for tumor antigens. In mice reconstituted with *Batf3*$^{-/-}$ bone marrow, adoptively transferred T cells were unable to migrate to the tumor site.[51] However, once reconstituted with activated DCs, this phenotype was rescued.[51] It is therefore possible that Flt3L, in combination with a TLR agonist, could potentiate ACT. Indeed, increased proliferation of adoptively transferred OT-I cells occurs in B16-OVA bearing mice treated with Flt3L and poly I:C.[49] CAR T cells have been engineered to express and secrete Flt3L.[53] Lai and colleagues demonstrate Flt3L-CAR T cells improve tumor clearance, especially in combination with poly I:C and anti-4-IBB. This is dependent on cDC1, with no significant reduction in tumor size observed in *Batf3*$^{-/-}$ mice. Importantly, Flt3L-CAR T cell therapy increases the host anti-tumor response with an increase in endogenous DC and T cells. In addition, improved host TCR diversity is observed. As a result, when mice are rechallenged with tumors lacking antigen, anti-tumor responses are improved.

Flt3/Flt3L signaling has been exploited for vaccines against infection. Incorporation of Flt3L into vaccines against infectious agents can enhance immunity by increasing DC

numbers and infiltration. Following subcutaneous immunization with DC-targeted antigen there is an increase in serum Flt3L alongside alterations in DC composition in skin-draining LNs.[56] Mice treated with Flt3L during immunization display increased antigen uptake, and upon antigen recall, improved $CD4^+$ T cell interferon gamma (IFNγ) production, $CD4^+$ T cell expansion and increased serum IgG. In addition, Flt3L treatment expands $CD8^-$ $CD24^+$ precursors of cDC1.[57] Mice vaccinated with these DC precursors prior to viral infection have increased specific memory T cell expansion and decreased viral load in comparison to mice vaccinated with cDC1.[57] During early stages of influenza A virus infection, there is a decrease in Flt3L and cDCs, impacting immune outcomes.[58] By treating mice with a Flt3L-encoding plasmid prior to infecting with influenza, Beshara and colleagues exploited the Flt3/Flt3L signaling pathway and effectively increased the number of DC progenitors and lung DCs, in addition to reducing the number of tissue-damaging inflammatory monocytes. This strategy protected mice against secondary bacterial infections.[58]

**Flt3 and autoimmunity**

While increased Flt3/Flt3L signaling may be desirable during infection and cancer, a genome-wide association study of more than 30,000 autoimmune thyroid disease (AITD) cases highlights this pathway can also elicit autoimmune disease.[59] Saevarsdottir and colleagues identified an intron variant of Flt3 impacting AITD, systemic lupus, rheumatoid arthritis (RA) and coeliac disease risk.[59] The intron variant has a premature stop codon predicted to generate a truncated non-functional protein. The reduction in Flt3 correlates with increased serum Flt3L and expansion of myeloid cells, indicative of a positive feedback loop between Flt3 receptor and ligand.[59] This is the first study to detail a germline mutation in *Flt3* leading to increased risk of autoimmunity. Increased Flt3L is a well-established hallmark of autoimmunity. Indeed, RA patients not only exhibit increased serum Flt3L but also significantly increased Flt3L in the synovial fluid of their joints, where most inflammation and tissue damage is observed.[60] It is hypothesized that increased Flt3L exacerbates autoimmunity in RA. In support of this, increased arthritis pathogenesis is observed in mice administered with Flt3L.[60]

In contrast, Flt3/Flt3L signaling can dampen autoimmunity via expansion of Tregs. Flt3L pre-treatment prevents death due to graft-versus-host-disease (GVHD) and protects mice against type 1 diabetes and inflammatory bowel disease.[43,44] In part this is due to increased cDC1s with protection lost when Tregs are depleted.[44] Unsurprisingly, the relationship between Tregs and DCs is also observed in mice harboring Flt3-ITD mutations, with progressively increased Tregs in $Flt3^{ITD/+}$ and $Flt3^{ITD/ITD}$ mice.[46] Indeed, when Tregs are selectively depleted with diphtheria toxin in $Flt3^{ITD/+}FoxP3^{DTR\text{-}GFP}$ or $Flt3^{+/+}FoxP3^{DTR\text{-}GFP}$ mice, there was faster reconstitution of Tregs in $Flt3^{ITD/+}$ mice.[46]

## Conclusion

Since its discovery, the Flt3/Flt3L signaling cascade has proved to be one of the most important pathways for the development and maintenance of DCs. Recent clinical strategies aim to use this pathway to exploit DCs to shape immune responses for desired outcomes. This is proving particularly useful in cancer treatment as our understanding of tumor infiltrating immune cells and their role in cancer progression and clearance grows. Given the relationship between DCs and Tregs, manipulating the Flt3/Flt3L cascade may also prove useful in the context of autoimmune disease. Currently, clinical strategies rely upon administration of recombinant Flt3L. Improving understanding of the biology of Flt3 in DCs would enable more sophisticated approaches, including the use of small molecule pharmaceuticals. To do this, further understanding of the transcription, trafficking and regulation of Flt3 in DCs, and their progenitors, is required, research that to date, has largely been neglected. Attention to this important aspect of DC biology will reveal novel targets for regulating DCs in healthy and malignant settings.

## Acknowledgments

This work was supported by National Health and Medical Research Council, Department of Health Australia grants or fellowships (1058193, 1113293, 1154502 and 1163090 [to JAV], and 1161101 and 1129672 [to JDM]), Australian Research Council, Department of Education and Training grants or fellowships (160103134, 170102471, 190102213 [to JAV] and 190101242, 180100844, 160101373, and 180100521 [to JDM]), a Human Frontiers Science Program grant (0064/2011 [to JAV]), and the Victorian State Government Operational Infrastructure Support and the Independent Research Institutes

Infrastructure Support Scheme of the Australian Government National Health and Medical Research Council.

**Author contributions**

**Kayla R Wilson:** Conceptualization; Writing – original draft; Writing - review & editing. **Jose A Villadangos:** Conceptualization; Supervision; Writing - review & editing. **Justine D Mintern:** Conceptualization; Funding acquisition, Supervision; Writing -review & editing.

**Conflicts of interest**

The authors declare no conflicts of interest.

**References**

1 Wculek SK, Cueto FJ, Mujal AM, Melero I, Krummel MF, Sancho D. Dendritic cells in cancer immunology and immunotherapy. *Nat Rev Immunol* 2020; **20**: 7–24.

2 Steinman RM, Cohn ZA. Identification of a novel cell type in peripheral lymphoid organs of mice. I. Morphology, quantitation, tissue distribution. *J Exp Med* 1973; **137**: 1142–1162.

3 e Sousa CR. Dendritic cells in a mature age. *Nat Rev Immunol* 2006; **6**: 476–483.

4 Miller JC, Brown BD, Shay T *et al.* Deciphering the transcriptional network of the dendritic cell lineage. *Nat Immunol* 2012; **13**: 888–899.

5 Hannum C, Culpepper J, Campbell D *et al.* Ligand for FLT3/FLK2 receptor tyrosine kinase regulates grouth of haematopoietic stem cells and is encoded by variant RNAs. *Nature* 1994; **368**: 643–648.

6 Lyman SD, James L, Johnson L *et al.* Cloning of the human homologue of the murine flt3 ligand: a growth factor for early hematopoietic progenitor cells. *Blood* 1994; **83**: 2795–2802.

7 Lyman SD, James L, Bos TV *et al.* Molecular cloning of a ligand for the flt3/flk-2 tyrosine kinase receptor: A proliferative factor for primitive hematopoietic cells. *Cell* 1993; **75**: 1157–1167.

8 Lyman SD, James L, Escobar S *et al.* Identification of soluble and membrane-bound isoforms of the murine flt3 ligand generated by alternative splicing of

mRNAs. *Oncogene* 1995; **10**: 149–157.

9 Chklovskaia E, Jansen W, Nissen C *et al.* Mechanism of flt3 Ligand Expression in Bone Marrow Failure: Translocation From Intracellular Stores to the Surface of T Lymphocytes After Chemotherapy-Induced Suppression of Hematopoiesis. *Blood* 1999; **93**: 2595–2604.

10 Saito Y, Boddupalli CS, Borsotti C, Manz MG. Dendritic cell homeostasis is maintained by nonhematopoietic and T-cell-produced Flt3-ligand in steady state and during immune responses. *Eur J Immunol* 2013; **43**: 1651–1658.

11 Chklovskaia E, Nissen C, Landmann L, Rahner C, Pfister O, Wodnar-Filipowicz A. Cell-surface trafficking and release of flt3 ligand from T lymphocytes is induced by common cytokine receptor γ-chain signaling and inhibited by cyclosporin A. *Blood* 2001; **97**: 1027–1034.

12 Horiuchi K, Morioka H, Takaishi H, Akiyama H, Blobel CP, Toyama Y. Ectodomain shedding of FLT3 ligand is mediated by TACE. *J Immunol* 2009; **182**: 7408–7414.

13 Fujita K, Chakarov S, Kobayashi T *et al.* Cell-autonomous FLT3L shedding via ADAM10 mediates conventional dendritic cell development in mouse spleen. *Proc Natl Acad Sci USA* 2019; **116**: 14714-14723.

14 Carotta S, Dakic A, D'Amico A *et al.* The transcription factor PU.1 controls dendritic cell development and Flt3 cytokine receptor expression in a dose-dependent manner. *Immunity* 2010; **32**: 628–641.

15 Gwin K, Frank E, Bossou A, Medina KL. Hoxa9 Regulates Flt3 in Lymphohematopoietic Progenitors. *J Immunol* 2010; **185**: 6572–6583.

16 Gwin KA, Shapiro MB, Dolence JJ, Huang ZL, Medina KL. Hoxa9 and Flt3 Signaling Synergistically Regulate an Early Checkpoint in Lymphopoiesis. *J Immunol* 2013; **191**: 745–754.

17 Volpe G, Walton DS, Del Pozzo W *et al.* C/EBPα and MYB regulate FLT3 expression in AML. *Leukemia* 2013; **27**: 1487–1496.

18 Volpe G, Clarke M, Garcìa P *et al.* Regulation of the flt3 gene in haematopoietic stem and early progenitor cells. *PLoS One* 2015; **10**: 1–18.

19 Kato T, Sakata-Yanagimoto M, Nishikii H *et al.* Hes1 suppresses acute myeloid leukemia development through FLT3 repression. *Leukemia* 2015; **29**: 576–585.

20 De Obaldia ME, Bell JJ, Wang X *et al.* T cell development requires constraint of the

myeloid regulator C/EBP-α by the Notch target and transcriptional repressor Hes1. *Nat Immunol* 2013; **14**: 1277–1284.

21 Holmes ML, Carotta S, Corcoran LM, Nutt SL. Repression of Flt3 by Pax5 is crucial for B-cell lineage commitment. *Genes Dev* 2006; **20**: 933–938.

22 Lyman SD, James L, Zappone J, Sleath PR, Beckmann MP, Bird T. Characterization of the protein encoded by the flt3 (flk2) receptor-like tyrosine kinase gene. *Oncogene* 1993; **8**: 815–822.

23 Turner AM, Lin NL, Issarachai S, Lyman SD, Broudy VC. FLT3 Receptor Expression on the Surface of Normal and Malignant Human Hematopoietic Cells. *Blood* 1996; **88**: 3383–390.

24 Zhang S, Broxmeyer HE. p85 subunit of PI3 kinase does not bind to human Flt3 receptor, but associates with SHP2, SHIP, and a tyrosine-phosphorylated 100-kDa protein in Flt3 ligand-stimulated hematopoietic cells. *Biochem Biophys Res Commun* 1999; **254**: 440–445.

25 Durai V, Bagadia P, Briseño CG *et al.* Altered compensatory cytokine signaling underlies the discrepancy between $Flt3^{-/-}$ and $Flt3l^{-/-}$ mice. *J Exp Med* 2018; **215**: 1417–1435.

26 Zhang S, Mantel C, Broxmeyer HE. Flt3 signaling involves tyrosyl-phosphorylation of SHP-2 and SHIP and their association with Grb2 and Shc in Baf3/Flt3 cells. *J Leukoc Biol* 1999; **65**: 372–380.

27 Sathaliyawala T, O'Gorman WE, Greter M *et al.* Mammalian target of rapamycin controls dendritic cell development downstream of Flt3 ligand signaling. *Immunity* 2010; **33**: 597–606.

28 Laouar Y, Welte T, Fu XY, Flavell RA. STAT3 Is Required for Flt3L-Dependent Dendritic Cell Differentiation. *Immunity* 2003; **19**: 903–912.

29 Onai N, Obata-Onai A, Tussiwand R, Lanzavecchia A, Manz MG. Activation of the Flt3 signal transduction cascade rescues and enhances type I interferon–producing and dendritic cell development. *J Exp Med* 2006; **203**: 227–238.

30 Lavagna-Sévenier C, Marchetto S, Birnbaum D, Rosnet O. FLT3 signaling in hematopoietic cells involves CBL, SHC and an unknown P115 as prominent tyrosine-phosphorylated substrates. *Leukemia* 1998; **12**: 301–310.

31 Rathinam C, Thien CBF, Flavell RA, Langdon WY. Myeloid leukemia development

in c-Cbl RING finger mutant mice is dependent on FLT3 signaling. *Cancer Cell* 2010; **18**: 341–352.

32 Scheffler JM, Sparber F, Tripp CH *et al.* LAMTOR2 regulates dendritic cell homeostasis through FLT3-dependent mTOR signalling. *Nat Commun* 2014; **5**: 5138.

33 Naik SH, Perié L, Swart E *et al.* Diverse and heritable lineage imprinting of early haematopoietic progenitors. *Nature* 2013; **496**: 229–232.

34 D'Amico A, Wu L. The Early Progenitors of Mouse Dendritic Cells and Plasmacytoid Predendritic Cells Are within the Bone Marrow Hemopoietic Precursors Expressing Flt3. *J Exp Med* 2003; **198**: 293–303.

35 Karsunky H, Merad M, Cozzio A, Weissman IL, Manz MG. Flt3 Ligand Regulates Dendritic Cell Development from $Flt3^+$ Lymphoid and Myeloid-committed Progenitors to $Flt3^+$ Dendritic Cells In Vivo. *J Exp Med* 2003; **198**: 305–313.

36 Audiger C, Lesage S. FLT3 Ligand Is Dispensable for the Final Stage of Type 1 Conventional Dendritic Cell Differentiation. *J Immunol* 2020; **205**: 2117–2127.

37 Ginhoux F, Liu K, Helft J *et al.* The origin and development of nonlymphoid tissue $CD103^+$ DCs. *J Exp Med* 2009; **206**: 3115–3130.

38 Maraskovsky E, Brasel K, Teepe M K *et al.* Dramatic increase in the numbers of functionally mature dendritic cells in Flt3 ligand-treated mice: multiple dendritic cell subpopulations identified. *J Exp Med* 1996; **184**: 1953–1962.

39 Waskow C, Liu K, Darrasse-Jèze G, Guermonprez P *et al.* The receptor tyrosine kinase Flt3 is required for dendritic cell development in peripheral lymphoid tissues. *Nat Immunol* 2008; **9**: 676–683.

40 Maraskovsky E, Daro E, Roux E *et al.* In vivo generation of human dendritic cell subsets by Flt3 ligand. *Blood* 2000; **96**: 878–884.

41 Mackarehtschian K, Hardin JD, Moore KA, Boast S, Goff SP, Lemischka IR. Targeted disruption of the flk2/flt3 gene leads to deficiencies in primitive hematopoietic progenitors. *Immunity* 1995; **3**: 147–161.

42 McKenna HJ, Stocking KL, Miller RE *et al.* Mice lacking flt3 ligand have deficient hematopoiesis affecting hematopoietic progenitor cells, dendritic cells, and natural killer cells. *Blood* 2000; **95**: 3489–3497.

43 Swee LK, Bosco N, Malissen B, Ceredig R, Rolink A. Expansion of peripheral

naturally occurring T regulatory cells by Fms-like tyrosine kinase 3 ligand treatment. *Blood* 2009; **113**: 6277–6287.

44 Darrasse-Jèze G, Deroubaix S, Mouquet H *et al.* Feedback control of regulatory T cell homeostasis by dendritic cells in vivo. *J Exp Med* 2009; **206**: 1853–1862.

45 Klein O, Ebert LM, Zanker D *et al.* Flt3 ligand expands $CD4^+$ $FoxP3^+$ regulatory T cells in human subjects. *Eur J Immunol* 2013; **43**: 533–539.

46 Lau CM, Nish SA, Yogev N, Waisman A, Reiner SL, Reizis B. Leukemia-associated activating mutation of Flt3 expands dendritic cells and alters T cell responses. *J Exp Med* 2016; **213**: 415–431.

47 Guermonprez P, Helft J, Claser C *et al.* Inflammatory Flt3L is essential to mobilize dendritic cells and for T cell responses during Plasmodium infection. *Nat Med* 2013; **19**: 730–738.

48 Barry KC, Hsu J, Broz ML *et al.* A natural killer–dendritic cell axis defines checkpoint therapy–responsive tumor microenvironments. *Nat Med* 2018; **24**: 1178–1191.

49 Salmon H, Idoyaga J, Rahman A *et al.* Expansion and Activation of $CD103^+$ Dendritic Cell Progenitors at the Tumor Site Enhances Tumor Responses to Therapeutic PD-L1 and BRAF Inhibition. *Immunity* 2016; **44**: 924–938.

50 Broz ML, Binnewies M, Boldajipour B *et al.* Dissecting the Tumor Myeloid Compartment Reveals Rare Activating Antigen-Presenting Cells Critical for T Cell Immunity. *Cancer Cell* 2014; **26**: 638–652.

51 Spranger S, Dai D, Horton B, Gajewski TF. Tumor-Residing Batf3 Dendritic Cells Are Required for Effector T Cell Trafficking and Adoptive T Cell Therapy. *Cancer Cell* 2017; **31**: 711-723.e4.

52 Hammerich L, Marron TU, Upadhyay R *et al.* Systemic clinical tumor regressions and potentiation of PD1 blockade with in situ vaccination. *Nat Med* 2019; **25**: 814–824.

53 Lai J, Mardiana S, House IG *et al.* Adoptive cellular therapy with T cells expressing the dendritic cell growth factor Flt3L drives epitope spreading and antitumor immunity. *Nat Immunol* 2020; **21**: 914-926.

54 Esche C, Subbotin VM, Maliszewski C, Lotze MT, Shurin MR. FLT3 ligand administration inhibits tumor growth in murine melanoma and lymphoma. *Cancer*

*Res* 1998; **58**: 380–383.

55 Sánchez-Paulete AR, Cueto FJ, Martínez-López M *et al.* Cancer immunotherapy with immunomodulatory anti-CD137 and anti–PD-1 monoclonal antibodies requires BATF3-dependent dendritic cells. *Cancer Discov* 2016; **6**: 71–79.

56 Anandasabapathy N, Feder R, Mollah S *et al.* Classical Flt3L-dependent dendritic cells control immunity to protein vaccine. *J Exp Med* 2014; **211**: 1875–1891.

57 Bedoui S, Prato S, Mintern J *et al.* Characterization of an Immediate Splenic Precursor of $CD8^+$ Dendritic Cells Capable of Inducing Antiviral T Cell Responses. *J Immunol* 2009; **182**: 4200–4207.

58 Beshara R, Sencio V, Soulard D *et al.* Alteration of Flt3-Ligand-dependent de novo generation of conventional dendritic cells during influenza infection contributes to respiratory bacterial superinfection. *PLoS Pathog* 2018; **14**: e1007360.

59 Saevarsdottir S, Olafsdottir TA, Ivarsdottir EV *et al.* FLT3 stop mutation increases FLT3 ligand level and risk of autoimmune thyroid disease. *Nature* 2020; **584**. doi:10.1038/s41586-020-2436-0.

60 Dehlin M, Bokarewa M, Rottapel R *et al.* Intra-articular fms-like tyrosine kinase 3 ligand expression is a driving force in induction and progression of arthritis. *PLoS One* 2008; **3**: e3633.

**Figure Captions**

**Figure 1.** Schematic of the structure of Flt3 and Flt3L. Flt3 comprises five extracellular immunoglobulin (Ig)-like domains at the N-terminus. These are followed by one transmembrane (TM) domain and a juxtamembrane (JM) domain. The C-terminus comprises 2 tyrosine kinase domains. The most common mutation in the *Flt3* gene is the internal tandem duplication (ITD), where an in-frame duplication of exons 14 and 15 is present in the JM domain. Membrane-bound Flt3L comprises of 5 extracellular domains, one TM domain and one cytosolic tail (CT). The arrow indicates cleavage site to form soluble Flt3L.

**Figure 2.** Schematic of the trafficking of Flt3**.** Flt3 is transcribed and translated as a monomer which traffics to the cell surface. During this journey it is glycosylated. Once at the surface, it binds to Flt3L which promotes dimerization and phosphorylation of Flt3.

Flt3 internalizes quickly and is degraded by either/or both the lysosomal and proteasomal degradation pathways.

**Figure 3.** Signaling pathways induced by activated Flt3**.** Flt3 signals through 3 pathways –MAPK (pink), STAT3 (blue) and PI3K (green). Dashed arrows indicate pathways that have only been demonstrated using transformed cell lines (not DCs) whereas solid lines indicate pathways confirmed in DCs or DC progenitors.

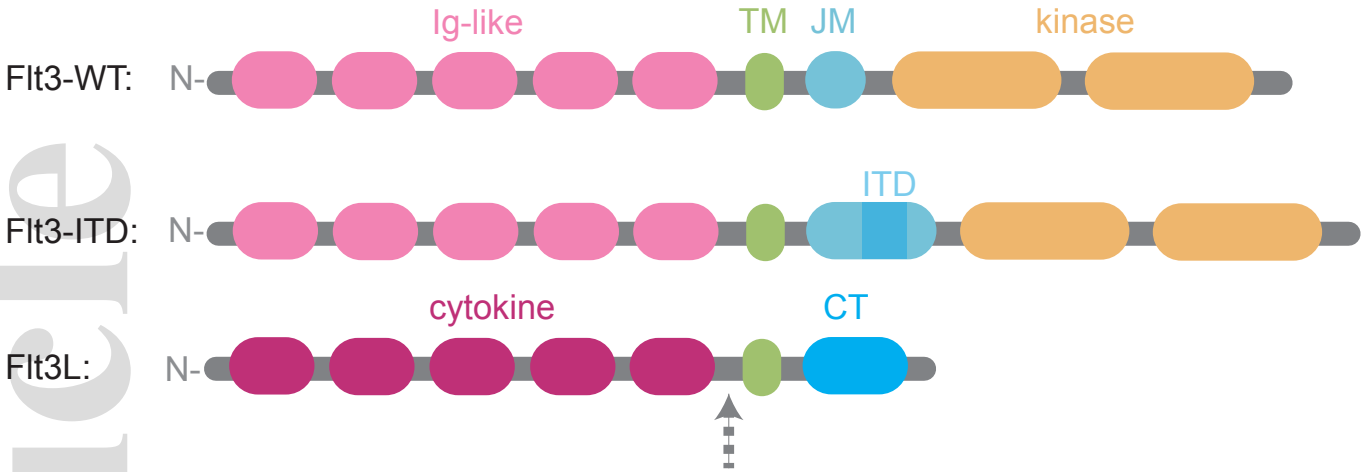

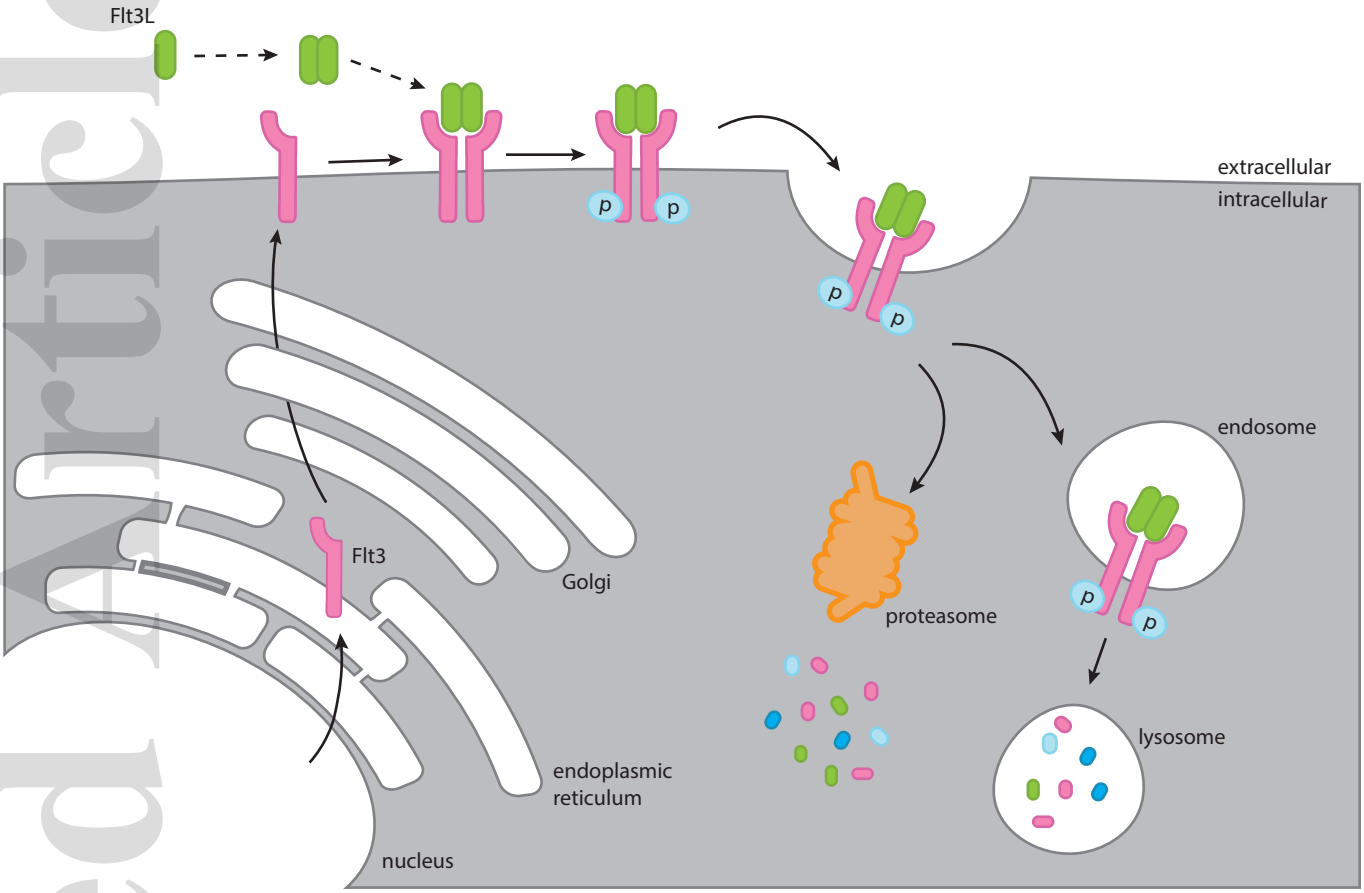

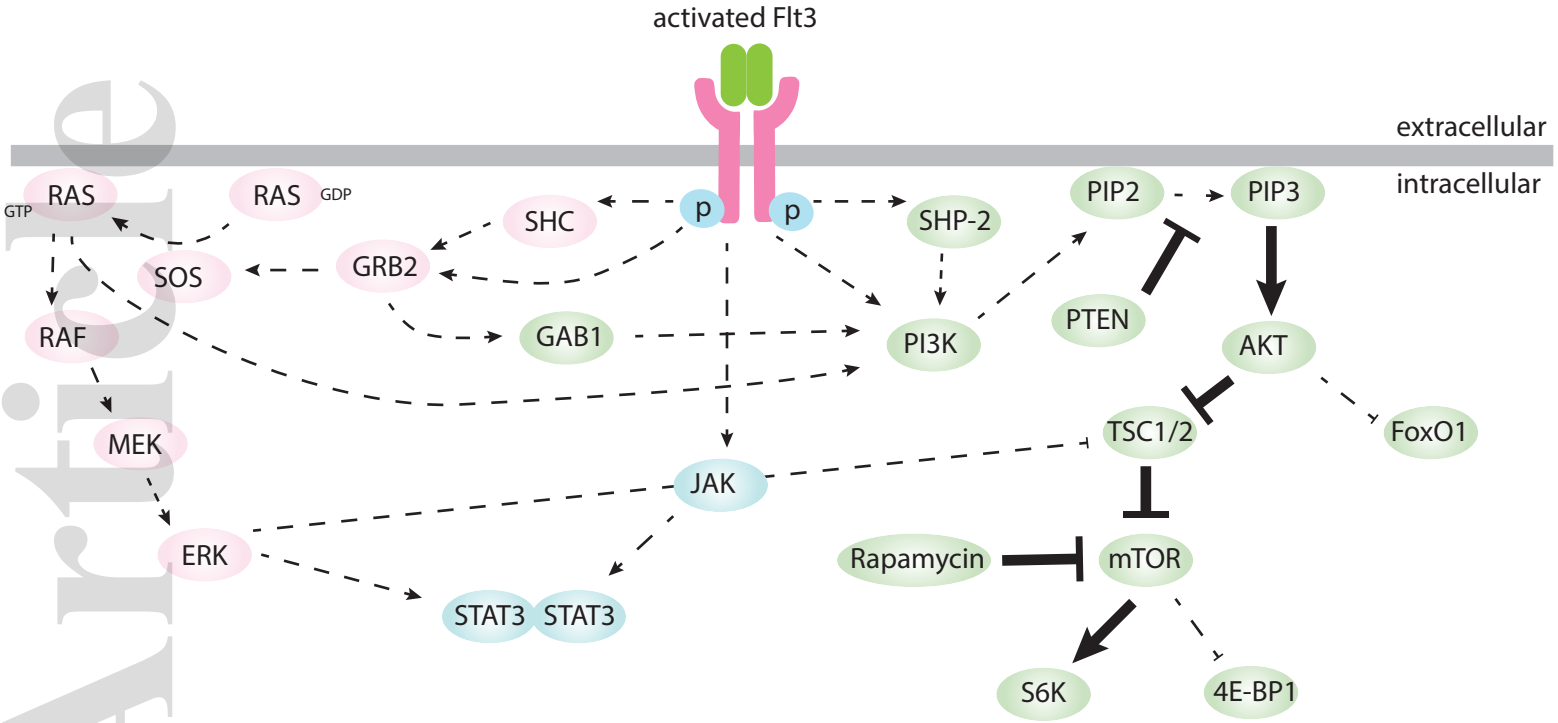

# Appendix 2

Genes enriched in Brie CRISPR/Cas9 genome wide screen Flt3$^{lo}$ samples sort 1.

| # | gene | FDR | p value | LFC |
|---|---|---|---|---|
| **1** | *Flt3* | 0.000309 | 2.52E-07 | 2.887 |
| **2** | *Cbfb* | 0.000309 | 2.52E-07 | 2.3517 |
| **3** | *Arih1* | 0.000309 | 2.52E-07 | 2.1677 |
| **4** | *Pagr1a* | 0.000309 | 2.52E-07 | 1.8764 |
| **5** | *Ep300* | 0.000309 | 2.52E-07 | 1.8003 |
| **6** | *Kmt2c* | 0.000309 | 2.52E-07 | 1.7347 |
| **7** | *Runx3* | 0.000309 | 2.52E-07 | 1.6758 |
| **8** | *Nf1* | 0.000309 | 2.52E-07 | 1.6627 |
| **9** | *Mau2* | 0.000309 | 2.52E-07 | 1.6439 |
| **10** | *Paxip1* | 0.00409 | 4.78E-06 | 1.5959 |
| **11** | *Flcn* | 0.000309 | 2.52E-07 | 1.54 |
| **12** | *Adnp* | 0.003825 | 4.28E-06 | 1.5065 |
| **13** | *Fbxl14* | 0.000309 | 2.52E-07 | 1.4652 |
| **14** | *Ahr* | 0.000309 | 2.52E-07 | 1.4184 |
| **15** | *Cnot11* | 0.000309 | 2.52E-07 | 1.4112 |
| **16** | *Nmt1* | 0.000309 | 2.52E-07 | 1.3751 |
| **17** | *Atxn7l3* | 0.045455 | 7.62E-05 | 1.3598 |
| **18** | *Runx1* | 0.000309 | 2.52E-07 | 1.29 |
| **19** | *Usp22* | 0.012907 | 1.84E-05 | 1.2061 |
| **20** | *Tnfrsf8* | 0.004332 | 5.28E-06 | 1.1253 |
| **21** | *Gnai2* | 0.002723 | 2.77E-06 | 1.1155 |
| **22** | *Fam49b* | 0.000309 | 2.52E-07 | 1.1059 |
| **23** | *Klhl10* | 0.031848 | 4.86E-05 | 1.0883 |
| **24** | *Keap1* | 0.000874 | 7.55E-07 | 1.0449 |
| **25** | *Bcor* | 0.011918 | 1.59E-05 | 1.0182 |
| **26** | *Fam193a* | 0.033057 | 5.21E-05 | 1.0146 |
| **27** | *Asxl2* | 0.020997 | 3.09E-05 | 1.0077 |

# Appendix 3

Genes enriched in Brie CRISPR/Cas9 genome wide screen Flt3$^{lo}$ samples sort 2.

| # | gene | FDR | p value | LFC |
|---|---|---|---|---|
| **1** | *Flt3* | 0.00033 | 2.52E-07 | 4.1242 |
| **2** | *Cbfb* | 0.00033 | 2.52E-07 | 2.9796 |
| **3** | *Arih1* | 0.00033 | 2.52E-07 | 2.7213 |
| **4** | *Pagr1a* | 0.00033 | 2.52E-07 | 2.6398 |
| **5** | *Paxip1* | 0.000928 | 7.55E-07 | 2.4543 |
| **6** | *Flcn* | 0.00033 | 2.52E-07 | 2.3511 |
| **7** | *Mau2* | 0.00033 | 2.52E-07 | 2.2275 |
| **8** | *Kmt2c* | 0.00033 | 2.52E-07 | 2.1618 |
| **9** | *Runx3* | 0.00033 | 2.52E-07 | 2.0864 |
| **10** | *Ube2m* | 0.002038 | 1.76E-06 | 2.084 |
| **11** | *Adnp* | 0.00033 | 2.52E-07 | 2.0729 |
| **12** | *Fbxl14* | 0.00033 | 2.52E-07 | 1.9433 |
| **13** | *Ep300* | 0.017777 | 1.99E-05 | 1.9222 |
| **14** | *Nf1* | 0.00033 | 2.52E-07 | 1.9181 |
| **15** | *Ahr* | 0.00033 | 2.52E-07 | 1.7693 |
| **16** | *Cnot11* | 0.005472 | 5.28E-06 | 1.7075 |
| **17** | *Lamtor4* | 0.011634 | 1.18E-05 | 1.7047 |
| **18** | *Runx1* | 0.00033 | 2.52E-07 | 1.6803 |
| **19** | *Asxl2* | 0.005472 | 5.28E-06 | 1.6049 |
| **20** | *Nmt1* | 0.00033 | 2.52E-07 | 1.5029 |
| **21** | *Fam193a* | 0.015323 | 1.64E-05 | 1.3993 |
| **22** | *Fam49b* | 0.00033 | 2.52E-07 | 1.2504 |

# Appendix 4

Genes enriched in Brie CRISPR/Cas9 genome wide screen Flt3$^{hi}$ samples sort 1.

| # | gene | FDR | P value | LFC |
|---|---|---|---|---|
| **1** | *Carm1* | 0.00099 | 2.52E-07 | 1.2669 |
| **2** | *Rhog* | 0.00099 | 2.52E-07 | 1.5257 |
| **3** | *Tcf7l2* | 0.00099 | 2.52E-07 | 1.6618 |
| **4** | *Med25* | 0.00099 | 2.52E-07 | 2.1183 |
| **5** | *Trp53* | 0.010608 | 3.77E-06 | 1.2054 |
| **6** | *Hes1* | 0.019183 | 7.80E-06 | 1.1008 |
| **7** | *Prex1* | 0.038119 | 1.94E-05 | 1.1775 |

# Appendix 5

Genes enriched in Brie CRISPR/Cas9 genome wide screen Flt3$^{hi}$ samples sort 2.

| # | gene | FDR | P value | LFC |
|---|---|---|---|---|
| **1** | *Med25* | 0.000165 | 2.52E-07 | 3.4241 |
| **2** | *Tcf7l2* | 0.000165 | 2.52E-07 | 2.3448 |
| **3** | *Rhog* | 0.000165 | 2.52E-07 | 2.3313 |
| **4** | *Arpc5* | 0.000165 | 2.52E-07 | 2.2988 |
| **5** | *Trp53* | 0.000165 | 2.52E-07 | 2.2367 |
| **6** | *Rcor1* | 0.000165 | 2.52E-07 | 2.1369 |
| **7** | *Carm1* | 0.000165 | 2.52E-07 | 1.5874 |
| **8** | *Dek* | 0.000165 | 2.52E-07 | 1.3919 |
| **9** | *Elf4* | 0.000165 | 2.52E-07 | 1.2765 |
| **10** | *Epc1* | 0.000165 | 2.52E-07 | 1.7871 |
| **11** | *Hes1* | 0.000165 | 2.52E-07 | 1.955 |
| **12** | *Jmjd6* | 0.000165 | 2.52E-07 | 1.6495 |
| **13** | *Kmt2d* | 0.000165 | 2.52E-07 | 1.1122 |
| **14** | *Marcks* | 0.000165 | 2.52E-07 | 1.0614 |
| **15** | *Mbd2* | 0.000165 | 2.52E-07 | 1.567 |
| **16** | *Mta2* | 0.000165 | 2.52E-07 | 1.4052 |
| **17** | *Mxi1* | 0.000165 | 2.52E-07 | 1.2518 |
| **18** | *Nckap1l* | 0.000165 | 2.52E-07 | 1.2602 |
| **19** | *Pcnxl3* | 0.000165 | 2.52E-07 | 1.3463 |
| **20** | *Prex1* | 0.000165 | 2.52E-07 | 1.7346 |
| **21** | *Rara* | 0.000165 | 2.52E-07 | 1.3856 |
| **22** | *Rxra* | 0.000165 | 2.52E-07 | 1.4642 |
| **23** | *Ssr2* | 0.000165 | 2.52E-07 | 1.2364 |
| **24** | *Suv39h1* | 0.000165 | 2.52E-07 | 1.59 |
| **25** | *Suv420h1* | 0.000165 | 2.52E-07 | 1.5461 |
| **26** | *Tm2d3* | 0.000165 | 2.52E-07 | 1.4425 |
| **27** | *Tsc22d2* | 0.000165 | 2.52E-07 | 1.3297 |
| **28** | *Ube2a* | 0.000165 | 2.52E-07 | 1.4698 |
| **29** | *Actr2* | 0.000437 | 7.55E-07 | 1.1965 |
| **30** | *Dot1l* | 0.000437 | 7.55E-07 | 1.1488 |
| **31** | *Maea* | 0.000437 | 7.55E-07 | 1.1661 |
| **32** | *Gid8* | 0.000688 | 1.26E-06 | 1.3039 |
| **33** | *Jmjd1c* | 0.000889 | 1.76E-06 | 1.2068 |

| | | | | |
|---|---|---|---|---|
| **34** | *Setd5* | 0.000889 | 1.76E-06 | 1.2419 |
| **35** | *Ccar1* | 0.001114 | 2.26E-06 | 1.2712 |
| **36** | *Mafb* | 0.001266 | 2.77E-06 | 1.0238 |
| **37** | *Ncstn* | 0.001266 | 2.77E-06 | 1.1446 |
| **38** | *Ssr3* | 0.001266 | 2.77E-06 | 1.2361 |
| **39** | *Wipf1* | 0.00143 | 3.27E-06 | 1.2092 |
| **40** | *Fbxo42* | 0.001515 | 3.77E-06 | 1.3577 |
| **41** | *Ncoa6* | 0.001515 | 3.77E-06 | 1.1937 |
| **42** | *Rarb* | 0.001515 | 3.77E-06 | 1.1368 |
| **43** | *Zfp148* | 0.001515 | 3.77E-06 | 1.2629 |
| **44** | *Unc119b* | 0.001809 | 4.78E-06 | 1.0119 |
| **45** | *Tecr* | 0.002842 | 7.80E-06 | 1.0887 |
| **46** | *Setd3* | 0.00297 | 8.30E-06 | 1.2151 |
| **47** | *Arpc4* | 0.00344 | 1.03E-05 | 1.2374 |
| **48** | *Epc2* | 0.00344 | 1.03E-05 | 1.3982 |
| **49** | *Gatad2a* | 0.00349 | 1.08E-05 | 1.1549 |
| **50** | *Rbm12* | 0.00358 | 1.18E-05 | 1.2697 |
| **51** | *Fam122a* | 0.005985 | 2.04E-05 | 1.1711 |
| **52** | *Tm2d2* | 0.007677 | 2.69E-05 | 1.3381 |
| **53** | *Zranb1* | 0.01052 | 3.85E-05 | 1.1365 |
| **54** | *Psenen* | 0.013663 | 5.21E-05 | 1.1704 |
| **55** | *Chd2* | 0.01408 | 5.51E-05 | 1.2682 |
| **56** | *Slc35a2* | 0.016606 | 6.67E-05 | 1.0476 |
| **57** | *Dock5* | 0.019138 | 7.98E-05 | 1.1312 |
| **58** | *Dpm3* | 0.021532 | 9.08E-05 | 1.0395 |
| **59** | *Ski* | 0.023122 | 9.99E-05 | 1.0636 |
| **60** | *Dpm2* | 0.026421 | 0.00011952 | 1.062 |
| **61** | *Rasgrp4* | 0.027228 | 0.00012455 | 1.3336 |
| **62** | *P2ry12* | 0.031172 | 0.00014417 | 1.0725 |
| **63** | *Zbtb14* | 0.033163 | 0.00015575 | 1.0527 |
| **64** | *Zfp384* | 0.036149 | 0.00017588 | 1.1869 |
| **65** | *Scaf1* | 0.036149 | 0.00017638 | 1.0687 |
| **66** | *Rap1gds1* | 0.049955 | 0.00025136 | 1.0083 |

# Appendix 6

Published October 1, 2021, doi:10.4049/jimmunol.2001426



# MHC Class II Ubiquitination Regulates Dendritic Cell Function and Immunity

**Kayla R. Wilson,* Devi Jenika,* Annabelle B. Blum,* Christophe Macri,* Bangyan Xu,* Haiyin Liu,* Patrick Schriek,* Dominik Schienstock,† Lauren Francis,* F. Victor Makota,* Satoshi Ishido,‡ Scott N. Mueller,† Mireille H. Lahoud,§ Irina Caminschi,†,§ Laura E. Edgington-Mitchell,*,¶,‖,# Jose A. Villadangos,*,† and Justine D. Mintern***

**MHC class II (MHC II) Ag presentation by dendritic cells (DCs) is critical for $CD4^+$ T cell immunity. Cell surface levels of MHC II loaded with peptide is controlled by ubiquitination. In this study, we have examined how MHC II ubiquitination impacts immunity using *MHC IIKR$^{KI/KI}$* mice expressing mutant MHC II molecules that are unable to be ubiquitinated. Numbers of conventional DC (cDC) 1, cDC2 and plasmacytoid DCs were significantly reduced in *MHC IIKR$^{KI/KI}$* spleen, with the remaining *MHC IIKR$^{KI/KI}$* DCs expressing an altered surface phenotype. Whereas Ag uptake, endosomal pH, and cathepsin protease activity were unaltered, *MHC IIKR$^{KI/KI}$* cDC1 produced increased inflammatory cytokines and possessed defects in Ag proteolysis. Immunization of *MHC IIKR$^{KI/KI}$* mice identified impairments in MHC II and MHC class I presentation of soluble, cell-associated and/or DC-targeted OVA via mAb specific for DC surface receptor Clec9A (anti-Clec9A-OVA mAb). Reduced T cell responses and impaired CTL killing was observed in *MHC IIKR$^{KI/KI}$* mice following immunization with cell-associated and anti-Clec9A-OVA. Immunization of *MHC IIKR$^{KI/KI}$* mice failed to elicit follicular Th cell responses and generated barely detectable Ab to anti-Clec9A mAb-targeted Ag. In summary, MHC II ubiquitination in DCs impacts the homeostasis, phenotype, cytokine production, and Ag proteolysis by DCs with consequences for Ag presentation and T cell and Ab-mediated immunity. *The Journal of Immunology*, 2021, 207: 1–10.**

Major histocompatibility class II (MHC II) molecules present peptide Ags derived from the endosomal pathway to $CD4^+$ T cells. This is essential for T cell activation during immune responses, but is also essential in thymic T cell selection and T cell maintenance in peripheral lymphoid organs. The stability and abundance of peptide-loaded MHC II (pMHC II) at the cell surface of APCs is regulated by ubiquitination. Ubiquitination occurs on lysine 225 (K225) in the β-chain of MHC II (1–3). The E3 ligase responsible for pMHC II ubiquitination in hematopoietic cells, including B cells and dendritic cells (DCs), is membrane-associated RING-CH-type finger (MARCH) 1 (4–6 and P. Schriek, H. Liu, A. C. Ching, P. Huang, N. Gupta, K. R. Wilson, M. Tsai, Y. Yan, C. F. Macri, L. F. Dagley, et al., manuscript posted on bioRxiv, DOI: 2021.04.15.439921), whereas MARCH8 is responsible for ubiquitination in thymic epithelial cells (7, 8, and P. Schriek et al., manuscript posted on bioRxiv, DOI: 2021.04.15.439921) and type II alveolar epithelial cells (P. Schriek et al., manuscript posted on bioRxiv, DOI: 2021.04.15.439921). Ubiquitination targets pMHC II for lysosomal degradation (9). As a result, DCs from mice lacking MARCH1 (*March1$^{-/-}$*) (6, and P. Schriek et al., manuscript posted on bioRxiv, DOI: 2021.04.15.439921) or expressing MHC II molecules with K225 mutated to R (*MHC IIKR$^{KI/KI}$*), which cannot be ubiquitinated, have increased surface MHC II expression (10). Despite surface MHC II being critical for T cell development, mice that lack MHC II ubiquitination have only minor alterations in their T cell compartments. We and others reported reduced regulatory T cells (11–13), but there is little impact on steady-state conventional T cell populations (11–13). The functional consequences for immunity are unclear, although little

*Department of Biochemistry and Pharmacology, Bio21 Molecular Science and Biotechnology Institute, The University of Melbourne, Parkville, Victoria, Australia; †Department of Microbiology and Immunology, Peter Doherty Institute for Infection and Immunity, The University of Melbourne, Parkville, Victoria, Australia; ‡Department of Microbiology, Hyogo College of Medicine, Nishinomiya, Japan; §Infection and Immunity Program, Monash Biomedicine Discovery Institute, Monash University, Clayton, Victoria, Australia; ¶Department of Biochemistry and Molecular Biology, Monash University, Clayton, Victoria, Australia; ‖Department of Oral and Maxillofacial Surgery, New York University College of Dentistry, Bluestone Center for Clinical Research, New York, NY; and #Drug Discovery Biology, Monash Institute of Pharmaceutical Sciences, Monash University, Parkville, Victoria, Australia

ORCIDs: 0000-0003-2023-7964 (K.R.W.); 0000-0002-0034-3527 (A.B.B.); 0000-0002-9618-3088 (C.M.); 0000-0002-2156-9074 (B.X.); 0000-0003-3103-6949 (H.L.); 0000-0002-0875-884X (P.S.); 0000-0001-8440-0009 (D.S.); 0000-0002-3838-3989 (S.N.M.); 0000-0001-8472-6201 (M.H.L.); 0000-0002-6810-6149 (L.E.E.-M.); 0000-0001-6771-8891 (J.A.V.); 0000-0002-3797-8577 (J.D.M.).

Received for publication December 18, 2020. Accepted for publication August 17, 2021.

This work was supported by Department of Health Australia, National Health and Medical Research Council grants or fellowships 1058193, 1113293, 1154502, and 1163090 (to J.A.V.) and 1161101 and 1129672 (to J.D.M.), Department of Education and Training, Australian Research Council (ARC) grants or fellowships 160103134, 170102471, and 190102213 to J.A.V. and 190101242, 180100844, 160101373, and 180100521 (to J.D.M.), a Human Frontiers Science Program grant (0064/2011 to J.A.V.), and the Australian Government's National Health and Medical Research Council Victorian State Government Operational Infrastructure Support and the Independent Research Institutes Infrastructure Support Scheme. L.E.E.-M. was supported by the Russell and Mab Grimwade Miegunyah Fund, funded at the University of Melbourne, which supplied a Grimwade Fellowship, and an ARC Discovery Early Career Researcher Award Fellowship (ARC, DE180100418).

Address correspondence and reprint requests to Prof. Jose A. Villadangos and Associate Prof. Justine D. Mintern, University of Melbourne, Parkville, Victoria 3010, Australia. E-mail addresses: j.villadangos@unimelb.edu.au (J.A.V.) and jmintern@unimelb.edu.au (J.D.M.)

The online version of this article contains supplemental material.

Abbreviations used in this article: BMDC, bone marrow–derived DC; cDC, conventional DC; CTV, CellTrace Violet; $CTV^{hi}$, splenocytes pulsed with $OVA_{257–264}$ and labeled with a high concentration of CTV; $CTV^{lo}$, splenocytes labeled with a low concentration of CTV; DC, dendritic cell; gMFI, geometric mean fluorescence intensity; MARCH, membrane-associated RING-CH-type finger; MHC I, MHC class I; MHC II, MHC class II; pMHC II, peptide-loaded MHC II; $T_{FH}$, T follicular helper; WT, wild-type.

analysis has been carried out to address this question. This is surprising, given the important role of APCs, particularly DCs, in initiating immunity.

An appealing hypothesis is that MHC II ubiquitination limits Ag presentation to prevent detrimental outcomes. In vitro Ag-presentation assays that investigate this scenario are inconclusive, showing increased (9), unaltered (14), or reduced (15–17) $CD4^+$ T cell priming in response to *MHC IIKR*$^{KI/KI}$ DC Ag presentation. This inconsistency may be due to differences in cell types, with some studies using bone marrow–derived DC (BMDC) (9, 14, 16) and others using bulk $CD11c^+$ DC (15, 17). Moreover, the impact of MHC II ubiquitination on MHC class I (MHC I) presentation has largely been ignored. We have previously described that a lack of MHC II ubiquitination reduces MHC I surface expression and impairs cross-presentation in vitro (18). From these studies, it is clear that an in-depth in vivo investigation is required to fully elucidate the impact of MHC II ubiquitination on DC Ag presentation and immunity.

In this study, we have systematically investigated the role of MHC II ubiquitination on primary DC function and in vivo immune outcomes. We have identified that in mice lacking MHC II ubiquitination there is a decrease in the number of splenic DCs. The remaining DCs have an altered surface phenotype accompanied by defects in Ag proteolysis and cytokine secretion. Functionally, these changes reduce in vivo $CD4^+$ and $CD8^+$ T cell priming in response to soluble, cell-associated and DC-targeted Ag. Importantly, ex vivo T cell priming revealed these changes were not simply due to reduced DC numbers but an intrinsic defect in DC function. Additionally, impairment in CTL killing, T follicular helper ($T_{FH}$) cell generation, and Ab responses were observed in *MHC IIKR*$^{KI/KI}$ mice following immunization. Our results demonstrate the importance of DC MHC II ubiquitination for effective immunity.

## Materials and Methods

### *Mice*

C57BL/6, *MHC IIKR*$^{KI/KI}$ (12), *IA*$\alpha^{-/-}$ (19), OT-II × Ly5.1 and OT-I × Ly5.1 mice were used at 6–12 wk of age. All mice were bred and maintained in specific pathogen–free conditions at the Melbourne Bioresources Platform at Bio21 Molecular Science and Biotechnology Institute. Experimental procedures were approved by the Animal Ethics Committee of the University of Melbourne (1714375).

### *Isolation of immune cells*

Primary splenic or thymic DCs were isolated as previously described (20). Splenic conventional DCs (cDCs) were stained with mAbs specific for CD11c (N418), CD8α (53-6.7), and CD11b (M1/70) (all BioLegend). Plasmacytoid DC (pDC) preparations were stained with BST-2 (927) and Siglec-H (551) (both BioLegend). Thymus DCs were identified with mAbs specific for CD11c (N418), CD8α (53-6.7), CD11b (M1/70), B220 (RA3-6B2), Sirpα (all BioLegend), and NK1.1 (PK136; BD Biosciences). In some experiments, cDC1 ($CD11c^+$ $CD8^+$ $CD11b^-$) and cDC2 ($CD11c^+$ $CD8^-$ $CD11b^+$) were sorted to purity by flow cytometry on a BD Influx (Murdoch Children's Research Institute Flow Cytometry and Imaging Facility). To obtain absolute cell numbers, an internal microsphere counting standard (BD Biosciences) was used.

For determining the expression of cell surface markers, single-cell suspensions were generated. Splenocytes were either treated with RBC removal buffer, or light cells were separated by density gradient separation in 1.077 g/cm$^3$ Nycodenz (Nycomed). Cells were stained with mAbs specific for CD3 (KT3-1.1), CD8α (53-6.7), CD11b (M1/70), CD11c (N418), CD19 (6D5), CD24 (M1/69), CD40 (FGK45.5), CD45R/B220 (RA3-6B2), CD80 (16-10A1), CD86 (GL1), CD135/Flt3 (A2F10), CD172 (Sirpα), CD205/DEC205 (NLDC-145), CD274/PD-L1 (10F.9G2), CD317/BST2 (927), CD370/Clec9A (7H11), H-2Kb (AF6-8815), IgD (11-26c.2a), IgM (RMM-1), Siglec-H (551), XCR1 (ZET) (all BioLegend), Ly-6C.2 (5075-3.6), or Ly-6G (1A8) (Walter and Eliza Hall Antibody Facility). Stained cells were acquired on the LSRFortessa (BD Biosciences) flow cytometer and analyzed on FlowJo software (Tree Star), with exclusion of cell doublets and dead cells in all cases identified based on forward and side scatter as well as staining with propidium iodide or DAPI. Statistical analysis was performed with Prism software.

### *Cytokines*

Splenic cDC1 and cDC2 were isolated and sorted to purity. A total of $1 \times 10^5$ DCs were cultured in completed medium (RPMI 1640 medium supplemented with 10% heat-inactivated FCS, 1% penicillin/streptomycin, 50 nM 2-ME, and 1% GlutaMAX) with or without 0.5 μM phosphorothioated CpG 1668 (Bioneer), 50 ng/ml IFN-γ (PeproTech), and 20 ng/ml GM-CSF (PeproTech) or 0.5 μM CpG alone. Supernatants were collected 18 h later and stored at −20°C. Cytokine secretion was determined using the BD Cytometric Bead Array Mouse Inflammation Kit according to the manufacturer's instructions (BD Biosciences).

### *Ag uptake, proteolysis, and endosomal pH analyses*

To assess Ag uptake, $5 \times 10^4$ purified cDC1 or cDC2 were incubated with 50 μg/ml OVA-Cy5 in complete medium for 0–90 min at 37°C. DCs were washed twice, and the fluorescence was measured by flow cytometry. As a control, DCs were pulsed with OVA-Cy5 for 90 min at 4°C. To assess Ag proteolysis and endosomal pH, $2.5 \times 10^5$ purified DCs were incubated with 20 μg/ml DQ-OVA (Life Technologies) or with 20 μg/ml dextran-pHrodo (Life Technologies) for 15 min at 37°C. Cells were washed twice, resuspended in complete medium and chased for the indicated time. At each time point, cells were kept on ice, and the fluorescence was measured by flow cytometry. As a control, DCs were pulsed with DQ-OVA or dextran-pHrodo for 15 min at 4°C, washed twice, and analyzed by flow cytometry. The signal was calculated for the 37°C chase time point by subtracting the geometric mean fluorescence intensity (gMFI) at 4°C. To normalize for dextran-pHrodo internalization, we simultaneously measured uptake of dextran-A647.

### *In vivo Ag-presentation assays*

Single-cell suspensions were generated from lymph nodes of OT-I × Ly5.1 or OT-II × Ly5.1 mice. Cells were stained with rat anti-mouse mAbs specific for CD11b (M1/70), F4/80 (F4/80), RBCs (TER119), Ly-6G/Ly-6C (RB68C5), MHC II (M5/114), CD45R (RA36B2), and CD4 (GK1.5) for OT-I T cells or CD8α (53-6.7) for OT-II cells. Cells were washed and incubated with BioMag anti-rat IgG-coupled magnetic beads (QIAGEN). After magnetic depletion, the $CD4^+$ or $CD8^+$ T cell–enriched supernatant was recovered. Cells were washed with PBS supplemented with 0.1% BSA and labeled with CellTrace Violet (CTV; Thermo Fisher Scientific). To enable accurate quantification of the number of OT-II or OT-I cells, mice also received transfer of a control population of CFSE (Thermo Fisher Scientific)–labeled splenocytes. Single-cell suspensions were treated with RBC removal buffer. Cells were washed with PBS, 0.1% BSA, and labeled with CFSE. Equal numbers of CTV-labeled OT-II or OT-I cells and CFSE-labeled splenocytes were pooled and resuspended in RPMI 1640, 2% FCS at $1 \times 10^7$ cells/ml, respectively, and injected i.v. Twenty-four hours later, mice received 50 μg (for OT-II–transferred mice) or 25 μg (for OT-I–transferred mice) soluble OVA (Sigma-Aldrich), $20 \times 10^6$ OVA-coated splenocytes, or 0.2 μg anti-Clec9A-OVA mAb (21) via i.v. injection. For OVA-coated splenocytes, single-cell suspensions were generated from spleens of C57BL/6 mice treated with RBC removal buffer, washed, and incubated with 10 mg/ml OVA protein (Sigma-Aldrich) in FCS-free RPMI 1640 at 37°C. Sixty-four hours after immunization, spleens were harvested, single-cell suspensions were generated, and RBCs were lysed. Cells were stained with mAbs specific for CD8α (53-6.7, BioLegend) or CD4 (GK1.5; Walter and Eliza Hall Antibody Facility) and Ly-5.1 (A20; BioLegend). The number of divided OT-II and OT-I was determined as the number of $CD4^+$ or $CD8^+$ $Ly\text{-}5.1^+$ cells that had undergone CTV dilution. The number of cells was normalized to the number of CFSE-labeled splenocytes recovered.

### *Ex vivo Ag-presentation assays*

Mice were immunized i.v. with 1 μg of anti-Clec9A-OVA mAb (22). One day later, spleens were harvested, and DC were isolated, as previously described, before sorting to purity. Sorted cDC1 ($CD11c^+$ $CD8^+$ $CD11b^-$) or cDC2 ($CD11c^+$ $CD8^-$ $CD11b^+$) (numbers indicated in figures) were cultured in vitro with $2.5 \times 10^4$ CTV-labeled OT-II or OT-I cells in complete medium. Four or five days later, the number of divided OT cells was determined.

### *In vitro Ag-presentation assays*

DCs were isolated as previously described, and cDC1 ($CD11c^+$ $CD8^+$ $CD11b^-$) and cDC2 ($CD11c^+$ $CD8^-$ $CD11b^+$) were sorted to purity. A total of $2.5 \times 10^4$ sorted cDC1 or cDC2 were cultured in vitro with $2.5 \times 10^4$ CTV-labeled OT-II cells and $OVA_{(323–339)}$ peptide. Sixty-eight hours later, the number of divided OT-II cells was determined by flow cytometry.

### *CTL assays*

Mice were injected with $2 \times 10^7$ OVA-coated splenocytes (prepared as previously described) or 1 μg of anti-Clec9A-OVA mAb, both with 1 μg of LPS as adjuvant. Six days later, single-cell suspensions of target cells (splenocytes) were prepared from spleens of wild-type (WT) mice. Half of the suspension ($OVA^+$ splenocytes pulsed with $OVA_{257–264}$ labeled with a high concentration of CTV [$CTV^{hi}$]) was pulsed with 1 μg of $OVA_{257–264}$ (Worthington Biochemical) and labeled with 5 mM CTV (Thermo Fisher Scientific). The other half of the suspension ($OVA^-$ splenocytes labeled with a low concentration of CTV [$CTV^{lo}$]) was labeled with 0.5 mM CTV only. An equal number of $OVA^+$ $CTV^{hi}$ and $OVA^-$ $CTV^{lo}$ target cells were pooled, and $10 \times 10^6$ target cells were injected i.v.; 36–42 h later, spleens were harvested and the percentage of OVA-specific lysis was determined as follows:

$$R = (\%\ CTV^{lo}/\%\ CTV^{hi})$$
$$\%\ \text{OVA-specific lysis} = [1 - (r_{\text{unprimed}}/r_{\text{primed}})] \times 100.$$

### *T cell characterization*

A total of $1 \times 10^4$ OT-II × Ly-5.1 or OT-I × Ly-5.1 cells were adoptively transferred into WT and *MHC IIKR*$^{KI/KI}$ mice. One day later, mice were immunized with 1 μg of anti-Clec9A-OVA mAb and 1 μg of LPS. Seven days later, spleens were harvested, single-cell suspensions were generated, and RBCs were lysed. Splenocytes were stained with mAbs specific for TCR Vα2 (B20.1; Walter and Eliza Hall Antibody Facility), Ly-5.1 (A20), PD-1 (29F.1A12), CD44 (IM7), and CD62L (MEL-14) (all BioLegend). For IFN-γ analysis, splenocytes were incubated with 1 μg/ml $OVA_{257–264}$ in the presence of BD GolgiPlug for 5 h at 37°C. For intracellular staining of IFN-γ and T-bet, splenocytes were permeabilized and fixed with a BD Cytofix/Cytoperm Kit or an eBioscience Foxp3/Transcription Factor Staining Buffer Set. Cells were stained for IFN-γ (XMG1.2) or T-bet (REA102; Miltenyi Biotec).

### *Induction and detection of Ab responses*

For $T_{FH}$ induction, $1 \times 10^6$ OT-II × Ly-5.1 cells were adoptively transferred into mice. One day later, mice were immunized with 0.5 μg anti-Clec9A-OVA mAb or PBS (no Ag control). Six days later, spleens were harvested, single-cell suspensions were generated, and RBCs were lysed. Cells were stained with mAbs specific for CD4 (GK1.5; Walter and Eliza Hall Antibody Facility), Ly-5.1 (A20), PD-1 (29F.1A12), CD44 (IM7) (all BioLegend), and CXCR5 (2G8; BD Biosciences). The number of OT-II and $T_{FH}$ cells was determined as the number of $CD4^+$ $Ly\text{-}5.1^+$ cells or $CD4^+$ $Ly\text{-}5.1^+CXCR5^+$ $PD\text{-}1^+$. For anti-rat Ig response, mice were injected i.v. with 2 μg of rat anti-Clec9A mAb (10B4), and serum samples were obtained at 2 wk postinjection. Anti-rat Ig reactivity was determined by ELISA. Nunc MaxiSorp (Thermo Fisher Scientific) plates were coated overnight at 4°C with 1.5 μg/ml rat GL117 mAb (Walter and Eliza Hall Antibody facility). Unbound Ab was removed by washing with PBS plus 0.05% Tween 20, PBS, and Milli-Q water. Serum samples were serially diluted in 5% skim milk powder in PBS and incubated at 4°C overnight. Captured mouse anti-rat Ig Abs were detected using anti-mouse IgG-HRP and visualized using 1-Step Ultra 3,3′,5,5′-Tetramethylbenzidine ELISA Substrate (Thermo Fisher Scientific). Absorbance at 440 nm was detected with a CLARIOstar plate reader (BMG LABTECH). Titers were considered positive when the absorbance was above 0.1 compared with blank.

### *Protease activity assay and cystatin C immunoblot*

To generate a large number of DCs, WT and *MHC IIKR*$^{KI/KI}$ mice were injected s.c. with $5 \times 10^6$ Flt3L-secreting B16 melanoma cells (22). Nine days later, spleens were harvested, and DCs were isolated as previously described (20). cDC1 and cDC2 were further separated by positive selection using MACS magnetic separation (Miltenyi Biotec). Purity >90% was determined by flow cytometry. Cells were lysed in PBS 0.1% Triton X-100 on ice for 20 min. Postnuclear supernatants equivalent to 80 μg of protein were acidified by adding 10× citrate buffer (final concentrations were 50 mM citrate [pH 5.5], 0.5% CHAPS, 0.1% Triton X-100, and 4 mM DTT). Where indicated, lysates were preincubated with the pan-cysteine cathepsin inhibitor E-64 (25 μM; Sigma-Aldrich) or DMSO vehicle at 37°C. A total of 1 μM BMV109, a fluorescently quenched pan-cysteine cathepsin activity-based probe, was added, and lysates were incubated at 37°C. Labeling reactions were stopped by addition of 5× sample buffer (50% glycerol, 200 mM Tris-Cl [pH 6.8], 10% SDS, 0.05% bromophenol blue, 6.25% 2-ME) followed by heating at 95°C for 5 min. Proteins were resolved on a 15% SDS-PAGE gel, and the gel was scanned for Cy5 fluorescence using a Typhoon flatbed laser scanner (GE Healthcare). For cystatin C immunoblots, proteins were transferred to nitrocellulose membranes and probed with goat anti-cystatin C (R&D Systems) and rabbit anti-actin (Sigma-Aldrich) Abs. After washing with PBS plus 0.05% Tween 20, blots were incubated with donkey anti-goat HRP (Novex; Life Technologies) and goat anti-rabbit IRDye 800CW (LI-COR Biosciences). IRDye 800CW immunoblots were scanned using Typhoon, and HRP labeling was visualized on a ChemiDoc MP Imaging System (Bio-Rad Laboratories) with the use of Amersham ECL Western blotting reagents (GE Healthcare). Protease activity and cystatin C (band intensity) were measured by densitometry using ImageJ. Values were normalized to actin (band intensity). Statistical analyses were performed using GraphPad Prism 8.

## Results

### *The inability to ubiquitinate MHC II impacts DC number and surface phenotype*

To investigate the impact of MHC II ubiquitination on DC biology, we used mice harboring a mutant MHC II unable to undergo ubiquitination (*MHC IIKR*$^{KI/KI}$) (12). First, we analyzed the number of splenic DCs. cDC1, cDC2, and pDCs were enriched by DNAse/collagenase digestion, followed by density centrifugation. A reduction in the number of cDC1 (61% decrease), cDC2 (50% decrease), and pDC (30% decrease) was detected in *MHC IIKR*$^{KI/KI}$ mice compared with WT mice (Fig. 1A). The decreased cell number was specific for splenic cDC and pDC, with no changes observed for splenic B cells (Fig. 1A) or thymic cDC1 and cDC2 (Fig. 1B).

The remaining cDC in *MHC IIKR*$^{KI/KI}$ spleen were profiled for their surface expression of characteristic DC markers (Fig. 1C, Supplemental Fig. 1). As expected, increased MHC II expression was observed on *MHC IIKR*$^{KI/KI}$ cDC1 (3.4-fold increase) and cDC2 (2.4-fold increase), whereas no changes were observed in CD86, a well-known MARCH1 substrate (15). Increased MHC II expression was accompanied by decreases in MHC I, CD24, and CD8, which we and others have previously reported as being reduced in the absence of MHC II ubiquitination (11, 15, 18). In addition, we detected previously undescribed, to our knowledge, reductions in CD11b, Sirpα, CD40, CD80, Flt3, XCR1, and DEC205. The only molecule besides MHC II to show increased expression was CD11c, most notably for *MHC IIKR*$^{KI/KI}$ cDC1 (Fig. 1C, Supplemental Fig. 1). Similar patterns were observed in splenic B cells, with increased MHC II expression correlating with small but significant decreases in the surface expression of IgM, PD-L1, CD19, and CD40 (Supplemental Fig. 1). These results indicate that impaired MHC II ubiquitination was sufficient to alter a variety of surface molecules, including integrins, chemokine receptors, and C-type lectin receptors.

### *An inability to ubiquitinate MHC II impacts DC function*

Given that we observed reduced costimulatory molecule expression (CD40 and CD80) on *MHC IIKR*$^{KI/KI}$ DCs, we next aimed to assess other parameters of Ag presentation. For efficient presentation by DCs, Ag must undergo endocytic uptake and proteolytic degradation. First, we measured OVA protein uptake. WT and *MHC IIKR*$^{KI/KI}$ cDC were purified and incubated with fluorescent soluble OVA-Cy5. In agreement with previous studies (23), we found cDC1 and cDC2 captured similar amounts of OVA. Similar uptake was observed by *MHC IIKR*$^{KI/KI}$ and WT cDC, demonstrating that a lack of MHC II ubiquitination does not alter uptake of OVA (Fig. 2A).

Once internalized, Ag is degraded and loaded onto MHC molecules. To investigate whether Ag proteolysis was impacted by a loss of MHC II ubiquitination, we used DQ-OVA, a self-quenched form of OVA that fluoresces once degraded. *MHC IIKR*$^{KI/KI}$ cDC1 and cDC2 were sorted to purity, and equal numbers of DCs were incubated with DQ-OVA. After Ag pulsing, excess DQ-OVA was

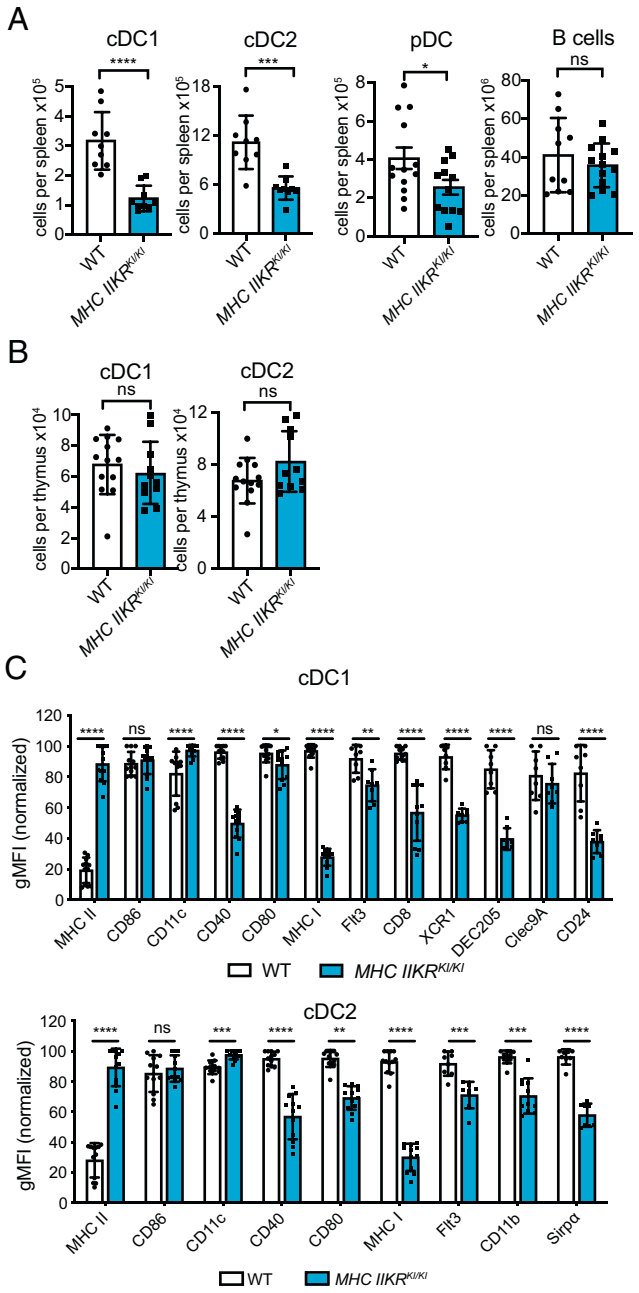


**FIGURE 1.** MHC II ubiquitination controls splenic DC number and cell-surface phenotype. Quantification of (**A**) splenic cDC1 ($CD11c^+$ $CD8^+$ $CD11b^-$), cDC2 ($CD11c^+$ $CD8^-$ $CD11b^+$), pDC ($BST\text{-}2^+$ $Siglec\text{-}H^+$), B cells ($CD19^+$ $B220^+$), and (**B**) thymic cDC1 ($XCR1^+$ $Sirp\alpha^-$) and cDC2 ($XCR1^-$ $Sirp\alpha^+$). Absolute numbers were determined as described in *Materials and Methods*. (**C**) WT and *MHC IIKR*$^{KI/KI}$ splenic cDC1 and cDC2 cell surface marker expression determined by flow cytometry. gMFI has been normalized to the maximum gMFI signal. (A–C) Symbols represent individual mice, with data pooled from a minimum of two independent experiments, displayed as mean ± SD. $^{****}p < 0.0001$, $^{***}p < 0.001$, $^{**}p < 0.01$, $^{*}p < 0.05$ by unpaired *t* test. ns, not significant.

removed by washing, and assessment of DQ-OVA fluorescence over time, as a read out of OVA proteolysis, was assessed by flow cytometry. In comparison with WT cDC1, *MHC IIKR*$^{KI/KI}$ cDC1, and to some extent cDC2 displayed reduced DQ-OVA proteolysis (Fig. 2B). The defect was specific to OVA, given that DQ-BSA, a self-quenched form of BSA underwent similar proteolysis in *MHC IIKR*$^{KI/KI}$ DC as in WT DC (Fig. 2C). Impaired proteolysis of DQ-OVA could result from alterations in the endosomal environment in *MHC IIKR*$^{KI/KI}$ cDC. To investigate this, we assessed endosomal pH using dextran-pHrodo. This is a pH-sensitive probe for which fluorescence is only detected once the probe enters an acidic environment. Purified WT and *MHC IIKR*$^{KI/KI}$ cDC1 and cDC2 were pulsed with dextran-pHrodo and chased for 120 min (Fig. 2D). As expected, fluorescence increased with time, indicative of dextran-pHrodo accessing an acidic environment. No difference was observed between *MHC IIKR*$^{KI/KI}$ and WT cDC, indicating no changes to endosomal pH in the absence of MHC II ubiquitination.

To examine protease activity, a fluorescently quenched activity-based probe, BMV109, was used to measure the activity of four cysteine cathepsins, which are key Ag-degrading enzymes (24–26). BMV109 irreversibly binds to cathepsins in an activity-dependent manner, giving rise to Cy5 fluorescence upon release of a QSY21-quenching group. As the binding is covalent, cathepsin binding can be detected by in-gel fluorescence as a surrogate measure of protease activity. A pan-cysteine cathepsin inhibitor, E-64, was first used to confirm the specificity of BMV109 for active papain-fold cysteine proteases. As expected, BMV109 did not bind cathepsins in the presence of E-64, confirming its specificity (Supplemental Fig. 2A). In agreement with previous studies (27), cysteine protease inhibitor cystatin C (CTS3) could only be detected in cDC1 (Supplemental Fig. 2B). Next, cysteine cathepsin protease activity was compared between *MHC IIKR*$^{KI/KI}$ DC and WT DC, and no differences were observed (Fig. 2E).

Given that cathepsin activity was normal in *MHC IIKR*$^{KI/KI}$ DCs, the reduction in Ag proteolysis together with altered cell surface phenotype suggest that a lack of MHC II ubiquitination could impact endocytic events. Because the production of cytokines is dependent on the endosomal trafficking of TLRs and their recognition of TLR ligands (28), we next investigated the capacity of *MHC IIKR*$^{KI/KI}$ DC to produce inflammatory cytokines. Splenic cDC1 and cDC2 were sorted to purity, and equal numbers were incubated in the presence of TLR9 ligand, CpG, and inflammatory cytokines IFN-γ and GM-CSF, conditions that elicit maximal IL-12 production (29). Supernatants were harvested after 18 h, and the presence of IL-6, IL-10, IL-12p70, TNF-α, and MCP-1 were measured using a BD Cytometric Bead Array assay. IL-10 and MCP-1 were not produced by either cDC1 or cDC2. *MHC IIKR*$^{KI/KI}$ cDC1 produced increased amounts of IL-6, IL-12, and TNF-α compared with WT cDC1, whereas the cytokine production of *MHC IIKR*$^{KI/KI}$ cDC2 was unaltered (Fig. 2F). Similar patterns, albeit at lower concentrations, were observed when DCs were treated with CpG alone (Supplemental Fig. 2C).

In summary, an inability to ubiquitinate MHC II reduces DC numbers, alters their surface phenotype, reduces proteolysis of some forms of Ag, and enhances cytokine production, in particular for the cDC1 subset, but does not impact DC endosomal pH or cysteine cathepsin protease activity.

MHC II expression levels, per se, rather than the extent of its ubiquitination, may regulate endosomal functions. If this were the case, such functions might also be affected in cells deficient in MHC II expression. To address this, we analyzed DCs from $I\!A\alpha^{-/-}$ mice. First, the cell surface phenotype was investigated. In contrast to the *MHC IIKR*$^{KI/KI}$ DCs, no alterations were observed, except for a slight increase in CD80 (Supplemental Fig. 3A). Next, we investigated the cytokine secretion of $I\!A\alpha^{-/-}$ cDC1 and cDC2 (Supplemental Fig. 3B). In agreement with previous studies (30), DCs lacking MHC II produced slightly less IL-6, IL-12, and TNF-α than WT DCs. Finally, we investigated Ag proteolysis using DQ-OVA, which proceeded similarly in WT and $I\!A\alpha^{-/-}$ DCs (Supplemental Fig. 3C). Overall, the impact of MHC II deficiency

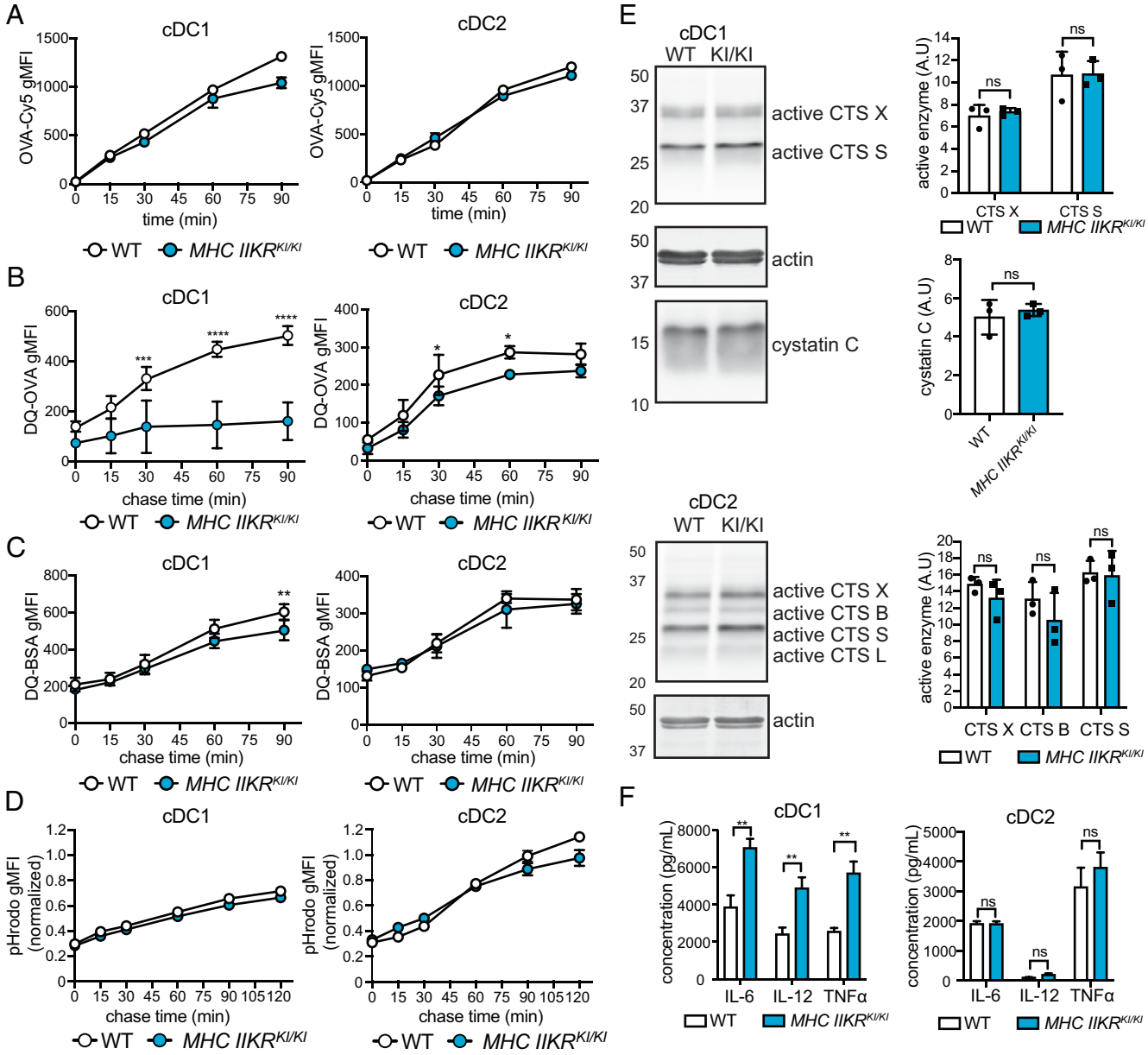


**FIGURE 2.** Lack of MHC II ubiquitination impairs Ag proteolysis and cytokine secretion without impacting Ag uptake, endosomal pH, or protease activity. (**A**) *MHC IIKR*$^{KI/KI}$ and WT cDC1 and cDC2 were sorted to purity and incubated at 37°C with 50 μg/ml OVA-Cy5 for the indicated times. Cells were washed before the Cy5 fluorescence was determined by flow cytometry. Data are from one experiment carried out in technical triplicate. (**B** and **C**) *MHC IIKR*$^{KI/KI}$ and WT cDC1 and cDC2 were sorted to purity and pulsed with 20 μg/ml (B) DQ-OVA or (C) DQ-BSA for 15 min at 37°C. Cells were washed and chased for the indicated time before the DQ signal was measured by flow cytometry. ****$p < 0.0001$, ***$p < 0.001$, *$p < 0.05$, two-way ANOVA with Bonferroni test for multiple comparisons. (**D**) *MHC IIKR*$^{KI/KI}$ and WT cDC1and cDC2 were sorted to purity and pulsed with 20 μg/ml dextran-pHrodo or dextran-A647 for 15 min at 37°C. Cells were washed, and dextran-pHrodo or dextran-A647 signal was measured by flow cytometry at different chase time points. To account for changes in uptake, dextran-pHrodo gMFI was normalized to dextran-A647. Data are from one experiment carried out in technical triplicate. (**E**) cDC1 (top panel) and cDC2 (lower panel) protease activity analysis. DCs were isolated as described in *Materials and Methods*. Cells were lysed before incubation with the pan-cathepsin (CTS) protease activity-based probe BMV109 (1 μM). Proteins were resolved on SDS-PAGE gel and Cy5 fluorescence was determined. Representative in-gel fluorescence of three independent experiments for WT or *MHC IIKR*$^{KI/KI}$ is shown. Quantification of protease activity or total protein expression is normalized to actin and displayed as mean ± SD. For cystatin C expression, blots were probed with goat anti-cystatin C and rabbit anti-actin (Sigma-Aldrich) Abs. Data are representative of three biological replicates. ns by unpaired Welch *t* test. (**F**) Cytokine secretion. cDC1 and cDC2 were sorted to purity and incubated with 0.5 μM CpG, 50 ng/ml IFN-γ, and 20 ng/ml GM-CSF. Supernatants were collected 18 h later, and cytokine secretion was determined using BD Cytometric Bead Array Mouse Inflammation Kit. Bars display mean ± SD from two independent experiments with cells pooled from eight mice. **$p < 0.01$, unpaired *t* test with Holm-Sidak correction for multiple comparisons. ns, not significant.

was negligible compared with that caused by lack of MHC II ubiquitination, suggesting that the altered phenotype of *MHC IIKR*$^{KI/KI}$ DCs is due to changes in MHC II trafficking rather than to altered MHC II surface expression.

### *An inability to ubiquitinate MHC II in APCs impairs MHC II Ag presentation in vivo*

Given the important role of MHC II in B cell and T cell immunity (31) and the dysregulation in Ag processing observed in *MHC*

*IIKR*$^{KI/KI}$ DCs, we next investigated the impact of MHC II ubiquitination on adaptive immunity. To investigate Ag presentation in a physiologically relevant setting, WT or *MHC IIKR*$^{KI/KI}$ mice were injected i.v. with CTV-labeled OT-II or OT-I. The following day, mice were immunized i.v. with one of three different forms of the model Ag OVA: 1) OVA protein, 2) cell-associated (splenocytes preincubated in vitro with OVA protein), and 3) OVA protein genetically fused to mAb against Clec9A (anti-Clec9A-OVA) (21). Clec9A was chosen as a receptor to measure receptor-mediated Ag uptake, as it is highly expressed by cDC1 (32) and is not altered in DCs with impaired MHC II ubiquitination (Fig. 1C). T cell priming with OCS (33) and anti-Clec9A-OVA (34) is cDC1 dependent. The number of dividing OT-II and OT-I cells in spleen was determined by flow cytometry 3 d following i.v. immunization. For all Ags tested, *MHC IIKR*$^{KI/KI}$ mice displayed a significant reduction in the number of dividing OT-II and OT-I cells (Fig. 3A). Therefore, a lack of MHC II ubiquitination impacts both MHC II and MHC I Ag presentation of soluble, cell-associated, and DC-targeted Ag in vivo.

Changes in in vivo T cell priming could be due to intrinsic alterations in DC function and/or the observed reduction in DC numbers (Fig. 1A). To control for the latter, ex vivo Ag-presentation assays were performed using equivalent numbers of isolated WT and *MHC IIKR*$^{KI/KI}$ DC. In this case, WT or *MHC IIKR*$^{KI/KI}$ mice were immunized with anti-Clec9A-OVA (21); 22 h later, spleens were harvested, and cDC1 were sorted to purity before an equal number of cells were incubated with CTV-labeled OT-II or OT-I cells. Proliferation was determined 4 or 3 d later for OT-II or OT-I, respectively. In agreement with in vivo analysis, reduced OT-II and OT-I priming was observed for *MHC IIKR*$^{KI/KI}$ cDC1 (Fig. 3B). Second, we tested the capacity of WT and *MHC IIKR*$^{KI/KI}$ cDC1 to present OVA peptide in vitro. WT and *MHC IIKR*$^{KI/KI}$ DCs were incubated with $OVA_{323–339}$ peptide and $IA^b$-$OVA_{323–339}$–specific OT-II T cells for 3 d. No change in OT-II proliferation was observed in vitro (Supplemental Fig. 4). Previously, we have demonstrated reduced OT-I proliferation when *MHC IIKR*$^{KI/KI}$ DC are pulsed with $OVA_{254–267}$ peptide (18). Together, these data demonstrate that a lack of MHC II ubiquitination causes DC-intrinsic impairments in Ag presentation.

### *An inability to ubiquitinate MHC II impairs CTL immune responses*

We investigated whether a lack of MHC II ubiquitination alters generation of effector CTL. WT and *MHC IIKR*$^{KI/KI}$ mice were immunized with cell-associated OVA or anti-Clec9A-OVA, with LPS used as an adjuvant. Six days later, mice were injected with target cells that comprised an equal mix of syngeneic splenocytes pulsed with CTV$^{hi}$ or without CTV$^{lo}$." Robust CTL responses were observed in WT mice immunized with cell-associated OVA (35) or anti-Clec9A OVA mAb (21). In contrast, reduced CTL killing was observed in *MHC IIKR*$^{KI/KI}$ mice in response to both immunogens (Fig. 4).

To further investigate T cell responses in *MHC IIKR*$^{KI/KI}$ mice, OT-II or OT-I cells were transferred into WT and *MHC IIKR*$^{KI/KI}$ mice before immunization with anti-Clec9A-OVA together with LPS as an adjuvant. Six days later, their number and phenotype

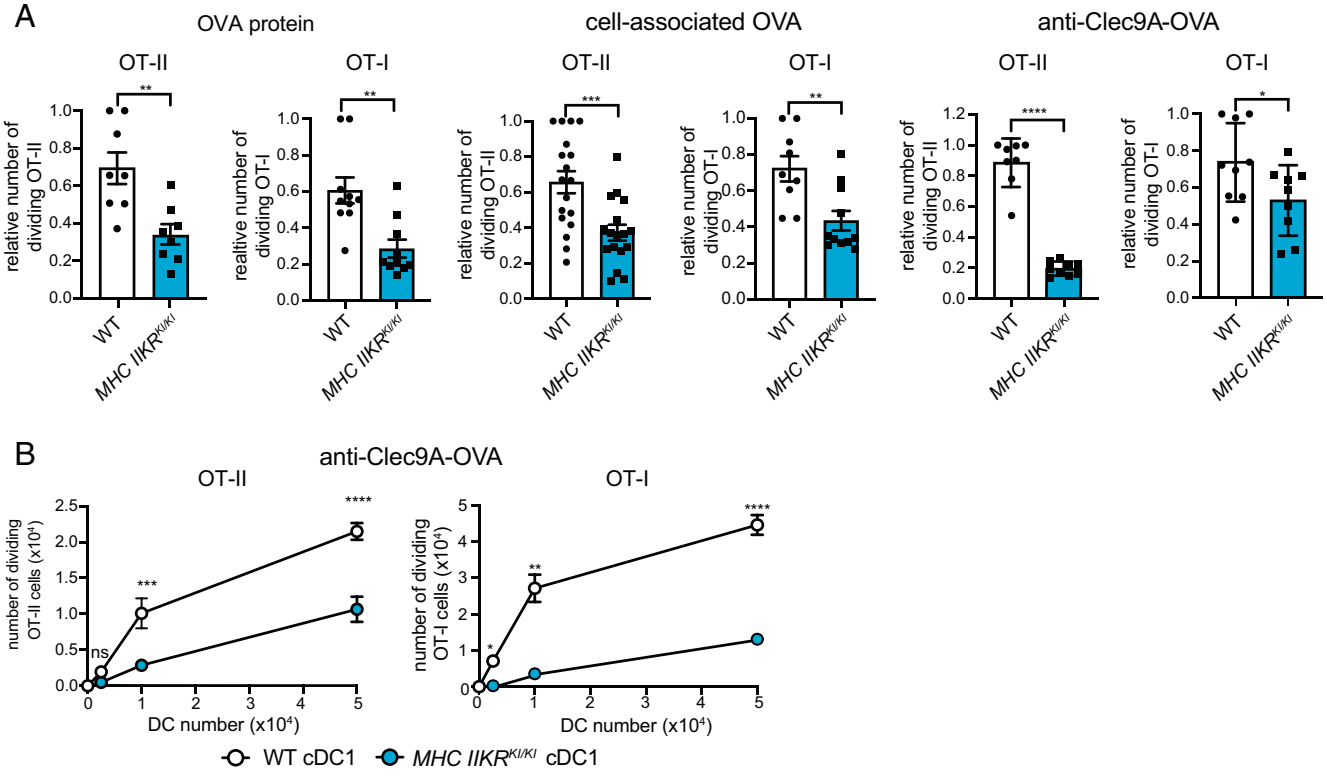


**FIGURE 3.** Lack of MHC II ubiquitination impairs DC Ag presentation in vivo and ex vivo. (**A**) Purified CTV-labeled OT-II or OT-I cells and CFSE-labeled BL6 mouse splenocytes were adoptively transferred into *MHC IIKR*$^{KI/KI}$ and WT mice. Twenty-four hours later, mice were injected with 50 μg (OT-II), 25 μg (OT-I) of soluble OVA protein, $20 \times 10^6$ OVA-coated splenocytes (cell-associated OVA), or 0.2 μg of anti-Clec9A-OVA mAb via i.v. injection (anti-Clec9A-OVA). Spleens were harvested 64 h later, and Ag-presentation capacity was assessed by flow cytometry as described in *Materials and Methods*. Each symbol represents an individual mouse with data pooled from at least two independent experiments displayed as mean ± SD. (**B**) WT and *MHC IIKR*$^{KI/KI}$ mice were i.v. injected with 1 μg of anti-Clec9A-OVA. Twenty-two hours later, spleen cDC1 were isolated and cell-sorted to purity. DCs were cultured ex vivo with $2.5 \times 10^4$ OT-I for 64 h or OT-II for 84 h, and divided OT-I cells were quantified by flow cytometry. Data are pooled from two independent experiments, and graphs show mean ± SD. $^{****}p < 0.0001$, $^{***}p < 0.001$, $^{**}p < 0.01$, $^{*}p < 0.05$ by two-way ANOVA with Bonferroni test for multiple comparisons. ns, not significant.

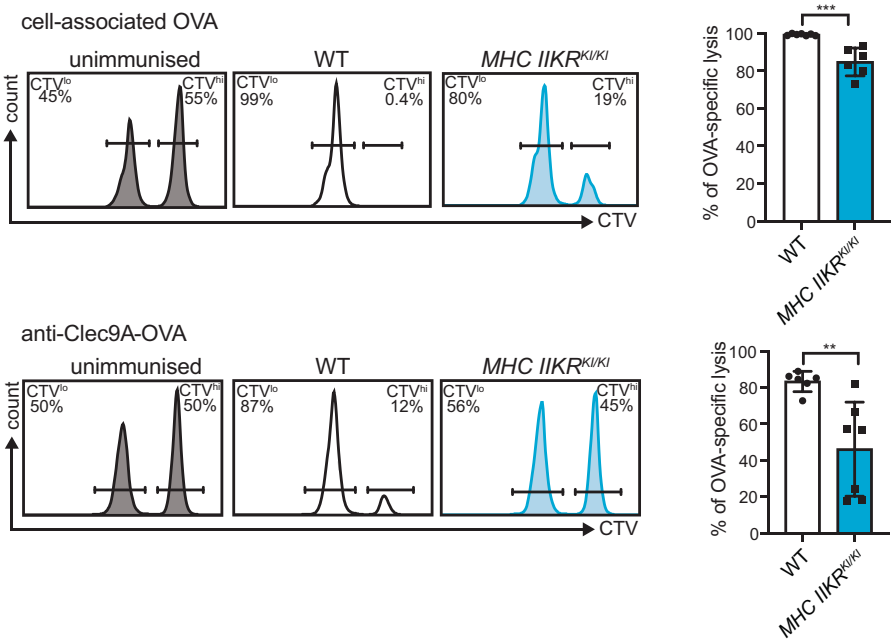


**FIGURE 4.** Lack of MHC II ubiquitination impairs CTL responses. *MHC IIKR*$^{KI/KI}$ and WT mice were immunized i.v. with $2.5 \times 10^7$ OVA-coated splenocytes (cell-associated OVA) or 1 μg of anti-Clec9A-OVA mAb (anti-Clec9A-OVA) in the presence of LPS. Six days later, mice were challenged with equal number of CTV$^{hi}$ (OVA$_{257–264}^+$) and CTV$^{lo}$ (OVA$^-$) target cells; 36–42 h later, the spleens were harvested, and the percentage lysis of CTV$^{hi}$ cells was determined by flow cytometry as described in *Materials and Methods*. Histograms are representative of killing in each group, including no Ag (unimmunized) negative control. Bars show mean ± SD and are data pooled from two independent experiments, with symbols representing individual mice. ***$p < 0.001$, **$p < 0.01$, unpaired *t* test.

were examined (Fig. 5). In response to immunization, *MHC IIKR*$^{KI/KI}$ mice had reduced numbers of OT-II cells accompanied by reduced PD-1 expression, a marker expressed by activated T cells (36), and a reduction in the percentage of CD62L$^-$CD44$^+$ OT-II cells. Expression of T-bet, indicative of Th1 differentiation, was unaltered (Fig. 5A). Reduced OT-I numbers were also observed in *MHC IIKR*$^{KI/KI}$ mice following immunization. These cells expressed lower PD-1, but did not differ in their expression of CD62L and CD44 or IFN-γ production when restimulated with Ag (Fig. 5B).

*An inability to ubiquitinate MHC II impairs Ab responses*

Finally, a role for MHC II ubiquitination in humoral immunity was assessed. WT and *MHC IIKR*$^{KI/KI}$ mice were immunized with rat anti-mouse Clec9A mAb, which elicits anti-rat Ig reactive Abs (21, 32). Generating germinal centers and Ab responses requires CD4$^+$ T$_{FH}$ cells. To investigate T$_{FH}$ cell induction, OT-II cells were transferred into WT and *MHC IIKR*$^{KI/KI}$ mice, and 1 d later, mice were immunized with anti-Clec9A-OVA mAb. Six days later, we examined production of T$_{FH}$, which upregulates PD-1 and CXCR5. WT mice injected with anti-Clec9A-OVA mAb had robust expansion of OT-II cells, with increased PD-1 and CXCR5 expression (21, 37). In contrast, reduced numbers of T$_{FH}$ cells were detected in *MHC IIKR*$^{KI/KI}$ mice (Fig. 6A). The reduction in T$_{FH}$ cells was associated with a barely detectable Ab response. Although a robust anti-rat Ig response was detected in WT mice, *MHC IIKR*$^{KI/KI}$ mice failed to generate serum anti-rat Ig in response to anti-Clec9A (Fig. 6B). Therefore, *MHC IIKR*$^{KI/KI}$ mice display significant impairments in humoral immunity.

## Discussion

Ubiquitination of MHC II plays an important role in regulating cell surface MHC II; however, the biological consequences of this post-translational modification are unclear. In this study we conduct, to our knowledge, the first comprehensive analysis in vivo and show that an absence of MHC II ubiquitination reduces splenic DC numbers, alters DC cytokine production, impairs DC Ag proteolysis, and ultimately reduces in vivo Ag presentation, CTL, and humoral immunity.

Previously, different in vitro Ag-presentation studies have yielded disparate outcomes and have focused on CD4$^+$ T cell priming only (9, 14–18). To our knowledge, this is the first study to demonstrate a reduction in MHC II and MHC I Ag presentation in response to soluble, cell-associated and anti-Clec9A mAb-targeted Ag following immunization of *MHC IIKR*$^{KI/KI}$ mice. These data are in agreement with a recent study identifying that *MHC IIKR*$^{KI/KI}$ mice have reduced CD4$^+$ T cell priming following immunization with OVA in the presence of CFA (17). Our study extends this work to different forms of Ag, including soluble, cell-associated, and Clec9A-targeted Ag, demonstrating that MHC II ubiquitination impacts MHC II presentation of Ag acquired via different intracellular routes. In addition, we demonstrated that MHC II ubiquitination impacts MHC I presentation in vivo. Reduced splenic DC numbers may contribute to this impairment, and in addition, ex vivo Ag-presentation assays demonstrate a cell-intrinsic defect in DC function. In agreement with this, *MHC IIKR*$^{KI/KI}$ DC isolated from mixed bone marrow chimeric mice generated from *MHC IIKR*$^{KI/KI}$ bone marrow have reduced in vitro CD4$^+$ T cell priming in comparison with the WT DC from the same mouse (17). Several parameters of DC biology are likely involved, including reduced costimulatory molecule and MHC I cell surface expression, altered cytokine secretion, and altered Ag proteolysis. An altered cell surface phenotype has previously been observed in cells lacking MHC II ubiquitination. Indeed, altered expression of CD80, CD40, CD71, PD-L1, ICOS-L (P. Schriek et al., manuscript posted on bioRxiv, DOI: 2021.04.15.439921), CD4, and CD8 (15) is detected on APCs lacking *Marchf1*, and *MHC IIKR*$^{KI/KI}$ BMDCs have reduced tetraspanin expression (11).

Elevated IL-6, IL-12, and TNF-α secretion described in this study is in contrast to other studies demonstrating that *MHC IIKR*$^{KI/KI}$ and *Marchf1*$^{-/-}$ DC have reduced IL-12 and TNF-α production (15, 17). This difference is likely due to differences in stimuli tested, with CpG (TLR9 agonist), IFN-γ, and GM-CSF used in this study, in contrast to LPS (TLR4 agonist). This study also shows that *MHC IIKR*$^{KI/KI}$ cDC1 have reduced OVA degradation, but overall, *MHC IIKR*$^{KI/KI}$ cDC1 or cDC2 do not exhibit a global Ag proteolysis defect. BSA degradation was similar to WT and, likewise, no defects in endosomal acidification or cathepsin activity were detected.

Impairments in DC Ag presentation in the absence of MHC II ubiquitination are likely due to excessive MHC II accumulation on the plasma membrane, which disrupts plasma membrane and lipid raft structure (11). Lipid rafts are important for Ag presentation and

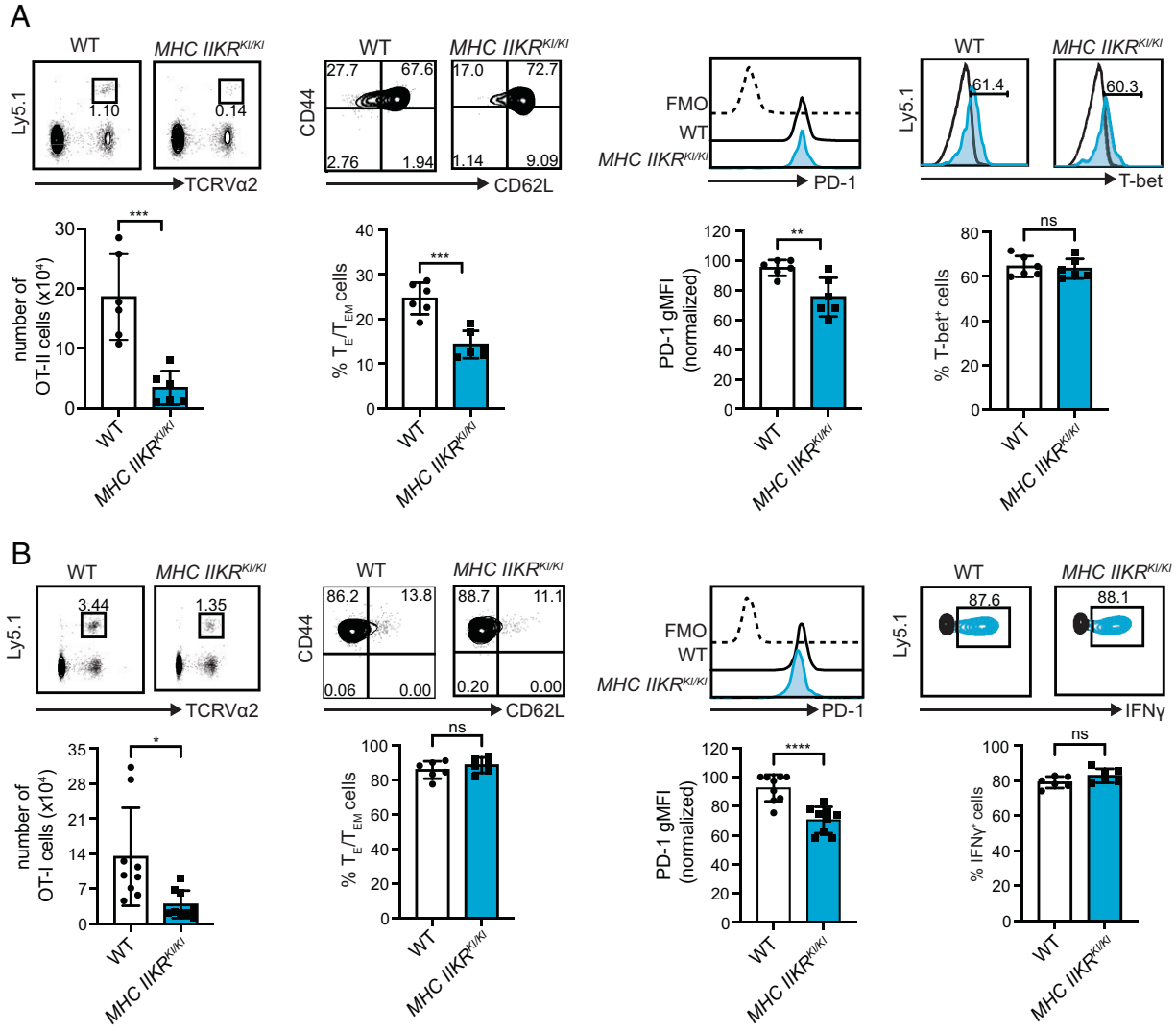


**FIGURE 5.** Lack of MHC II ubiquitination impairs $CD4^+$ and $CD8^+$ T cell responses. A total of (**A**) $1 \times 10^4$ OT-II or (**B**) OT-I cells were adoptively transferred into *MHC IIKR*$^{KI/KI}$ and WT mice. One day later, mice were immunized with 1 μg of anti-Clec9A-OVA mAb and 1 μg of LPS. Seven days later, spleens were harvested, and the number of OT-II and OT-I cells, surface PD-1, CD44 and CD62L, and intracellular IFN-γ and T-bet expression was determined. For IFN-γ analysis, cells were incubated with 1 μg/ml $OVA_{257–264}$ in the presence of BD GolgiPlug for 5 h at 37°C before intracellular staining as described in *Materials and Methods*. Data are from two independent experiments, with symbols representing individual mice. $^{****}p < 0.0001$, $^{***}p < 0.001$, $^{**}p < 0.01$, $^{*}p < 0.05$ by unpaired *t* test. ns, not significant.

if disrupted can lead to reduced APC and T cell conjugate formation, and reduced T cell activation (38, 39). In agreement with this, *Marchf1*-deficient and *MHC IIKR*$^{KI/KI}$ BMDC engage thymocytes at a lower frequency (11), and when pulsed with OVA, *Marchf1*-deficient and *MHC IIKR*$^{KI/KI}$ spleen $CD11c^+$ DCs are unable to form stable conjugates with $CD4^+$ T cells to the same extent as WT DCs (17). Altered MHC II trafficking in the absence of its ubiquitination has been previously described, with reduced pMHC II degradation (9), MHC II internalization (13, 18), and increased recycling (9). The downstream consequences for T cell priming were examined, and reduced numbers and impaired phenotype of $CD4^+$ (OT-II) and $CD8^+$ (OT-I) T cells following Clec9A-OVA immunization was identified. This likely accounts for impaired CTL immunity following immunization with cell-associated or Clec9A-targeted Ag and, similarly, poor Ab responses. Indeed, we also observe reduced induction of $CD4^+$ $T_{FH}$ cells in *MHC IIKR*$^{KI/KI}$ mice, in accordance with longer TCR:pMHC II interactions being required to promote their differentiation (40, 41).

*MHC IIKR*$^{KI/KI}$ mice failed to generate Ab responses to DC-targeted Ag. This is in conflict to previous studies that show normal Ab responses for *MHC IIKR*$^{KI/KI}$ mice (14). The discrepancy could stem from the different mouse models, with *MHC IIKR*$^{KI/KI}$ mice used in this study as opposed to *MHC IIKR-GFP* mice, or differences in immunization timing and Ag. Our study immunized with rat anti-Clec9A mAb, which specifically relies on cDC1 presentation, whereas the previous analysis used protein (OVA and hen egg lysozyme) and influenza A virus infection, all of which will engage other DC subsets, including cDC2, that we show in this study are less impacted by a lack of MHC II ubiquitination. Importantly, changes in Ab production could also be due to alterations in B cell biology. Indeed, MHC II is regulated by MARCH1-mediated ubiquitination in B cells. In germinal center B cells, in particular, MHC II expression is dynamically regulated by ubiquitination as the cells cycle between the light and dark zones (42). A lack of MHC II ubiquitination in germinal center B cells leads to prolonged peptide presentation that may impact the presented peptide repertoire and, in

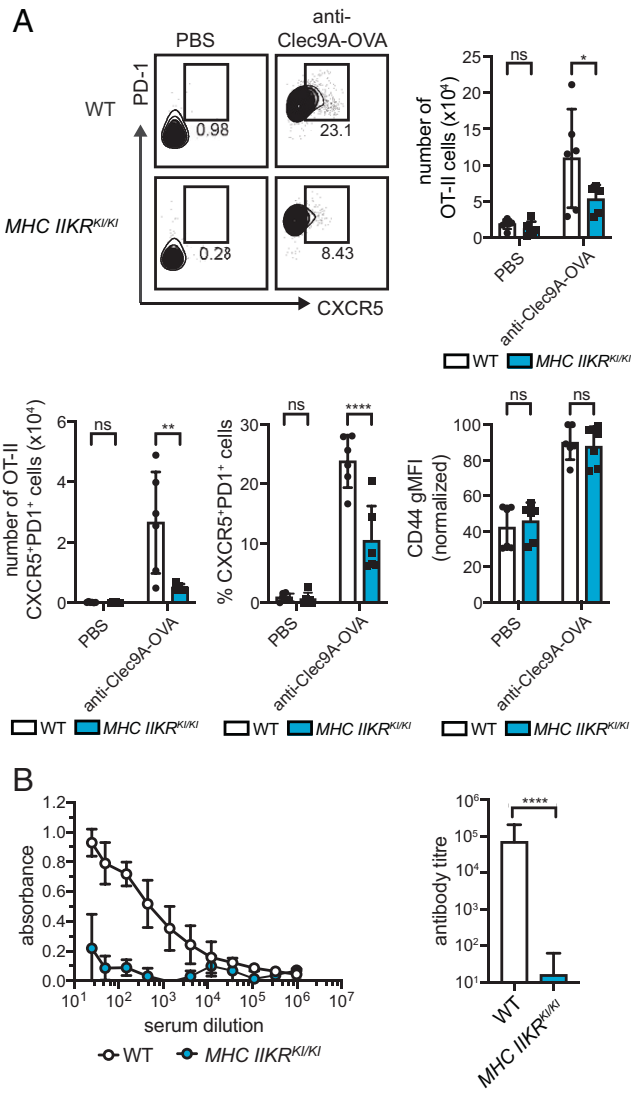


**FIGURE 6.** Lack of MHC II ubiquitination impairs Ab responses. (**A**) $T_{FH}$ induction. A total of $1 \times 10^6$ OT-II × Ly-5.1 cells were adoptively transferred into *MHC IIKR*$^{KI/KI}$ and WT mice. Twenty-four hours later, mice were injected with PBS (no Ag) or 1 μg of anti-Clec9A-OVA mAb. Six days later, spleens were harvested, and the number of OT-II cells and OT-II CXCR5$^+$ PD1$^+$ ($T_{FH}$) cells was determined. The activation status of OT-II cells was assessed by staining for CD44. gMFI has been normalized to the maximum gMFI signal. Data are from two independent experiments, with $n = 6$ mice. ****$p < 0.0001$, **$p < 0.01$, *$p < 0.05$, two-way ANOVA with Sidak test for multiple comparisons. (**B**) Ab production. WT and *MHC IIKR*$^{KI/KI}$ mice were injected i.v. with 2 μg of anti-Clec9A mAb (10B4), and serum anti-rat reactivity was measured by ELISA 14 d after injection. Representative anti-rat Ig response is shown (left). Bars show mean titers ± SD with $n = 10$ mice; data are pooled from two independent experiments performed in duplicate. ****$p < 0.0001$, Mann–Whitney *U* test. ns, not significant.

turn, delay affinity maturation (42). Therefore, it is possible that this too contributes to the decreased Ab production observed in *MHC IIKR*$^{KI/KI}$ mice.

In this study we identify the importance of MHC II ubiquitination in DC, T cell, and B cell responses. Evolutionary conservation of MARCH ligases and the target residue of ubiquitination in MHC II (K225), may therefore have been driven not by a simple requirement to regulate MHC II surface expression but to prevent secondary effects induced by the excessive deposition of MHC II on the cell surface.

## Disclosures

The authors have no financial conflicts of interest.

## References


1. Ohmura-Hoshino, M., Y. Matsuki, M. Aoki, E. Goto, M. Mito, M. Uematsu, T. Kakiuchi, H. Hotta, and S. Ishido. 2006. Inhibition of MHC class II expression and immune responses by c-MIR. *J. Immunol.* 177: 341–354.
2. Shin, J. S., M. Ebersold, M. Pypaert, L. Delamarre, A. Hartley, and I. Mellman. 2006. Surface expression of MHC class II in dendritic cells is controlled by regulated ubiquitination. *Nature* 444: 115–118.
3. van Niel, G., R. Wubbolts, T. Ten Broeke, S. I. Buschow, F. A. Ossendorp, C. J. Melief, G. Raposo, B. W. van Balkom, and W. Stoorvogel. 2006. Dendritic cells regulate exposure of MHC class II at their plasma membrane by oligoubiquitination. *Immunity* 25: 885–894.
4. De Gassart, A., V. Camosseto, J. Thibodeau, M. Ceppi, N. Catalan, P. Pierre, and E. Gatti. 2008. MHC class II stabilization at the surface of human dendritic cells is the result of maturation-dependent MARCH I down-regulation. *Proc. Natl. Acad. Sci. USA* 105: 3491–3496.
5. Young, L. J., N. S. Wilson, P. Schnorrer, A. Proietto, T. ten Broeke, Y. Matsuki, A. M. Mount, G. T. Belz, M. O'Keeffe, M. Ohmura-Hoshino, et al. 2008. Differential MHC class II synthesis and ubiquitination confers distinct antigen-presenting properties on conventional and plasmacytoid dendritic cells. *Nat. Immunol.* 9: 1244–1252.
6. Matsuki, Y., M. Ohmura-Hoshino, E. Goto, M. Aoki, M. Mito-Yoshida, M. Uematsu, T. Hasegawa, H. Koseki, O. Ohara, M. Nakayama, et al. 2007. Novel regulation of MHC class II function in B cells. *EMBO J.* 26: 846–854.
7. Liu, H., R. Jain, J. Guan, V. Vuong, S. Ishido, N. L. La Gruta, D. H. Gray, J. A. Villadangos, and J. D. Mintern. 2016. Ubiquitin ligase MARCH 8 cooperates with CD83 to control surface MHC II expression in thymic epithelium and CD4 T cell selection. *J. Exp. Med.* 213: 1695–1703.
8. von Rohrscheidt, J., E. Petrozziello, J. Nedjic, C. Federle, L. Krzyzak, H. L. Ploegh, S. Ishido, A. Steinkasserer, and L. Klein. 2016. Thymic CD4 T cell selection requires attenuation of March8-mediated MHCII turnover in cortical epithelial cells through CD83. *J. Exp. Med.* 213: 1685–1694.
9. Cho, K.-J., E. Walseng, S. Ishido, and P. A. Roche. 2015. Ubiquitination by March-I prevents MHC class II recycling and promotes MHC class II turnover in antigen-presenting cells. *Proc. Natl. Acad. Sci. USA* 112: 10449–10454.
10. Walseng, E., K. Furuta, B. Bosch, K. A. Weih, Y. Matsuki, O. Bakke, S. Ishido, and P. A. Roche. 2010. Ubiquitination regulates MHC class II-peptide complex retention and degradation in dendritic cells. *Proc. Natl. Acad. Sci. USA* 107: 20465–20470.
11. Oh, J., J. S. A. Perry, H. Pua, N. Irgens-Möller, S. Ishido, C.-S. S. Hsieh, and J.-S. S. Shin. 2018. MARCH1 protects the lipid raft and tetraspanin web from MHCII proteotoxicity in dendritic cells. *J. Cell Biol.* 217: 1395–1410.
12. Oh, J., N. Wu, G. Baravalle, B. Cohn, J. Ma, B. Lo, I. Mellman, S. Ishido, M. Anderson, and J.-S. Shin. 2013. MARCH1-mediated MHCII ubiquitination promotes dendritic cell selection of natural regulatory T cells. *J. Exp. Med.* 210: 1069–1077.
13. Liu, H., K. R. Wilson, P. Schriek, C. Macri, A. B. Blum, L. Francis, M. Heinlein, C. Nataraja, J. Harris, S. A. Jones, et al. 2020. Ubiquitination of MHC Class II Is Required for Development of Regulatory but Not Conventional CD4$^+$ T Cells. *J. Immunol.* 205: 1207–1216.
14. McGehee, A. M., K. Strijbis, E. Guillen, T. Eng, O. Kirak, and H. L. Ploegh. 2011. Ubiquitin-dependent control of class II MHC localization is dispensable for antigen presentation and antibody production. *PLoS One* 6: e18817.
15. Ohmura-Hoshino, M., Y. Matsuki, M. Mito-Yoshida, E. Goto, M. Aoki-Kawasumi, M. Nakayama, O. Ohara, and S. Ishido. 2009. Cutting edge: requirement of MARCH-I-mediated MHC II ubiquitination for the maintenance of conventional dendritic cells. *J. Immunol.* 183: 6893–6897.
16. Ishikawa, R., M. Kajikawa, and S. Ishido. 2014. Loss of MHC II ubiquitination inhibits the activation and differentiation of CD4 T cells. *Int. Immunol.* 26: 283–289.
17. Kim, H. J., J. Bandola-Simon, S. Ishido, N. W. Wong, V. N. Koparde, M. Cam, and P. A. Roche. 2021. Ubiquitination of MHC Class II by March-I Regulates Dendritic Cell Fitness. *J. Immunol.* 206: 494–504.
18. Wilson, K. R., H. Liu, G. Healey, V. Vuong, S. Ishido, M. J. Herold, J. A. Villadangos, and J. D. Mintern. 2018. MARCH1-mediated ubiquitination of MHC II impacts the MHC I antigen presentation pathway. *PLoS One* 13: e0200540.
19. Köntgen, F., G. Süss, C. Stewart, M. Steinmetz, and H. Bluethmann. 1993. Targeted disruption of the MHC class II Aa gene in C57BL/6 mice. *Int. Immunol.* 5: 957–964.
20. Vremec, D. 2010. The isolation of mouse dendritic cells from lymphoid tissues and the identification of dendritic cell subtypes by multiparameter flow cytometry. *Methods Mol. Biol.* 595: 205–229.
21. Lahoud, M. H., F. Ahmet, S. Kitsoulis, S. S. Wan, D. Vremec, C.-N. Lee, B. Phipson, W. Shi, G. K. Smyth, A. M. Lew, et al. 2011. Targeting antigen to mouse dendritic cells via Clec9A induces potent CD4 T cell responses biased toward a follicular helper phenotype. *J. Immunol.* 187: 842–850.
22. Mach, N., S. Gillessen, S. B. Wilson, C. Sheehan, M. Mihm, and G. Dranoff. 2000. Differences in dendritic cells stimulated in vivo by tumors engineered to secrete granulocyte-macrophage colony-stimulating factor or Flt3-ligand. *Cancer Res.* 60: 3239–3246.
23. Schnorrer, P., G. M. N. N. Behrens, N. S. Wilson, J. L. Pooley, C. M. Smith, D. El-Sukkari, G. Davey, F. Kupresanin, M. Li, E. Maraskovsky, et al. 2006. The

dominant role of CD8+ dendritic cells in cross-presentation is not dictated by antigen capture. *Proc. Natl. Acad. Sci. USA* 103: 10729–10734.
24. Verdoes, M., K. Oresic Bender, E. Segal, W. A. van der Linden, S. Syed, N. P. Withana, L. E. Sanman, and M. Bogyo. 2013. Improved quenched fluorescent probe for imaging of cysteine cathepsin activity. *J. Am. Chem. Soc.* 135: 14726–14730.
25. Edgington-Mitchell, L. E., M. Bogyo, and M. Verdoes. 2016. Live Cell Imaging and Profiling of Cysteine Cathepsin Activity Using a Quenched Activity-Based Probe. In *Activity-Based Proteomics: Methods and Protocols*. H. S. Overkleeft, and B. I. Florea, eds. Springer, New York. 145–159.
26. Villadangos, J. A., and H. L. Ploegh. 2000. Proteolysis in MHC class II antigen presentation: who's in charge? *Immunity*. 12: 233–239.
27. El-Sukkari, D., N. S. Wilson, K. Hakansson, R. J. Steptoe, A. Grubb, K. Shortman, and J. A. Villadangos. 2003. The protease inhibitor cystatin C is differentially expressed among dendritic cell populations, but does not control antigen presentation. *J. Immunol.* 171: 5003–5011.
28. Lee, B. L., and G. M. Barton. 2014. Trafficking of endosomal Toll-like receptors. *Trends Cell Biol.* 24: 360–369.
29. Hochrein, H., M. O'Keeffe, T. Luft, S. Vandenabeele, R. J. Grumont, E. Maraskovsky, and K. Shortman. 2000. Interleukin (IL)-4 is a major regulatory cytokine governing bioactive IL-12 production by mouse and human dendritic cells. *J. Exp. Med.* 192: 823–833.
30. Liu, X., Z. Zhan, D. Li, L. Xu, F. Ma, P. Zhang, H. Yao, and X. Cao. 2011. Intracellular MHC class II molecules promote TLR-triggered innate immune responses by maintaining activation of the kinase Btk. *Nat. Immunol.* 12: 416–424.
31. Cosgrove, D., D. Gray, A. Dierich, J. Kaufman, M. Lemeur, C. Benoist, and D. Mathis. 1991. Mice lacking MHC class II molecules. *Cell* 66: 1051–1066.
32. Caminschi, I., A. I. Proietto, F. Ahmet, S. Kitsoulis, J. Shin Teh, J. C. Y. Lo, A. Rizzitelli, L. Wu, D. Vremec, S. L. H. van Dommelen, et al. 2008. The dendritic cell subtype-restricted C-type lectin Clec9A is a target for vaccine enhancement. *Blood* 112: 3264–3273.
33. Hildner, K., B. T. Edelson, W. E. Purtha, M. Diamond, H. Matsushita, M. Kohyama, B. Calderon, B. U. Schraml, E. R. Unanue, M. S. Diamond, R. D. Schreiber, T. L. Murphy, and K. M. Murphy. 2008. Batf3 deficiency reveals a critical role for CD8alpha+ dendritic cells in cytotoxic T cell immunity. *Science* 322: 1097–1100.
34. Caminschi, I., D. Vremec, F. Ahmet, M. H. Lahoud, J. A. Villadangos, K. M. Murphy, W. R. Heath, and K. Shortman. 2012. Antibody responses initiated by Clec9A-bearing dendritic cells in normal and Batf3$^{(-/-)}$ mice. *Mol. Immunol.* 50: 9–17.
35. Carbone, F. R., and M. J. Bevan. 1990. Class I-restricted processing and presentation of exogenous cell-associated antigen in vivo. *J. Exp. Med.* 171: 377–387.
36. Sharpe, A. H., and K. E. Pauken. 2018. The diverse functions of the PD1 inhibitory pathway. *Nat. Rev. Immunol.* 18: 153–167.
37. Kato, Y., A. Zaid, G. M. Davey, S. N. Mueller, S. L. Nutt, D. Zotos, D. M. Tarlinton, K. Shortman, M. H. Lahoud, W. R. Heath, and I. Caminschi. 2015. Targeting antigen to Clec9A primes follicular Th cell memory responses capable of robust recall. *J. Immunol.* 195: 1006–1014.
38. Hiltbold, E. M., N. J. Poloso, and P. A. Roche. 2003. MHC class II-peptide complexes and APC lipid rafts accumulate at the immunological synapse. *J. Immunol.* 170: 1329–1338.
39. Anderson, H. A., E. M. Hiltbold, and P. A. Roche. 2000. Concentration of MHC class II molecules in lipid rafts facilitates antigen presentation. *Nat. Immunol.* 1: 156–162.
40. Tubo, N. J., A. J. Pagán, J. J. Taylor, R. W. Nelson, J. L. Linehan, J. M. Ertelt, E. S. Huseby, S. S. Way, and M. K. Jenkins. 2013. Single naive CD4+ T cells from a diverse repertoire produce different effector cell types during infection. *Cell* 153: 785–796.
41. Benson, R. A., M. K. L. MacLeod, B. G. Hale, A. Patakas, P. Garside, and J. M. Brewer. 2015. Antigen presentation kinetics control T cell/dendritic cell interactions and follicular helper T cell generation in vivo. *eLife* 4: e06994.
42. Bannard, O., S. J. McGowan, J. Ersching, S. Ishido, G. D. Victora, J. S. Shin, and J. G. Cyster. 2016. Ubiquitin-mediated fluctuations in MHC class II facilitate efficient germinal center B cell responses. *J. Exp. Med.* 213: 993–1009.